Ecole Doctorale Lorraine de Chimie et Physique Moléculaires (SESAMES)
UFR Science et Techniques de la Matière et des Procédés
Nancy Université – Université Henri Poincaré

Nancy-Université

Thèse en vue de l'obtension du titre de

Docteur de l'université Henri Poincaré

(Spécialité Chimie Informatique et Théorique)

Fonction et modulation des canaux potassiques voltage-dépendants: Etude par simulations de dynamique moléculaire

On the function and modulation of voltage-gated potassium channels: Insights from large-scale all-atom molecular dynamics simulations.

Lucie Delemotte

Equipe de Chimie et Biochimie Théoriques
UMR 7565 Structure et Réactivité des Systèmes Moléculaires Complexes

Cette thèse est présentée et soutenue le 22 septembre 2011

Rapporteurs :	Pr. Erik Lindahl	Center for biomembrane research, Stockholm University, Suède
	Dr. Marc Baaden	Laboratoire de biochimie théorique, Université Pierre et Marie Curie, Paris, France (CR CNRS - HDR)
Examinateurs :	Dr. Gildas Loussouarn	Institut du thorax, université de Nantes, France (CR CNRS HDR)
	Pr. Michael L. Klein	Institute for computational molecular science, Temple University, Philadelphia, USA
	Pr. Xavier Assfeld	UMR SRSMC, Nancy Université, France
	Dr. Mounir Tarek	UMR SRSMC, Nancy Université, France (DR CNRS)

Note: The main text of this thesis is in English. The introduction and conclusion are presented in both languages and each chapter starts with a short summary of the content in French.

Acknowledgments

I would like to thank:

Dr. Marc Baaden and Pr. Erik Lindahl *for agreeing to review this work*

Mounir, Werner and Mike, *for what I learned from you. Thanks to you, I hope this is just the beginning.*

Adèle, Eva, Jennifer, Pascale, Vale. *Merci d'avoir été là pour remplir le labo de douceur féminine* ;-) *I will miss you girls !*

Adil, Agostino, Ahcène, Alain, Alexandrine, Anne-Gaëlle, Antonio, Aurore, Axel, Béatrice, Camille, Catherine, Céline, Chao, le petit groupe CIES, le CINES, Claude, Claudia, Christian, Christophe, Chuong, Damjan, Daniel, David, Delphine, Domenica, Elke, Emiliano, Fabien, Francesca, Francis, François, Gérald, Giacomo, Giulia, Greg, Jean-Louis, Jean-Loup, Jens, Jérôme, Jonathan, Julien, Kathy, Laëtitia, Laure, Liz, Luca, Luciann, Luisa, le Made In France, Manolo, Marilia, Marwa, Michaël, Muhannad, Mylène, the NAMD/VMD team, Nico, Nirmala, Ophélie, Paolo, Peppe, Peter, Quy, Rafael, Sébastien, Sefer, Sharon, Soraya, Thibault, Valeria, YanYan, Xavier *for your scientific and/or personal support. All of you have made these three years, in Nancy or elsewhere, an great time.*

Annie, Luc, Maël, Martin et l'ensemble de ma famille, proche ou éloignée. *Vous êtes le socle sur lequel je peux m'appuyer. Merci pour tout le soutien que vous m'avez apporté.*

Ralph-Olivier, *plus que tout, mon rayon de soleil*. *Merci d'avoir partagé l'ensemble avec moi* ♥.

Résumé

Contexte : Les canaux ioniques voltage-dépendant (CIVD) sont des protéines transmembranaires (TM) ubiquitaires qui sont impliquées dans la transmission de signaux électriques dans les cellules excitables. Lors d'une variation du potentiel TM, ces canaux subissent un changement conformationnel donnant lieu à leur ouverture/fermeture, grâce à la sensibilité de résidus conservés chargés positivement (basiques) appartenant au domaine sensible à la tension (DST). La mutation de ces résidus peut donner lieu à de nombreuses maladies génétiques. Durant les quelques dernières 50 années, des études par électrophysiologie, pharmacologie, spectroscopie et autres techniques ont permis de révéler des détails sur la fonction de tels canaux. Toutefois, certaines questions concernant leur dynamique à l'échelle moléculaire sont encore matière à débat intense. Nous mettons a profit dans ce travail une technique complémentaire, la dynamique moléculaire (DM), qui peut contribuer à apporter un éclairage nouveau sur la relation entre structure et fonction dans ces CIVD.

Résultats principaux : Partant de la structure cristallographique du canal potassique Kv1.2 dans sa conformation ouverte (ou activée), nous avons mené des simulations de DM du canal inséré dans son environnement lipidique et soumis à un potentiel hyperpolarisant. Nous avons pu suivre la désactivation du DST et ainsi découvrir trois états intermédiaires entre les conformations ouverte et fermée. Les estimations de la charge liée à l'ouverture/fermeture (« gating charge ») et les contacts moléculaires en fonction de la conformation du canal sont en accord avec les résultats expérimentaux publiés. Nous proposons donc un modèle complet de la désactivation qui réconcilie les modèles divergents qui étaient jusqu'alors proposés. Par ailleurs, nous avons caractérisé l'effet de mutations des résidus chargés positivement du DST impliquées dans des maladies génétiques. Nous montrons que celles-ci donnent lieu à l'apparition de courants de fuite qui dépendent de la conformation du canal. Ces résultats révèlent les éléments moléculaires clé impliqués dans ces courants “omega” qu'il est possible de détecter par électrophysiologie. Nous proposons une généralisation aux autres membres de la famille des CIVD en indiquant dans quelles conditions ces fuites peuvent être critiques.

Travaux en cours : Dans le but d'étendre ces résultats à d'autres membres de la famille des CIVD, qui sont impliqués dans des maladies génétiques, nous avons choisi de nous intéresser à la sous-famille des canaux potassiques Kv7. Nous proposons un modèle du domaine TM de quelques membres de cette famille, et étudions par DM leur activation et l'effet de la mutation de résidus basiques du DST qui sont impliquées dans le syndrome du QT long du coeur, les attaques néonatales familiales bénignes ou la surdité lentement évolutive.

Publications: 1- Delemotte, L., Dehez, F., Treptow, W., & Tarek, M. (2008). Modeling membranes under a transmembrane potential. *J. Phys. Chem. B*, *112*(18), 5547-5550.

2- Delemotte, L., Treptow, W., Klein, M. L., & Tarek, M. (2010). Effect of Sensor Domain Mutations on the Properties of Voltage-Gated Ion Channels: Molecular Dynamics Studies of the Potassium Channel Kv1.2. *Biophys. J*, *99*(9), L72-L74.

3- Delemotte, L., Tarek, M., Klein, M. L., Amaral, C., & Treptow, W. (2011). Intermediate states of the Kv1.2 voltage sensor from atomistic molecular dynamics simulations. *Proc. Nat. Acad. Sci. USA,* 108, 6109-6114.

Abstract

Background: Voltage gated ion channels (VGCs) are ubiquitous transmembrane proteins involved in electrical signaling in excitable cells. Their gating (opening-closing), triggered by changes in the TM voltage, proceeds through a sensing mechanism involving conserved positively charged (basic) residues belonging to the voltage sensor domain (VSD). Mutation of these residues can lead to various genetic diseases. Details on the function of such channels have been revealed thanks to many years of experimental investigations, using electrophysiology, molecular biology, pharmacology, spectroscopy techniques and others. However, many questions concerning the molecular level gating process of these proteins still remain under active debate. We use here a complementary technique, molecular dynamics (MD) simulations, that can contribute to provide new light on the VGC structure/function relationship.

Main Results: Starting from the "open state" crystal structure of the potassium VGC Kv1.2, we have carried out large-scale all-atom MD of the channel embedded in its lipidic environment submitted to a hyperpolarized potential. This has allowed to follow the deactivation of the VSD and to uncover three intermediate states between the open and closed conformations. We report gating charge calculations or else state dependent molecular contacts that comply with experimental results and propose accordingly a model of the entire deactivation that conciliates the diverging views proposed so far. We have also characterized the effect of specific mutations of basic residues of the VSD involved in genetic diseases. The latter are shown to induce a perturbation of the VSD structure and lead to the appearance of state-dependent leak currents. These results unveil the key elementary molecular processes involved in these "omega" currents detected by electrophysiology. We propose a generalization to other members of the voltage gated ion channel family, indicating which type of residues may lead to the appearance of such currents, and under which condition these leaks may be critical.

Work in progress: Wishing to extend all these findings to other members of the potassium VGCs family which are implicated in genetic diseases, we have selected to study the Kv7 subfamily. In this scope, we put forward a model of the transmembrane domain of a few Kv7 channels, and studied by molecular dynamics simulations their activation properties and the effect of VSD basic residues mutations that are implicated in long QT syndrome, in benign familial neonatal seizures or in slowly progressive deafness.

Related published papers: 1- Delemotte, L., Dehez, F., Treptow, W., & Tarek, M. (2008). Modeling membranes under a transmembrane potential. *J. Phys. Chem. B*, *112*(18), 5547-5550.

2- Delemotte, L., Treptow, W., Klein, M. L., & Tarek, M. (2010). Effect of Sensor Domain Mutations on the Properties of Voltage-Gated Ion Channels: Molecular Dynamics Studies of the Potassium Channel Kv1.2. *Biophys. J*, *99*(9), L72-L74.

3- Delemotte, L., Tarek, M., Klein, M. L., Amaral, C., & Treptow, W. (2011). Intermediate states of the Kv1.2 voltage sensor from atomistic molecular dynamics simulations. *Proc. Nat. Acad. Sci. USA,* 108(15), 6109-6114.

Table of Contents

Table of Abbreviations

1D one dimensional
3D three dimensional
ABF adaptative biasing force
AP action potentials
BNFS benign neonatal familial seizures
CAP cell-attached patch
Cav voltage-gated calcium channels
CNG cyclic nucleotide gated
EAG ether-à-go-go
EP electrostatic potential
FRET fluorescence resonance energy transfer
HaTx hanatoxin
HCN hyperpolarization-activated cyclic nucleotide
hSkMI human skeletal muscle
IOP inside-out patch
Kv voltage-gated potassium
LRET luminescence (or lanthanide) resonance energy transfer
MD molecular dynamics
MTS methylthiosulfonate
MTSET trimethylammonium-ethyl methanethiosulfonate
NaChBac bacterial voltage sensitive sodium channel
NaChR nicotinic acetylcholine receptor
Nav voltage-gated sodium channels
NMR nuclear magnetic resonance
NPT constant pressure and temperature
NVT constant volume and temperature
OMIM online mendelian inheritance in man
OOP outside-out patch
PCMBS p-chloromercuribenzenesulfonate
PBCs periodic boundary conditions
PIP2 phosphatidylinositol-4,5-bisphosphate
POCP ceramide-1-phosphate
POCR ceramide
POPC palmitoyl-oleoyl-phosphatidylcholine
PME particle mesh ewald
PNH peripheral nerve hyperexcitability
ppWC permeabilized-patch WC-configuration
SCAM substituted cysteine accessibility method
SMase C sphingomyelinase C
SMase D sphingomyelinase D
SPGM sphingomyelin
T1 tetramerization domain
TEA tetra-ethyl-ammonium
TM transmembrane
TRP transient receptor potential
TTX tetrodotoxin
STX saxitoxin
VGCs voltage-gated ion channels
VSD voltage-sensor domain
VSTX1 voltage-sensor toxin
WC whole cell recording
WT wild type

1- INTRODUCTION

"The key to growth is the introduction of higher dimensions of consciousness into our awareness."

-Lao Tzu

Les cellules excitables ont été découvertes au début des années 1950 et leur rôle crucial dans la transmission de l'influx nerveux au sein des organismes supérieurs a été reconnu grâce à l'avènement des techniques d'électrophysiologie. En effet, lorsqu'une impulsion de potentiel électrique est appliquée à ces cellules, elles répondent en donnant lieu à l'apparition d'un courant au travers de leurs membranes. Sur le plan moléculaire, ceci provient du transport d'ions au travers de ces dernière. Une vingtaine d'années plus tard, on a découvert que ce transport voltage-dépendant d'ions au travers des membranes excitables survenait au travers de protéines membranaires. Ces macromolécules, appelées canaux ioniques voltage-dépendants (CIVD), sont en fait des pores qui peuvent être ouverts ou fermés en fonction de la polarisation de la membrane. Depuis, on a découvert que ces canaux sont impliqués dans un grand nombre de fonctions biologiques car ils sont localisés dans toutes les cellules excitables comme le cœur, le système nerveux et de nombreux autres organes tels que l'oreille interne, l'estomac ou le foie... De ce fait, ces protéines sont sensibles à un grand nombre de facteurs de modulation, comme d'action de peptides d'inactivation, de drogues ou d'anesthésiants, ou la modification des lipides qui les entourent... D'une manière similaire, les mutations génétiques qui touchent ces canaux peuvent avoir un effet dramatique et donner lieu à un grand nombre de maladies héréditaires (appelées canalopathies) comme le syndrome du QT long, des maladies neurologiques telles que l'épilepsie, les paralysies périodiques de différents types, la surdité héréditaire...

Avec l'avènement des techniques dites de «patch-clamp», les expériences d'électrophysiologie ont permis la découverte d'une caractéristique essentielle des canaux ioniques voltage-dépendants: lors de leur activation, ils produisent des courants de très petite magnitude et de nature transitoire qui ont été appelés courants de « gating » et qui sont dûs à la réorganisation des charges de la protéine. L'intégrale de ces courants, la charge de « gating », provient du transport de charges de la protéine au travers du capaciteur que forme la membrane et constitue l'une des propriétés fondamentales des canaux. Au début des années 1980, lorsque les premiers canaux voltage-dépendants ont été séquencés, on a pu montrer qu'ils sont tous organisés de la même manière, en tétramères, chaque monomère contenant six hélices transmembranaires. Le repliement et l'assemblage des deux hélices de l'extrémité N-terminale de chaque sous-unité (S5 et S6) forment le pore, la région qui est responsable du transport des ions d'un côté à l'autre de la membrane. Les quatre autres (S1-S4) constituent un domaine auxiliaire qui est responsable de la sensibilité aux changements dans le voltage transmembranaire : le domaine sensible à la tension (DST). Parmi ces hélices, le segment S4 contient un grand nombre de résidus chargés positivement (4 à 7, le plus souvent des arginines) qui sentent et répondent aux fluctuations du potentiel transmembranaire (*i.e.* du champ électrique local). Ces résidus sont les composants au niveau moléculaire qui sont responsables des courants de « gating » : en effet, lors de l'activation, soit lorsque le canal passe de l'état au repos (fermé) à l'état activé (ouvert), la charge de « gating » totale (12 à 14 charges élémentaires par canal) est transportée au travers de la membrane principalement par les résidus basiques de S4.

Le mouvement de la charge électrique au sein du domaine sensible à la tension, *i.e.* la charge de « gating », est une propriété fondamentale qui détermine non seulement la dépendance au voltage de l'activation du canal, mais contraint aussi les modèles physiques qui permettent d'expliquer le mouvement de charge au sein du DST et donc son fonctionnement. Pour décrire ce dernier, trois modèles principaux ont été proposés. Dans le premier, appelé le *modèle en vis,* S4 se déplace par rapport au reste du domaine dans un mouvement de translation (de ~10 à 20 Å le long de la normale à la membrane) combiné à une rotation (le long de son propre axe, de 180°). Ce modèle implique aussi un phénomène caractéristique : la réorganisation des interactions électrostatiques dans le DST. En effet, afin de stabiliser S4 dans une orientation transmembranaire, les arginines sont engagées dans des ponts salins avec des résidus chargés négativement appartenant aux autres hélices (S1-S3) du DST. A partir de données provenant d'expériences de mutagénèse, ce modèle met en jeu la formation de certains ponts salins tandis que d'autres sont rompus lorsque S4 bouge en réponse au champ électrique produit par le potentiel transmembranaire. Le deuxième modèle met en jeu au contraire une réorganisation conséquente du champ électrique au voisinage de S4 et un mouvement de S4 d'une magnitude réduite. Ce modèle, basé principalement sur des expériences de fluorescence est appelé le *modèle transporteur*. Enfin, le *modèle paddle*, qui a été abandonné depuis, implique le large mouvement de l'ensemble S3-S4 d'une position parallèle à la surface de la membrane dans l'état au repos à une position verticale dans 'état activé. Un nombre important d'études a été conduit afin de réconcilier ces modèles et une vision relativement consensuelle a fini par émerger ces dernières années : le mouvement transmembranaire de S4 est probablement d'une magnitude intermédiaire et le réarrangement des ponts salins lors de l'activation est important pour le fonctionnement correct du canal. L'évènement qui a généré la plus grande avancée dans la compréhension du mécanisme moléculaire des canaux ioniques sensibles à la tension a vraisemblablement été la résolution de la structure cristallographique à haute résolution d'un canal potassique voltage-dépendant : le Kv1.2. Dans cette structure, le pore est ouvert et le domaine sensible à la tension est dans sa conformation « activée », *i.e.* avec S4 en position haute. Cette structure, qui est d'une manière générale en bon accord avec de nombreuses mesures d'électrophysiologie, a permis de révéler de nombreux détails au niveau moléculaire tel que le réseau de ponts salins impliqué dans l'état activé du domaine sensible à la tension, l'interaction des têtes polaires des lipides avec les résidus basiques du haut de S4, la courbure de l'hélice S6 qui est importante pour la fermeture du canal, etc... ***Le contexte bibliographique détaillé de ce travail est introduit au chapitre 2.***

Malgré les progrès remarquables faits ces dernières décennies dans la compréhension des détails du fonctionnement des CIVD au niveau moléculaire, certaines questions essentielles restent en suspens, parmi lesquelles :

- Dans Kv1.2, quelle est *l'étendue du mouvement* des résidus basiques de S4 et comment *la force électrique* agit-elle sur eux ? A quoi ressemblent les *états intermédiaires* et *au repos* du canal ?
- Quelle est le mécanisme de *couplage* entre l'activation (désactivation) du DST et

l'ouverture (fermeture) du pore ?

- Comment peut-on expliquer au niveau moléculaire les *canalopathies* qui sont la conséquence de la *mutation* des résidus chargés positivement de S4 ?
- Comment les *lipides modulent*-ils l'activation/désactivation du domaine sensible à la tension et que se passe-t-il lorsque les *têtes polaires* des lipides proches du canal sont modifiées ?

L'objectif principal de ce travail est de contribuer à répondre à ces questions grâce à l'utilisation de simulations de dynamique moléculaire état de l'art. Cet ensemble de méthodes repose sur l'intégration des équations classiques du mouvement, connaissant les interactions entre les paires de particules du système. L'avantage principal de cette technique est la possibilité d'obtenir des informations au niveau moléculaire que la plupart des techniques expérimentales ne peuvent atteindre. De plus, comme ce travail le démontrera, l'information tirée des simulations de dynamique moléculaire (position, charges, vitesses des atomes...) permet d'évaluer des quantités mesurables expérimentalement. On mesura ainsi par exemple la charge de « gating » d'une manière cohérente avec les mesures d'électrophysiologie. En effet, nous avons mis en place une méthode (protocole) qui permet d'appliquer un potentiel transmembranaire d'une manière équivalente à ce qui est fait par patch clamp. Nous avons également développé et comparé des procédés pour mesurer la charge de « gating » *in silico*. ***Ces dernières, ainsi que les protocoles et les méthodes de simulation de dynamique moléculaires seront exposées en détail dans le chapitre 3.***

L'essentiel de notre travail a consisté à modéliser le canal Kv1.2 dans son intégralité, inséré dans son environnement lipidique (une bicouche lipidique de phosphatidyl-choline), et plongé dans une solution ionique à 150 mM de KCl. Les résultats sont basés sur l'analyse d'une simulation de 2.2 μs du canal soumis à un potentiel hyperpolarisé de ~ -600 mV et de simulations biaisées conduites afin de générer les dernières étapes de la désactivation. Nous avons ainsi obtenu cinq états du domaine sensible à la tension au long de la désactivation. Les conformations correspondantes, α, -β, γ and δ- et ε représentent les états ouvert, intermédiaire et fermé du canal, respectivement. Nous avons aussi décrit en détail le mouvement de S4 et de ses résidus chargés, les interactions entre les domaines sensibles à la tension et les lipides aux alentours, les propriétés électriques du DST, parmi lesquelles la forme du champ électrique local ou les contributions des différents composants moléculaires à la charge de « gating » et finalement le couplage de l'action du domaine sensible à la tension à la fermeture du pore. Dans l'ensemble, nos résultats indiquent que c'est le *modèle en vis* qui permet de décrire le mieux l'opération du DST.

Grâce à l'utilisation des configurations du Kv1.2 déterminées dans la première partie de ce travail, nous avons ensuite étudié l'effet au niveau moléculaire des mutations des résidus chargés positivement de S4 qui sont impliquées dans des maladies génétiques. Certaines d'entre elles perturbent la structure du domaine sensible à la tension et donnent lieu à l'apparition de courants de fuite au travers du DST. Ces résultats dévoilent les mécanismes moléculaires qui sont impliqués dans ces courants « oméga » détectés par électrophysiologie.

Après une étude extensive des différentes mutations dans les états ouvert et fermé du Kv1.2, nous proposons un modèle du mécanisme donnant lieu à l'apparition des courants « oméga », indiquant quel type de résidus peut générer ces derniers et sous quelles conditions ces fuites peuvent être critiques.

Dans une dernière étude déclenchée par l'apparition de nouveaux résultats expérimentaux, nous nous sommes intéressés à la modulation des DST par les lipides et nous avons étudié l'impact de la modification de la nature de leurs têtes polaires sur l'activation du DST. Cette étude est basée sur la simulation du Kv1.2 dans une variété de bicouches asymétriques contenant de la sphyngomyéline, du céramide-1-phosphate ou du céramide dans la couche supérieure, qui mime des membrane d'oocytes naturelles ou modifiées. Nous montrons en particulier que, en dépit du rôle essentiel des interactions entre lipides et résidus basiques de S4, la charge de « gating » n'est pas affectée par la modification des têtes polaires des lipides. Ces résultats suggèrent que la modification de la tête polaire lipidique affecte surtout la cinétique de transition d'une conformation du DST à l'autre – quand bien même des simulations supplémentaires (à l'échelle de la centaine de nanosecondes) n'ont pu démontrer que de telles transitions pouvaient être accélérées par l'altération de la tête polaire des lipides. ***Les résultats des ces trois études sont présentés au chapitre 4.***

Enfin, souhaitant étendre ces résultats à d'autres membres de la famille des canaux ioniques voltage-dépendants qui sont impliqués dans des maladies génétiques, nous avons entrepris une étude de plusieurs membres de la famille de Kv7. Ainsi, nous avons construit des modèles moléculaires du domaine sensible à la tension des Kv7.1, Kv7.2 et Kv7.4 dans leur conformation ouverte et fermée qui sont en accord avec ceux du Kv1.2. Nous avons débuté l'étude de leurs propriétés électriques (*e.g.* de leur charge de « gating ») et de l'effet de mutations de résidus basiques de S4 qui sont impliqués dans le syndrome du QT long, dans des attaques bénignes familiales néonatales ou encore dans une forme de surdité progressive. La comparaison de nos résultats avec les données expérimentales est aujourd'hui en cours. ***Les résultats préliminaires de cette étude sont rapportées au chapitre 5.***

Excitable cells were discovered in the early 1950s and were recognized to be crucial for the function of superior organisms thanks to the introduction of electrophysiology techniques. Indeed, these cells are responsible for the transmission of the nervous influx and when an electrical voltage pulse is applied to them, they respond by giving rise to a current flow through their membrane. On a molecular level, this is manifested by the transport of ions through the latter. Twenty years later, it was discovered that transmembrane proteins were involved in the voltage dependent transport of ions across the membranes of excitable cells. These macromolecules, called *voltage-gated ion channels (VGCs),* are essentially pores that can be found in open or closed states depending on the polarization of the membrane. Since then, it was shown that these channels are implicated in a wide variety of biological functions, as they are found in all excitable cells, *i.e.* in the heart, in the nervous system (central and peripheral) and in many other organs such as the inner ear, liver or stomach... As such, these proteins are sensitive to a large number of *modulating factors*, *e.g.* action of inactivation peptides, drugs or anesthetics, alteration of the lipids embedding them... Similarly, *genetic mutations* of these channels can have dramatic effects and give rise to a large number of familial genetic diseases (so-called *channelopathies*) like long QT heart syndrome, several neurological diseases including epilepsy, seizures or periodic paralyzes of different kinds, deafness...

With the advent of voltage clamp techniques, electrophysiology experiments allowed the discovery in the 70s of a characteristic feature of VGCs: when going from closed to open state, they produce tiny, transient currents that were named *gating currents*. The integral of these currents is called the *gating charge* and is a fundamental property of the channels. In the early 80s, when the first VGCs were sequenced, it was found that they have a common structure with 4 units each containing six transmembrane helices. The fold and assembly of the two helices at the N-terminus of each unit (S5 and S6) form the pore, the region that is responsible for the transport of ions from one side of the membrane to the other. The other four (S1-S4) constitute an auxiliary domain that is responsible for sensing the TM voltage change: the *voltage sensor domain (VSD)*. Among them, the fourth transmembrane segment (*S4*) contain a large number *positively charged residues* (4 to 7, mostly arginines) that sense and respond to the TM voltage changes (*i.e.* the local electric field). These residues are the molecular level components responsible for the gating currents: indeed, following activation, *i.e.* when VGCs go from the resting (closed) state to the activated (open) one, the total gating charge (~ 12 to 14 elementary charges) is transported across the membrane mostly by the S4 basic residues.

The electrical charge movement within the VSD, *i.e.* the gating charge, is a fundamental property that not only determines the voltage dependency of the channel activation, but also constraints the physical models for charge translocation in the VSD and therefore its operation. To describe the latter, three main models have been proposed. In the first one, called the *helical screw model*, S4 moves independently from the rest of the voltage sensor domain in a screw-like motion, translating by ~ 10 to 20 Å while rotating about its own axis

by 180°. This model also involves a characteristic feature: the reorganization of salt bridges within the VSD. Indeed, to stabilize S4 in a transmembrane (TM) orientation despite its high charge, the arginines are involved in salt bridges with negatively charged residues of the other (S1-S3) transmembrane segments. Based on mutagenesis studies, this model implies that several salt bridges are broken while others are formed when S4 moves in response to the electric field induced by the TM voltage. The second model involves instead a large reorganization of the electric field in the vicinity of S4 with only a small overall displacement of S4. This model, supported mostly by fluorescence measurements is called the *transporter model.* Finally, the *paddle model*, that has since then been abandoned, involves a large movement of the "S3-S4 paddle" from a position parallel to the membrane surface in the resting state to a vertical position in the activated one. A large number of studies was performed to reconcile these models and a rather unified picture has emerged in the last couple of years: the TM movement of S4 is likely of intermediate magnitude and the salt bridge rearrangement within the VSD is important for proper channel function. The event that has probably triggered the biggest advance in the comprehension of the molecular mechanism of VCGs is the determination of the high resolution crystal structure of the first mammalian potassium channel: the *Kv1.2*. In this structure, the pore was found to be open and the VSD in an activated state, *i.e.* with S4 in an 'up' state. This structure, overall consistent with a large number of previous electrophysiology measurements, has revealed many molecular details such as the salt bridge network involved in the activated state of the VSD, the interaction of lipid head groups with the top positive residues of S4, the kink in the S6 helix that is important for the closure of the channel, a possible mechanism for fast inactivation and others... ***The detailed bibliographical context of this work is introduced in chapter 2.***

Despite the outstanding progress achieved over the last few decades in understanding the molecular level details of VGC function thanks to exquisite quantitative electrophysiology experiments and the breakthrough achievements, several key questions remain to be answered, among which:

- In Kv1.2, what is the *extent of the movement* of S4 basic residues and how does the *electrical driving force* act upon them ? What do the *intermediate* and *resting states* look like ?
- What is the structural basis of the *coupling* of the VSD activation/deactivation to pore opening/closing ?
- How can one explain the *genetic diseases* following the *mutation* of S4 positively charged residues on a molecular level ?
- How do lipids *modulate* the activation/deactivation of the VSD and what happens when altering the *lipid headgroups* close to the channel?

The main aim of this work is to specifically address these questions using state of-the-art classical *molecular dynamics (MD) simulations*. This class of methods relies on the integration of the classical equations of motion, provided a good description of all the

interactions between pairs of particles of the system is available. Its main advantage is that it can provide information on a molecular level that most experiments cannot reach. Furthermore, and as will be demonstrated in this work, the information from MD simulations (position, charges, velocities of atoms...) enables to evaluate quantities that can be measured experimentally, *e.g.* the gating charge, in a way that complies with electrophysiology measurements. We have indeed devised a method (protocol) allowing to apply a TM potential, in a way that complies with voltage clamp experiments. We have also developed and compared schemes for measuring *in-silico* the gating charge… ***The latter, along with the protocols and MD simulations methods will be described in details in chapter 3.***

The main thrust of our work consisted in modeling the entire Kv1.2 channel, embedded in a mimic of lipid environment (a phosphatidyl-choline lipid bilayer), solvated in KCl salt solution. The results are based on the analyzes of a 2.2 μs large scale simulation of the system submitted to a deactivating TM potential of ~ -600 mV and of subsequent biased (steered) MD simulations conducted to generate the last steps of the deactivation. We uncovered hence 5 states of the channels VSDs along the deactivation, conformation of which α, -β, γ and δ- and ε correspond respectively to the open, intermediate and closed states of the channel. The simulations were used to describe in detail the motion of the S4 helices and their charges, the interactions between the VSDs and the surrounding lipids, the electrical properties of the VSD among which the shape of the local electric field within the VSD or the contributions of molecular components involved in the gating charge and finally coupling of VSD operation to Kv1.2 pore gating. Overall, between the different models proposed, our results advocate the *sliding helix* model.

Using the configurations of Kv1.2 determined in the first part of this work, we then studied the molecular level effect of selected mutations of S4 positively charged residues involved in genetic diseases. Some well-defined mutations are herein shown to induce a perturbation of the VSD structure and lead to the appearance of state-dependent leak currents through this domain. These results hence unveil the key elementary molecular processes involved in these "omega" currents detected by electrophysiology. Based on an extensive study of most mutations performed both for the open and closed conformations of the Kv1.2, we propose a model of the mechanism involved, indicating which type of residues may lead to the appearance of omega currents, and under which condition these leaks may be critical.

In a third study triggered by new experimental evidence, we focused on the modulation of VSD function by lipids, and studied the impact associated to modification of the nature of their polar head groups on the VSD activation. The study is based on simulations of the Kv1.2 channel in a variety of assymetric lipid bilayer containing sphygomyelin, ceramide-1-phosphate or ceramide in the upper leaflet, that mimic natural or modified oocyte cell membranes. We show in particular that, despite the key role the interactions between the lipids and S4 basic residues play, the gating charge is not highly affected by the change in the lipids characteristics. These results suggest that the change in the lipid head groups affects mostly the kinetics of transition from one VSD conformation to the other - even though additional simulations (in the 100 ns range) could not directly show that such transitions could be sped

up upon modifications of the upper lipid head groups. ***The results concerning the three above-mentioned studies are presented in chapter 4.***

Finally, wishing to extend all these findings to other members of the VGC family which are implicated in genetic diseases, we have undertaken the study of several members of the Kv7 subfamily. In this scope, we have built molecular models of the transmembrane domain of Kv7.1, Kv7.2 and Kv7.4 channels in their open and closed conformations that are consistent with those of the Kv1.2. We have initiated a study of their electrical properties (*e.g.* gating charge) and of the effect of VSD basic residue mutations that are implicated in long QT syndrome, in benign familial neonatal seizures or in slowly progressive deafness. Comparison of our findings with experimental data are now in progress. ***The preliminary results of this investigation are presented in chapter 5.***

2- OBJECTS

"To know an object is to lead it
through a context which the
world provides"
-William James

Ce chapitre s'attache à présenter au lecteur les différents objets qui ont été étudiés durant ce travail de thèse. Afin d'amener le lecteur à bien comprendre les enjeux et les problématiques liées aux canaux potassiques voltage-dépendants, nous décrivons les différents objets intervenant dans ces questions, en partant d'une description grossière (échelle micrométrique) pour aller vers une description plus fine (échelle nanométrique). Ainsi, nous présentons d'abord les membrane biologiques, leur composants et leurs propriétés physiques, puis plus particulièrement les membranes des cellules excitables (avec leurs propriétés électriques) et enfin les canaux ioniques sensibles au voltage, mettant l'accent sur leur structure, leur fonction et les moyens pour moduler leur opération.

La membrane plasmique constitue l'enveloppe des cellules biologiques. Elle est constituée d'une bicouche continue de lipides dans laquelle sont insérées des protéines. Sa composition précise varie en fonction du type de cellule. La membrane joue de nombreux rôles dans le métabolisme de la cellule : elle en définit les limites, elle sert à la reconnaissance d'autres cellules, ou encore de molécules venant du milieu extracellulaire, et également au transport sélectif de molécules vers l'intérieur de la cellule ou depuis le cytoplasme vers le milieu externe. Puisque la membrane est composée surtout de lipides, le transport de molécules polaires, chargées ou volumineuses y est souvent restreint. Même si la thermodynamique qui guide le transport est favorable au transfert d'une espèce d'un côté de la membrane vers l'autre, le cœur lipidique de la membrane peut constituer une barrière. Dans ce cas, des protéines transmembranaires peuvent faciliter le transport. Dans le cas du transport sélectif d'ions, ces protéines sont alors appelées canaux ioniques. Lorsque leur ouverture dépend de l'état de polarisation de la membrane, *i.e.* du potentiel transmembranaire, ils sont alors appelés canaux ioniques voltage-dépendants et ont une rôle particulièrement important dans le fonctionnement des cellules excitables.

Les membranes des cellules excitables, comme toutes les membranes par ailleurs, ont à la fois les propriétés électriques d'une résistance et d'un capaciteur. Nous décrivons ici plus particulièrement les résultats obtenus pour l'axone géant du calmar, la cellule excitable utilisée historiquement en électrophysiologie. Lorsqu'une impulsion de voltage est appliquée à ces axones, ils répondent en générant des courants électriques. Ces courants sont très spécifiques, et viennent de la conduction d'ions potassium et d'ions sodium selon un schéma précis. Le courant de sodium et rapide et dirigé depuis l'extérieur de la cellule vers le cytoplasme et s'inactive rapidement, tandis que le courant de potassium est plus lent et dirigé vers l'extérieur de la cellule indiquant des voies de transports différentes pour chacun de ces ions. D'un point de vue moléculaire, ce transport est effectué au travers de canaux ioniques sensibles au potentiel (voltage-dépendants). Ces canaux constituent une grande famille qui ont des propriétés structurales et fonctionnelle communes : ils sont tétramériques, leur assemblage forme un pore central qui est lui même composé d'un filtre de sélectivité, qui permet de sélectionner un type d'ion et d'une barrière qui peut s'ouvrir et se fermer, et de quatre domaines auxiliaires qui confèrent aux canaux leur sensibilité au voltage (les domaines sensibles à la tension). C'est l'activation et la désactivation de ces domaines qui va agir sur

l'ouverture/fermeture du pore. D'un point de vue fonctionnel, ces canaux s'ouvrent de manière stochastique et ce n'est que lorsque l'on observe un ensemble de canaux et que l'on regarde la moyenne de leur comportements que l'on trouve un schéma de fonctionnement macroscopique.

Les canaux ioniques voltage-dépendants sélectifs au potassium (canaux Kv) constituent la famille la plus diverse des canaux sensibles au potentiel. Leur séquençage a révélé que chaque monomère a six hélices transmembranaires. S1-S4 forment les domaines sensible à le tension et S5-S6 le pore. S4 porte un grand nombre de résidus chargés positivement (surtout des arginines) qui constituent le détecteur de changement du potentiel. En plus du courant ionique, en réponse à une impulsion de voltage, des courants transitoires peuvent être mesurés, de magnitude ~200 fois inférieur au courant ionique, et qui proviennent du réarrangement des résidus chargés de la protéine. Ces courant (appelés « courant de gating ») surviennent avant l'ouverture du canal et donc avant l'arrivée du courant ionique. De nombreux modèles ont été proposés pour expliquer ces propriétés. Tous impliquent le mouvement vertical de S4, perpendiculairement au plan de la membrane, avec l'exposition de résidus spécifiques en fonction de l'état de polarisation de la membrane. Pour ce qui est des deux modèles principaux, S4 est transférée soit d'une vingtaine d'Å (modèle *en vis*) soit de quelques Å seulement (modèle *du transporteur*). Tandis que le débat n'est pas encore clos, d'autres caractéristiques de l'activation continuent à être révélées, parmi lesquelles le rôle des lipides adjacents au canal, la présence d'un centre de transfert de charge au sein du domaine sensible à la tension et la possibilité pour l'hélice S4 de passer transitoirement en conformation 3_{10}. Par ailleurs, avec le rôle prépondérant que jouent les résidus chargés de S4, il est facile d'imaginer que la mutation d'un seul de ces résidus puisse être critique pour la fonction du canal, comme en témoignent le grand nombre de maladies génétiques héréditaires dues à ces mutations. Ainsi, un phénomène particulier a été révélé : la mutation de résidus spécifiques de S4 donne lieu à l'apparition de courants de fuite qui dépendent de la conformation du canal et qui pourraient être l'origine moléculaire de maladies génétiques neuronales, du cœur ou des muscles squelettiques.

Nous concluons ce chapitre en présentant plus particulièrement les canaux potassiques voltage-dépendants d'intérêt dans cette thèse : le Kv1.2, seul canal dont la structure cristallographique à haute résolution a été révélée et qui nous sert donc de prototype pour l'ensemble de cette grande famille. Dans cette structure, le pore est en conformation ouverte et le domaine sensible a la tension en conformation activée, laissant en suspens la question du mécanisme de la désactivation. Nous proposons également un résumé des informations obtenues jusqu'ici grâce à la dynamique moléculaire. Nous présentons finalement la famille des Kv7, et plus particulièrement les Kv7.1, le Kv7.2 et le Kv7.4. Ceux-ci sont particulièrement intéressants car ils sont impliqués dans de nombreuses maladies génétiques et constituent ainsi des cibles de choix en pharmacologie.

This chapter aims at presenting the objects that have been investigated during this three years work: voltage-gated potassium (Kv) channels. In order to bring the reader to understand the fascinating properties of these proteins, and the questions that are still under active debate in the scientific community, we start by introducing the matrix that embeds these channels: the plasma membrane, by reviewing its composition and its function. In a second part, we describe excitable cells using a historical approach. We try to show what was known before the discovery of voltage gated channels (VGCs) and how scientists discovered these macromolecules before presenting the properties of the members of this large family. This all brings us to introduce in a third part Kv channels, their structural and functional features, their means of modulation and finally, most specifically the specific channels we studied here: Kv1.2 and a few members of the Kv7 family.

1 The biological cell membrane

Every complex living organism is divided into functional units called cells. The biological membrane is an enclosing membrane that acts as a barrier, within or around these cells. The particular membrane that delineates the cell is called the plasma membrane but other membranes are also found that separate internal organelles, such as mitochondria, the nucleus or the endoplasmic reticulum from the rest of the cell (Fig. 2.1).

Their major role is to isolate the interior of the cell (called the cytoplasm) or of the organelle. The plasma membrane also controls the transport of solutes in and out of the cell in order to ensure proper function and metabolism. To do so, the plasma membrane has a specific property: it is selectively permeable to molecules, depending on their chemical and/or physical properties, rationalizing its essential role in the cell's life (Lodish et al. 2000) (Alberts et al. 2002) (Karp 2009). In this part, we start by describing the structure of the plasma membrane and its different components. We then focus on the role of the membrane by describing its various functions.

1.1 Structure and Composition

The overall membrane structure can be viewed as a continuous lipid bilayer, whose main role is to isolate the cell's cytoplasm from the surroundings. Within this matrix, several types of molecules (especially proteins) are embedded, or anchored and serve various mechanical or chemical purposes. According to the 1972 fluid mosaic model by Singer and Nicolson (Singer & Nicolson 1972), the membrane may be envisioned as a 2D hydrophobic matrix in which free lateral diffusion of lipids and proteins occurs. It was later shown that membranes are in fact heterogeneous and composed by different micro-domains of diverse functions and

structures (Engelman 2005). For example, lipid rafts, that play a role in many cellular functions, such as membrane fusion, signal transduction..., are usually rich in cholesterol and sphyngolipids, resulting in thick regions where the lipid hydrophobic tails are more ordered (Brown & London 2000) (Edidin 2003).

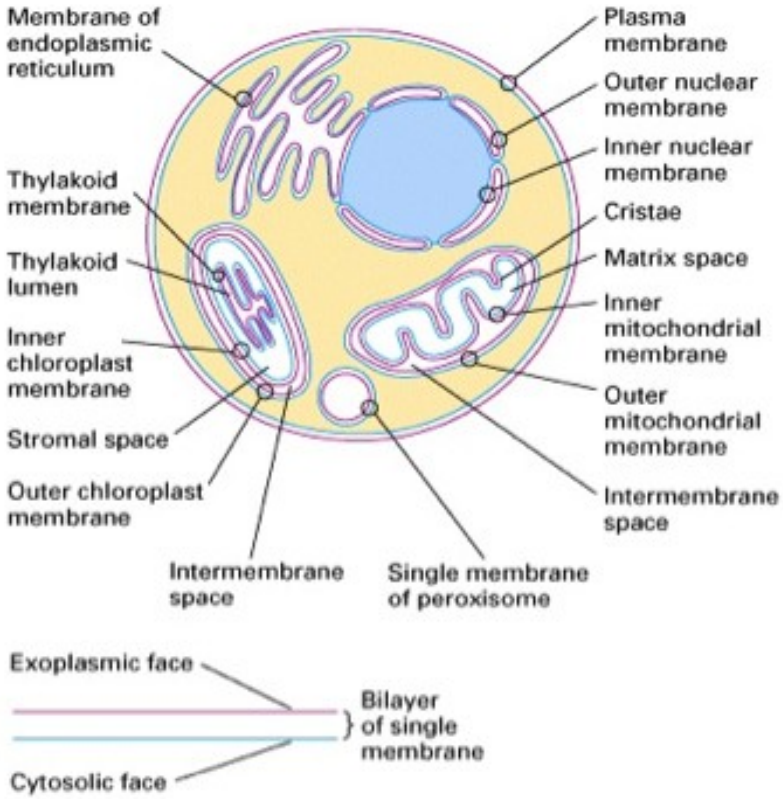

Figure 2.1: Scheme of the different membranes of the cell. The internal medium (cytoplasm) is represented as light yellow and the membranes are represented as cyan and pink lines.

1.1.1 Lipids

The main components of plasma membranes of animal cells are lipids. Four major phospholipids (phosphatidylcholine, phosphatidylethanolamine, phosphatidylserine, and sphingomyelin) account together for more than half of the lipids in most membranes (Dowhan 1997). The common property of these phospholipid molecules is that they are constituted by two main parts: 1- a hydrophilic head-group (negatively charged in the case of phosphatidylserine or polar and zwitterionic in the case of phosphatidylcholine, phosphatidylethanolamine and sphyngomyelin), and 2- usually two hydrophobic tails, consisting of long, fatty acid hydrocarbon chains (either saturated or unsaturated depending on the lipid). Due to their amphiphilic nature, in the presence of water, lipids have a tendency to self-assemble to isolate their hydrophobic tails from the solvent (Fig 2.2). Depending on the lipid/water ratio, the temperature and other factors, several assemblies can be formed to

minimize the contact between hydrocarbon tails and water molecules: *e.g.* micelles, bilayers, hexagonal or cubic phases.. The one adopted in the plasma membrane is the bilayer: the polar head-groups face the solution, enabling the insulation of the hydrophobic tails from the water molecules. In the case of a cell membrane, they thereby form a continuous lipid bilayer that completely isolates the intracellular medium from the extracellular one.

Depending on the specific cell, the different phospholipids mentioned above may be asymmetrically distributed between the two leaflets of the membrane bilayer. The outer leaflet of the plasma membrane consists for instance mainly of phosphatidylcholine and sphingomyelin, whereas phosphatidylethanolamine and phosphatidylserine are the predominant phospholipids of the inner leaflet. In addition to those, the plasma membrane also contains glycolipids and cholesterol. The glycolipids, in which the polar head group contains carbohydrates are found exclusively in the outer leaflet of the plasma membrane, with their carbohydrate portions exposed on the cell surface. Cholesterol, on the other hand, which is a major membrane constituent of animal cells, can be found in both leaflets of the bilayer and participates mainly in the control of mechanical and elastic properties of the membrane (Wolfe 1993) (Alberts et al. 2002).

Due to the presence of the hydrophobic core, membranes mostly constitute a barrier for polar and charged species while allowing for the diffusion of hydrophobic species. This hydrophobicity ensures that the transport of the polar and charged molecules is well controlled by the cell since it necessitates the mediation by membrane proteins.

To assume a lot of the biological functions necessary for the cell machinery, *e.g.* the passive and active transport of matter, the capture and storage of energy, the control of the ionic balance or the cellular recognition and signaling, cells therefore require the assistance of membrane proteins.

1.1.2 Membrane proteins

As a general definition, a membrane protein is a polypeptide chain that is attached to, or associated to the membrane of a cell or an organelle (White 1994). Depending on their location, and on their interaction with the membrane, they can be divided into three major categories.

Integral proteins are in permanent interaction with the membrane and can in turn be divided into transmembrane (TM) proteins, which entirely span the membrane (and which we will focus on in the rest of this chapter) and monotopic proteins that are attached to the membrane only from one side

Peripheral proteins are proteins external to the membrane, that are transiently bound to the latter by non covalent interactions

Lipid-anchored proteins are on the other hand permanently (because covalently) bound to the lipids of the membrane.

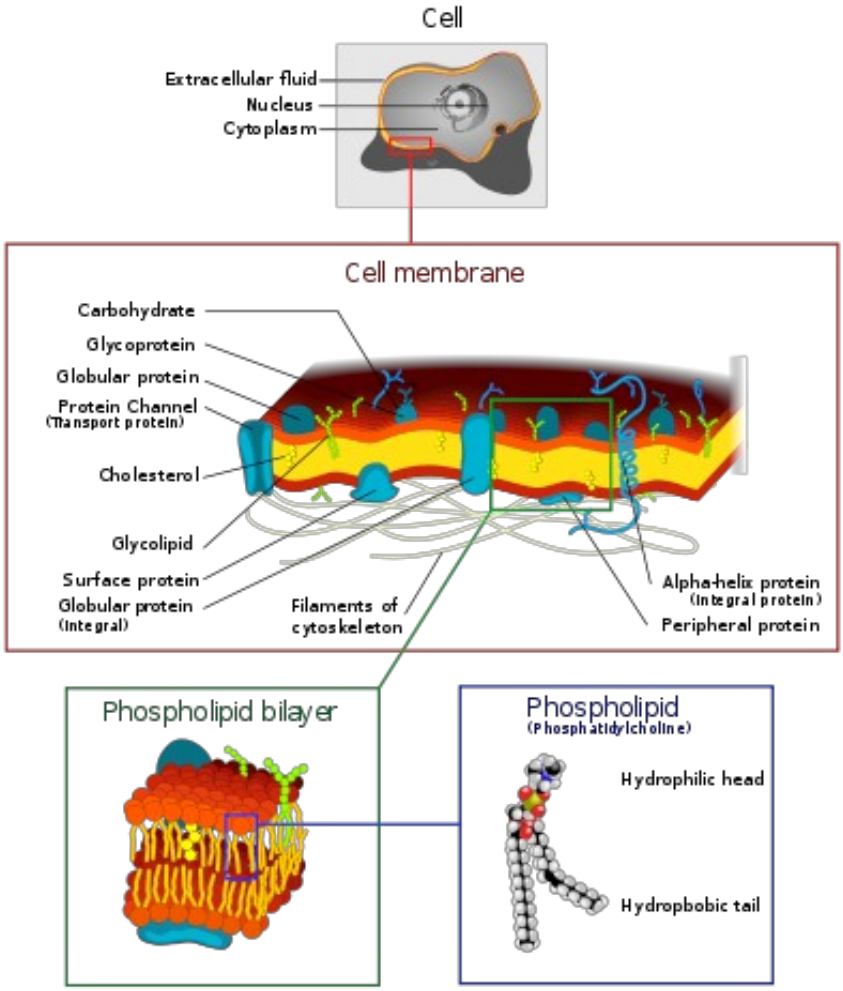

Figure 2.2: Illustration of the structure of a biological membrane. The principal component is the phospholipid molecule, composed of a hydrophilic head and two hydrophobic tails, that self-assembles into a bilayer. This bilayer constitute the matrix to embed other types of molecules. This continuous bilayer forms the outer shell of the cell and isolates the cytoplasm from the extra-cellular medium.

All these proteins carry out a wide range of functions, such as a role in the structure (achieved through the interaction of structural proteins with microfilaments of the cytoskeleton), in cellular recognition (achieved through cell adhesion proteins), in the production of a variety of chemicals essential to cell function (through membrane enzymes), in the connection of cell's internal and external solutions (through membrane receptor proteins) and finally in the transport of solutes across the membrane (achieved by carrier proteins and channel proteins).

As all proteins, membrane proteins are made of a sequence of amino acids and fold into 3-dimensional structures that depend on the properties of the various amino-acids, and on the interaction with the environment. Depending on their secondary structure, transmembrane proteins can be classified into two main categories: alpha helical proteins and beta barrels (Karp 2009). Alpha helical proteins, which constitute the larger proportion are constituted by one or more transmembrane alpha-helices. In the case of multiple segments, these are connected together by hydrophilic loops that protrude on both sides of the membrane. Their tertiary structure is then most of the time a bundle of helices. Beta barrels are much scarcer (mostly found in bacteria or internal organelles) and are made of interconnected beta sheets that define a barrel shape (von Heijne 1999).

1.2 Role and function

Due to its composition, the plasma membrane carries out a large number of functions that are essential to the cell's life. Not only it has a structural role, it is also involved in a large number of processes vital to the life of the organism such as cell adhesion, cell signaling or selective transport of solutes into and out of the cell (Lodish et al. 2000).

1.2.1 Structural role

The most obvious role of the plasma membrane is to delineate the cell and is in that sense important for the cell's structure. Furthermore, the structural proteins embedded in the lipid bilayer play a crucial role as they interact with the structure that provides a frame and a shape to the cell, the cytoskeleton.

1.2.2 Cell adhesion

Cellular adhesion is the process that involves the binding of the cell to the extracellular matrix or to other cells. The membrane proteins involved in such processes, called cell adhesion molecules belong to four families: immunoglobulins, selectins, integrins or cadherins. They are all constituted by a transmembrane helical domain that enables the anchoring of the protein, an intracellular domain that interacts with the cytoskelton and an extracellular domain that is in charge of the molecular recognition of other cells or of the extracellular matrix.

1.2.3 Cell signaling

Living organisms constantly receive and interpret signals from their environment, that come in the form of light, heat, water, odors, touch, or sound, or of signals from other cells, including signals for cell division and differentiation. These messages often reach the cell through its membrane in the form of chemicals, such as hormones or cytokines. A large number of membrane proteins is therefore devoted to the recognition of such molecules and to the response to such stimuli. Typical responses of cells to external signals include activation of G-proteins, production of second messengers, activation of protein kinases, and the release of calcium ions from membranes. These mechanisms are particularly important because errors while processing cellular information can be responsible for diseases such as cancer (Martin 2003).

1.2.4 Selective transport

The last crucial role of the plasma membrane, which is also the one that is of particular interest to this work, is the selective transport of solutes through the membrane. This transmembrane transport is driven by the thermodynamic equilibrium of the whole system. However, except for gases and small apolar molecules that will be able to cross the hydrophobic barrier directly through the lipids, diffusion of other species across the membrane is not always possible due to its hydrophobic nature. For polar, charged and larger molecules, for instance, the transport will have to be facilitated through transmembrane proteins.

1.2.4.1 Thermodynamical principles

As any chemical process, transport across the cell membrane is guided by thermodynamics: the system always tends to minimize its free energy ΔG (Mathews et al. 1999). As in any type of diffusion, thermal motion is involved, but it operates in a random fashion with respect to direction and as such, does not represent a driving force for the transport across the membrane.

In the presence of a concentration difference between both sides of the membrane, the movement of species a and b is guided by the chemical potential of the solutions with:

$$\Delta G = \mu_b - \mu_a = RT \ln \frac{C_b}{C_a} \quad [2.1]$$

where μ_ι is their respective chemical potential of the solutions and C_ι their respective concentration. The free energy is minimized when the concentrations are equal on both sides of the membrane, rationalizing the transport of solutes along their concentration gradient.

In addition, charged molecules such as ions experience an additional driving force when subjected to electric fields. The combination of both chemical and electrostatic potentials, called electrochemical potential, completely describes the driving force for an ion's

translocation, that causes its flow across a membrane (Hille 2001). This potential may be expressed as:

$$\Delta G = RT \ln \frac{C_b}{C_a} + ZF \Delta V \quad [2.2]$$

where Z is the charge of the solute, F Faraday's constant and ΔV the transmembrane potential. Equilibrium is reached when the electrostatic potential (field strength) is uniform. In this case, ions will be transported in the absence of an ion gradient (no chemical potential) or even against their concentration gradient (uphill movement).

The last case is that of active transport, where an external free energy ΔG^r is added to the chemical or electrochemical free energy.

$$\Delta G = RT \ln \frac{C_b}{C_a} + \Delta G^r \quad [2.3]$$

ΔG^r may originate from a favorable thermodynamic process, *e.g.* the hydrolysis of ATP or the transport of another solute along its electrochemical gradient. In such a case, compounds can be transported against their chemical or even electrical free energy.

1.2.4.2 Transporters, channels and pumps

One distinguishes three types of membrane proteins, depending on their transport properties: for polar and charged molecules that move along their electrochemical gradient, diffusion proceeds through transmembrane proteins called *channels* rather than through the hydrophobic core of the membrane. Such a transport is known as facilitated diffusion.

Active transport concerns transport against an electrochemical potential. The proteins involved are then called *transporters* and translocate various ions and molecules along with other solutes. They are able to displace certain solutes against their gradient while transporting others along their gradient (either in the same or in opposite directions).

Pumps are membrane proteins that also transport chemicals against their gradients, using the energy they get from the hydrolysis of compounds such as ATP. One of the most important pumps in animal cells is the sodium potassium pump because it helps maintain the resting potential in excitable cells by pumping 3 Na^+ ions out of the cell, while pumping 2 K^+ ions in (see paragraph 2 of this chapter).

1.2.4.3 Ion channels are gated by multiple stimuli

Ion flux is particularly important for the function of cells as it is the vector of electric current in and between cells. The proteins that mediate passive transport of ions are called ion channels. The human genome has over 200 genes encoding ion channels, illustrative of their variety and specificity. Quite amazingly, such proteins are able to reach a very high selectivity

to a type of ions as well as a very high conductance for a single protein. Moreover, most of them bear an ability to open and close depending on their environmental conditions, a conformational change known as gating (Hille 2001).

Ion channels can be categorized in terms of two factors: their selectivity to ions (defining potassium, sodium, calcium and chloride channels) and the stimuli to which they respond (defining ligand gated, voltage gated, mechanosensitive, temperature gated, light gated, pH gated…). We choose here to list briefly the various ion channels families based on the stimuli to which they are sensitive.

Ligand-gated ion channels, also called ionotropic receptors, are gated by the binding of specific ligands (more precisely second messenger molecules). Examples of such channels include the cation-permeable nicotinic acetylcholine receptor (NaChR), the glutamate-gated receptor, the ATP-gated P2X receptors, GABA-A receptors, or the 5HT3 serotonin receptor. All these channels consist at least of an extracellular domain that binds the ligand and a TM domain that constitutes the pore region of the channel. The pore can be selective to either one type of ion (sodium in the NaChR, chloride in the GABA-A receptors) or to cations in general (as is the case for the glutamate-gated receptor or the ATP-gated P2X receptors). Among this family, the calcium-activated potassium selective channels are gated by intracellular Ca^{2+}. Their members are divided into three sub-categories: BK channels, IK channels and SK channels based on their conductance (respectively big, intermediate, and small conductance).

Mechanosensitive channels (e.g. the MscL channel) open in response to mechanic stimuli, *e.g.* stretching of the membrane, pressure, displacement… They are involved in the senses of touch, hearing and balance, as well as in cardiovascular regulation and osmotic homeostasis.

Cyclic nucleotide gated (CNG) channels are characterized by activation following binding of intracellular cAMP or cGMP with specificity varying by member. These channels are primarily permeable to monovalent cations such as K^+ and Na^+. Hyperpolarization-activated cyclic nucleotide gated channels (HCN) are also opened by hyperpolarization of the membrane (see below for a definition). This family of channels is involved in the olfactory, the visual and other systems.

The large family of *voltage-gated* ion channels has the general property of being gated by changes in the TM potential. They are divided into three large groups, voltage gated sodium channels (Nav), voltage gated potassium channels (Kv) and voltage gated calcium channels (Cav). Nav channels are largely responsible for action potential creation and propagation. They open and inactivate very rapidly, allowing the influx of sodium down its concentration gradient. Like calcium, the reversal potential of sodium is very positive and sodium current is always inward. Kv channels play a major role in the repolarization of the cell membrane after initiation of the action potential. They are activated by membrane depolarization (see paragraph 2 for the definition of membrane polarization states), upon which these channels open, allowing the efflux of potassium from the cell, down its electrochemical gradient. Ca_v channels play an important role in the function of muscles and neurons since their opening results in the influx of calcium into the cell, which in turn activates a number of metabolic

pathways. All the above are very often located in excitable cells, and the next part will review most particularly their role in these cells.

To be complete, one should note that various other stimuli can trigger the gating of ion channels, including light (rhodopsins), temperature (members of the Transient Receptor Potential (TRP) ion channel superfamily), pH and others… Also, one should mention here that there are types of channels that are gated by multiple stimuli. For instance, the HCN channels mentioned above are gated both by membrane hyperpolarization and by binding of cyclic nucleotides. Another example is that of voltage-gated proton channels that also open with depolarization, but in a strongly pH-sensitive manner.

2 The excitable cell

Excitable cells constitute a large category of cells, including nerve, heart, muscle or else sensory cells. They encompass all the cells that are able to respond to an electrical stimulus and to propagate tiny electrical currents (action potentials (AP)) along the cell. This involves changing the membrane's electrical state due to the in- and out-flows of ions through ion channels. In this section, we start by describing the electrical properties of the membranes. We then proceed by describing the classical biophysics of the squid giant axon, the first excitable cell to ever be investigated. The last part of the section will be dedicated to the thorough description of the ion channels of excitable cells.

2.1 Electrical properties of the membrane

Because of its chemical composition, the biological membrane has well-defined electrical properties that play an important role in the transport of ions. A lot of what we know on excitable cells and the way they exchange ions comes from electrical measurements. It is therefore useful to remind here the simple, yet efficient electrical models that can be used to describe the plasma membrane.

2.1.2 The membrane as a resistor

Because membranes do not contain free ions themselves, and because they mostly prevent the free exchange of ions, the current (I) across them is very low, even when applying a relatively high voltage difference (U). Following from Ohm's law (R = U/I), their resistance R is very high and their conductance, g = 1/R is very low.

Artificial membranes made of pure phospholipid bilayers have a conductance per unit area (g_A) of $\sim 10^{-13}\ \Omega^{-1}m^{-2}$ (Goldup et al. 1970) The conductance of biological membranes on the other hand, is higher by several orders of magnitude, which is rationalized by the presence of

membrane proteins permeable to charged species (ion channels and other transporters/pumps) (Cole 1968).

2.1.3 The membrane as a capacitor

The cell can be envisioned as an inner solution (the cytoplasm) separated from the external solution by an extremely thin insulator. Such a narrow gap between two conductors defines an electrical capacitor of capacitance C=Q/V, with Q the charge that are separated by the insulator and V the potential difference arising therefrom. For model bilayers, it amounts to ~0.8 ∓F/cm2 (Almers 1978), and interestingly, it is very close for real cell membranes (1.0 ∓F/cm^2) (Hille 2001) (Cole 1968).

2.1.4 Equivalent electrical circuit

Following from its intrinsic properties, the membrane can be envisioned as a capacitor and a resistor at the same time. Therefore, it may be represented by an electrical equivalent circuit consisting of a capacitor C in parallel with a resistor R (Fig. 2.3).

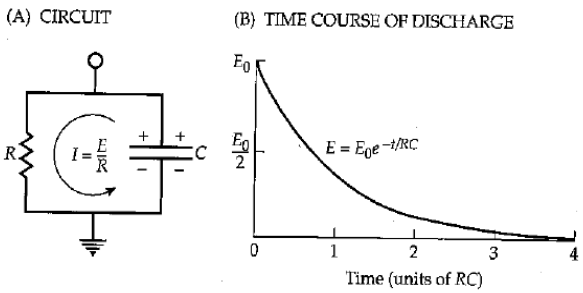

Figure 2.3: RC circuit and corresponding discharge. The circuit is constituted by a resistor and a capacitor connected in parallel. At time t=0, the capacitor is charged to E_0 and begins to discharge through the resistor. From (Hille 2001).

This resistance-capacitance (RC) circuit has very simple electrical properties. Solving the differential equation that follows from applying Ohm's law to this model

$$\frac{d\Delta V}{dt} = \frac{I_C}{C} = -\frac{\Delta V}{RC} \quad [2.4]$$

enables evaluating the time dependance of the transmembrane voltage E along the time *t* as

$$\Delta V(t) = \Delta V(0) e^{\frac{-t}{RC}} = \Delta V(0) e^{\frac{-t}{\tau}} \quad [2.5]$$

Starting from any initial state, the transmembrane potential ΔV decays exponentially, with a time constant of τ = RC, where C is the capacitance of the membrane patch, and R is the net resistance.

In general, as we will see in the following paragraphs, various membrane models of excitable cells are made up of such pieces and the most complex models can be easily derived

from these simple biophysical models.

2.2 Electrophysiology of the squid giant axon

Excitable cells respond when they are excited by an electrical impulse. This paragraph aims at describing this behavior from a kinetic point of view using simple thermodynamical laws and without having to refer to the molecular components of the membrane, very much as was done by Hodgkin and Huxley (Hodgkin & Huxley 1952d), and others in the first half of the 20th century. One will see how it is possible using quite simple experimental techniques and classical biophysical notions to understand how excitable cells respond to electrical impulses.

Early electrophysiology experiments involved measuring the membrane potential with glass micropipette electrode filled with a salt solution. Due to the size of the first electrodes, it was important to find an experimental setup that made it possible to measure voltages. As such, the first neurons in which such measurements were made possible are squid giant axons (Young 1936). We use this system to introduce the concepts useful to study excitable cells. Later, in the last part of this chapter, we will try to link these concepts together with the function of the molecular components of excitable membranes.

2.2.1 Resting potential and other membrane polarization states

The reversal potential, also called the Nernst potential, is the transmembrane potential at which there is no net ion flux through the membrane. This value is determined by the laws of thermodynamics cited in the previous section and can be derived directly from the application of the Nernst equation (a special case of the Boltzmann equation):

$$E_{M^{n+}} = \frac{RT}{nF} \ln \frac{[M]_o}{[M]_i} \quad [2.6]$$

where M is an ion with a charge of n^+, R the gas constant, F the Faraday constant and the subscripts o and i refer to the outer and inner media respectively. In excitable cells, four ions are relevant (according to their concentration): K^+, Na^+, Ca^{2+} and Cl^-. Knowing their relative concentrations in the extra- and intracellular media can enable us to calculate the equilibrium potential of each ion. In mammalian skeletal muscles, for instance, $[K^+]_o$ = 4 mM, and $[K^+]_i$ = 155 mM, leading to an equilibrium potential of E_K=-98 mV. This means that in a cell containing only K^+ ions, if the pathways that allow the flow of K+ are open, the ions will flow through the membrane until E_{K+} is reached, *i.e.* -98 mV. Using the same equation, it is possible to determine the equilibrium potential of Cl^- (E_{Cl}) = -90 mV), of Na^+ (E_{Na} = +67 mV) and of Ca^{2+} (E_{Ca} = +129mV).

From a biological point of view, all cells have a resting potential, which is the TM potential of the cell when it is not in any special excited configuration. From an experimental point of view, when approaching a voltage recording electrode (linked to the ground) from the surface

of an excitable cell, the recorded voltage changes abruptly to a negative value when the pipette comes in interaction with the cell's interior. This corresponds to the resting potential. Its magnitude varies according to the type of cells, but in most excitable cells, it amounts to ~ -70 mV (with the interior of the cell negative with respect to the exterior). Following from the reversal potential values given above (E^K = -98 mV), electrophysiologists from the first half of the 20th century imagined that such a negative resting potential could be possible if only K^+ permeative pathways were open when the cell is at rest. Then the resting potential would be close to the equilibrium potential of K^+ (E_K).

Modern biology confirms this hypothesis and adds to that the activity of the sodium/potassium ATPase. This extremely important pump creates a charge imbalance by pumping two potassium ions (K^+) into the cell for every three sodium ions (Na^+) it pumps out of it, resulting in a net loss of positive charges within the cell: Binding 3 Na^+ ions from the intracellular medium triggers the hydrolysis of an ATP molecule and thereby the phosphorylation of the cytoplasmic side of the pump, causing a structural change in the protein that exposes the Na^+ ions to the exterior. In this conformation, the pump can bind two K^+ ions from the extracellular medium, causing the dephosphorylation of the pump, reverting it to its previous conformational state, and therefore transporting K^+ ions into the cell.

When the membrane is found in a state other than the resting state, a special terminology is used: when the TM potential is brought to a value higher than the resting potential (up to positive TM voltages), one speaks of membrane depolarization. When the TM potential is brought down, on the other hand, to reach more negative values, the membrane state is referred to as hyperpolarization.

2.2.2 The action potential (AP)

When an electrical impulse is applied to an excitable cell such as a neuron, the recorded TM voltage signal (one electrode outside and one electrode inside of the cell) is very particular (Fig. 2.4) (Hodgkin & Huxley 1939) (Curtis & Cole 1940): Starting from the resting potential, the voltage increases slowly to a value called the threshold potential. The TM voltage then increases very rapidly to a value above 0 mV (depolarization). After reaching its peak value, the TM potential then decreases (repolarization) before going slightly under the resting potential (hyperpolarization) and then going back to its original resting value.

Before 1930, the explanations put forward to account for this shape were vague and not consensual. Electrical impedance measurements starting in 1923 showed that the action potential corresponds to a large increase in the conductance while the capacitance remained roughly unchanged, and that this increase, contrary to what was initially assumed was not due to membrane breakdown. Moreover, these measurements showed that the increase in conductance occurred only when the membrane potential was above the resting potential. These results are summarized in Cole's book (Cole 1968).

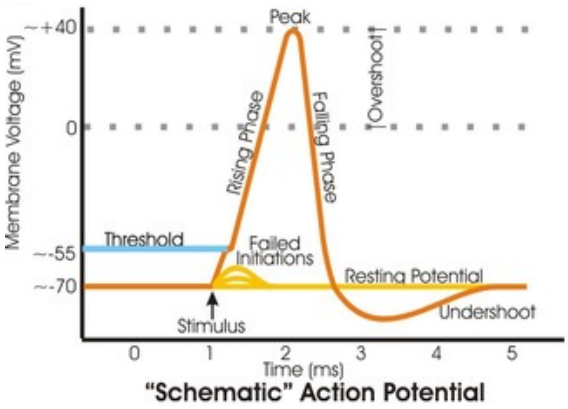

Figure 2.4: A schematic view of an idealized action potential illustrates its various phases.

Looking more closely at the shape of the action potential led Cole and Curtis to propose an electrical equivalent circuit for the membrane (Fig. 2.5). The initial, exponentially rising foot of the potential represents the discharging of the membrane while the next part, for the rest of the rise, the membrane generates its own net inward current (thanks to the resting potential created by concentration differences). In this circuit, the capacitor is set in parallel with a branch containing a resistor and a battery in series.

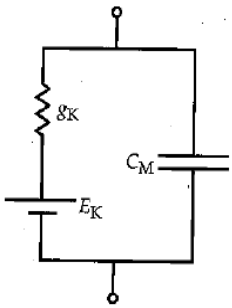

Figure 2.5: Equivalent electrical circuit where the bilayer capacitor is set in parallel with the branch containing a resistor and a battery in series (mimicking the sodium and potassium gradients across the membrane).

The other information brought by the study of the action potential comes from the overshoot of the TM potential (potentials rising above 0 mV). Indeed, one would expect that discharging the membrane would lead to a TM potential of 0 mV. However, here, it reaches positive voltages before decreasing back. Following from the reversal potential considerations described in the previous paragraph, considering E_{Na} ~67 mV, the overshoot can be explained if the membrane becomes selectively permeable to sodium ions. This was confirmed by experiments where the concentration of sodium in the outer solution was modified (Hodgkin & Katz 1949).

2.2.3 Voltage-dependent ionic currents (I_{Na}, I_K)

After the introduction of the voltage clamp experimental setup, it became possible to address directly the questions of permeability changes (Hodgkin et al. 1949). In this setup, the TM potential is clamped to a certain value while the response in current is measured (see Annex 1).

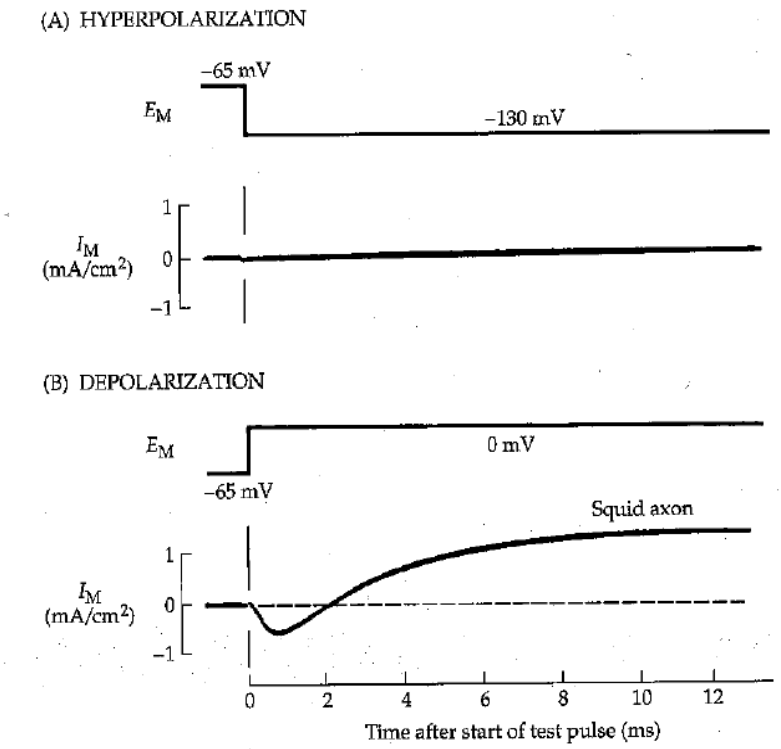

Figure 2.6: Currents in the squid giant axon when clamped from a resting potential (-65 mV) to (A) a hyperpolarized voltage (-130 mV) and to (B) a depolarized voltage (0 mV). From (Hille 2001).

When the TM voltage is held down to negative voltages (hyperpolarization), a tiny inward current is observed (Fig. 2.6.A). On the other hand, when the TM voltage is held up to positive potentials, the response is quite different: an inward current arises first before reducing until an outward current arises (Fig. 2.6.B).

Hodgkin and Huxley, in their series of papers of 1952 (Hodgkin & Huxley 1952a) (Hodgkin & Huxley 1952d) (Hodgkin & Huxley 1952b), explained the shape of these currents based on two working hypotheses: 1. Each type of ion moves down its electrochemical gradient. For instance, Na^+ ions flow inwards below E_{Na} and outwards above E_{Na}, and when the voltage is clamped to E_{Na}, the flow of Na^+ ions is then null and 2. If the ionic current comes from more than one ion, varying the concentration of one type of ion could help understand which type of ion intervenes in the ionic response. They were able to deduce therefrom that the inward current occurring at the beginning of the clamping was due to Na^+ flow and that the outward current, occurring later was due to K^+ flow.

2.2.4 Axon response

2.2.4.1 Electrical circuit equivalent

This led Hodgkin and Huxley to design an electrical equivalent circuit containing for the first time branches representing solely the conduction of Na^+ and K^+ ions (Hodgkin & Huxley 1952c). Along the capacitor branch, the Na^+ branch and the K^+ branch, they introduced another branch, that corresponds to a minor component of the current and that they called a leakage current (Fig. 2.7). We now know that this current consists mainly of Cl^- conduction.

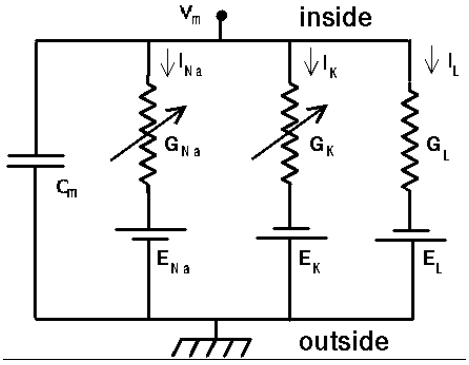

Figure 2.7: Electrical circuit equivalent of excitable cell membranes. Four branches are set in parallel: one for the membrane capacitor, one for the conduction of Na, one for K and one for the "leak" current.

In this model, the resistors of the K^+ and Na^+ branches are time- and voltage- dependent. Such a model enables calculating the conductance changes in the squid axon and is also able to reproduce experimental observables: The larger the depolarization, the larger and faster the changes in g_{Na} and g_K. When the depolarization is very large, however, both conductances reach a plateau value.

2.2.4.2 The Hodgkin and Huxley kinetic model

The Hodgkin-Huxley kinetic model deriving from above enables the description of electrical responses such as the response to voltage clamp, or the reproduction of the action potential… In this model, the conductances of Na^+ and K^+ are expressed separately.

For K^+, upon depolarization, g_K follows a S shaped time course, while upon repolarization, it follows an exponential decay (Fig. 2.8). In order to explain such a behavior, Hodkin and Huxley proposed that the opening of the K^+ pathways were controlled by four *"gating particles"*, each of which can be in the "correct" position to open the channel with a probability n, that is voltage dependent. The probability that all four particle are in the "correct" position is then n^4. The evolution of the current ascribed to K^+ can then be written in the form :

$$I_K = n^4 g_K (E - E_K) \quad [2.7]$$

with g_K the maximum conductance that can be reached by K^+.

If each particle moves from "correct" to "incorrect" position with first order kinetics, this will lead to the distribution of particles described by n relaxing exponentially to a new value. With this mathematical form; when n rises exponentially from 0, n^4 follows a S shaped time course while when n decreases exponentially to 0, n^4 follows an exponential decay, reproducing well the I_K experimental response to voltage clamp.

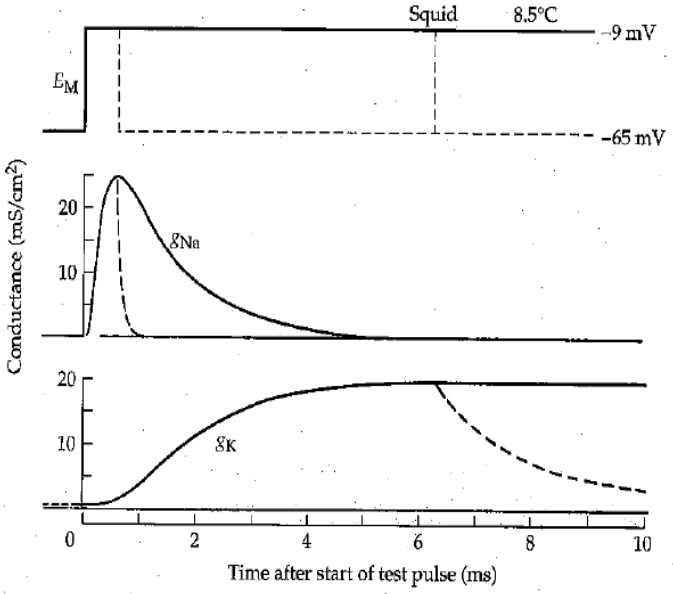

Figure 2.8: Separation of the Na (g_{Na}) and K conductances (g_K) in a squid axon when holding to a depolarized voltage. The main difference comes from the fact that g_{Na} inactivates when g_K remains maximum for the duration of the pulse. Dashed lines indicate the response when the voltage is held back down to -65 mV. Note the rapid response of g_{Na} with respect to g_K. From (Hille 2001).

For Na^+, the same logic is followed but because Na^+ current is inactivated (along with being activated), there has to be two types of gating particles: an activating particle called m and an inactivating particle called h. To reproduce empirically the response of I_{Na} to voltage clamp, Hodgkin and Huxley set the number of activating particles to 3 and of inactivating particles to 1.

The mathematical form is then:

$$I_{Na} = m^3 h g_{Na} (E - E_{Na}) \quad [2.8]$$

At rest, *m* is low and *h* is high. During depolarization, *m* rises while *h* falls and m^3h has the experimental form of the current. After depolarization, *h* rises and *m* decreases and m^3h stays at a low value, as in experimental recordings.

Adding up these two members, plus another one of the same type for the leak yields the

mathematical form of the total ionic current:

$$I_i = n^4 g_K (E - E_K) + m^3 h g_{Na} (E - E_{Na}) + g_L (E - E_L) \quad [2.9]$$

This mathematical form enables reproducing in a satisfactory manner the current curves g_{Na} and g_K, but also the shape of the action potential.

2.3 Voltage-gated ion channels (VGCs)

After these first electrophysiology experiments, a variety of scientists from different disciplines set out to determine what was the molecular basis of voltage dependent ionic conduction. Pharmacologists were the first (1965 to 1975), and biophysicists, chemists, geneticists and cell biologists followed to unravel which molecules were responsible for ionic transport and how these worked (for a short description of the methods used for VGC studies, refer to Annex 1). It was determined that these were integral, transmembrane proteins that act as channels (passive transport) and that are selective to a single ion type. This paragraph describes the extent of the ion channel family while underlining the common structural and functional features of their members.

2.3.1 The VGC superfamily

Setting out to determine which type of molecules conducts the ions, pharmacologists started by proving that the molecular pathways for K^+ and Na^+ were distinct. Their experiments consisted in testing the effects of a variety of drugs: tetrodotoxin (TTX) and saxitoxin (STX) were shown to suppress the Na^+ component of the ionic current in giant axons of invertebrate neurons, leaving the K^+ current invariant (Narahashi et al. 1964) (Nakamura et al. 1965) (Kao 1966). Tetra-ethyl-ammonium (TEA), on the other hand, blocks K^+ current selectively, leaving Na+ current invariant (Tasaki & Hagiwara 1957). These two experiments showed that sodium and potassium ions are conducted by different macromolecules that are not sensitive to the same drug. These macromolecules have since then been called channels.

Moving to distinct cell types, it was also shown that the plasma membranes of other cells contained a large variety of ion channels. Their difference lies in their activation and inactivation kinetics, in the drug concentration needed to reach half activity, in their sensitivity to neurotransmitters or other intracellular messengers.

Much later, advances in molecular genetics lead to the possibility to sequence the genes encoding ion channels and to look at the phylogenetic of ion channel families. Other ion selective channels were then discovered, like the ones selective to Cl^- and Ca^{2+}. All these channels have the same kind of structure: they are all integral proteins made of alpha-helices bundles, linked to each other by intra- and extracellular loops. The most diverse family is the one of K^+ selective channels (Fig 2.9), as they can be made of homotetramers of 2

transmembrane segments (K_{ir} channels), of an assembly of such motives (K_{2P}) channels, or else of homotetramers of 6 TM segments (Kv, K_{Ca}, CNG, HCN or TRP channels). Voltage-gated channels that are selective to Na^+ (Nav) or to Ca^{2+} (Cav) on the other hand are much less diverse, as they are all constituted by heterotetramers of 6 TM segments each.

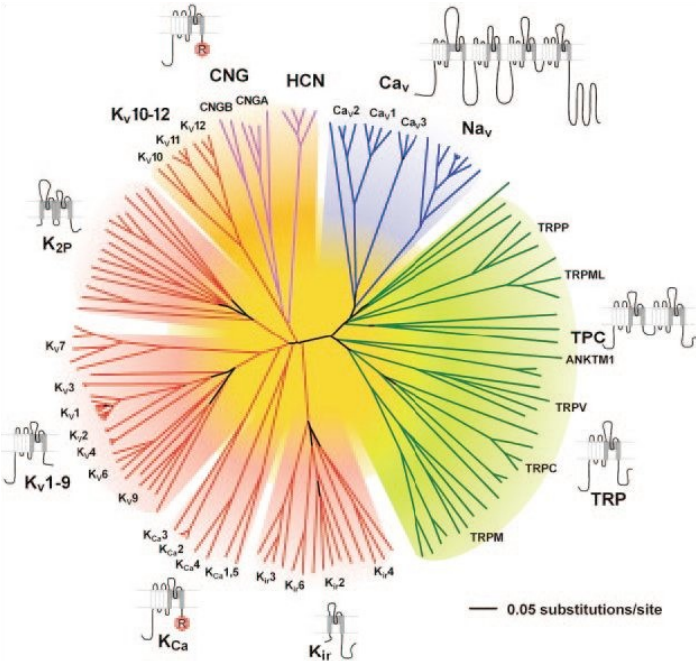

Figure 2.9: A schematic view of the phylogenetic tree of the voltage-gated ion channel superfamily. This global view of the 143 members of the structurally related ion channel genes highlights seven groups of ion channel families and their membrane topologies. Four-domain channels (Cav and Nav) are shown as blue branches, potassium-selective channels are shown as red branches, cyclic nucleotide-gated channels are shown as magenta branches, and TRP and related channels are shown as green branches. Background colors separate the ion channel proteins into related groups: light blue, Cav and Nav; light green, TRP channels; light red, potassium channels, except Kv10–12, which have a cyclic nucleotide binding domain and are more closely related to CNG and HCN channels; light orange, Kv10–12 channels and cyclic nucleotide-modulated CNG and HCN channels. From (Yu et al. 2005).

Obviously, different cells carry different types of ion channels. However, it is noteworthy that a single cell by itself contains a large variety of VGCs, enabling a fine reaction to an electrical signal.

2.3.2 Common structural features

More than pointing out at the differences between VGCs, it is interesting to note the common structural features these ion channels share. Indeed, it seems that complex 6 TM voltage-gated ion channels have evolved from a more primitive type of ion channels, *e.g.* those found in bacteria and that bear only 2 TM segments.

2.3.2.1 The pore

The first common feature is that these ion channels transport ions as water filled pores. This was first shown once more by pharmacologists, who discovered that the block by tetra-ethyl-ammonium (TEA) of K^+ channels could be reversed by applying a high concentration of potassium on the extracellular side and then a hyperpolarizing pulse, suggesting that K^+ can displace TEA from its binding site. (Armstrong & Binstock 1965) (Armstrong 1966) They inferred that this could be possible if TEA binds inside of the pore that is also used to conduct ions. Next, counting the number of ions that could pass through the protein before TEA blocked it also gave conductivity values that could be reached only by channels (as opposed to transporters, in which conductance is much smaller) (Armstrong 1969). All this pointed in favor of the presence of a water-filled conduction pathway for ions.

2.3.2.2 The selectivity filter and the gate

Electrophysiology measurements and the discovery of the primary structure of ion channels brought a large number of answers about the function of ion channels. However, up to 1998, structural information was still missing. Then, the discovery that ion channels in bacteria were homologous to ion channels in eucaryotes enabled the production of proteins in large quantities, as is needed to produce crystals used in X-ray diffraction (see Annex 1).

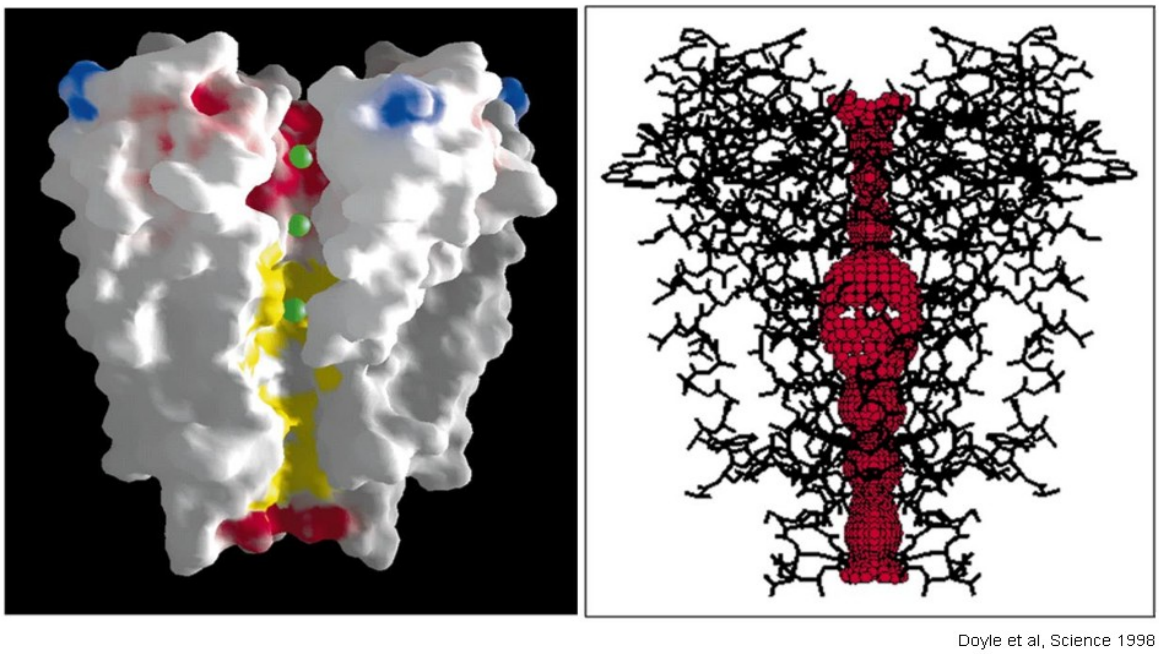

Figure 2.10: Side view of the KcsA structure, illustrating the presence of the selectivity filter screening for ions, of the pore and the gate. (Left) Space filling representation. Ions are represented as green spheres. (Right) Illustration of the solvent accessible volume in red. From (Doyle, Cabral, et al. 1998).

The first Xray structure of an ion channel came out in 1998 (Doyle, Cabral, et al. 1998). The authors managed to crystallize the KcsA channel, a K^+ ion channel from the bacterium Streptomyces lividans. This structure confirmed features that were inferred earlier (Fig 2.10): the KcsA structure displays a homotetramer of two TM helices (TM1 for the outermost and TM2 for the innermost) joined by an extracellular re-entering P-loop, with an aqueous pore in the middle. On the extracellular side of the pore lies the selectivity filter (P-loop, that screens K^+ ions from others) and on the intracellular side, a large vestibule filled with water molecules (that is also the place where TEA can bind to the selectivity filter) is ended by a narrower region, where the four subunits join to form a gate. This is the region that opens and closes to let ions through or not.

2.3.2.3 The voltage sensor domain (VSD)

The bacterial ion channel KcsA is homologous to the pore region of the more complex 6 TM segments VGCs that are commonly found in mammals (Kv, Nav and Cav). Their pore is similar to the ones found in bacterial channels, as they have two TM helices (called in such VGCs S5 and S6) linked by a reentrant P-loop. Cloning of these channels revealed that they contain four additional TM segments, the so-called voltage sensor domains that confer them their sensitivity to voltage (Fig. 2.11). Within the VSD, there is a TM segment called S4 that bears a large number of positively charged (basic) residues (their number varying between 4 and 7). The other three segments (S1 to S3) bear 4 negatively charged amino-acids (following Kv1.2 numbering: Glu^{183} (called E1 hereafter) on S1, Glu^{126} (E2) on S2, Asp^{259} (D3) on S3 and Glu^{136} (E4) on S2).

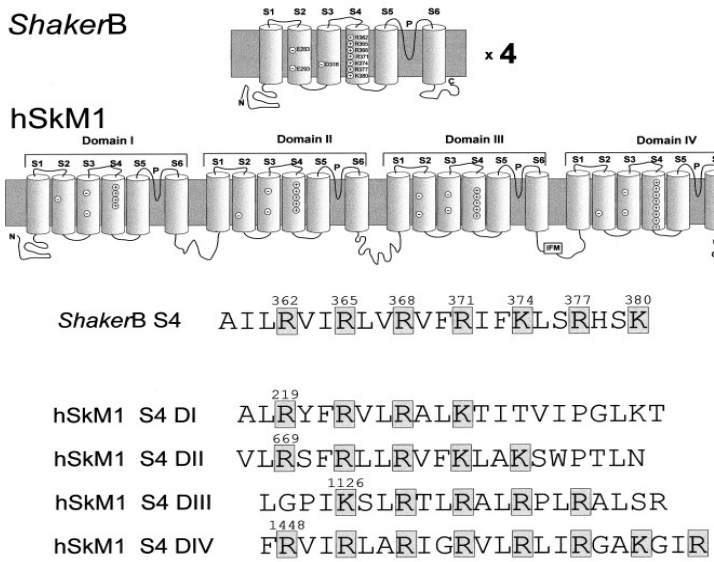

Figure 2.11: Transmembrane segments of voltage-gated channels, S1 to S4 form the voltage-sensor domain. Top: Subunit of Shaker (a Kv channel from the Kv1 family). Four of these subunits are assembled into a functional channel. Middle: human skeletal muscle Na channel (hSkM1) α-subunit. Bottom: amino acid sequences of the S4 segments for ShakerB and for the S4 segments in all 4 domains of the hSkM1 channel.

We will develop extensively how these voltage-sensing entities function in the case of voltage-gated potassium (Kv) channels in the next chapter.

2.3.2.4 Pore gating and coupling to VSD operation

Although they both involve the innermost helix of the pore, gating mechanisms are different in bacterial 2 TM-segments ion channels and in mammalian 6-TM VGCs. In bacterial K^+ channels, the closed state has the S6-like TM2 segments in a straight conformation that leads to their crossing in a bundle to close the pore at its intracellular end (Doyle, Cabral, et al. 1998) The open state shows a bend in the TM2 segments, at the level of highly conserved glycine residue, which leads to opening of the intracellular mouth of the pore (Jiang, Lee, Chen, Cadene, Chait & MacKinnon 2002a) (Jiang, Lee, Chen, Cadene, Chait & MacKinnon 2002b) In VGCs, on the other hand, a conserved proline-valine-proline (PVP) motif in the S6 segment seems to serve the same purpose

It is well admitted that S4 is responsible for voltage sensing and that it is the molecular trigger for pore opening and closing. However, the mechanism by which the VSD function is coupled to pore gating is not completely understood. Indeed, the structure of the Kv1.2 displays limited contacts between the pore-forming and voltage-sensing modules (Long, Campbell & Roderick 2005a), consistent with the idea that these modules function in a largely independent manner. Of course, the pore is covalently attached to the VSD through the S4–S5 linker. Both site-directed mutagenesis studies and structural studies support the idea that this linker communicates the conformational change in the voltage sensor to the pore-forming domain through a pulling/twisting force on the S5 segment in an allosteric mechanism (Long, Campbell & MacKinnon 2005b) (Soler-Llavina et al. 2006). Also, many studies have shown that the S4-S5 linker has to be compatible with the pore inner helix (S6) tail for proper function in a variety of VGCs, indicating a direct interaction between these two parts of the protein (Lu et al. 2002) (Tristani-Firouzi et al. 2002) (Ding & Horn 2003) (Decher et al. 2004) (Caprini et al. 2005)(Labro et al. 2008).

Also, other functional interactions between VSD and pore domain were shown to occur, that seem to act as pivots for the voltage sensor to be able to pull on the S4–S5 linker: between the extracellular end of the S4 segment and the extracellular end of the S5 segment on one hand (Broomand 2003) (Gandhi et al. 2003) and between an extracellular site in the S1 segment of the VSD and the S5 segment (Lee et al. 2009) on the other. Interestingly, it was shown that activation of a single VSD is enough to open the *Shaker* activation gate provided that the other three VSDs are all in an activated conformation (Gagnon & Bezanilla 2009).

2.3.3 Common functional features

Following from their common structural features, there are also several functional features that can also be pointed out as common to the various families.

2.3.3.1 Stochastic opening

Since the introduction of patch clamp and gigaseal setup (see Annex 1), it became possible to record signals from single channels. When the first response of single ion channels to sustained depolarization was recorded in 1981, it was found that VGCs seemed to open abruptly (on the millisecond time scale), but also to close as abruptly, despite the sustained depolarization (Hamill et al. 1981).

Hodgkin and Huxley also noted that, when trying to reproduce the measurements, the patterns of opening and closing were always different, indicating that the opening/closing processes are stochastic in nature. Only when reproducing these measurements a large number of times, it appeared that the sum of these traces constituted a signal similar to the microscopic K^+ or Na^+ current. It should be noted here that this behavior is not unique to VGCs but is inherent to all molecular reactions.

2.3.3.2 Voltage-dependent opening of the gate

Amazingly, with just electrical signal recordings and by building kinetic models that could reproduce current and voltage traces, the electrophysiologists from the first half of the 20th century were able to determine that 1- ions had to be transported through the membrane in a selective manner and that 2- these pathways were opened by the action of *"gating particles"* (that Hodgkin and Huxley called *n*, *m* and *h*) in a voltage dependent manner. They reasoned in the following way: because voltage drives this gating process, the electric field must do work by displacing some charged particles of the system. After ruling out the possibility that the response is due to changes in the concentration of ions, or to a change in the membrane structure (*e.g.* squeezing), the idea that the field acts upon charges or dipoles that pertain to the channel was tested: because depolarization causes the pathways to open, it must be that negative charges are carried inwards, that positive charges are carried outwards or else both.

Hodgkin and Huxley had also pointed out that if such a phenomenon occurred, a transient current preceding the ionic current initially called "carrier current", should be measurable (Hodgkin & Huxley 1952c). Because of challenges in the measurement systems, and the need to eliminate ionic and capacitive currents, these now called "gating currents" were only first measured in the 1970s in skeletal muscle (Schneider & Chandler 1973) and in the squid giant axon (Armstrong & F. Bezanilla 1973) (Keynes & Rojas 1974).

Since then, gating currents were widely used to study the electrophysiology of ion channels. The typical trace obtained after suppressing ionic and capacitive currents is presented in fig. 2.13. As can be seen, gating current are transient (they go back to 0 after a few ms) and of very low amplitude (~200 times lower than ionic currents). The integral of such currents is called the gating charge and represents the total charge that is transported within the protein during opening (or closing) of the channel.

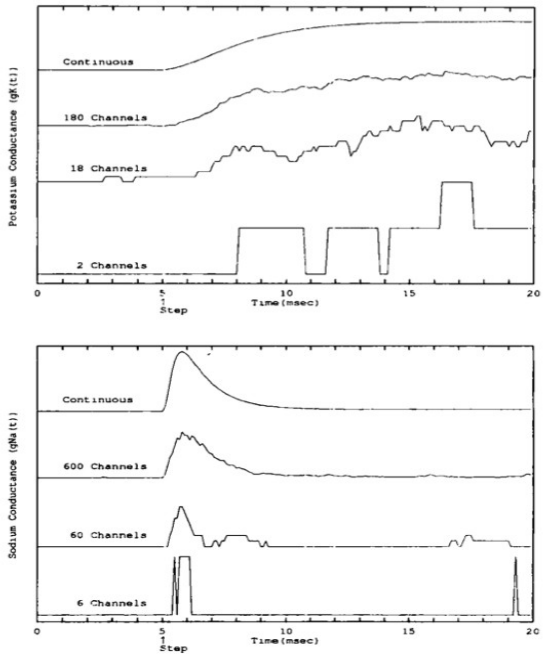

Figure 2.12: Illustration of the stochastic nature of the opening of voltage gated sodium (top) and potassium (bottom) channels. Only when looking at a large number of channels is it possible to reconstitute the macroscopic behavior of the current. From (Strassberg & DeFelice 1993)

This "gating charge" is an important quantity that was measured in a variety of VGCs and using various methods. Its values range from 8 to 16 elementary charges. Using the integral of the gating current and combining it with counting the number of channels by non stationary fluctuation analysis, Shoppa et al. Estimated the gating charge to be 12-14 e per Shaker channel (see paragraph 3) (Schoppa et al. 1992) (Seoh et al. 1996). Using a different strategy to count the number of channels (α-KT scorpion toxin binding), Aggarwal and MacKinnon found values within the same range (Aggarwal & MacKinnon 1996). Using a kinetic multi-state gating model to fit measured curves of the gating charge as a function of voltage (G/V curves) (Zagotta, Hoshi, Dittman, et al. 1994) or measuring limiting slopes near -75 mV (Noceti et al. 1996) led to values of 12-16 e for the same channels. Other experiments were conducted on Nav and Cav channels leading to similar values (Hirschberg et al. 1995) (Noceti et al. 1996).

Today, we understand the molecular basis for this voltage sensing process: when the membrane is depolarized, the positively charged amino-acids of the S4 helix move towards the outside of the membrane and it is these residues, when moving within the TM potential difference, that produce the gating current and therefore the gating charge. This voltage-dependent gating process and particularly the models that were developed to rationalize it will be detailed in the case of Kv channels in paragraph 3 of this chapter.

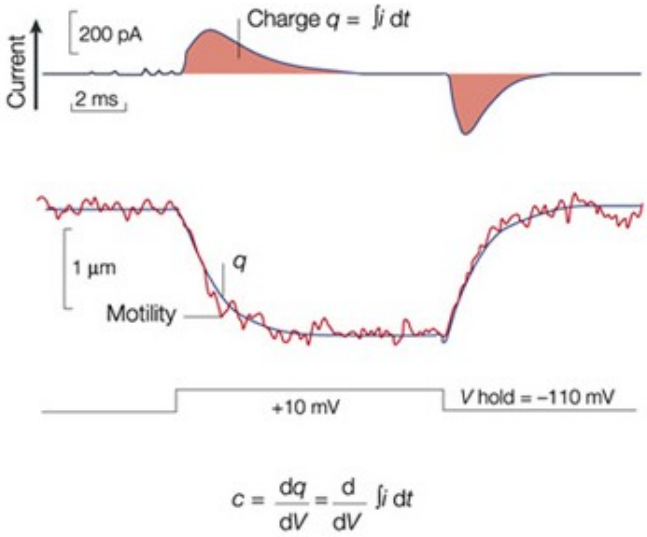

Figure 2.13: Gating currents and gating charge. Bottom: Typical gating current curve obtained when holding the TM potential from -110 mV to +10 mV. Top: Corresponding gating charge, q, calculated as the integral of the gating current. The gating charge per channel can be obtained by dividing this quantity by the total number of channels in the voltage clamp patch. From (Dallos & Fakler 2002).

3 Voltage gated potassium channels (Kv channels)

We now come to the description of Kv channels which constitute the center of attention of this work. In this section, we describe what is known of their structure and their function and we present the challenges and main unknowns that remain today. We also briefly describe means of modulation of Kv channels, with a particular focus on mutations giving rise to leak currents. We later present in details the Kv channels we have specifically worked on: the Kv1.2 channel and some members of the Kv7 family.

3.1 Structure and function

Among all ion channels, the potassium selective channels constitute the most diverse family. Today, over 80 genes of K^+ ion channels have been identified in mammals (Honoré 2008) and over 40 for the sole Kv sub-family (Gutman et al. 2005). We describe here the features of Kv channels in terms of sequence, structure, electrical and mechanical properties.

3.1.1 The sequence and secondary structure are revealed

Well before the first crystal structures were published, sequencing enabled reconstructing the primary structure of Kv channels. The secondary structure predictions led to the following

observations: the number of amino acids in the various sequences of the Kv families appears to be very variable but a common pattern emerges. All channels have 6 TM segments, named S1 to S6 connected by intra- and extra-cellular loops. Interestingly, they were also found to assemble as tetramers, making them very similar to Na_v or Ca_v channels; which possess a single sequence of four repeats of 6 TM domains each. Among the 6 TM segments, the last two (S5 and S6) are separated by a reentrant loop, called the P loop. Their homology to the 2 TM channels designated them as the perfect candidates for the pore domain. The other 4 TM segments (S1 to S4) constitute a separate domain, the voltage sensor domain (VSD), and confer to the Kv channels their sensitivity to voltage. Among the four TM segments of the VSD, S4 contains a large variable number of conserved positively charged amino-acids (mostly ARG and more rarely LYS), 4 to 7, that are also sometimes referred to as gating charges (Fig. 2.14). In the Kv1.2 for example, there are 6 charges: R^{294} (called R1 hereafter), R^{297} (R2), R^{300} (R3), R^{303} (R4), K^{306} (K5) and R^{309} (R6). These S4 charged residues are always arranged in the same way: two consecutive positive charges in S4 are separated by two hydrophobic amino-acids, such that when the amino-acid chain is folded in a α-helix, all positive residues are located on the same side of the helix (when looking at the helix from the top, the gating charges are almost aligned). In fact, because an α-helix has a pitch of 3.6 residues per turn, the charged residues arrange in a stride describing a slow helical periodicity of the opposite handedness.

Kv1.1	AIL**R**VI**R**LV**R**VF**R**IF**K**LS**R**HS
Kv1.3	AIL**R**VI**R**LV**R**VF**R**IF**K**LS**R**HS
Kv1.4	AIL**R**II**R**LV**R**VF**R**IF**K**LS**R**HS
Kv1.5	AIL**R**VI**R**LV**R**VF**R**IF**K**LS**R**HS
Kv1.6	AIL**R**VI**R**LV**R**VF**R**IF**K**LS**R**HS
Kv1.7	AIL**R**VI**R**LV**R**VF**R**IF**K**LS**R**HS
Kv1.10	AIL**R**II**R**LV**R**VF**R**IF**K**LS**R**HS
Kv2.1	RVVQIF**R**IM**R**IL**R**IL**K**LA**R**HS
Kv3.1	GFL**R**VV**R**FV**R**IL**R**IF**K**LT**R**HF
Kv4.1	GAFVTL**R**VF**R**VF**R**IF**K**FS**R**HS
Kv5.1	QAVQAL**R**IM**R**IA**R**IF**K**LA**R**HS
Kv6.1	LVL**R**VL**R**AL**R**ILYVM**R**LA**R**HS
Kv7.1	SAL**R**GI**R**FLQIL**R**MLHVD**R**QG
Kv9.2	RVAQVL**R**LM**R**IF**R**IL**K**LA**R**HS
Kv11.2	QVL**R**VM**R**LM**R**IF**R**IL**K**LA**R**HS

Figure 2.14: Sequence alignment of the S4 segments in different members of the Kv channel family, illustrating the conservation of the basic residues.

The importance of these S4 charged residues was gradually pointed to: they are responsible for voltage sensing and mutating one or more of them may considerably alter the response of the channel to changes in TM voltage and be responsible for genetic diseases (see paragraph 3.2.3).

In the other segments S1 to S3, it is also possible to find conserved residues: the first group

is constituted by the negatively charged residues in these helices (3 glutamic acids and 1 aspartic acid), that were thought to constitute the negative binding sites for S4 gating charges and participate in the voltage sensing process (Catterall 1986) (Guy & Seetharamulu 1986). Also, a phenylalanine residue is conserved on S2 among all VGCs (Ramsey et al. 2006) (Sasaki et al. 2006). Its possible role as a transfer center is discussed in more details later on.

3.1.2 Voltage dependence of conductance and gating charge movement

Up to now, gating currents were measured only in a few Kv channels, *e.g.* Kv1.1 (Bezanilla et al. 1991), Kv2.1 (Taglialatela & Stefani 1993), Kv1.5 (Fedida et al. 1996), Kv4.2 (Dougherty & Covarrubias 2006), Kv7.4 (Miceli, Cilio, et al. 2009), Kv10.1 (Tang et al. 2000) and Kv11.1 (Piper, Varghese, et al. 2003).

First, we recall that the time integral of the gating current at a particular voltage V is called the gating charge or *Q(V)* and that ionic conductance/voltage (*G/V* or *I/V*) and gating current/voltage (*Q/V*) functional dependence can be derived from electrophysiology experiments. These dependencies can be built from both single channel recordings or from regular patch clamp, in which case these relationships are valid for a population of channels. Although some discrepancies can be witnessed, in terms of voltage sensitivity, magnitudes, ability to inactivate or not and so on, a general pattern emerges for all VGCs and most particularly Kv channels: all *G/V* and *Q/V* relationships display a sigmoid shape with asymptotes at extreme potentials.

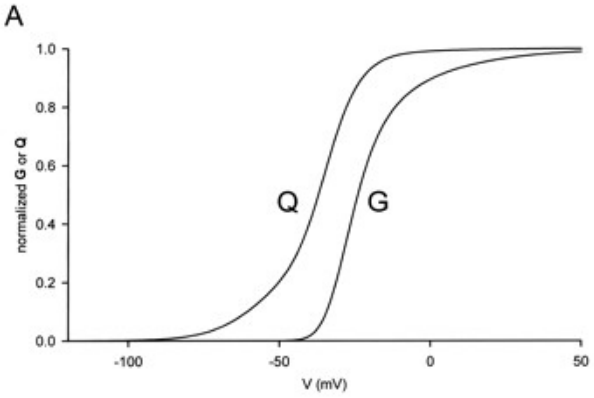

Figure 2.15: Voltage (V) dependence of conductance (G) and gating charge movement (Q) for a voltage-dependent ion channel. From (Bezanilla 2000).

At negative, hyperpolarized resting potentials, the channels are closed and the ionic current is null. Under depolarization, the channels start to open and Q increases, indicating the movement of gating charges in the electric field. Then, G starts to increase, signaling the opening of the channels gate and the flow of ions through them. When reaching a definite

value of the TM hyperpolarized potential, both Q and G reach a plateau value, completing the S-shape of the Q/V and G/V relationship. Q reaches a plateau because the gating charges have reached their extreme positions while G stops increasing because the conductivity through the pore has reached its maximum value. Note that the G/V curve is always shifted to the right with respect to the Q/V curve, which clearly indicates that the gating charges movement occurs prior to channel opening and ionic conduction.

3.1.3 Element of the activation mechanism

3.1.3.1 Kinetic models show that there are intermediate kinteic states

In early kinetic models, such as the Hodgkin/Huxley model described in paragraph 2.2.3, the channel could be found in two states: open or closed. Accordingly, the probability of finding the channel in the open state depends on the gating charge z_g and on the non-electrical work required to open the channel w.

Subsequent models introduced more complex parameters to fit the kinetics of the curves of ionic current (so called *I/V* relationships) and of the *Q/V* curves. As each channel has four VSDs that can be found in a resting or activated state, the kinetic models should account for similar events taking place in each of these VSDs and also for a coordinated event to open the channel.

In the Zagotta-Hoshi-Aldrich model (Zagotta, Hoshi & Aldrich 1994), each VSD can be found in two different resting states and in one activated state but to open, the channel requires that all four subunits be in the activated state (Fig. 2.16).

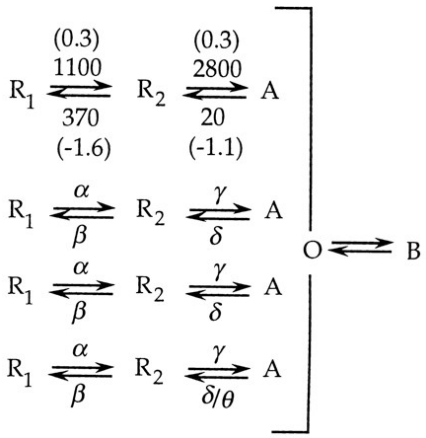

Figure 2.16: Zagotta-Hoshi-Aldrich kinetic model involving two successive transitions in each subunit, from resting state R1 to resting state R2, and from resting state R2 to activated state A. To open (state B), the channel requires that all for subunits be in the activate state.

Later, other groups, extending the study to a broader voltage range, proposed the same

types of models, but introducing additional states (Schoppa & Sigworth 1998) (Baker et al. 1998) (Loboda & Armstrong 2001) (Sigg et al. 2003) (Zheng & Sigworth 1998) (Kanevsky & Aldrich 1999).

Experiments have proven that activation of each of the VSDs proceeded in multiple steps rather than in a single resting to activated transition. Especially, an early component of the gating current in *Shaker* channels with a time constant of 12 μsec was recorded (Sigg et al. 2003). This fast component, so-called the "loose" charge, was found to be part of the gating current associated with the opening and closing of the channel and is the fastest component of gating current resolved so far. As the electrophysiology measurements became more and more sophisticated, new kinetic models accounting for the latest experiments have been proposed (Lacroix et al. 2011).

In all of these models, the VSD goes from a state S_i to another S_{i+1} by carrying a gating charge z_i. The total gating charge is then the addition of all these gating charges in all subunits. Note here that during a single transition, one or more charged residues may cross part or the entirety of the electric field across the membrane. The gating charge associated with each step z_i may then be written as

$$z_i = \sum_j z_j \left(\delta_{ji} - \delta_{(j(i+1))}\right) \quad [2.10]$$

with the sum running over all residues j. δ_{ji} is the so-called electrical distance, the fraction of the electric field crossed by the residue j during transition from state I to state i+1. Such a step can be related to probability finding one state rather than the other, and therefore to the probability of opening the channel's gate through:

$$\frac{p_2}{p_1} = e^{\frac{-(w_{12} - z_{g2} q_e E_M)}{k_B T}} = e^{z_{g2} q_e \frac{(E_M - E_2)}{k_B T}} \quad [2.11]$$

where E_i is the midpoint potential for the transition of charge z_i, w_{12} the nonelectrical work needed to go from state 1 to state 2 and E_M the membrane potential.

Such phenomenological models are very useful to help interpret electrophysiology results. However, they miss the molecular level description of the intermediate states. We will see later that simulation tools such as molecular dynamics are useful to provide answers to these questions.

3.1.3.2 Mutagenesis reveals the importance of S4

Sequencing of VGCs led to think of S4 as the domain sensitive to changes in the TM voltage, due to the presence of a large number of positively charged residues. Single-sited mutagenesis (see Annex 1) seemed like the perfect tool to probe whether residues participate in the sensing of the voltage and/or in the structural rearrangements consecutive to the stimuli. Indeed, early studies on the Kv1.1 revealed that neutralizing any of the five first basic residues

shifted the midpoint of the I/V activation curve, indicating a perturbation of the voltage sensing. Additionally, mutating a pair of these residues reduced the steepness of gating, indicating probably a reduction of the gating charge (Papazian et al. 1991) (Liman & Hess 1991).

Newer methods enabling the direct measurement of the total gating charge also permitted testing if the mutagenesis of several residues altered the gating charge. Both Aggarwal and MacKinnon, and Seoh et al. found in 1996 (Aggarwal & MacKinnon 1996) (Seoh et al. 1996) that the residues carrying the most gating charge in Shaker (Kv1.1) were the first 4 positively charged residues, giving each a drop of at least 4e for the whole channel (4 mutations, one in each subunit). The same experiments tested whether mutation of the negative residues of S2 and S3 led also to a reduction in the gating charge. One of them, E^{293} was hence showed to participate in the gating charge for as much as 4e. Mutation of neutral residues on the other hand did not lead to alteration of the total gating charge.

3.1.3.3 Arginines are transported from one side of the membrane to the other

Substituting S4 basic residues by neutral amino-acids brought information about the role played by the latter. The reduced gating charge could come from at least two factors: losing a positively charged amino-acid could reduce the gating charge, even if the extent of the S4 movement was the same, because one less charge would be transported across the electric field. Or, it could also mean that S4 became less sensitive to voltage and therefore the extent of S4 movement would be reduced. Bezanilla and coworkers then set out to measure the extent of S4 movement with minimal perturbation of the nature of S4. They then tested the effect of substitution of arginines by histidines, an amino-acid that could be manipulated under a physiological range of pH. (Starace et al. 1997). In Shaker, they found that substituting R2, R3 or R4 by histidine gave rise to a proton current through the voltage sensor (after blocking the conduction through the central pore), indicating that these residues are transported from the intracellular media to the extracellular media during activation. R1 on the other hand seems to be in contact with both the outside and the inside at hyperpolarized voltages (Starace & Bezanilla 2001) (Starace & Bezanilla 2004). Finally, they found that K4 and R5 are not transported through the electric field during activation.

At the same period, cysteine accessibility techniques were used to look into the state-dependent exposure of the S4 basic residues, using (trimethylammonium)ethyl methanethiosulfonate (MTSET) (Larsson et al. 1996) or *p*-chloromercuribenzenesulfonate (PCMBS) (Yusaf et al. 1996) as cysteine reagents. Larsson et al. mutated charged residues to cysteine, whereas Yusaf et al. mutated uncharged residues in an attempt to preserve the charge of the S4 segment. Both came to the conclusion that R1 and R2 become accessible from the extracellular medium in the activated state. In the same state, Larsson et al. found that R3 was inaccessible, but Baker et al., who extended their study by combining a fluorescent reporter with the exposure changes of cysteine found R3 to be accessible (Baker et al. 1998). In the resting hyperpolarized state, R2 and R3 were found to be accessible from the intracellular medium. For R1, incoherent results were found, Larsson et al. found it to be exposed while

Baker et al. found it to be in a buried position.

Taken altogether, all these results indicate that the gating charges are located in water crevices, explaining the stability of charged residues in a TM position, and that some conformational change occurs during depolarization which results in a large change in the exposure of the S4 basic residues (Bezanilla 2000).

3.1.3.4 Many models describe VGC gating

Three main models describing the conformational changes of the VSD involved during deactivation of the channel have been proposed to rationalize the transfer of a large gating charge across the low dielectric membrane in VGCs. All of them are associated with the motion of S4 (Fig 2.17). Since 15 years, there have been a large number of reviews describing and updating these models as knowledge about Kv channels was evolving (Yellen 1998) (Bezanilla 2000) (Horn 2000) (Gandhi & Isacoff 2002) (Cohen, Grabe, et al. 2003) (Ahern & Horn 2004) (Blaustein & Miller 2004) (Bezanilla 2005a) (Tombola, Pathak, et al. 2005) (Tombola, Pathak & Isacoff 2006) (Catterall 2010).

In the *sliding helix* (or *helical screw*) model (Catterall 1986) (Guy & Seetharamulu 1986), the positively charged residues of the S4 segment, which are located at every third position, form sequential ion pairs with acidic residues on neighboring TM segments. Altogether, S4, which remains tilted with respect to the membrane plane, rotates about its axis while translating perpendicularly to the membrane plane, and during the process changes the exposure of the S4 basic residues. This model was adapted a few years later by several groups (Durell et al. 1998) (Keynes & Elinder 1999) (Gandhi & Isacoff 2002) (Durell et al. 2004) who estimated that the S4 helix should rotate by 180° and translate by 13.5 Å to satisfy geometrical constraints and to account for the transport of the total gating charge.

The *transporter* model (or *helical-twist*, *helical-tilt* model) derives from measurements of a focused electrical field within the membrane, and suggests that during activation, the latter is reshaped. Accordingly, it is posited that S4 does not need to move its charges physically very far across the membrane, and that just a change in tilt and rotation is enough to transport the total gating charge (Starace et al. 1997) (Bezanilla 2000) (Bezanilla 2002)As such, it is an evolved version of the simpler *rotation in place* (Cha et al. 1999) and the *moving orifice* models (Yang, George, et al. 1996).

A third model was introduced following publication of the first KvAP (a bacterial voltage gated ion channel from the archeabacterium *Aeropyrum Pernix*) crystallographic structure (Jiang, Lee, et al. 2003) (Jiang, Ruta, et al. 2003). In this structure, the position of the S3–S4 helical hairpin with respect to the pore domain suggested a gating mechanism in which the hairpin moves through the membrane in a *paddle*-like motion translocating S4 basic residues across the membrane, and reaching a TM position only in the activated state. This model differs drastically from the two others, because it involves exposing the S4 basic residues to the membrane core. Following the publication of this KvAP crystal structure, a large number of groups argued that this model was incompatible with the 10 years of experiments

conducted up to then and subsequent experiments were done leading the group of MacKinnon to admit that the KvAP structure likely represented a nonnative state of the channel, that the paddle model was highly unlikely (Lee et al. 2005) (Butterwick & MacKinnon 2010) and to propose a revised paddle model in which the voltage-sensor paddles (top of S3 of S4 helices) moves perpendicularly to the membrane, relative to the S1 and S2 helices. This movement translates S4 by ~15 Å.

The most recent two crystal structures of the Kv1.2 channel (Long, Campbell & Roderick MacKinnon 2005a)and of the Kv1.2-Kv2.1 paddle chimera (Long et al. 2007) have made it possible to propose molecular models of the VSD response, most of which have now converged towards the *sliding helix* model (Shafrir et al. 2008) (Campos et al. 2007) (Pathak et al. 2007) (Catterall 2010).

3.1.3.5 How far does S4 move ?

The question however still remains, as to how to characterize precisely the extent of the movement of S4 (small in the transporter model, intermediate in the helical screw model and large in the paddle model), the focusing of the electric field (which is very strong in the transporter model, intermediate in the helical screw and mild in the original paddle model) and to reconcile the various measurements that were done up to now. We attempt here to build a list of the various measurements and indicate which kind of model they mostly support. The reader is referred to Annex 1 for a description of the experimental methods cited hereafter.

Most of the experiments advocating a small movement of S4 rely on fluorescence measurements. The first ones carried out in Shaker (Cha et al. 1999) (Glauner et al. 1999) indicated voltage-dependent distance changes between S4 segments of adjacent subunits of up to 3-5 Å. Later, Bezanilla and coworkers used fluorescence resonance energy transfer (FRET) implicating eGFP attached at the bottom of S6 as a donor and sulforhodamine + methylthiosulfonate (MTS) as acceptor linked to extracellular regions distance to find that the charges do not move more than 2 Å perpendicularly to the membrane, suggesting that the region associated with the S4 segment undergoes a rotation and possible tilt, rather than a large transmembrane movement (Bezanilla 2005b).

Islas et al. studied how the reduction of the ionic strength of the intra- or extracellular media altered the gating charge (Islas & Sigworth 2001). They proposed that the VSD contains water crevices separated by a thin hydrophobic zone (3 to 7 Å) which is the zone where the electric field collapse and through which the arginines are transported.

Histidine scanning mutagenesis by using a cysteine reactive electrochromic fluorophore (the ANEP chromophore) was used to analyze the electric field in the VSD (Asamoah et al. 2003). They found here dynamical changes in the electric field during the gating process, reducing the need to transport physically S4 basic residues far across the membrane and therefore showing support to the transporter model.

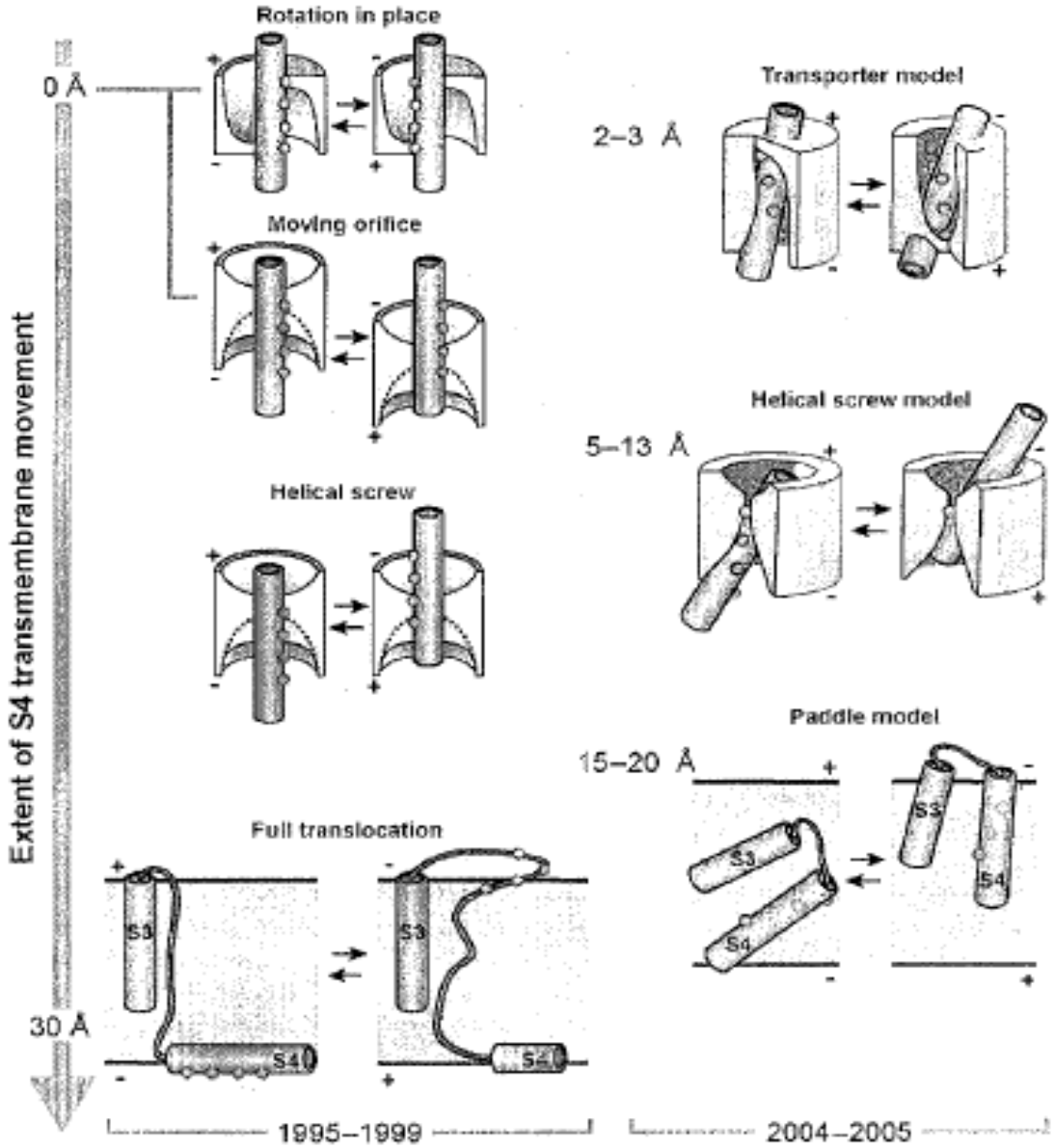

Figure 2.17: Models of the voltage sensor movement. In each model, the resting conformation is represented on the left while the activated conformation is shown on the right. From (Francesco Tombola, Medha M. Pathak & Ehud Y. Isacoff 2006).

Bell et al. used MTSET reactivity experiments to suggest that, in HCN channels, S4 lies in a water-filled gating canal with a very narrow barrier between the external and internal solutions, that the internal crevice is much larger than the external one and argue that this pattern of reactivity is incompatible with the classical gating models or with the KvAP paddle model (Bell et al. 2004)

Ahern and Horn substituted R1 with cysteine and then restored the original charge of S4 by adding positively charged cysteine reactive probes of various length. The shorter the linker, the deeper the charge was moving into the electric field. As soon as the linker reached 4 Å, they found that the contribution of the gating charge was eliminated, leading them to propose that the depth of the electric field between the outside and the position of R1 at rest is ~4 A and 8 Å at most (Ahern & Horn 2005).

Later, luminescence resonance energy transfer (LRET) has been used to monitor the conformational movements of voltage-gated potassium channels in oocyte membranes (Posson et al. 2005). Extracellular domains residues of S4 were labeled with terbium chelates, and the acceptors were subsequently added to the channels by introducing a rhodamine, fluorescein, or bodipy-labeled scorpion toxin that binds to the channel's extracellular pore. Here again, the measured translation distances are no more than 2 Å. Recent FRET experiments using dipycrilamide, a lipid soluble organic anion, as an acceptor and rhodamine as a donor attached at different positions on S4 also find that no large translation occurs during depolarization (Chanda et al. 2005).

It should be noted, however, that most of these experiments show that the electric field is focused within the voltage-sensor domain, and that therefore, a large movement of S4 is not necessary. On the other hand, they do not completely rule it out.

The accessibility to cysteine methods were widely used to test which residues were exposed to the solvent in the different conformational states. A newer variant of the method, involving monitoring the electrostatic field close to R1 in the different states (Elinder et al. 2001) suggested that during activation of the channel, R1 moves from a position far away (>20 Å) to a position close (8 Å) to a S5 residue, the whole extent of the S4 translation being ~12 Å.

Swartz and coworkers used the hanatoxin peptide (HaTx), which binds to the extracellular part of the voltage sensors (to S3 more precisely) and locks the channel in the resting state. They showed that HaTx partitions into the membrane and binds tightly to the voltage-sensor paddle. Using brominated lipids, they conducted fluorescence quenching experiments (with the tryptophan from the toxin) and showed that the toxin does not penetrate deeper that 8Å from the surface (Lee et al. 2003) (Phillips et al. 2005). This led them to think that the VSD paddle moves a relatively small distance. If S4 moves on its own, on the other hand, it is possible that the movement is larger (> 10 Å).

Disulfide scanning experiments were conducted in Shaker, showing further support to the sliding-helix model and supporting a rather large S4 motion (although qualitative) (Broomand 2003) (Gandhi et al. 2003). Ahern and Horn, using their electrical positively charged probes

introduced into the voltage-sensor paddle of Shaker also found a good agreement with the sliding helix model (Ahern & Horn 2004). Using electrophysiology, Tombola et al. find leak currents (called omega currents) through the VSD when mutating specific residues (R1 in the closed state, R4 in the open one) and deduce from these observations that S4 must move ~10-13Å vertically (Tombola, Pathak, Gorostiza, et al. 2006). These very interesting experiments will be described in more details in the paragraph concerning the mutation of S4 residues (paragraph 3.2.3).

Papazian's group coupled electrophysiology and molecular modeling in both ether-à-go-go (EAG) and Shaker (Silverman et al. 2003). They found that two conserved arginines of the S4 voltage sensor move sequentially into an extracellular gating pocket, where they interact with an acidic residue in S2, in agreement with a rather large movement of S4. Grabe's group interpret experiments on human skeletal muscle (hSkMI) Na^+ channels and both Shaker and EAG K^+ channels by finding that the electrostatic profile across the sensor is smoothly varying and that large motions of S4 are necessary to describe the gating charge (Lecar, Larsson, et al. 2003).

After the publication of the Kv1.2 crystal structure (Long, Campbell & MacKinnon 2005a), it was finally possible to make molecular models of good quality and several groups took advantage of this to interpret their data by building models of different channels. The group of Catterall built the first model of the closed state of Kv1.2 using the rosetta membrane method (Yarov-Yarovoy et al. 2006). They explain that the gating movement can be viewed as a sum of two previously suggested mechanisms: translation (2–4 Å) plus rotation (≈180°) of the S4 segment as proposed in the original “sliding helix” or “helical screw” models coupled with a rolling motion of the S1–S3 segments around S4, similar to recent “transporter” models of gating.

Also, early fluorescence-based methods had already pointed to the possible large movements of S4 (Gandhi et al. 2000). Using voltage-clamp fluorometry (Pathak et al. 2007), the group of Isacoff refined the closed-state model proposed above and suggested a molecular mechanism of activation in which S4 rotates by 180 as it moves ‘‘outward’’ by 6–8 Å. Posson and Selvin continued LRET experiments, looking at a larger number of S3 and S4 positions and reached an altogether different conclusion. In their final model, they find rather that S4 moves moderately, by 10 ± 5 Å , 5 ± 2 Å of which are vertical and that this movement is with respect to a static S3 helix (Posson & Selvin 2008).

Finally, even the members of Bezanilla's group deduced from late histidine scanning mutagenesis, disulfide and metal bridges experiments in the Shaker K channel (Campos et al. 2007) that S4 moves relatively to rather static S1 and S2, in an axial rotation of ≈180° and a transmembrane (vertical) movement of ≈6.5 Å, moving the gating charge across a focused electric field.

MacKinnon and coworkers tested various positions in S3b (the extracellular half of S3) and S4 using avidin/biotin binding experiments: because biotin has a length of ~17Å, and because avidin cannot penetrate the membrane, it is possible to test which residues are accessible from

the extracellular medium or from the intracellular medium and if they are less than ~17Å away from the surface (Fig. 2.18). In KvAP, looking at positions 121 and 122 (which correspond to the two amino-acids between R2 and R3), they found that biotin is accessible to avidin from the intracellular side when the channel is closed and from the extracellular side when it is opened. Given the length of the tether to which biotin is attached, and constraints for avidin binding, this binding requires that the paddles move a large distance, which they estimate ~20Å (Jiang, Ruta, et al. 2003) (Ruta et al. 2005). They first argued that these measurements supported the paddle model. One should however note that they are not incompatible with the sliding helix one.

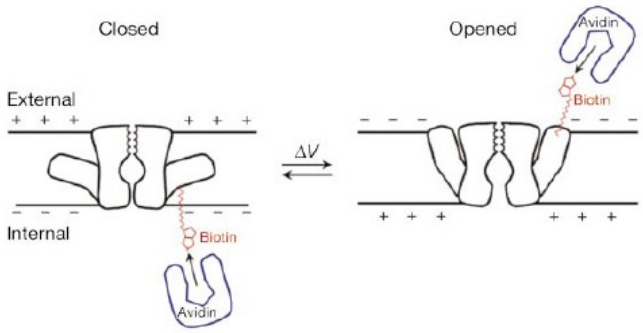

Figure 2.18: Illustration of the avidin/biotin binding experiments. Biotin is attached to a specific position and it is tested wether avidin coming from the extra-cellular medium or from the intra-cellular one is able to bind with biotin. One should note that this scheme represents the paddle model. However, the most recent understanding indicates that such a binding is possible in the case of another model, e.g. the sliding helix one. From (Jiang, Ruta, et al. 2003)

Finally, a recent study using cysteine pairing in S4 and S3b of Shaker (Broomand & Elinder 2008) found that a disulfide bond forms between residues 325 in S3b and 360 in S4 in the closed state, while it forms between 325 and 366 in the open state, leading them to come to the conclusion that S4 slides 16–26 Å along S3b and showing further support to the helical-screw model.

Taken altogether, these results describing the extent of S4 motion might seem contradictory. However, several attempts have been taken at reconciling these various views (Tombola, Pathak & Isacoff 2006) (Jogini & Roux 2007) (Pathak et al. 2007).

1- Experiments have been conducted on different channels, most of them on Shaker, Kv1.2 and KvAP. One should keep in mind that, whereas Kv1.2 and Shaker are very close in terms of sequence and function, KvAP is quite different and that it is possible that the mechanism of gating in the two families varies quite a bit.

2- All the experiments involving mutagenesis introduce an alteration of the structure, the function and probably the dynamics of the channel (Durell et al. 2004). One should always remember that mutating a charge to an uncharged residue, or a small to a much bulkier residue probably introduce changes in the function and experimental results should be treated with

care.

3- Finally, the different experiments that were used introduce biases that can over- or under-estimate the distances that are measured. Indeed, in fluorescence studies small distances contribute more to energy transfer and therefore weigh more heavily on average than larger distances, leading globally to an underestimation of distances (Selvin 2002). On the other hand, avidin binding may lock the channel in extreme positions which are scarcely visited otherwise, leading altogether to overestimation of measured distances (Jiang, Ruta, et al. 2003).

From all the above, we can deduce that the whole experimental body of investigations supports the helical-screw model and points towards translation of S4 of intermediate magnitude.

3.1.3.6 New features are still discovered

The crystal structures of the Kv1.2 (Long, Campbell & MacKinnon 2005a) and of the Kv1.2/2.1 paddle chimera (Long et al. 2007) have shown that the VSD is embedded in the membrane, S4 being mostly shielded away from the lipids. However, in this open state, the top gating charges R1 and R2 seem to come in interaction with the lipids head-groups, making stable electrostatic interaction with the phosphate negatively charged groups. Prior to the crystal structure determination, Cuello et al. using site-directed spin labeling and electron paramagnetic resonance spectroscopy showed that the S4 segment of KvAP is likely located at the protein/lipid interface (Cuello et al. 2004). MacKinnon and coworkers inferred also from the study of the action mechanism of a voltage-sensor toxin (VSTX1, from the Chilean Rose Tarantula) that the sensor in voltage-dependent K^+ channels had to be located at the membrane–protein interface (Lee & MacKinnon 2004). Further evidence came later from the fact that modifying the lipid headgroup (most particularly removing the phosphate group) altered the function of Kv channels, proving the importance of S4/lipid interactions (Schmidt et al. 2006) (Ramu, Xu, et al. 2006) (Xu, Ramu, et al. 2008)

The fact that negatively charged residues constitute binding sites for S4 basic residues has been known since a long time. In Shaker, E^{283} in S2 and R^{368} and R^{371} in S4 on one hand and K^{374} in S4 and E^{293} in S2 and D^{316} in S3 on the other form a network of strong, local, electrostatic interactions that stabilize the structure of the channel in the two extreme states (open and resting respectively) (Fig. 2.19) (Papazian et al. 1995) (Tiwari-Woodruff et al. 1997).

Using charge reversal mutagenesis, Zhang et al. found the same kind of interactions in the HERG channel (Zhang et al. 2005). A most direct evidence came from the groups of Catterall and of Cui, who probed interactions in different channels, and found that ion pairs form within the VSD in a sequential manner. Charge reversal mutagenesis in Kv7.1 (Wu, Delaloye, et al. 2010) and disulfide locking in NaChBac (a bacterial voltage sensitive sodium channel of which the VSD is very similar to that of K^+ channels) (DeCaen et al. 2009) showed that the S4 segment moves outward during activation from an inward position in which R1 interacts with

E2 (in S2) to an outward position in which R4 interacts with E4, and the R1–R4 gating charges interact sequentially with E2 and then E4 to form ion pairs as S4 moves (Catterall 2010).

Finally, noting that F^{233}, a phenylalanine pertaining to S2, was very conserved in all classes of Kv channels, a combination of a large number of experiments, including mutations with natural and unnatural amino acids, MacKinnon and coworkers used electrophysiological recordings and X-ray crystallography to show that this residue plays the role of a *charge transfer center* that facilitates the movement of positively charged amino acids across the membrane field (Tao et al. 2010). They find that the S4 basic residues go through this transfer center one at a time during activation. The authors posited accordingly that the Kv1.2 channel has three intermediate kinetic states between the closed and the open channels.

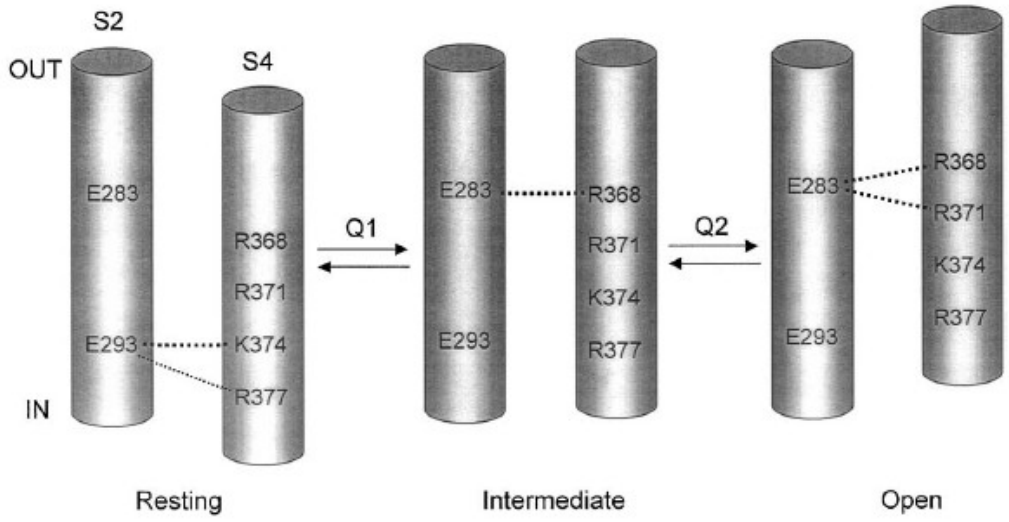

Figure 2.19: Model of putative salt bridges between negatively charged residues of the S2 helix and positively charged residues of the S4 helix in the Shaker channel. The S2 and S4 transmembrane helices are as indicated in the first pair of helices. The S3 helix is omitted for clarity, but is also thought to participate in the same interactions as residue E^{293}.Each pair of helices represents a different gating state of the channel. 'Q1' and 'Q2' denote the two separate gating charge components. From (Fedida & Hesketh 2001).

This view has been complemented by Bezanilla and coworkers who have conducted electrophysiology experiments in Shaker F^{290} mutants (analogs of Kv1.2 F^{233} mutants), of which the results suggest that the conserved phenylalanine residue controls the transfer of R4 during gating while not affecting the movement of the other three gating arginines (Lacroix & Bezanilla 2011).

The hypothesis that S4 adopts a 3_{10} helix structure during deactivation (Kosower 1985) has been left out when the Kv1.2 crystal structure was released because in this activated state (Long, Campbell & MacKinnon 2005a), the S4 helix was in the form of a regular α-helix. The Kv1.2/2.1 chimera structure (Long et al. 2007) on the other hand, displayed a 10 residue 3_{10} helix stretch in the middle of S4 and the MlotiK (a non-voltage dependent channel that also

has an auxiliary domain resembling the VSD of Kv channels) structure in which 11 residues at the S4 C-terminus displayed a 3_{10} helix conformation in the activated state (Clayton et al. 2008) reinstated the idea that S4 might go from α-helix to 3_{10} helix during channel activation. It was realized later by Villalba-Gaelea et al. that Kv channels have three separate states: resting, active (corresponding to the real open state) and relaxed (corresponding to an open-inactivated conformation, possibly the one captured in X-ray structures reached after prolonged depolarization) (Villalba-Galea et al. 2008). The authors suggest that S4 is in a 3_{10} helix conformation in the resting and active state and in a α-helix conformation in the relaxed state, as found in the X-ray crystal structure. Shafrir et al. (Shafrir et al. 2008) also revived this hypothesis when they proposed models of the open and closed state of the NaChBac that involved secondary structure changes of S4.

From an purely structural point of view, the hypothesis of a 3_{10} helix makes sense because it enables to align the basic residues and to slightly extend S4, allowing for salt bridge contacts with the S2 and S3 negative charge without resorting to large rotation and tilt of S4. The 3_{10} helical structure, however, is not very stable energetically and as a result is rarely found in membrane proteins. It has been suggested that it could be stabilized by the TM electric field (Swartz 2008). Simulations recently focused on this issue (Khalili-Araghi et al. 2010) (Schwaiger et al. 2011) The findings will be presented in more detail in paragraph 3.3.1.

3.1.3.7 Molecular models of the VSD deactivation are proposed

To date, only the structure of the activated voltage sensor has been determined. (Long, Campbell & MacKinnon 2005a). In order to have a complete view of the process associated with the response to depolarization, and in particular to develop models of the resting state, structural modeling has been used. Hence, the resting state structure of Kv1.2 was proposed on the basis of the ROSETTA Membrane ab initio structural modeling program (Yarov-Yarovoy et al. 2006). Relaxation of the model in a membrane environment using molecular dynamics simulations revealed a second resting state structure with the S4 segment drawn even farther toward the intracellular side of the membrane (Pathak et al. 2007). Independently, Grabe et al constructed a down state model of the channel using six pairs of interacting residues as structural constraints and verified this model by engineering suppressor mutations on the basis of spatial considerations (Grabe et al. 2006) and Tombola et al. proposed yet another model of the resting conformation of the VSD of Kv1.2 that they tested using leak current measurements consecutive to S4 mutations (see paragraph 3.2.3) (Tombola, Pathak, Gorostiza, et al. 2006).

In 2008, Clayton et al. solved the structure of MlotiK in its closed state (Clayton et al. 2008). In this non voltage gated potassium-selective channel, the first for basic residues of S4 are replaced by uncharged residues. In addition, two of the acidic countercharges are also absent in this channel. Although differences with a voltage-gated channel are expected, this structure provides us with a good idea of what a closed Kv channel looks like, mostly in the pore region. The packing of the VSD domain and the interaction between the VSD and the pore on the other hand seem to be quite different than the ones in VGCs. Anyhow, this

structure shows that it is possible to find a rather long stretch of S4 in a 3_{10} helix conformation.

Finally, models of the resting states of other channels (Hv1, NaChBac and the plant KAT) channel have also been derived from homology modeling methods, using among others, the MlotiK structure as templates (Shafrir et al. 2008) (Schow et al. 2010). All these models bear similarities, in that they place S4 in a low position with respect to the activated state and that the bundle made of S1-S3 is rather static, in agreement with the helical-screw movement. The total extent of the S4 movement, however, varies among the models from ~10 to ~20Å. More models of the Kv1.2 and its response to depolarization have been derived. These are more thoroughly described in the next part dedicated to this particular channel.

3.2 Modulation and dysfunction of the VSD

3.2.1 Means of modulation of VSD function

The "normal function" of Kv channels can be altered by a variety of factors. The first of these is a naturally occurring phenomenon that has been observed for a long time in some channels: inactivation. Phenomenologically, electrophysiology measurements have shown that some channels stop conducting when they are submitted to prolonged depolarization, leading to inactivating currents (*e.g.* the Na^+ current presented in the previous part). Their gate remains open but the channels lie essentially in a non-conductive state. Two types of mechanisms have been identified: N-type inactivation, or fast inactivation, has been attributed to the blockade of the pore by an inactivation peptide, pertaining either to the C-terminus of some channels, or to auxiliary β subunits that interact with the channel's intracellular tetramerization (T1) domain. C-type inactivation, or slow inactivation, on the other hand is attributed to a conformational change in the selectivity filter. These naturally occurring phenomena confer to the channels the ability to become non conductive, even in an open state.

As VGCs are essential to the proper function of excitable cells, they constitute the primary targets of drugs, whether naturally present as in the poison (toxin) of some animals and plants, or of synthetic curative drugs used in medicine. The most frequently used drugs in therapy today are blocking drugs (local anesthetics, antiarrhythmics, antiepileptics). Nearly all bind inside of the pore or at the channel extracellular entrance, blocking thereby ion conduction (Rodríguez de la Vega et al. 2003). Due to the conservation of the pore domain among the voltage gated ion channel family, they are not highly selective to one special category of ion channels. For others, a mechanism of inhibition has been proposed in which anesthetics dissociate the channel by changing the lateral pressure of the membrane (van den Brink-van der Laan et al. 2004). This corresponds to anew inhibition mechanism still largely unknown at the molecular level. It is possible that some antagonists such as toxins share at least to a certain extent this indirect mode of action (Lee & MacKinnon 2004).

To target specifically one channel, current efforts are devoted to finding drugs that target

the VSDs, which have a greater diversity in terms of sequence. It is interesting to note here that natural toxins, such as scorpion HaTx already target the VSD in a highly specific manner and prevent the gating by hindering the deactivation of these domains.

3.2.2 Modulation by lipids

Another mean of modulating the function of ion channels is acting on the lipids interacting with the channels. As has been stated above, the top gating charges interact with the lipid head-groups in the open state of the channel. When these lipids are modified, the channel function is in turn altered (Schmidt et al. 2006). There are natural enzymes (*e.g.* sphyngomyelinase) that use this mechanism to hinder the function of Kv channels. Approaching from the extracellular side of the channels, these enzymes chemically transform the lipid head-groups Enzymes that remove the choline group from the lipids, leaving the negatively charged headgroup favor the open state of the channel (*e.g.* Smase D), whereas the enzymes that remove the entire headgroup of the channel, leaving no phosphate group to anchor R0 and R1, favor the closed state of the channel (*e.g.* Smase C) (Ramu, Xu, et al. 2006) (Xu, Ramu, et al. 2008). Other types of lipids are known to modify the function of VGCs. Phosphatidylinositol-4,5-bisphosphate (PIP2) is known to modulate the function of cardiac ion channels such as Kir6.2, Kir2.1, Kv11.1 (hERG), and Kv7.1 (KCNQ1) (Park et al. 2005)(Rodriguez et al. 2010) (Huang et al. 1998) (Bian et al. 2001) (Hilgemann & Ball 1996) (Zhang et al. 2003)

3.2.3 Single point mutations

Finally, mutations in the sequence of voltage gated ion channels lead to alteration of the function of VGCs and some lead to the appearance of leak currents through the VSD.

3.2.3.1 Channelopathies

A large number of diseases is due to the dysfunction of VGCs, following from inherited genetic mutations in their genes. The first that were described concerned neuromuscular disorders but we now know that they can affect a variety of other areas (tissues of any excitable cell) such as the heart, the muscles...

It is interesting to note that one gene encoding a particular ion channel can suffer from various mutations, causing either the same disease, or a different one. For example, the Kv7.1, encoded by the KCNQ1 gene and found in the heart cells, totalizes 49 mutations that lead to 5 different phenotypes: long QT syndrome types 1 and 2, short QT syndrome, Jervell and Lange-Nielsen syndrome 1 or atrial fibrillation (Online Mendelian Inheritance in Man (OMIM) database).

Usually these mutations can be spread throughout the ion channel sequence, in the voltage sensor domain, the pore, or in the N- and C-termini domains, leading to molecular scale

effects that should be drastically different. In this work, we focus on the mutations within the VSD, and most particularly affecting the S4 basic residues.

3.2.3.2 "Omega" leak currents

Mutations of the charged residues of S4 in K^+, Na^+ or Ca^{2+} voltage gated ion channels have been shown to impair cellular function and have been linked to a large number of inherited channelopathies leading to epilepsy, long QT syndrome, and paralyses (Lehmann-Horn & Jurkat-Rott 1999). Most of these mutations modify the physical properties of VGCs, *e.g.* sensitivity to voltage changes, which in turn alters conduction through the central (alpha) pore (Bao et al. 1999) (Jurkat-Rott et al. 2000) (Soldovieri et al. 2007)

Recently, however, specific mutations have been identified that lead to the appearance of another current component aside from the alpha conduction. This so-called "omega" or gating-pore current was attributed to a non specific leakage of cations through a conduction pathway within the VSD, indicating that R1 in the S4 segment of Shaker sterically hinders ion passage through the gating-pore (Tombola, Pathak, et al. 2005). Substitution of the latter in the voltage sensor with histidine, R1H, allows a H^+ current to flow at hyperpolarized potentials (Starace & Bezanilla 2004), while a R4H mutant allows a proton flux at depolarized potentials (Starace & Bezanilla 2001). Moreover, mutations of R1 into smaller, uncharged residues give rise to an influx of a non-selective cation current, called "omega current", through an unidentified yet pathway through the VSD (Tombola, Pathak, Gorostiza, et al. 2006).

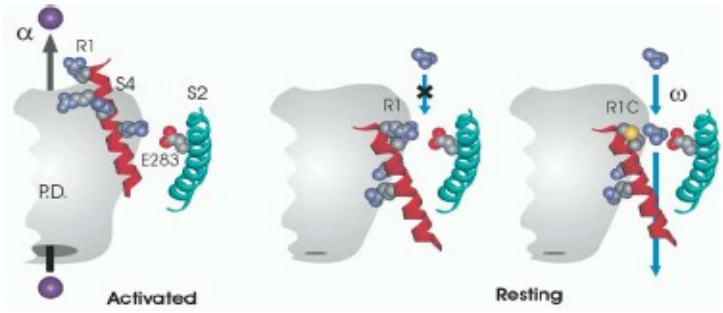

Figure 2.19: Proposed location of the omega pore within the VSD by Tombola et al. 2005: Model of S4 and S2 lining the omega pore. An inward helical-screw motion of S4 ratchets R3, R2, and R1, successively, into the position occupied by R4 in the structure until R1 faces E^{283} in the resting state. Substitution of R1 with smaller side chains opens the pathway for ion flux at rest. The S4 helix is shown up to position G^{381} in Shaker (KvAP G^{134}). Side chains displayed in space-filling CPK scheme.

In Na^+ VGCs, such currents were correlated with mutations that cause normo- and hypo-kalemic periodic paralysis (Sokolov et al. 2005) (Sokolov et al. 2007) (Struyk & Cannon 2007) (Sokolov et al. 2008). Interestingly, in this channel, mutation of residues R2 or R3 in one of the four S4 helices allows an influx of cations through the omega pore in a state-

dependent manner: the omega current is observed only when the channel is in its hyperpolarized conformation. Under depolarization, the omega pore closes and the canonical ion-selective pore opens.

3.3 Specific VGCs of interest

In this work, we have focused on a few channels. We naturally started off with the Kv1.2 channel, the only channel for which a high resolution crystal structure (2.9 Å) was resolved (Long, Campbell & MacKinnon 2005a). As such, it was the first that was possible to study on a molecular level using molecular dynamics simulations (MD) without resorting to homology modeling. It served us as a paradigm for the entire Kv family during the whole first part of the study. After elucidating the function of this prototype, we moved to members of the Kv7 sub-family because of their potential as targets for drugs their mutations -such as the ones described above- are responsible for genetic diseases.

3.3.1 The Kv1.2 as a prototype

The first Kv1 sequence was found in the fruit fly Drosophila melangoster and was named Shaker because mutation of the gene encoding this channel led to restless flies with shaking legs. Since then, several vertebrate potassium channels with similar amino acid sequences were found and the family now consists of at least 6 genes (encoding Kv1.1, Kv1.2, Kv1.3, Kv1.4, Kv1.5 and Kv1.6) which are mostly expressed in the brain, but can also be found in non-excitable cells, such as lymphocytes. Among them, the Kv1.2 is a channel member of this Shaker family encoded by the KCNA2 gene, that is uniformly distributed in the heart and brain. In the Kv1.2 sequence, S4 has six positively charged residues, from intra- to extracellular position, 4 arginines, 1 lysine and 1 more arginine (R1, R2, R3, R4, K5 and R6). The group of MacKinnon succeeded in 2005 to crystallize the Kv1.2 channel from the rat brain in complex with a β subunit (Long, Campbell & MacKinnon 2005a) and resolved the structure of the entire complex at a 2.9 Å resolution. This structure was also refined by applying a novel normal-mode-based X-ray crystallographic refinement method, which enabled to bring up large parts of the 37% missing densities (Chen et al. 2010).

3.3.1.1 The tetrameric assembly

Preceding the first S1 TM segment, the N-terminus of Kv1.2 has a large N-terminus intracellular domain (T1 domain). The domains from each of the four subunits of the Kv1.2 channel come together to form the tetramerization domain at the intracellular membrane surface. This domain is a docking site for β subunits, a tetrameric whose particular role has not been revealed yet but that seems to have a role in the catalytic activity of aldo-keto reduction (Sewing et al. 1996) (Yu et al. 1996). In the Kv1.2 crystal, it seems that this auxiliary subunit was very important to enable contacts between the proteins of different cells. The global structure has an *I4* symmetry, the four-fold symmetry axis running through the

center of the main pore. The dimensions of the tetramer are 135x95x95 $Å^3$. In the direction perpendicular to the membrane, the transmembrane domain extends by ~30 Å and the T1/β subunit by ~40 Å. As expected, the pore domain, formed by the S5-S6 segments are quite similar to the KscA pore. The VSDs on the other hand, are organized in an unexpected manner with respect to the pore: the VSD of one subunit sits next to the pore domain of the adjacent subunit (Fig. 2.20) and the connection between the VSD and the pore of the same subunit is made by the S4-S5 linker, a α-helix that is located at the bottom membrane layer/solution interface, perpendicular to the membrane plane. The VSD structures are described in more detail below

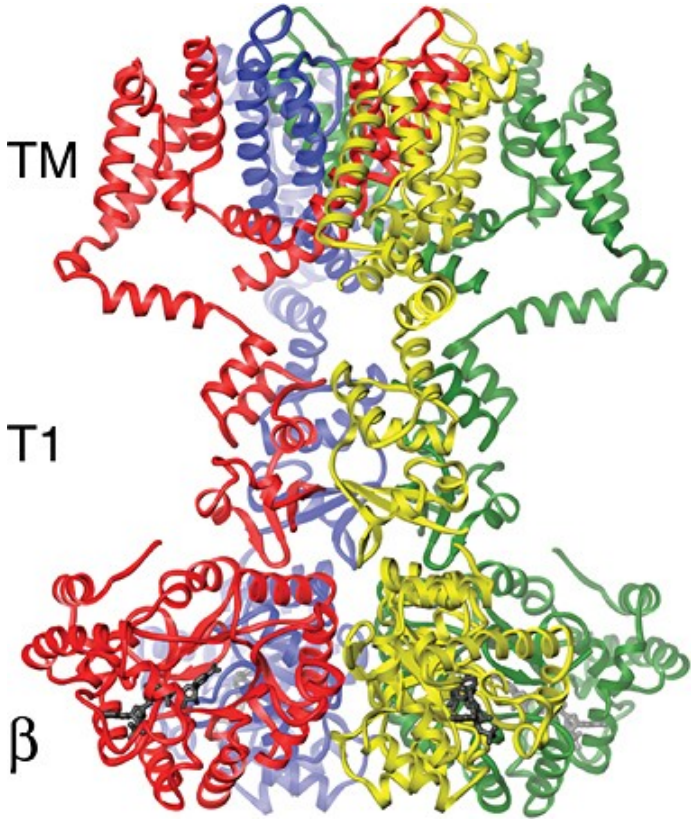

Figure 2.20: Side view of the Kv1.2/β subunit complex in a ribbon representation. The four subunits of the channel are colored uniquely, highlighting the arrangement of the VSDs with respect to the pore. TM indicates the location of the pore domain, T1 and β the location of the intracellular transmembrane domain and of the β subunit respectively. From (Long, Campbell & Roderick MacKinnon 2005a).

3.3.1.2 Open pore and inactivation peptide binding site

As in other ion channels, the pore domain is divided into two major regions: at the extracellular side, the selectivity filter controls the passage of ions and favor the transport of K+ with respect to other ions whereas at the intracellular side, the gate defines the open and closed state of the channel. The selectivity filter of the Kv1.2 is very similar to the one of other ion channels, such as the KscA described above.

The rest of the pore domain, however, is quite different. Based on the diameter of the pore at the bundle crossing (~12 Å), the pore lies in an open state. The inner helix of the pore (S6) contains the amino-acid sequence Pro-Val-Pro, conserved among Kv channels, and this area shows a kink in the helix, leading the C-terminus to be more parallel to the bilayer plane than the rest of S6. This kink is thought to be important for coupling of the VSD to the gate and for the actual gating of the channel (Long, Campbell & MacKinnon 2005b).

The S1 segment is separated from the T1 domain by a linker that was not resolved in the initial structure, but whose function seems to be to space the tetramerization domain from the rest of the channel. The ions or then have to go through the portals (15 to 20 Å wide) defined by these linkers to reach the gate and later the selectivity filter. These regions are also important for the N-type inactivation (or fast or "ball and chain" inactivation) of the channel that occurs after prolonged depolarization (see paragraph 3.2.1). The inactivation peptide, that belongs to the N-terminus of the β subunit for example, has to go through these portal to reach its binding site within the pore. The crystal structure provides an idea of the mechanism associated with this inactivation: the authors show that there is a region located ~10 residues from the N-terminus that is rich in negative amino acids that could bind to the positively charged at the T1 surface. The N-terminus itself is hydrophobic and should locate within the open pore.

3.3.1.3 VSD structure and coupling to the pore

Electron densities are weak in the VSD region. The backbones were easily identified as TM alpha helices but the side chains were not all resolved: most side chains are present in the model on S2, S4 and the S4-S5 linker but S1 and S3 were built as polyalanine helices. The loops connecting the helices were also omitted in the original structure model. The S1-S4 bundle shows a rather tight packing, in sharp contrast with the KvAP structure (Jiang, Lee, et al. 2003) and S1 to S4 are all perpendicular to the membrane plane.

In the refined structure (Chen et al. 2010), as well as in the paddle chimera (Long et al. 2007), the side chains and the loops are refined, enabling a better characterization of the VSD. In the two structures, the S4 basic residues and the negative residues of S1-S3 are quite well aligned. Importantly, R3 is engaged in a salt bridge with E^{183}, R4 with E^{226}, K5 with D^{259} and R6 with E^{236}, while R1 and R2 face the lipid head-groups of the top bilayer. This corresponds to an activated state of the VSD, in agreement with the open pore state.

Both structures have revealed the presence of a hydrophobic layer in the midpoint of the VSD. This layer is ~10 Å thick and is composed of 10 completely buried residues V^{172}, I^{173}, S^{176}, I^{177}, F^{180} on S1, C^{229}, I^{230}, F^{233} on S2 and A^{262} and I^{263} on S3. This zone is thought to be important for the shape of the electric field: it could enable focusing the transmembrane field and help reduce the extent by which S4 needs to move to account for the total gating charge (see methods, paragraph 4.2).

The coupling between the VSD and the pore occurs through the amphiphatic helix bridging between S4 of the VSD and S5 of the pore (S4-S5 linker). This linker is located along the

pore, with its hydrophilic face facing the solution and hydrophobic face facing the hydrophobic core of the membrane. Importantly, it crosses over the top of the S6 inner helix from the same subunit and makes many amino-acid contacts with it. The kink in the S6 helix makes the bottom half of S6 a "receptor" for this linker. When the channel is submitted to a hyperpolarized TM voltage, S4 is thought to move down and exert a pressure on the S4-S5 linker , which will in turn press on the S6 helix, causing the gate to close.

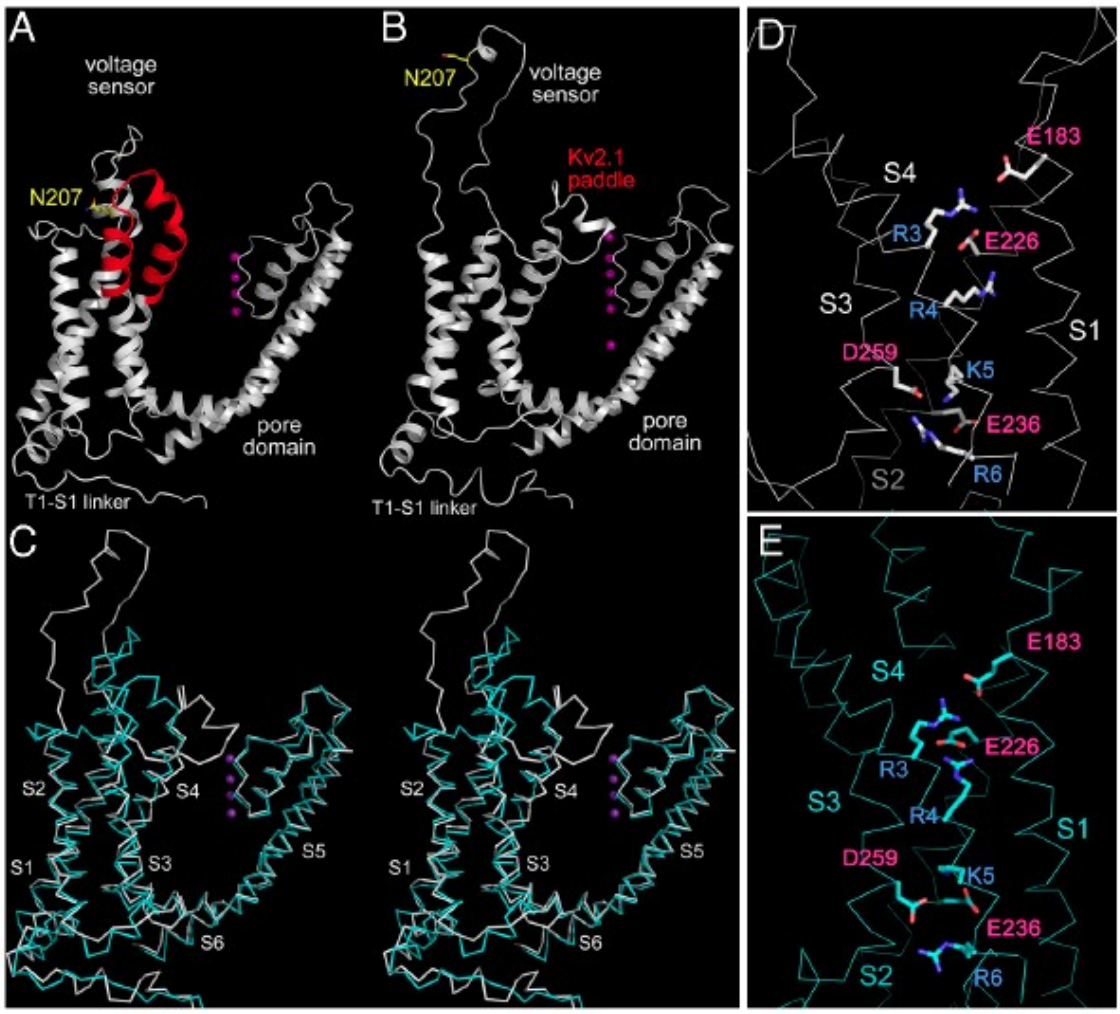

Figure 2.21: Comparison of the transmembrane portions of the final Kv1.2 structure and the paddle-chimera structure. (A) Ribbon diagram of the paddle chimera structure with the chimera paddle region colored in red. (B) Ribbon diagram of the final Kv1.2 structure. (C) Stereo view of the superposition of transmembrane portion of the final Kv1.2 structure (White) and the paddle-chimera structure (Cyan). Potassium ions are shown as purple spheres in A–C. (D) The voltage sensors of the final Kv1.2 structure (White). (E) The voltage sensors of the paddle-chimera structure (Cyan). Key residues were shown as sticks for positive gating charges (Blue) and their interacting negatively charged residues (Red). From (Chen et al. 2010).

3.3.1.4 Results from Molecular dynamics (MD) studies

The resolution of the crystal structure of the Kv1.2 channel has provided the MD community with the first really trustworthy starting conformation to investigate the dynamical properties of a Kv channel. Accordingly, as soon as the Kv1.2 structure was published, several groups (including ours) embedded the channel in a membrane/solution environment and set out to investigate the structural, dynamical and electrical properties of the latter.

3.3.1.4.1 Results on the pore

The crystal structure of the Kv1.2 represents the open state of the channel, enabling the conduction of K^+ ions through the main pore. The first MD studies showed that the pore volume is large enough to let ions through and that the conduction pathway seems to involve going through the S1-T1 linkers (Treptow & Tarek 2006). Along the S6 segment, MD simulations enabled the identification of V^{478} as the residue constituting the main gate (Treptow & Tarek 2006). Furthermore, coupling between the position of S4 and the state of the pore was carried out showing that gating involves the S4-S5 linker that brings S6 in its open/closed position through salt bridges between a positive charge at the end of S4 and a negative charge at the end of S6 (Nishizawa & Nishizawa 2009). Finally, the permeation mechanism through the selectivity filter of the Kv1.2 was thoroughly examined (hundreds of events were sampled) revealing a "knock on" mechanism in which translocation of two ions is driven by a third ion (Jensen et al. 2010).

3.3.1.4.2 Focused electric field

Gating charges environment: a lot of focus was dedicated to the elucidating of the environment of the S4 basic residues. First, several groups reconstructed the missing side chain residues and observed the following properties: R1 and R2 are turned towards the lipid head-groups and seem to interact with the lipids in the open state (Sands & Sansom 2007). Because water crevices protrude into the VSD from the intra- and the extra-cellular media, all the S4 basic residues lie in a solution environment, rationalizing the focused electric field necessary to transport 12-14e during activation (Treptow & Tarek 2006) (Jogini & Roux 2007) (Freites et al. 2006) (Nishizawa & Nishizawa 2008) (Krepkiy et al. 2009). Using continuum electrostatic computations, Jogini and Roux determined that the TM potential sensed by the S4 basic residues varies mostly over the outer half of the membrane ("focused electric field"), and they further calculated that assuming such an electric field, a 10-15 Å vertical translocation of S4 was needed to account for the 12-14 e gating charge.

3.3.1.4.3 Response to hyperpolarization

Starting from 2008, attention was devoted to the closed state and the VSD mechanism associated with the deactivation of the channel. Two strategies were adopted: the first was to simulate the open (crystal structure) and closed (homology model of (Pathak et al. 2007)) channel and investigate the changes between both. The second was to submit the open conformation to a hyperpolarized TM potential and observe the rearrangement consecutive to such an application.

Using the model by Pathak et al., Han and Zhang observed a variety of properties and their differences over 45 ns simulations of the open and closed state channel (stability, environment of the S4 basic residues, salt bridge arrangements, and further interactions between the VSD and the pore), concluding that only the sliding helix model could enable going from one to the other state (Han & Zhang 2008). Khalili-Araghi et al. pushed the calculations further (over 0.5 μs) and using continuum electrostatic calculations, measured the total gating charge associated to the activation of the channel (12 to 13e, provided one considers S4 in a slightly lower position than originally proposed by Pathak et al.) and revealed that a large portion of S4 seems to be in a 3^{10} helix conformation, also in agreement with other results from simulations (Bjelkmar et al. 2009) (Schow et al. 2010), enabling salt bridge interaction of most S4 basic residues with S2/S3 acidic residues in the closed state and that the applied electric field varies rapidly over a narrow region of 10-15Å in the outer leaflet of the membrane, allowing the transport of 12 to 13 e without full translocation of S4 across the membrane (Khalili-Araghi et al. 2010).

Applying a hyperpolarization to the membrane, on the other hand, was conducted by at least 3 groups. Two of them adopted the electric field method, in which a external force is applied to charged residues of the system (see chapter 3). Nishizawa et al. found that applying a strong electric field (0.1 V/nm) to an isolated Kv1.2 VSD resulted in a displacement of S4 in a screw-like axial rotation, S4 basic residues formed serial interactions with E^{183} and E^{226} and that the total extend of S4 translation amounted to 6.7 A. They identified two intermediate states, which they find to be in good agreement with kinetic models such as the ZHA one (Nishizawa & Nishizawa 2008). The group of Lindahl led a very long simulation (1 μs) of an entire Kv1.2 channel (Bjelkmar et al. 2009). They found a large rotation of S4 (120°), changes in hydrogen bonding patterns and as mentioned above, extension of 3^{10} helix stretch but almost no translation of S4. They imply that the final downwards translation that is necessary to complete the deactivation process is partly entropic explaining the slow nature of the process. The same authors also investigated the energetic cost of dragging S4 basic residues downwards when S4 is in a 3^{10} helical conformation when compared to a α-helical one (Schwaiger et al. 2011) using steered MD and applying the Jarzynski equation. For the first transition, *i.e.* when R4 passes through the gating charge transfer center, they find that the free energy is ~twice lower with the 3^{10} helix conformation and leads to less distortion of the rest of the VSD, leading them to support the hypothesis according to which S4 adopts a 3^{10} helix conformation during activation/deactivation.

Finally, another strategy was adopted by our group, using explicit ion dynamics to apply a hyperpolarising potential (Treptow et al. 2009). This enabled observing the first step of the response of the Kv1.2 to hyperpolarization (rotation of the top S4 and first rearrangement of the salt bridges in a collective downward motion of the S4 basic residues). This procedure also enabled the direct calculation of the gating charge associated to the first step of the response (~-0.45 e per subunit) and the elucidation that S4 basic residues are responsible for most of the transport of the gating charge.

3.3.2 The Kv7 family

The Kv7 family, which is encoded by the KCNQ gene, has a great physiological role, as the five members of this family Kv7.1, Kv7.2, Kv7.3, Kv7.4 and Kv7.5 can be found in the heart, brain, muscles, stomach, inner ear and others… As such, they have been more and more studied as potential targets to treat diseases coming from the alteration of membrane excitability (Miceli, Soldovieri, Martire, et al. 2008). Furthermore, four of the five members of this family were found to be implicated in channelopathies, leading to long QT syndrome, neonatal epilepsy, neuromyotonia… (Maljevic et al. 2010).

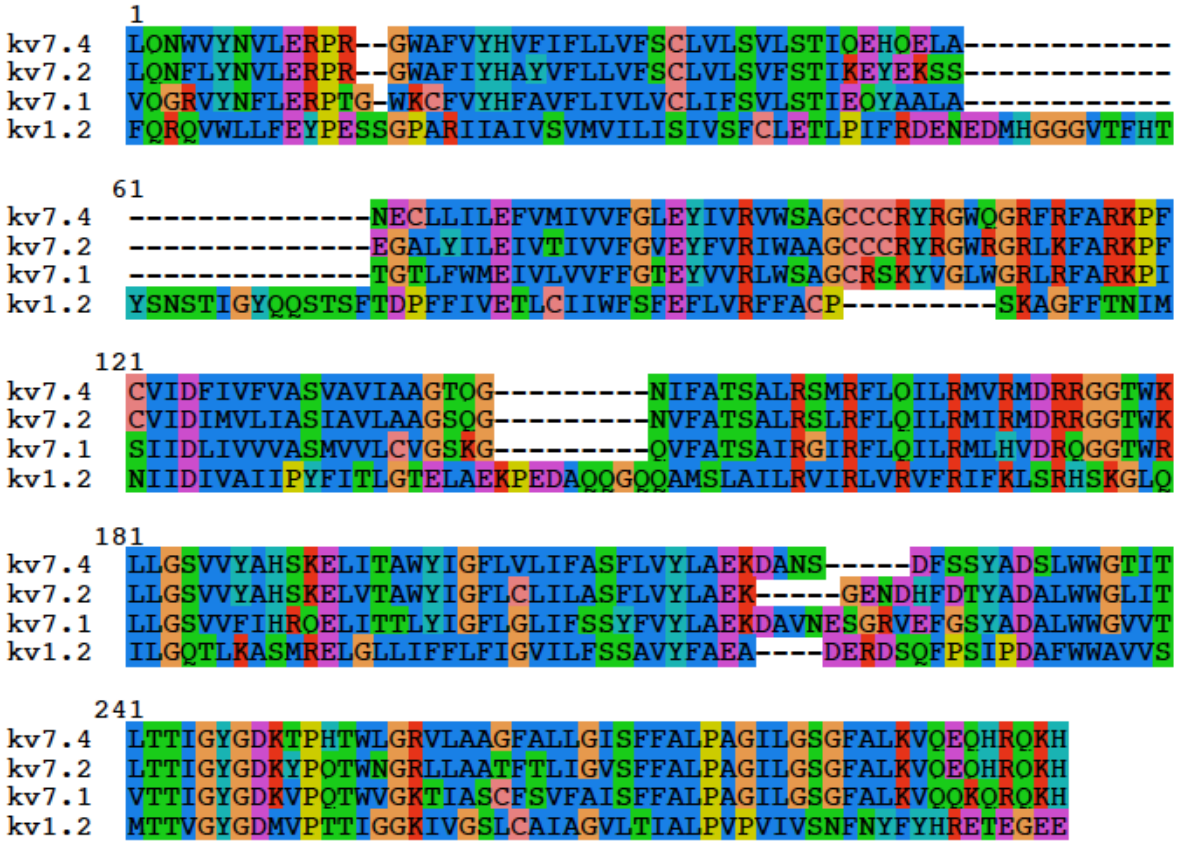

Figure 2.22: Sequence alignment of the Kv7 with the Kv1.2 of known structure highlighting the importance of S4 basic residues and of the two acidic countercharges of S2.

The channels pertaining to this family have the same 6 TM segment topology than other members of the Kv channel family, *i.e.* S1-S4 constituting the VS domain and S5-S6 making up the pore domain. A particularity of these channels, with respect to others of the Kv family is their large C-terminal, intracellular domain: four segments were identified as conserved helices (Helices A to D). Helices C and D are important for the tetramerization of the channel (Xu & Minor Jr. 2009) (Howard et al. 2007), and help explain why $K_V7.1$ does not tetramerize with other members of the Kv7 family. Helices A and B on the other hand constitute a

recognition pattern for calmodulin, a small soluble Ca^{2+} binding protein, that helps relay the cytosolic Ca^{2+} signal (Yus-Nájera et al. 2002). Through an unknown mechanism, it seems that Kv7.1 channels are stimulated by an increase of intracellular Ca^{2+} concentration via calmodulin (Bai et al. 2005) (Shamgar et al. 2006). Kv7.1 channels activity has further been shown to to be modulated by a change in PIP2 concentration, a lipid bearing two negative charges, but the molecular process involved remains unknown (Suh & Hille 2008). All this activity and modulation due to C-terminal structure is beyond the scope of this study and will not be further discussed. Such channels also have a tendency to associate with β-subunits, characterized by their ability to alter the conduction properties of Kv channels. The most important of these is the subunit encoded by the KCNE genes.

In Kv7.1, the S4 segment contains 4 gating charges (Fig. 2.22), which is the lowest number found in the Kv family. Indeed the sequent alignment shows that when compared to Kv1.2, R3 is replaced by a glutamine and K5 by a histidine, leaving only four arginines, R1, R2, R4 and R6. In Kv7.2 and Kv7.4, five gating charges are present, only R3 is replaced by a glutamine. In both cases on the other hand, the four negatively charged residues of S1-S3 are conserved. A recent charge reversal mutagenesis study revealed that, as suspected in other VGCs, in K_v7.1, one of the negatively charged residues of S2, E2 interacts with various S4 gating charges (R1 to R4) in a state-dependent manner (Wu, Delaloye, et al. 2010). As in the Kv1.2 crystal structure, R4 is close to E2 in the open state whereas R1 seems to be close to E2 in the resting state. They therefore conclude that E2 is engaged in electrostatic interactions with S4 arginines in a sequential manner during S4 movement during activation.

Homology models of the Kv7.1 channel have been proposed mostly by the team of C. Sanders. The open state model was built on the basis of the Kv1.2 X-ray structure whereas the closed state model relies on the closed state of the same Kv1.2 model proposed by Yarov-Yarovoy et al, (Yarov-Yarovoy et al. 2006). They used these models to locate the residues that were mutated in channelopathies. They further proposed models of the interaction between Kv7.1 and KCNE1 (Kang et al. 2008) (Van Horn et al. 2011)

Electrophysiology experiments on members of the Kv7 family revealed the following information: the macroscopic gating current has very slow kinetics, both during activation and inactivation (Adams et al. 1982) (Safiulina et al. 2008). Recently, and despite technical challenges related to the low expression levels of Kv7 channels in the plasma membrane, gating currents measurement were successful in two members of the family Kv7.4 and Kv7.5 (Miceli, Soldovieri, et al. 2009). The per channel gating charge, on the other hand, was never measured due to difficulties to count precisely Kv7 channels in the plasma membrane. On the other hand, the authors infer from their results that in Kv7.4, VSD movement is followed by a slow and/or low bearing charge step leading to pore opening.

Interestingly, whereas mutations leading to channelopathies have been identified over the entire sequence of Kv channels, two members of this family, the Kv7.1 and the Kv7.2 were found to be affected by mutations in the S4 region, and most particularly at the level of the S4 basic residues. In Kv7.1, which is a channel that is found mainly in the heart, Lupoglazoff et al reported that the mutation of R^{231}, the second arginine of S4, into cysteine led to Long QT

syndrome of type 1 and to Fetal brachycardia (Lupoglazoff et al 2003). Mutation of the second and fourth arginines of S4 (R^{207} and R^{214}) in the Kv7.2, a channel mostly present in the brain led to Benign Neonatal Familial Seizures (BNFS), myokymia and Peripheral Nerve Hyperexcitability (PNH) (Dedek et al. 2001) (Castaldo et al. 2002) (Wuttke et al. 2007). Moreover, a mutation of a negative residue in the VSD of Kv7.1, $E^{160}K$, was also shown to lead to long QT syndrome (Splawski et al. 2000).

Electrophysiology measurements of S4 gating charge mutants of the Kv7.2 channel were recently reported (Miceli, Soldovieri, Hernandez, et al. 2008). These indicate that every S4 gating charge is important for the voltage-dependent gating of Kv7.2 in the sense that they all modify the G/V relationship. Mutation of R2 (R^{201}), especially yielded channels that "behaved as K^+-selective leak channels that were largely open at all test potentials." Mutation of R3 (R^{207}) to W has induced a larger change than mutation to Q, possibly because of its necessary translocation through the gating charge transfer center during activation.

References

Adams, P.R., Brown, D. A. & Constanti, A., 1982. M-currents and other potassium currents in bullfrog sympathetic neurones. *The Journal of Physiology*, 330(1), p.537 -572.

Aggarwal, S.K. & MacKinnon, R., 1996. Contribution of the S4 segment to gating charge in the Shaker K+ channel. *Neuron*, 16(6), p.1169–1177.

Ahern, C.A. & Horn, R., 2005. Focused electric field across the voltage sensor of potassium channels. *Neuron*, 48(1), p.25-29.

Ahern, C.A. & Horn, R., 2004a. Specificity of charge-carrying residues in the voltage sensor of potassium channels. *The Journal of General Physiology*, 123(3), p.205 -216.

Ahern, C.A. & Horn, R., 2004b. Stirring up controversy with a voltage sensor paddle. *Trends in Neurosciences*, 27(6), p.303-307.

Alberts, B. et al., 2002. *Molecular biology of the cell* 4e éd., New York: Garland Science.

Almers, W., 1978. Gating currents and charge movements in excitable membranes. *Reviews of Physiology Biochemistry and Pharmacology*, 82, p.96-190.

Armstrong, C. M. & Bezanilla, F., 1973. Currents related to movement of the gating particles of the sodium channels. *Nature*, 242(5398), p.459-461.

Armstrong, C.M., 1969. Inactivation of the potassium conductance and related phenomena caused by quaternary ammonium ion injection in squid axons. *The Journal of General Physiology*, 54(5), p.553 -575.

Armstrong, C.M., 1966. Time course of tea+-induced anomalous rectification in squid giant axons. *The Journal of General Physiology*, 50(2), p.491 -503.

Armstrong, C.M. & Binstock, L., 1965. Anomalous rectification in the squid giant axon injected with tetraethylammonium chloride. *The Journal of General Physiology*, 48(5), p.859 -872.

Asamoah, O.K. et al., 2003. A fluorometric approach to local electric field measurements in a voltage-gated ion channel. *Neuron*, 37(1), p.85–98.

Bai, C.-X. et al., 2005. Role of nitric oxide in Ca2+ sensitivity of the slowly activating delayed rectifier K+ current in cardiac myocytes. *Circulation Research*, 96(1), p.64-72.

Baker, O. et al., 1998. Three transmembrane conformations and sequence-dependent displacement of the s4 domain in Shaker K channel gating. *Neuron*, 20(6), p.1283-1294.

Bao, H. et al., 1999. Voltage-insensitive gating after charge-neutralizing mutations in the S4 segment of Shaker channels. *The Journal of General Physiology*, 113(1), p.139 -151.

Bell, D.C. et al., 2004. Changes in local S4 environment provide a voltage-sensing mechanism for mammalian hyperpolarization–activated HCN channels. *The Journal of general physiology*, 123(1), p.5.

Bezanilla, F et al., 1991. Molecular basis of gating charge immobilization in Shaker potassium channels. *Science*, 254(5032), p.679 -683.

Bezanilla, F., 2005a. The voltage-sensor structure in a voltage-gated channel. *Trends in biochemical sciences*, 30(4), p.166–168.

Bezanilla, F., 2002. Voltage sensor movements. *The Journal of general physiology*, 120(4), p.465.

Bezanilla, F., 2005b. Voltage-gated ion channels. *IEEE Transactions on Nanobioscience*, 4(1), p.34-48.

Bezanilla, Francisco, 2000. The voltage sensor in voltage-dependent ion channels. *Physiological Reviews*, 80(2), p.555-592.

Bian, J., Cui, J. & McDonald, T.V., 2001. Herg K+ channel activity is regulated by changes in phosphatidyl inositol 4,5-bisphosphate. *Circulation Research*, 89(12), p.1168-1176.

Bjelkmar, P. et al., 2009. Conformational changes and slow dynamics through microsecond polarized atomistic molecular simulation of an integral Kv1.2 ion channel *plos computational biology*, 5(2), p.e1000289.

Blaustein, R.O. & Miller, C., 2004. Shake, rattle or roll. *Nature*, 427(6974), p.499–500.

van den Brink-van der Laan, E. et al., 2004. Small alcohols destabilize the KcsA tetramer via their effect on the membrane lateral pressure. *Biochemistry*, 43(20), p.5937-5942.

Broomand, A., 2003. Molecular movement of the voltage sensor in a K channel. *The Journal of General Physiology*, 122(6), p.741-748.

Broomand, A. & Elinder, F., 2008. Large-scale movement within the voltage-sensor paddle of a potassium channel—support for a helical-screw motion. *Neuron*, 59(5), p.770-777.

Brown, D.A. & London, E., 2000. Structure and function of sphingolipid- and cholesterol-rich membrane rafts. *Journal of Biological Chemistry*, 275(23), p.17221 -17224.

Butterwick, J.A. & MacKinnon, R., 2010. Solution structure and phospholipid interactions of the isolated voltage-sensor domain from KvAP. *Journal of Molecular Biology*, 403(4), p.591-606.

Campos, F.V. et al., 2007. Two atomic constraints unambiguously position the S4 segment relative to S1 and S2 segments in the closed state of Shaker K channel. *Proceedings of the National Academy of Sciences*, 104(19), p.7904 -7909.

Caprini, M. et al., 2005. Molecular compatibility of the channel gate and the N terminus of S5 segment for voltage-gated channel activity. *Journal of Biological Chemistry*, 280(18), p.18253.

Castaldo, P. et al., 2002. Benign familial neonatal convulsions caused by altered gating of KCNQ2/KCNQ3 potassium channels. *Journal of Neuroscience*, p.199.

Catterall, W.A., 2010. Ion channel voltage sensors: structure, function, and pathophysiology. *Neuron*, 67(6), p.915-928.

Catterall, W.A., 1986. Voltage-dependent gating of sodium channels: correlating structure and function. *Trends in*

Neurosciences, 9, p.7-10.

Cha, A. et al., 1999. Atomic scale movement of the voltage-sensing region in a potassium channel measured via spectroscopy. *Nature*, 402(6763), p.809-813.

Chanda, B. et al., 2005. Gating charge displacement in voltage-gated ion channels involves limited transmembrane movement. *Nature*, 436(7052), p.852-856.

Chen, X. et al., 2010. Structure of the full-length Shaker potassium channel Kv1. 2 by normal-mode-based X-ray crystallographic refinement. *Proceedings of the National Academy of Sciences*, 107(25), p.11352.

Clayton, G.M. et al., 2008. Structure of the transmembrane regions of a bacterial cyclic nucleotide-regulated channel. *Proceedings of the National Academy of Sciences*, 105(5), p.1511 -1515.

Cohen, B.E., Grabe, M. & Jan, L. Y, 2003. Answers and questions from the KvAP structures. *Neuron*, 39(3), p.395–400.

Cole, K.S., 1968. *Membranes, ions and impulses. A chapter of classical biophysics*, University of california, Berkeley.

Cuello, L.G., Cortes, D.M. & Perozo, E., 2004. Molecular architecture of the KvAP voltage-dependent K+ channel in a lipid bilayer. *Science*, 306(5695), p.491 -495.

Curtis, H.J. & Cole, K.S., 1940. Membrane action potentials from the squid giant axon. *Journal of Cellular and Comparative Physiology*, 15(2), p.147-157.

Dallos, P. & Fakler, B., 2002. Prestin, a new type of motor protein. *Natural Reviews Molecular Cell Biology*, 3(2), p.104-111.

DeCaen, P.G. et al., 2009. Sequential formation of ion pairs during activation of a sodium channel voltage sensor. *Proceedings of the National Academy of Sciences*, 106(52), p.22498.

Decher, N., Chen, J. & Sanguinetti, M.C., 2004. Voltage-dependent gating of hyperpolarization-activated, cyclic nucleotide-gated pacemaker channels: molecular coupling between the S4-S5 linker and C-linkers. *Journal of Biological Chemistry*, 279, p.13859-13865.

Dedek, K. et al., 2001. Myokymia and neonatal epilepsy caused by a mutation in the voltage sensor of the KCNQ2 K+ channel. *Proceedings of the National Academy of Sciences*, 98(21), p.12272 -12277.

Ding, S. & Horn, R., 2003. Effect of S6 tail mutations on charge movement in Shaker potassium channels. *Biophysical Journal*, 84(1), p.295-305.

Dougherty, K. & Covarrubias, M., 2006. A dipeptidyl aminopeptidase–like protein remodels gating charge dynamics in kv4.2 channels. *The Journal of General Physiology*, 128(6), p.745 -753.

Dowhan, W., 1997. Molcular basic for membrane phospholipid diversity: why are there so many lipids? *Annual Review of Biochemistry*, 66(1), p.199-232.

Doyle, D.A., Cabral, J.M., et al., 1998. The structure of the potassium channel: molecular basis of K+ conduction and selectivity. *Science*, 280, p.69-77.

Doyle, D.A., Cabral, J.M., et al., 1998. The structure of the potassium channel: molecular basis of K+ conduction and selectivity. *Science*, 280(5360), p.69 -77.

Durell, S. R, Shrivastava, I.H. & Guy, H. R, 2004. Models of the structure and voltage-gating mechanism of the shaker K+ channel. *Biophysical journal*, 87(4), p.2116–2130.

Durell, S.R., Hao, Y. & Guy, H. R., 1998. Structural models of the transmembrane region of voltage-gated and other K+ channels in open, closed, and inactivated conformations. *Journal of Structural Biology*, 121(2), p.263-284.

Edidin, M., 2003. The state of lipid rafts: from model membranes to cells. *Annual Review of Biophysics and Biomolecular Structure*, 32(1), p.257-283.

Elinder, F., Männikkö, R. & Larsson, H.P., 2001. S4 charges move close to residues in the pore domain during activation in a K channel. *The Journal of General Physiology*, 118(1), p.1 -10.

Engelman, D.M., 2005. Membranes are more mosaic than fluid. *Nature*, 438(7068), p.578-580.

Fedida, D. & Hesketh, J.C., 2001. Gating of voltage-dependent potassium channels. *Progress in Biophysics and Molecular Biology*, 75(3), p.165–199.

Fedida, D., Bouchard, R. & Chen, F.S., 1996. Slow gating charge immobilization in the human potassium channel Kv1. 5 and its prevention by 4-aminopyridine. *The Journal of Physiology*, 494(Pt 2), p.377.

Ferrer, T. et al., 2006. The S4-S5 linker directly couples voltage sensor movement to the activation gate in the Human Ether-a'-go-go-related gene (hERG) K+ channel. The *Journal of Biological Chemistry*, 281, p.12858-12864.

Freites, J. A, Tobias, D. J & White, S. H, 2006. A voltage-sensor water pore. *Biophysical journal*, 91(11), p.L90–L92.

Gagnon, D.G. & Bezanilla, F., 2009. A single charged voltage sensor is capable of gating the Shaker K + channel. *Journal of General Physiology*, 133(5), p.467-483.

Gandhi, C.S. et al., 2003. The orientation and molecular movement of a K+ channel voltage-sensing domain. *Neuron*, 40(3), p.515–525.

Gandhi, C.S., Loots, E. & Isacoff, Ehud Y, 2000. Reconstructing voltage sensor-pore interaction from a fluorescence scan of a voltage-gated K+ channel. *Neuron*, 27(3), p.585-595.

Gandhi, C.S. & Isacoff, Ehud Y., 2002. Molecular models of voltage sensing. *The Journal of General Physiology*, 120(4), p.455 -463.

Glauner, K.S. et al., 1999. Spectroscopic mapping of voltage sensor movement in the Shaker potassium channel. *Nature*, 402(6763), p.813-817.

Goldup, A., Ohki, S. & Danielli, J.F., 1970. Black lipid films. Dans *Recent Progress in Surface Science*. New York: J. F. Danielli, A. C. Riddiford & H. Rosenberg, p. 193.

Grabe, M. et al., 2006. Structure prediction for the down state of a potassium channel voltage sensor. *Nature*,

445(7127), p.550-553.

Gutman, G.A. et al., 2005. International Union of Pharmacology. LIII. Nomenclature and molecular relationships of voltage-gated potassium channels. *Pharmacological reviews*, 57(4), p.473.

Guy, H R & Seetharamulu, P., 1986. Molecular model of the action potential sodium channel. *Proceedings of the National Academy of Sciences*, 83(2), p.508 -512.

Hamill, O.P., Marty, A. & Neher, E., 1981. Improved patch-clamp techniques for high-resolution current recording from cells and cell-free membrane patches. *Pflugers Archiv European Journal of Physiology*, 391(2), p.85-100.

Han, M. & Zhang, J.Z.H., 2008. Molecular dynamic simulation of the Kv1.2 voltage-gated potassium channel in open and closed state conformations. *The Journal of Physical Chemistry B*, 112(51), p.16966-16974.

von Heijne, G., 1999. Recent advances in the understanding of membrane protein assembly and structure. *Quarterly Reviews of Biophysics*, 32(4), p.285-307.

Hilgemann, D.W. & Ball, R., 1996. Regulation of cardiac Na+,Ca2+ exchange and KATP potassium channels by PIP2. *Science*, 273(5277), p.956 -959.

Hille, B., 2001. *Ion channels of excitable membranes* 3e éd., Sunderland, MA: Sinauer Associates Inc.

Hodgkin, A.L. & Huxley, A.F., 1939. Action potentials recorded from inside a nerve fibre. *Nature*, 144(3651), p.710-711.

Hirschberg, B. et al., 1995. Transfer of twelve charges is needed to open skeletal muscle Na+ channels. *The Journal of General Physiology*, 106(6), p.1053 -1068.

Hodgkin, A.L. & Katz, B., 1949. The effect of sodium ions on the electrical activity of the giant axon of the squid. *The Journal of Physiology*, 108(1), p.37.

Hodgkin, A.L., Huxley, A.F. & Katz, B., 1949. Ionic currents underlying activity in the axon of the squid. *Archive Science Physiology*, 3, p.129-150.

Hodgkin, A.L. & Huxley, A.F., 1952a. Currents carried by sodium and potassium ions through the membrane of the giant axon of Loligo. *The Journal of physiology*, 116(4), p.449.

Hodgkin, A.L. & Huxley, A.F., 1952b. The dual effect of membrane potential on sodium conductance in the giant axon of Loligo. *The Journal of physiology*, 116(4), p.497.

Hodgkin, A.L. & Huxley, A.F., 1952c. A quantitative description of membrane current and its application to conduction and excitation in nerve. *The Journal of Physiology*, 117(4), p.500 -544.

Hodgkin, A.L. & Huxley, A.F., 1952d. The components of membrane conductance in the giant axon of Loligo. *The Journal of physiology*, 116(4), p.473.

Honoré, E., 2008. Alternative translation initiation further increases the molecular and functional diversity of ion channels. *The Journal of Physiology*, 586(23), p.5605 -5606.

Horn, R., 2000. Conversation between voltage sensors and gates of ion channels. *Biochemistry*, 39(51), p.15653-15658.

Van Horn, W.D., Vanoye, C.G. & Sanders, C.R., 2011. Working model for the structural basis for KCNE1 modulation of the KCNQ1 potassium channel. *Current Opinion in Structural Biology*, In Press.

Howard, R.J. et al., 2007. Structural Insight into KCNQ (Kv7) Channel Assembly and Channelopathy. *Neuron*, 53(5), p.663-675.

Huang, C.-L., Feng, S. & Hilgemann, D.W., 1998. Direct activation of inward rectifier potassium channels by PIP2 and its stabilization by G[beta][gamma]. *Nature*, 391(6669), p.803-806.

Islas, L.D. & Sigworth, F. J, 2001. Electrostatics and the gating pore of Shaker potassium channels. *The Journal of General Physiology*, 117(1), p.69.

Jensen, M.Ø. et al., 2010. Principles of conduction and hydrophobic gating in K+ channels. *Proceedings of the National Academy of Sciences*, 107(13), p.5833 -5838.

Jiang, Y., Lee, A., et al., 2003. X-ray structure of a voltage-dependent K+ channel. *Nature*, 423(6935), p.33–41.

Jiang, Y., Ruta, V., et al., 2003. The principle of gating charge movement in a voltage-dependent K+ channel. *Nature*, 423(6935), p.42–48.

Jiang, Y., Lee, A., et al., 2002a. Crystal structure and mechanism of a calcium-gated potassium channel. *Nature*, 417(6888), p.515-522.

Jiang, Y., Lee, A., et al., 2002b. The open pore conformation of potassium channels. *Nature*, 417(6888), p.523-526.

Jogini, V. & Roux, B., 2007. Dynamics of the Kv1. 2 voltage-gated K+ channel in a membrane environment. *Biophysical journal*, 93(9), p.3070–3082.

Jurkat-Rott, K. et al., 2000. Voltage-sensor sodium channel mutations cause hypokalemic periodic paralysis type 2 by enhanced inactivation and reduced current. *Proceedings of the National Academy of Sciences*, 97(17), p.9549.

Kanevsky, M. & Aldrich, Richard W., 1999. Determinants of voltage-dependent gating and open-state stability in the S5 segment of Shaker potassium channels. *The Journal of General Physiology*, 114(2), p.215 -242.

Kang, C. et al., 2008. Structure of KCNE1 and Implications for How It Modulates the KCNQ1 Potassium Channel. *Biochemistry*, 47(31), p.7999-8006.

Kao, C.Y., 1966. Tetrodotoxin, saxitoxin and their significance in the study of excitation phenomena. *Pharmacological Reviews*, 18(2), p.997 -1049.

Karp, G., 2009. *Cell and molecular biology* 6e éd., John Wiley & Sons Inc.

Keynes, R. D. & Rojas, E., 1974. Kinetics and steady-state properties of the charged system controlling sodium conductance in the squid giant axon. *The Journal of Physiology*, 239(2), p.393 -434.

Keynes, R.D. & Elinder, F., 1999. The screw–helical voltage gating of ion channels. *Proceedings of the Royal Society of London. Series B: Biological Sciences*, 266(1421), p.843 -852.

Khalili-Araghi, F. et al., 2010. Calculation of the gating charge for the Kv1.2 voltage-activated potassium channel. *Biophysical Journal*, 98(10), p.2189-2198.

Kosower, E.M., 1985. A structural and dynamic molecular model for the sodium channel of Electrophoruselectricus. *FEBS Letters*, 182(2), p.234-242.

Krepkiy, D. et al., 2009. Structure and hydration of membranes embedded with voltage-sensing domains. *Nature*, 462(7272), p.473-479.

Labro, A.J. et al., 2008. Kv channel gating requires a compatible S4-S5 linker and bottom part of S6, constrained by non-interacting residues. *The Journal of General Physiology*, 132(6), p.667 -680.

Lacroix, J. J & Bezanilla, F., 2011. Control of a final gating charge transition by a hydrophobic residue in the S2 segment of a K+ channel voltage sensor. *Proceedings of the National Academy of Sciences*, 108(16), p.6444.

Lacroix, J.J., Labro, A.J. & Bezanilla, F., 2011. Properties of deactivation gating currents in shaker channels. *Biophysical Journal*, 100(5), p.L28-L30.

Larsson, H. Peter et al., 1996. Transmembrane movement of the shaker K+ channel S4. *Neuron*, 16(2), p.387-397.

Lecar, H., Larsson, H. P & Grabe, M., 2003. Electrostatic model of S4 motion in voltage-gated ion channels. *Biophysical journal*, 85(5), p.2854–2864.

Lee, H.C., Wang, J.M. & Swartz, K. J, 2003. Interaction between extracellular Hanatoxin and the resting conformation of the voltage-sensor paddle in Kv channels. *Neuron*, 40(3), p.527–536.

Lee, S.-Y. & MacKinnon, R., 2004. A membrane-access mechanism of ion channel inhibition by voltage sensor toxins from spider venom. *Nature*, 430(6996), p.232-235.

Lee, S.-Y., Banerjee, A. & MacKinnon, R., 2009. Two separate interfaces between the voltage sensor and pore are required for the function of voltage-dependent K+ channels *PLoS Biology*, 7(3), p.e47.

Lee, S.-Y. et al., 2005. Structure of the KvAP voltage-dependent K+ channel and its dependence on the lipid membrane. *Proceedings of the National Academy of Sciences of the United States of America*, 102(43), p.15441 -15446.

Lehmann-Horn, F. & Jurkat-Rott, K., 1999. Voltage-gated ion channels and hereditary disease. *Physiological reviews*, 79(4), p.1317.

Liman, E.R. & Hess, P., 1991. Voltage-sensing residues in the S4 region of a mammalian K+ channel. *Nature*, 353(6346), p.752-756.

Loboda, A. & Armstrong, C. M, 2001. Resolving the gating charge movement associated with late transitions in K channel activation. *Biophysical Journal*, 81(2), p.905–916.

Lodish, H. et al., 2000. *Molecular cell biology* 4e éd., W. H. Freeman and Company.

Long, S.B., Campbell, E.B. & MacKinnon, R., 2005a. Crystal structure of a mammalian voltage-dependent shaker family K+ channel. *Science*, 309(5736), p.897 -903.

Long, S.B., Campbell, E.B. & MacKinnon, R., 2005b. Voltage Sensor of Kv1.2: structural basis of electromechanical coupling. *Science*, 309(5736), p.903 -908.

Long, S.B. et al., 2007. Atomic structure of a voltage-dependent K+ channel in a lipid membrane-like environment. *Nature*, 450(7168), p.376-382.

Lu, Z., Klem, A.M. & Ramu, Y., 2002. Coupling between voltage sensors and activation gate in voltage-gated K+ channels. *The Journal of General Physiology*, 120(5), p.663 -676.

Lupoglazoff, J.-M. et al., 2003. Long QT syndrom in neonates : Conduction disorders associated with HERG,mutations and sinus bradycardia with KCNQ1 mutations. *J.A.C.C*, 43, p.826-830.

Maljevic, S. et al., 2010. Kv7 channelopathies. *Pflügers Archiv - European Journal of Physiology*, 460(2), p.277-288.

Martin, G.S., 2003. Cell signaling and cancer. *Cancer Cell*, 4(3), p.167-174.

Mathews, C.K., Van Holde, K.E. & Ahern, K.G. éd., 1999. *Biochemistry* 3e éd., Prentice Hall.

Miceli, F., Cilio, M.R., et al., 2009. Gating currents from neuronal Kv7.4 Channels: General features and correlation with the ionic conductance. *Channels*, 3(4), p.277-286.

Miceli, F., Soldovieri, M.V., Hernandez, C.C., et al., 2008. Gating consequences of charge neutralization of arginine residues in the S4 segment of Kv7.2, an epilepsy-linked K+ channel subunit. *Biophysical Journal*, 95(5), p.2254-2264.

Miceli, F., Soldovieri, M.V., et al., 2009. Neutralization of a unique, negatively-charged residue in the voltage sensor of KV7.2 subunits in a sporadic case of benign familial neonatal seizures. *Neurobiology of Disease*, 34(3), p.501-510.

Miceli, F., Soldovieri, M.V., Martire, M., et al., 2008. Molecular pharmacology and therapeutic potential of neuronal Kv7-modulating drugs. *Current Opinion in Pharmacology*, 8(1), p.65-74.

Nakamura, Y., Nakajima, S. & Grundfest, H., 1965. Analysis of spike electrogenesis and depolarizing k inactivation in electroplaques of electrophorus electricus. *The Journal of General Physiology*, 49(2), p.321 -349.

Narahashi, T., Moore, J.W. & Scott, W.R., 1964. Tetrodotoxin Blockage of Sodium Conductance Increase in Lobster Giant Axons. *The Journal of General Physiology*, 47(5), p.965 -974.

Nishizawa, M. & Nishizawa, K., 2009. Coupling of S4 helix translocation and S6 gating analyzed by molecular-dynamics simulations of mutated Kv channels. *Biophysical journal*, 97(1), p.90–100.

Nishizawa, M. & Nishizawa, K., 2008. Molecular dynamics simulation of Kv channel voltage sensor helix in a lipid membrane with applied electric field. *Biophysical journal*, 95(4), p.1729–1744.

Noceti, F. et al., 1996. Effective gating charges per channel in voltage-dependent K+ and Ca2+ channels. *The Journal of General Physiology*, 108(3), p.143 -155.

Papazian, D.M. et al., 1995. Electrostatic interactions of S4 voltage sensor in shaker K+ channel. *Neuron*, 14(6), p.1293-1301.

Papazian, D.M. et al., 1991. Alteration of voltage-dependence of Shaker potassium channel by mutations in the S4 sequence. *Nature*, 349(6307), p.305-310.

Park, K.-H. et al., 2005. Impaired KCNQ1-KCNE1 and Phosphatidylinositol-4,5-Bisphosphate interaction underlies the long QT syndrome. *Circulation Research*, 96(7), p.730-739.

Pathak, M.M. et al., 2007. Closing in on the resting state of the Shaker K+ channel. *Neuron*, 56(1), p.124-140.

Phillips, L.R. et al., 2005. Voltage-sensor activation with a tarantula toxin as cargo. *Nature*, 436(7052), p.857-860.

Piper, D.R. et al., 2003. Gating currents associated with intramembrane charge displacement in HERG potassium channels. *Proceedings of the National Academy of Sciences of the United States of America*, 100(18), p.10534 -10539.

Posson, D.J. & Selvin, P.R., 2008. Extent of voltage sensor movement during gating of Shaker K+ channels. *Neuron*, 59(1), p.98-109.

Posson, D.J. et al., 2005. Small vertical movement of a K+ channel voltage sensor measured with luminescence energy transfer. *Nature*, 436(7052), p.848-851.

Ramsey, I.S. et al., 2006. A voltage-gated proton-selective channel lacking the pore domain. *Nature*, 440(7088), p.1213-1216.

Ramu, Y., Xu, Y. & Lu, Z., 2006. Enzymatic activation of voltage-gated potassium channels. *Nature*, 442(7103), p.696-699.

Rodríguez de la Vega, R.C. et al., 2003. Novel interactions between K+ channels and scorpion toxins. *Trends in Pharmacological Sciences*, 24(5), p.222-227.

Rodriguez, N. et al., 2010. Phosphatidylinositol-4,5-Bisphosphate (PIP2) stabilizes the open pore conformation of the Kv11.1 (hERG) channel. *Biophysical Journal*, 99(4), p.1110-1118.

Ruta, V., Chen, J. & MacKinnon, R., 2005. Calibrated measurement of gating-charge arginine displacement in the KvAP voltage-dependent K+ channel. *Cell*, 123(3), p.463-475.

Safiulina, V.F. et al., 2008. Low expression of Kv7/M channels facilitates intrinsic and network bursting in the developing rat hippocampus. *The Journal of Physiology*, 586(22), p.5437 -5453.

Sands, Z.A. & Sansom, M.S.P., 2007. How does a voltage sensor interact with a lipid bilayer? Simulations of a potassium channel domain. *Structure*, 15(2), p.235-244.

Sasaki, M., Takagi, M. & Okamura, Y., 2006. A voltage sensor-domain protein is a voltage-gated proton channel. *Science*, 312(5773), p.589 -592.

Schmidt, D., Jiang, Q.-X. & MacKinnon, R., 2006. Phospholipids and the origin of cationic gating charges in voltage sensors. *Nature*, 444(7120), p.775-779.

Schneider, M.F. & Chandler, W.K., 1973. Voltage dependent charge movement in skeletal muscle: a possible step in excitation-contraction coupling. *Nature*, 242(5395), p.244-246.

Schoppa, N.E. & Sigworth, F. J., 1998. Activation of Shaker potassium channels: II. Kinetics of the V2 mutant channel. *The Journal of general physiology*, 111(2), p.295.

Schoppa, N. et al., 1992. The size of gating charge in wild-type and mutant Shaker potassium channels. *Science*, 255(5052), p.1712 -1715.

Schow, E.V. et al., 2010. Down-state model of the voltage-sensing domain of a potassium channel. *Biophysical Journal*, 98(12), p.2857-2866.

Schwaiger, C.S. et al., 2011. 310-helix conformation facilitates the transition of a voltage sensor s4 segment toward the down state. *Biophysical Journal*, 100(6), p.1446-1454.

Selvin, P.R., 2002. Principles and biophysical applications of lanthanide-based probes. *Annual Review of Biophysics and Biomolecular Structure*, 31, p. 275-301.

Seoh, S.A. et al., 1996. Voltage-sensing residues in the S2 and S4 segments of the Shaker K+ channel. *Neuron*, 16(6), p.1159–1167.

Sewing, S., Roeper, J. & Pongs, O., 1996. Kv[beta]1 subunit binding specific for Shaker-related potassium channel [alpha] subunits. *Neuron*, 16(2), p.455-463.

Shafrir, Y., Durell, S.R. & Guy, H.R., 2008. Models of voltage-dependent conformational changes in NaChBac channels. *Biophysical Journal*, 95(8), p.3663-3676.

Shamgar, L. et al., 2006. Calmodulin is essential for cardiac IKS channel gating and assembly: Impaired function in long-QT mutations. *Circulation Research*, 98(8), p.1055-1063.

Sigg, D., Bezanilla, F. & Stefani, E., 2003. Fast gating in the Shaker K+ channel and the energy landscape of activation. *Proceedings of the National Academy of Sciences*, 100(13), p.7611.

Silverman, W.R., Roux, B. & Papazian, D.M., 2003. Structural basis of two-stage voltage-dependent activation in K+ channels. *Proceedings of the National Academy of Sciences*, 100(5), p.2935 -2940.

Singer, S.J. & Nicolson, G.L., 1972. The fluid mosaic model of the structure of cell membranes. *Science*, 175(4023), p.720 -731.

Sokolov, S., Scheuer, T. & Catterall, W.., 2008. Depolarization-activated gating pore current conducted by mutant sodium channels in potassium-sensitive normokalemic periodic paralysis. *Proceedings of the National Academy of Sciences*, 105(50), p.19980 -19985.

Sokolov, S., Scheuer, T. & Catterall, W.A., 2007. Gating pore current in an inherited ion channelopathy. *Nature*, 446(7131), p.76-78.

Sokolov, S., Scheuer, T. & Catterall, W.A., 2005. Ion permeation through a voltage- sensitive gating pore in brain

sodium channels having voltage sensor mutations. *Neuron*, 47(2), p.183-189.

Soldovieri, M. V. et al., 2007. Correlating the clinical and genetic features of benign familial neonatal seizures (BFNS) with the functional consequences of underlying mutations. *Channels*, 1, p.228-233.

Soler-Llavina, G.J., Chang, T.-H. & Swartz, K.J., 2006. Functional interactions at the interface between voltage-sensing and pore domains in the Shaker Kv channel. *Neuron*, 52(4), p.623-634.

Splawski, I. et al., 2000. Spectrum of mutations in long-QT syndrome genes : KVLQT1, HERG, SCN5A, KCNE1, and KCNE2. *Circulation*, 102(10), p.1178-1185.

Starace, D.M. & Bezanilla, F., 2001. Histidine scanning mutagenesis of basic residues of the S4 segment of the Shaker K+ channel. *The Journal of general physiology*, 117(5), p.469.

Starace, D.M., Stefani, E. & Bezanilla, F., 1997. Voltage-dependent proton transport by the voltage sensor of the Sshaker K+ channel. *Neuron*, 19(6), p.1319–1327.

Starace, D.M. & Bezanilla, Francisco, 2004. A proton pore in a potassium channel voltage sensor reveals a focused electric field. *Nature*, 427(6974), p.548-553.

Strassberg, A.F. & DeFelice, L.J., 1993. Limitations of the Hodgkin-Huxley formalism: effects of single channel kinetics on transmembrane voltage dynamics. *Neural Computation*, 5(6), p.843-855.

Struyk, A.F. & Cannon, S.C., 2007. A Na+ channel mutation linked to hypokalemic periodic paralysis exposes a proton-selective gating pore. *The Journal of general physiology*, 130(1), p.11.

Suh, B.-C. & Hille, B., 2008. PIP2 is a necessary cofactor for ion channel function: How and why? *Ann. Rev. Biophys.*, 37, p.175-195.

Swartz, Kenton J., 2008. Sensing voltage across lipid membranes. *Nature*, 456(7224), p.891-897.

Taglialatela, M & Stefani, E., 1993. Gating currents of the cloned delayed-rectifier K+ channel DRK1. *Proceedings of the National Academy of Sciences*, 90(10), p.4758 -4762.

Tang, C.-Y., Bezanilla, F. & Papazian, D.M., 2000. Extracellular Mg2+ modulates slow gating transitions and the opening of drosophila Ether-à-Go-Go potassium channels. *The Journal of General Physiology*, 115(3), p.319 -338.

Tao, X. et al., 2010. A gating charge transfer center in voltage sensors. *Science*, 328(5974), p.67-73.

Tasaki, I. & Hagiwara, S., 1957. Demonstration of two stable potential states in the squid giant axon under tetraethylammonium chloride. *The Journal of General Physiology*, 40(6), p.859 -885.

Tiwari-Woodruff, S.K. et al., 1997. Electrostatic interactions between transmembrane segments mediate folding of Shaker K+ channel subunits. *Biophysical Journal*, 72(4), p.1489-1500.

Tombola, F., Pathak, M.M. & Isacoff, E.Y., 2005. How far will you go to sense voltage? *Neuron*, 48(5), p.719–725.

Tombola, F., Pathak, M.M. & Isacoff, E.Y., 2006. How does voltage open an ion channel? *Annual Review of Cell*

and Developmental Biology, 22(1), p.23-52.

Tombola, F., Pathak, M.M. & Isacoff, E.Y., 2005. Voltage-sensing arginines in a potassium channel permeate and occlude cation-selective pores. *Neuron*, 45(3), p.379-388.

Tombola, F., Pathak, M.M., Gorostiza, P., et al., 2006. The twisted ion-permeation pathway of a resting voltage-sensing domain. *Nature*, 445(7127), p.546-549.

Treptow, W. & Tarek, M., 2006. Environment of the gating charges in the Kv1.2 Shaker potassium channel. *Biophysical journal*, 90(9), p.L64–L66.

Treptow, W. & Tarek, M., 2006. Molecular restraints in the permeation pathway of ion channels. *Biophysical Journal*, 91(3), p.L26-L28.

Treptow, W., Tarek, M. & Klein, M.L., 2009. Initial response of the potassium channel voltage sensor to a transmembrane potential. *Journal of the American Chemical Society*, 131(6), p.2107-2109.

Tristani-Firouzi, M, Chen, J & Sanguinetti, M., 2002. Interactions between S4-S5 linker and S6 transmembrane domain modulate gating of Herg potassium channels. *Journal of Biological Chemistry*, 277, p.18994 - 19000.

Villalba-Galea, C.A. et al., 2008. S4-based voltage sensors have three major conformations. *Proceedings of the National Academy of Sciences*, 105(46), p.17600.

White, S.H., 1994. *Membrane protein structure: experimental approaches*, Oxford university press.

Wolfe, S.L., 1993. *Molecular and cellular biology*, Belmont, California: Wadsworth Publishing Company.

Wu, D., Delaloye, K., et al., 2010. State-dependent electrostatic interactions of S4 arginines with E1 in S2 during Kv7.1 activation. *The Journal of General Physiology*, 135(6), p.595-606.

Wuttke, T. V. et al., 2007. Peripheral nerve hyperexcitability due to dominant-negative KCNQ2 mutations. *Neurology*, 69(22), p.2045 -2053.

Xu, Q. & Minor Jr., D.L., 2009. Crystal structure of a trimeric form of the Kv7.1 (KCNQ1) A-domain tail coiled-coil reveals structural plasticity and context dependent changes in a putative coiled-coil trimerization motif. *Protein Science*, 18(10), p.2100-2114.

Xu, Y., Ramu, Y. & Lu, Z., 2008. Removal of phospho-head groups of membrane lipids immobilizes voltage sensors of K+ channels. *Nature*, 451(7180), p.826-829.

Yang, N., George, A.L. & Horn, R., 1996. Molecular basis of charge movement in voltage-gated sodium channels. *Neuron*, 16(1), p.113-122.

Yarov-Yarovoy, V., Baker, D. & Catterall, W.A., 2006. Voltage sensor conformations in the open and closed states in rosetta structural models of K+ channels. *Proceedings of the National Academy of Sciences*, 103(19), p.7292 -7297.

Yellen, G., 1998. The moving parts of voltage-gated ion channels. *Quarterly Reviews of Biophysics*, 31(03), p.239-295.

Young, J.Z., 1936. Structure of nerve fibres and synapses in some invertebrates. *Cold Spring Harbor Symposia on Quantitative Biology*, 4, p.1 -6.

Yu, W., Xu, J. & Li, M., 1996. NAB domain is essential for the subunit assembly of both [alpha]-[alpha] and [alpha]-[beta] complexes of Shaker-like potassium channels. *Neuron*, 16(2), p.441-453.

Yus-Nájera, E., Santana-Castro, I. & Villarroel, A., 2002. The identification and characterization of a noncontinuous calmodulin-binding site in noninactivating voltage-dependent KCNQ potassium channels. *Journal of Biological Chemistry*, 277(32), p.28545-28553.

Yusaf, S.P., Wray, D. & Sivaprasadarao, A., 1996. Measurement of the movement of the S4 segment during the activation of a voltage-gated potassium channel. *Pflugers Archiv European Journal of Physiology*, 433(1-2), p.91-97.

Zagotta, W.N., Hoshi, T., Dittman, J., et al., 1994. Shaker potassium channel gating. II: Transitions in the activation pathway. *The Journal of General Physiology*, 103(2), p.279 -319.

Zagotta, W.N., Hoshi, T. & Aldrich, R. W, 1994. Shaker potassium channel gating. III: Evaluation of kinetic models for activation. *The Journal of General Physiology*, 103(2), p.321.

Zhang, H. et al., 2003. PIP2 activates KCNQ channels, and its hydrolysis underlies receptor-mediated inhibition of M currents. *Neuron*, 37(6), p.963-975.

Zhang, M. et al., 2005. Interactions between charged residues in the transmembrane segments of the voltage-sensing domain in the hREG channel. *Journal of Membrane Biology*, 207(3), p.169-181.

Zheng, J. & Sigworth, F.J., 1998. Intermediate conductances during deactivation of heteromultimeric Shaker potassium channels. *The Journal of General Physiology*, 112(4), p.457 -474.

Appendix 1

This appendix aims at describing briefly the experimental techniques that were used to study excitable cells and their membranes. However, many experimental and computational techniques have been used to study ion channels from different angles and have each in their own way been involved in understanding better voltage gated ion channels, making this field extraordinarily multidisciplinary (chemistry, pharmacology, biology, molecular biology and biophysics, physics, computer science…). In order to explain what type of information can be extracted from electrophysiology, structural, physical and molecular biology techniques, we catalog here the techniques that have been most useful to study Kv channels. This section does not aim at reviewing in details these techniques but rather should enable the reader to understand the different shortcomings of the following techniques and help understand in the rest of the chapter why the information coming from different experimental techniques seem contradictory.

1 Electrophysiology techniques

Electrophysiology is the study of electrical properties (voltage and current) of biological systems. Electrophysiology can be applied to a lot of systems, from entire animals, excised tissues to single cells or even small membrane patches containing a single channel. Whereas all these techniques are important and have been extremely useful to understand the electric properties of organs or even organisms, we focus here on the description of the protocols used for microscopic systems, in the view of studying voltage gated ion channels.

1.1 Voltage clamp

Voltage clamp is an electrophysiology technique, due to Kenneth Cole and George Marmount in the 1940s, that enables measuring the current flowing through the membrane while holding a constant transmembrane (TM) potential (also named “clamping”). In this setup, one set of two electrodes (one of them inside of the cell, in the intra-cellular medium, and the other one lying in the extra-cellular medium) is used to apply the TM voltage, *i.e.* the voltage difference between both sides of the membrane, and another one is used to pass the current to the membrane. The “voltage” electrodes measure the TM potential, and the voltage clamp device determines how far this voltage is from the user defined “holding potential”. This information is fed back to the “current” electrodes, which produce a current that leads the “measured TM potential” to equal the “holding TM potential”. Thus, the clamp circuit produces a current equal and opposite to the current flowing through the membrane.

Using this technique requires the substraction of transient capacitive currents, that are passed as the recording electrodes are charged. This technique is very much used to build

current/voltage curves, which are essential for the study of voltage-gated ion channels (see below).

1.2 Current clamp

In contrast, the current clamp circuit controls the amplitude of the injected current and records the variations of the TM voltage. This technique is used to study how a cell responds to an electrical impulse. For example, injecting a depolarizing current large enough across an excitable membrane generates an electrical response in the form of an action potential (see paragraph 2.2.2) during which the transmembrane potential rises abruptly before falling back to its original level as suddenly.

1.3 Patch clamp / Single channel recordings

Conventional recordings such as the ones described above involve impaling a cell with a fine electrode, rationalizing the historical use of giant squid axons (~0.5 μ m in diameter) as study systems. Patch-clamp recording, introduced by Erwin Neher and Bert Sakman in the late 1970s and early 1980s (Neher & Sakmann 1976) and who received the Nobel Prize of medecine for it in 1991, takes an altogether different approach. The patch clamp microelectrode is a micropipette with a relatively large tip diameter (~1 μm). The open tip is pressed against a cell's surface and when suction is applied to the inside of the pipette, a tight seal forms between the cell's membrane and the pipette's tip (Hamill et al. 1981). Due to this, the setup is also called the gigaseal technique.

There are multiple patch clamp configurations for a variety of experimental observations (Sakmann & Neher 2009) (Fig. A.1):

Cell-attached (CAP) or on-cell configuration: Once the seal is formed, the cell remains intact and the recording is performed without disrupting the interior of the cell. The solution inside of the pipette (representing the extra-cellular medium) on the other hand can be controlled. This configuration is useful when the ion channel under study is sensitive to unknown cytosolic factors and to test whether the channel's activity is altered with the patch excision (see below). The biggest drawback of this configuration is that the TM potential is difficult to control because the unknown resting cell membrane potential adds to the applied TM potential during measurement.

Inside-Out (IOP): After applying the suction, the micropipette is rapidly taken away from the cell, excising thereby a membrane patch. With this method, both the intracellular and extracellular media can be controlled, enabling to study the effect of intracellular compound on the channels. In this configuration, the original cytosolic composition is lost.

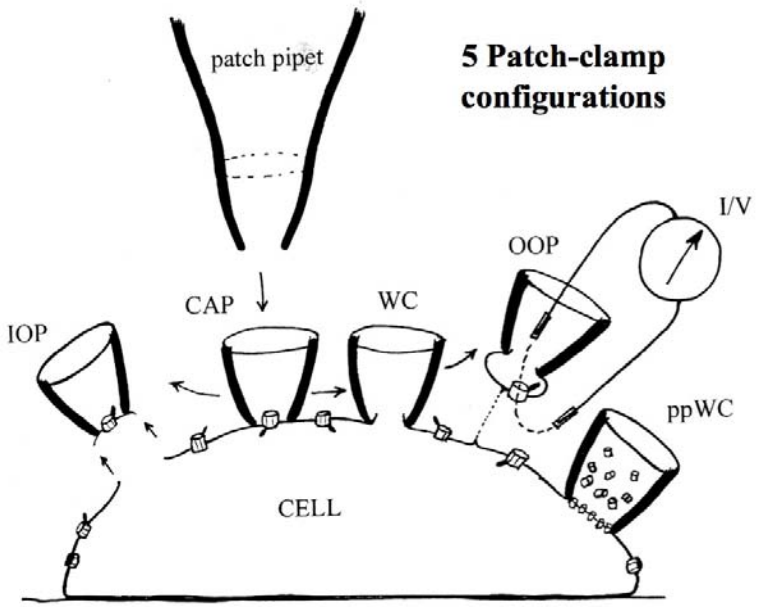

Figure A.1: Illustration of the five different patch clamp configuration. From conference slides by Ypey and Defelice, Erice school on Ion channels and transporters, 2005.

Whole cell recording (WC): In this configuration, the suction applied to the micropipette is larger that in the cell-attached configuration, destroying the membrane patch inside of the pipette's tip. The interior of the cell is then in direct contact with the electrode and the signal is recorded for the ensemble of the membrane components of the cell. Here again, the main problem is the loss of cytosolic factors that can be of importance for channel function.

Outside-Out (OOP): This is the experimentally most challenging measurement since it involves a large number of steps. After the whole-cell patch is formed, the electrode can be slowly moved away from the cell, stretching out a bleb of membrane. When the electrode is pulled far enough away, this bleb will detach from the cell and reform as a convex membrane at the tip of the electrode. In this configuration, the original outside of the membrane faces outward from the electrode while the original inside faces the inside of the pipette (leading to a configuration that is the opposite of the inside-out configuration. This experimental setup makes single channel recordings possible, with the advantage of being able to make the composition of the "extracellular" solution vary easily.

Permeabilized-patch WC-configuration (ppWC): In this configuration, the CAP is not actually ruptured for direct access to the inside of the cell, but made permeable by adding artificial ion channels (monovalent cation channel-forming antibiotics) via the pipette solution (Horn & Marty 1988) . The great advantage of this configuration is that it allows intracellular voltage and current-clamp measurements on relatively intact cells, *i.e.* cells with a near normal cytoplasmic composition, is in contrast to the perfused WC-configuration.

All these patch clamp configurations can be used both in voltage- or current-clamp modes.

2 Structural techniques

These structural techniques are probably the latest to have been applied to biological molecules as complex as voltage-gated ion channels but are also probably those that have given the most answers to the questions as to how Kv channels work. Among these, X-ray crystallography is probably the most trusted by the scientific community. We complete this paragraph by a short summary on NMR, in solution or in solid state, which has also proven to be useful in Kv channel studies.

2.1 X-Ray crystallography

X-Ray crystallography is an extremely powerful method that enables solving the 3D arrangement of atoms within a crystal. While this technique has been very widely used to study small molecules, it was introduced for proteins in the late 1950s. X-ray crystallography relies on the diffraction of a beam of X-ray by a crystal. The crystal is mounted on a goniometer, the instrument that allows an object to be rotated to a precise angular position, that is revolved along its axis and a beam of X-ray is aimed at it. When a X-ray hits an electron pertaining to an atom, it is reflected elastically, *i.e.* diffracted (or scattered). When the electrons are arranged in a crystal, most reflections cancel out due to incoherencies in the waves, but some of them add constructively in a few directions determined by Bragg's law:

$$2d\sin\theta = n.\lambda \quad [A.1]$$

d being the distance between two planes in the crystal, q the incidence angle of the X-Ray wave, n an integer and λ the wavelength of the X-ray beam. Altogether, this produces a diffraction pattern that can be resolved in terms of atomic positions.

From this simplified description, one understands the importance of having crystals of good quality, where the repetition distance d is highly homogeneous. For membrane proteins, and especially for ion channels, this is a very challenging task, due to many bottlenecks.

First, membrane proteins are usually not found abundantly and it is crucial to enhance their expression and achieve good quality purification. Most of the time, these two early steps prove to be difficult. Furthermore, before producing crystals, it is necessary to solubilize the proteins. Membrane proteins are mainly hydrophobic and therefore, this step requires introducing detergents or other means of solubilization, which later often interferes with crystallization. The crystals produced are then often small, poorly ordered and anisotropic which in turn leads to bad quality diffraction patterns.

In order to enhance the crystallization, some workarounds have been proposed. Among them, the introduction of antibody fragments as spacers has enabled the crystallization of the first voltage gated potassium channel, the KvAP (Jiang et al. 2003a). However, as it turned out later to be the case in this structure, introduction of such molecules can lead to crystallization

of the proteins in a non-native state. Since then however, two crystal structures of Kv channels (the Kv1.2 in 2005 (Long et al. 2005) and the Kv1.2/2.1 paddle chimera, in which the top of S3 and S4 (the so-called paddle) from the Kv2.1 are inserted in the Kv1.2 channel, in 2007 (Long et al. 2007) were resolved. In both studies, during purification and crystallization, it was necessary to keep the protein in a mixture of detergents and lipids. In the Kv1.2/2.1 paddle chimera structure, a few lipid molecules were resolved, giving information as to how lipids interact with the channel (see below). Moreover, the Kv1.2 was crystallized in the presence of a β subunit, a subunit that binds from the intracellular side to the channel and that seems to have enhanced the crystallization process.

2.2 Other structural techniques : solid and liquid-state NMR, Electron microscopy

Other experimental techniques give direct information on the structure of molecules and have been applied to proteins: among them, nuclear magnetic resonance (NMR) and electron spectroscopy are the most widely used.

NMR spectroscopy relies on the spin properties of certain nuclei, *i.e.* where nuclei with magnetic properties absorb and reemit electromagnetic energy. Its many variants permit to gather a variety of information, going from the local environment of a given nucleus to the proximity in space or via bonds between two given nuclei. Much of the recent innovation within NMR spectroscopy has been within the field of protein NMR. In contrast to X-ray crystallography however, NMR is most of the time limited to relatively small proteins. However, it is often very useful to obtain high-resolution information on unstructured parts proteins, where X-ray crystallography fails. Because of the much higher number of atoms present in a protein molecule in comparison with a small organic compound, the basic 1D spectra become crowded with overlapping signals to an extent where direct spectra analysis becomes untenable. Therefore, multidimensional (2, 3 or 4D) experiments have been devised to deal with this problem.

For ion channels, or any other type of membrane proteins, the transmembrane domains of the proteins have to be preserved in a native-like environment. Most of the time, detergent micelles are used but one can easily understand that the 3D structure can be lost during the preparation of the sample. To be trustworthy, such results thus have to be correlated with other measures of stability or activity.

When lipid bilayers are used, they provide the protein with a physical and chemical environment most similar to a natural membrane, but the large size and slow tumbling of lipid bilayer vesicles require the use of solid-state NMR methods. While the upper limit on the size of the macromolecular complexes to which solution NMR methods can presently be applied has been pushed well past 50 kD, solid state methods for structure determination of membrane proteins are more technically challenging and are still being developed. These techniques have been used to probe the structure of the KscA for instance (Chill et al. 2006) or to elucidate the

structure of the C and/or N- termini of ion channels (Baker et al. 2006).

Cryo-electron microscopy uses a particle beam of electrons to illuminate the sample. Whereas the resolution of optical miscroscopy is of the order of 200 nm, electron microscopy enables to get to the order of 0.2 nm. On the scale of proteins, this is still a rather low resolution but this technique is useful to access information of the 3-D assembling of proteins (quaternary structure) as has been done for the Nicotinic Acetylcholine Receptor (nAChR) (Unwin 1993).

3 Molecular Biology related techniques

Molecular biology techniques have recently made huge progress, making it possible today to engineer mutant proteins of all kinds and, in combination with other techniques (optical, electrophysiology...), to identify important residues in terms of structure and/or function.

3.1 Site directed mutagenesis

Site directed mutagenesis relies on the ability to engineer mutants of proteins that have just one amino acid that is altered with respect to the wild type sequence.

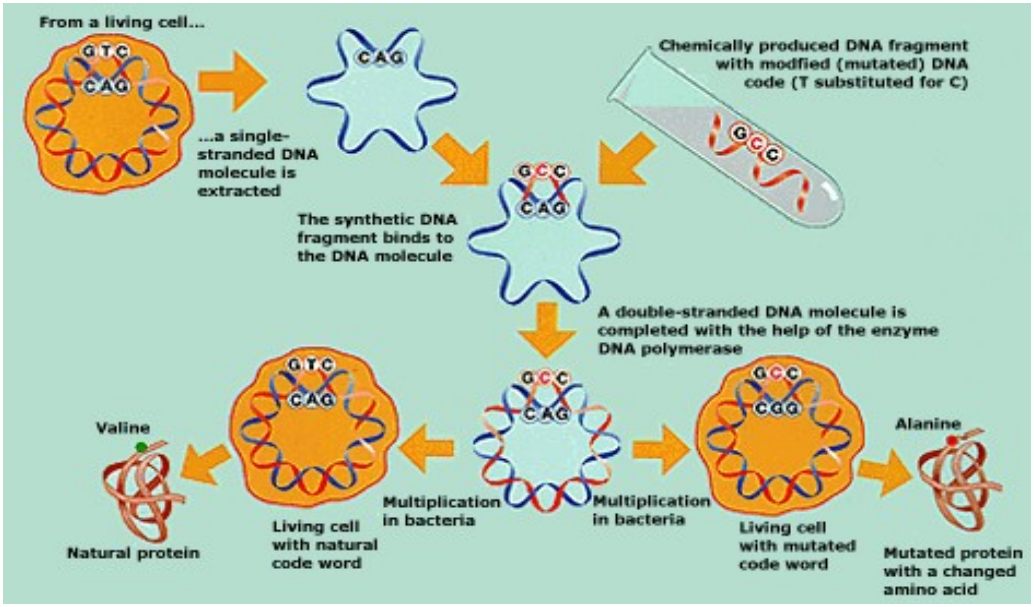

Figure A.2: Scheme of the site directed mutagenesis technique employed to produce proteins that contain a single mutation.

The basic procedure requires synthesizing a short DNA fragment (primer) that contains the desired base change (Fig. A.2). Besides, a single stranded DNA molecule is extracted from a

living cell. When put together, the primer binds to the single stranded DNA molecule, and a double stranded DNA molecule is completed thanks to the action of the DNA polymerase enzyme. This double stranded DNA is then replicated in bacteria, producing thereby two types of proteins: the wild type (WT) protein and the single amino-acid mutant.

A variety of properties can then be assessed by looking at the difference in the properties of WT channels or mutant ones. When using such a technique, however, attention must be payed because mutagenesis introduces a change in the primary structure and can potentially alter the 3-D structure. Similarly, one should also keep in mind that such mutations can alter the function of Kv channels (a first check is to verify that the mutant's properties are similar to those of the WT) and therefore special attention has to be payed when interpreting the data of such experiments.

3.2 Charge reversal mutagenesis

Charge reversal mutagenesis is a particular case of site directed mutagenesis in which a charged amino acid is mutated to another charged amino-acid of opposite charge (for example an arginine residue to a glutamic acid). This is particularly useful to probe salt bridges interactions in proteins. Coupling charge reversal mutagenesis of a positive residue residue to charge reversal of a negative residue partner enables detecting whether these residues are engaged in a particular salt bridge. In the case of Kv channels, it also enables “locking” the channel in a particular conformational state (open, closed or any intermediate state).

3.3 Substituted cysteine accessibility method (SCAM) and cycteine cross-linking

SCAM uses the site-directed mutagenesis described above coupled to chemical modification (Baker 2007). Indeed, after introducing a cysteine in place of the amino-acid whose location one wants to probe, it is possible to introduce thiol (SH) specific reagents, *i.e.* derivatives of methanethiosulfonate (MTS). MTS reagents react with cysteine residues in aqueous environments ~10^9 times faster than cysteine residues buried inside the protein or at the protein/lipid interface enabling the characterization of the residue's environment depending on the membrane polarization state (Akabas et al. 1994). Many methods deriving from this technique have also been developed to look at precise issues in Kv channels. For example, Ahern and Horn substituted specific positively charged residues with cysteine and then restored the original charge of S4 by adding positively charges cysteine reactive probes of various length. They then looked at the value of the gating charge of this mutant, arguing that the shorter the linker, the deeper the charge was moving into the electric field. As soon as the linker reached 4 Å, they found that the contribution of the gating charge was eliminated, leading them to propose a given depth of the electric field between the outside and the position of the mutated residue (Ahern & Horn 2004).

Another useful related technique, that involves introducing mutations to cysteine is cysteine cross-linking: A cross link is a bond that forms between two chains or between two residues that are far apart in the primary sequence of a protein. Because two cysteine residues can bond in a reductive environment, introducing cysteines at particular places in Kv channels helps probe wether two of such residues are close to one another in a given state. As well as charge reversal mutagenesis, this strategy can also be used to lock the channel in a special conformational state.

4 Biophysical techniques

4.1 Fluorescence based methods

The structural methods described above provide atomic scale resolution of ion channel structures, capturing essentially one isolated low-energy state. As explained before, Kv channels are able to open and close in response to changes in the TM voltage and during this process, they go through a variety of intermediate states that can be more or less stable. They may also be found in the complex medium of the cell, where local environmental factors, such as lipidic environment, TM voltage… can influence their structure and make it difficult to capture the extent of these changes using only structural methods. Along with the other methods described in this paragraph, fluorescence based methods have emerged as a powerful technique to access this kind of information, providing a real-time view into the conformation of Kv channels, as the experiments can be performed in living cells and with small quantities of protein (Taraska & Zagotta 2010).

Generally, fluorescent molecules absorb photons of particular wavelengths, thereby enabling a single paired electron to go from a low energy ground state to higher energy excited states. Once in one of these excited state, the electron quickly loses some energy through vibrational relaxation between high-energy excited states and finally falls back to the lower-energy ground state. The released photon has a lower energy and the emitted wave thus a longer wavelength. Because fluorophores exists in an excited state for a finite amount of time, we can take advantage of fluorescence techniques to probe the conformational movements of voltage-gated ion channels (VGCs). It is then necessary to attach a chosen fluorophore to a given amino-acid along the VGC sequence. The fluorescence techniques used can be divided in three categories: environmentally induced changes in fluorescence, fluorescence resonance energy transfer (FRET) and luminescence RET (LRET).

- *Environmentally induced changes in fluorescence* : The quantum yield and spectral characteristics of some fluorophores are very sensitive to the polarity of the environment. Looking at the fluorescence properties of such fluorophores attached to certain amino-acids of Kv channels while depolarizing or hyperpolarizing the

membrane can enable monitoring the conformational change in the region of the amino-acid. When labeling an amino-acid that lies at the interface between lipid and solution, changes in fluorescence can indicate that the residue is buried when the membrane is depolarized and exposed when the membrane is hyperpolarized and vice-versa. The same kind of strategy can also be used to monitor the changes in the local electric field: the ANEP chromophore that has proven to be a sensitive molecular indicator of transmembrane electrical events (Zhang et al. 1998) and by coupling the Di-1-ANEPIA probe to cysteines, it is possible to monitor changes in the local electrostatic field (Asamoah et al. 2003). However, it is often difficult to glean much information from the observation that one fluorophore-labeled residue exhibits a large change in fluorescence. On the other hand, if multiple residues localized to a specific region show similar changes in fluorescence, then it is likely that the structural domain is rearranging during the conformational transition.

- *FRET*: fluorescence (also called Forster) resonance energy transfer is the transfer of excited state energy from one fluorophore (donor) to another (acceptor) through dipole-dipole resonance coupling (Forster 1949) . The transfer of energy is only dependent on the distance between the partners. enabling to measure the distances between two amino-acids. In practice, for Kv channels, it is often used to monitor distance change between two amino-acids during conformational change when the polarity of the membrane is reversed. Also, attaching the acceptor molecule to a particular area of the lipid can enable to monitor quite precisely the position of the amino acid with respect to the membrane. Practical limitations come mostly from the size of fluorophores, their means of attachment and the potential disrupting effect they will have on the 3-D structure of the channel.

- *LRET*: luminescence (or lanthanide) resonance energy transfer is closely related to FRET but a luminescent lanthanide metal ion is used as the donor instead of an organic fluorophore (Selvin 2002). In most cases, organic fluorophores such as rhodamine or fluorescein are used as acceptor molecules. The main advantage of LRET over FRET is that lanthanide ions have multiple emission dipoles and the chance that the orientation of the probe will have a large impact on the efficiency of energy transfer is less than that of an organic fluorophore, that some probe combinations have extremely long R0 values (R0 being the distance at which 50% of the energy is transferred), enabling monitoring interactions up to 100 Å apart and that the extremely long excited state lifetime of lanthanide probes allows for more straightforward measurements of donor or acceptor lifetimes.

4.2 Avidin/biotin binding experiments

To probe wether a residue is accessible from one side of the membrane or the other, it is possible to take advantage of the strong affinity of avidin towards biotin. Indeed, biotin binds within a deep cleft inside the core of avidin, which is a rigid protein molecule (Fig. A.3). The

laboratory of MacKinnon developed the following strategy (Jiang et al. 2003b): they first introduce cysteine residues at specific locations in the channel, biotinylate the cysteine (add a linker to which biotin is attached), reconstitute the channels into planar lipid membranes, and finally determine whether avidin binds from the internal or external side and whether binding depends on membrane depolarization. Also, the distance from the cysteine α-carbon to the surface of avidin is 10Å and since avidin is large (the tetramer is a 57-kDa protein), it cannot fit into clefts on the channel and therefore cannot penetrate the surface. Therefore, for avidin to bind to a tethered biotin, the cysteine α-carbon has to be within 10Å of the bulk aqueous solution on either side of the membrane.

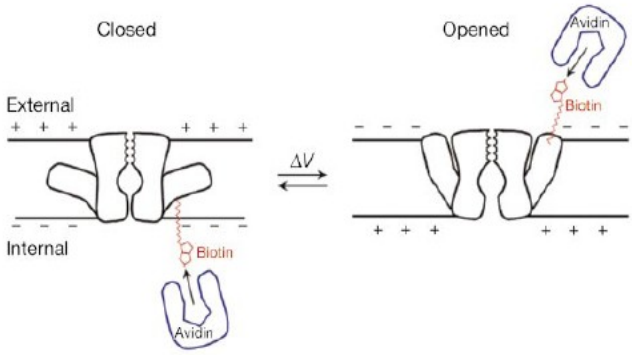

Figure A.3: Scheme of the Avidin/Biotin binding experiments. From (Jiang et al. 2003b).

It should be noted that in this technique, the use of avidin may lock the protein in an extreme position, overevaluating thereby the extent of the conformational change.

4.3 Toxin binding

Toxins or drugs often target voltage gated ion channel because they affect thereby the excitable cells of the nervous system, the heart or the muscles. Besides, they can also be used to study the function of ion channels. A lot of toxins target the main pore and were used in the early days of ion channel studies to probe which type of ion was conducted and other properties (Narahashi et al. 1964). Most recently, toxins that affect the voltage sensor of ion channels by binding to the loops in the extracellular medium have been used to study the conformational change during activation.

For example, Hanatoxin was added to the extracellular medium and was shown to interact with the voltage-sensor domain at negative potentials, indicating that the loop between S3 and S4 was exposed to the extracellular medium even in the resting state (Lee et al. 2003).

References

Ahern, C.A. & Horn, R., 2004. Specificity of charge-carrying residues in the voltage sensor of potassium channels. *The Journal of General Physiology*, 123(3), p.205 -216.

Akabas, M.H. et al., 1994. Identification of acetylcholine receptor channel-lining residues in the entire M2 segment of the α subunit. *Neuron*, 13(4), p.919-927.

Asamoah, O.K. et al., 2003. A fluorometric approach to local electric field measurements in a voltage-gated ion channel. *Neuron*, 37(1), p.85–98.

Baker, G., 2007. *Handbook of neurochemistry and molecular neurobiology* 3e éd., Glen Baker, Susan Dunn, Andrew Holt, Abel Lajtha.

Baker, K.A. et al., 2006. NMR-derived dynamic aspects of N-type inactivation of a Kv channel suggest a transient interaction with the T1 domain. *Biochemistry*, 45(6), p.1663-1672.

Chill, J.H. et al., 2006. NMR study of the tetrameric KcsA potassium channel in detergent micelles. *Protein Science*, 15(4), p.684-698.

Forster, T., 1949. Experimentelle und theoretische untersuchung deszwischenmolekularen ubergangs von elektronenanregungsenergie. *Zeitschrift Fur Naturforschung Section a-a Journal of Physical Sciences*, 4, p.321-327.

Hamill, O.P., Marty, A. & Neher, E., 1981. Improved patch-clamp techniques for high-resolution current recording from cells and cell-free membrane patches. *Pflugers Archiv European Journal of Physiology*, 391(2), p.85-100.

Horn, R. & Marty, A., 1988. Muscarinic activation of ionic currents measured by a new whole recording method. *Journal of General Physiology*, 92(2), p.145-159.

Jiang, Y. et al., 2003a. X-ray structure of a voltage-dependent K+ channel. *Nature*, 423(6935), p.33–41.

Jiang, Y. et al., 2003b. The principle of gating charge movement in a voltage-dependent K+ channel. *Nature*, 423(6935), p.42–48.

Lee, H.C., Wang, J.M. & Swartz, K.J., 2003. Interaction between extracellular Hanatoxin and the resting conformation of the voltage-sensor paddle in Kv channels. *Neuron*, 40(3), p.527–536.

Long, S.B., Campbell, E.B. & MacKinnon, R., 2005. Crystal structure of a mammalian voltage-dependent Shaker family K+ channel. *Science*, 309(5736), p.897 -903.

Long, S.B. et al., 2007. Atomic structure of a voltage-dependent K+ channel in a lipid membrane-like environment. *Nature*, 450(7168), p.376-382.

Narahashi, T., Moore, J.W. & Scott, W.R., 1964. Tetrodotoxin blockage of sodium conductance increase in lobster giant axons. *The Journal of General Physiology*, 47(5), p.965 -974.

Neher, E. & Sakmann, B., 1976. Single channel currents recorded from membrane of denervated frog muscle

fibers. *Nature*, 260(5554), p.799-802.

Sakmann, B. & Neher, E., 2009. *Single-channel recording* 2e éd., Springer.

Selvin, P.R., 2002. Principles and biophysical applications of lanthanide-based probes. *Annual Review of Biophysics and Biomolecular Structure*, 31, p. 275-301.

Taraska, J.W. & Zagotta, W.N., 2010. Fluorescence applications in molecular neurobiology. *Neuron*, 66(2), p.170-189.

Unwin, N., 1993. Nicotinic acetylcholine receptor at 9 Å resolution. *Journal of Molecular Biology*, 229(4), p.1101-1124.

Zhang, J. et al., 1998. Membrane electric properties by combined patch clamp and fluorescence ratio imaging in single neurons. *Biophysical Journal*, 74(1), p.48-53.

3- METHODS

" First, have a definite, clear, practical ideal; a goal, an objective. Second, have the necessary means to achieve your ends; wisdom, money, materials and methods. Third, adjust all your means to that end"

-Aristotle

Ce chapitre s'intéresse aux méthodes que nous avons développées et utilisées lors de ce travail de thèse. Toutes ces méthodes sont des techniques de simulation au niveau moléculaire et se divisent essentiellement en deux parties : d'une part, les méthodes que nous avons utilisées sans avoir à les développer, telles que la dynamique moléculaire, la modélisation par homologie ou encore les méthodes permettant d'évaluer le potentiel électrostatique et de l'autre, les méthodes que nous avons nous-mêmes mises en place afin d'étudier les propriétés bien spécifiques des canaux ioniques : les méthodes ayant pour but d'appliquer un potentiel transmembranaire et les méthodes permettant d'évaluer la charge de « gating ».

Le domaine d'étude des canaux ioniques a bénéficié des résultats de nombreux domaines expérimentaux (électrophysiologie, diverses techniques de spectroscopie, pharmacologie, crystallographie haute résolution...) qui ont permis de collecter un nombre impressionnant de données et de proposer des modèles du fonctionnement de ces protéines membranaires. Cependant, il reste des questions en suspens, en particulier au niveau moléculaire. La modélisation moléculaire est une technique théorique qui peut permettre en principe, en complément d'autres techniques, d'atteindre ce niveau de description.

En dynamique moléculaire, les atomes sont représentés par des particules classiques (qui ont une charge partielle et une masse constantes) et l'interaction entre ces dernières est définie par une fonction d'énergie potentielle qui décrit les interactions liées (liaisons, angles et dièdres) et les interactions non liées (électrostatiques et de van der Waals). Afin de limiter le temps de calcul, le nombre de particules doit être réduit (il peut alors aller jusque quelques centaines de milliers). Pour éviter les effets de bord, on calcule alors les interactions de ce système (qui contient dans notre cas le canal ionique inséré dans une bicouche lipidique, cet ensemble étant plongé dans une solution ionique) avec les images de ce dernier dans les trois directions de l'espace (appelé conditions périodiques aux limites). Le traitement des interactions a longue portée (électrostatiques) fait appel a l'utilisation des sommes d'Ewald, une technique qui divise le calcul entre deux contribution, à courte et à longue portée qui convergent rapidement dans l'espace direct et réciproque, respectivement. La connaissance des interactions à chaque instant permet ainsi de calculer la position des atomes après un pas de temps très court (de l'ordre de la femtoseconde) grâce à l'intégration des équations de Newton. C'est la répétition de cette étape un très grand nombre de fois qui permet de reconstituer l'évolution du système au cours du temps. Afin de nous positionner dans des conditions proches de l'expérience, il est possible de se placer dans des conditions de température et pression constante grâce à l'utilisation l'algorithmes spécifiques.

Afin de produire une structure pour des protéines dont la structure cristallographique n'a pas encore été résolue, nous avons également fait appel à la modélisation par homologie. Celle-ci s'appuie sur le principe selon lequel des protéines de séquences proches ont des également des repliements tridimensionnels proches. A partir d'un alignement de séquences d'une protéine de structure tridimensionnelle connue et d'une protéine de structure inconnue, on peut ainsi construire un modèle tridimensionnel de cette dernière.

Plus spécifiquement à cette étude, nous avons aussi conçu et utilisé des techniques pour calculer le potentiel électrostatique en chaque point de nos systèmes de particules. Ainsi, connaissant la position et la charge des différentes particules du système au cours du temps, nous avons pu calculer le potentiel électrostatique en tout point de l'espace grâce à l'application de l'équation de Poisson. Pour des systèmes composés d'une bicouche lipidique solvatée, nous avons ainsi pu déterminer le profil de potentiel le long de la normale à la membrane et ainsi déterminer le potentiel transmembranaire (*i.e.* la différence de potentiel entre les deux bains de part et d'autre de la membrane). Nous avons également fait appel à plusieurs techniques pour appliquer un potentiel transmembranaire. La technique historique consiste à appliquer un champ électrique, soit une force constante dirigé dans une direction donnée pour les particules chargées positivement et dans la direction opposée pour les particules chargées négativement. La polarisation des molécules, notamment d'eau, donne alors lieu à l'apparition d'un potentiel transmembranaire. Nous avons également élaboré une technique différente, qui est plus proche des conditions expérimentales lors de l'utilisation de « patch clamp ». Alors que dans ces expériences, où la membrane est chargée par l'application d'un potentiel entre deux électrodes placées de part et d'autre de la membrane, notre méthode considère un déséquilibre de charge entre les deux côtés de la membrane, *i.e.* le déplacement d'une particule chargée d'un côté à l'autre de la membrane. Afin que le système ne communique pas avec ses images dans la direction de la normale à la membrane et ainsi annule le déséquilibre de charge, nous avons inséré une couche de vide entre deux systèmes images puis réalisé nos simulations dans un système à volume constant. Puisque la membrane est un capaciteur, la séparation des charges donne alors lieu à l'apparition d'un voltage transmembranaire égal au quotient de la charge surfacique par la capacitance.

Finalement, nous avons adapté des méthodes de calcul de la charge de « gating », quantité bien spécifique aux protéines membranaires telles que les canaux ioniques voltage-dépendants. Cette charge correspond à l'intégrale des courants de « gating » qui sont mesurés lorsque des charges « accrochées » à la protéine se réorganisent en réponse à l'application d'un potentiel transmembranaire. D'une part, l'utilisation de la méthode de déséquilibre de charge pour appliquer le potentiel transmembranaire permet de mesurer directement cette charge de « gating ». En effet, puisque le déséquilibre de charge est fixe, toute chute du potentiel transmembranaire provient directement de la réorganisation de la protéine. Nous pouvons donc déduire de cette chute la charge transportée au cours de ce changement conformationnel. Nous avons d'autre part adapté une méthode de calcul énergétique des charges de « gating ». La charge de « gating » étant fonction du produit de la charge partielle portée par chaque résidu par la fraction du potentiel transmembranaire qu'elle traverse lors d'une transition en réponse à un potentiel transmembranaire, cette méthode a pour avantage de permettre d'identifier les résidus contribuant le plus à cette grandeur. Les valeurs obtenues par ces deux méthodes peuvent ensuite être comparées entre elles et aux valeurs mesurées expérimentalement.

As mentioned in chapter 2, the field of voltage gated ion channels has benefited from a large number of experimental techniques, *e.g.* structural biology, electrophysiology measurements, pharmacological data and spectroscopy techniques of various kinds, among others. Theoretical methods such as molecular simulations have stepped in a little later. The main advantage of these computational techniques is that they can provide information on a molecular level that most experimental ones cannot reach. The information from molecular dynamics (MD) simulations for instance (*e.g.* position, charges, velocities of atoms...) can enable to calculate a variety of quantities that can be measured by experiments. As an illustration, patch clamp electrophysiology measurements enable recording currents. In simulations, it is possible to follow ionic charge displacement and, using laws of physics, to calculate the same quantities. This enables, first, to validate the models and protocols used in simulations, and then, to predict behaviors that cannot be easily accessed through classical experiments.

This chapter aims at presenting all the general methods that were both used and specifically developed during this thesis. First, we will briefly describe the principles of molecular modelling methods that we mostly used here without further development. Then, we will present the protocols and methods developed in order to enable us to calculate the electrostatic properties of the simulated systems. In a third part, we will describe the methods we set up to apply transmembrane (TM) potentials in order to be in conditions close to patch clamp experiments. Finally, we will describe the two main methods we devised to monitor the gating charge, a quantity that is essential in the study of voltage gated ion channels (VGCs).

1 Molecular Modeling

Molecular modeling encompasses all theoretical methods and computational techniques used to model (or mimic) the structure or behavior of molecular systems. Ranging from quantum chemistry, where electrons are considered explicitly, to coarse grain simulations, where several atoms or group of atoms are represented by one particle, these simulations have enabled tackling a wide range of problems in chemistry and physics or more recently in biological domains. Here, we have used fully atomistic simulations, in which one atom is represented by one interaction center with its charge, mass and specific interaction properties.

1.1 Molecular dynamics (MD) simulations

Molecular dynamics refers to a family of computational methods aimed at simulating macroscopic behaviors through the numerical integration of the classical equations of motion of a microscopic many-body system. Macroscopic properties are expressed as functions of particle coordinates and/or momenta, which are computed along a phase space trajectory

generated by classical dynamics (Allen & Tildesley 1987) (Leach 2001). When performed under conditions corresponding to laboratory scenarios, MD simulations can provide a detailed view of the structure and dynamics of a macromolecular system. They can also be used to perform "computer experiments" that could not be carried out in the laboratory, either because they do not represent a physical behavior, or because the necessary controls cannot be achieved.

1.1.1 Force fields and potential energy function

MD simulations involve characterizing the forces between all particles in the considered system, deriving them from a potential energy function, also called a force field, and designated hereafter by U (Allen & Tildesley 1987) (Frenkel & Smit 2002) (Leach 2001). Force fields most commonly used in biophysics, such as GROMOS (Schuler et al. 2001), CHARMM (MacKerell Jr. et al. 1998) and AMBER (Case et al. 1999), are based on a classical treatment of particle-particle interactions that does not allow bond dissociation: the function U is written in terms of interactions between pairs of atoms and is typically divided into "bonded" and "non-bonded" terms. The bonded interactions consist of intramolecular harmonic bond stretching (E_{bond}), angle bending (E_{angle}), and dihedral angle deformation inside individual molecules ($E_{torsion}$). Non-bonded interactions include intermolecular electrostatic (E_{el}) and van der Waals terms (E_{vdw}). The former are calculated from the coulombic interaction of partial charges assigned to each atom, whereas the latter describe short-range repulsion and long-range attractions between pairs of atoms.

Its common mathematical form is then typically:

$$U = E_{bond} + E_{angle} + E_{torsion} + E_{el} + E_{vdw} \quad [3.1]$$

With:

$$E_{bond} = \sum_{i,j} k_{ij}^{b} (r_{ij} - r_{ij}^{0})^2 \quad [3.2]$$

$$E_{angle} = \sum_{i,j,k} k_{ijk}^{a} (\alpha_{ijk} - \alpha_{ijk}^{0})^2 \quad [3.3]$$

$$E_{torsion} = \sum_{i,j,k,l} k_{ijkl}^{t} [1 + \cos(n\,\omega_{ijkl} - \omega_{ijkl}^{0})] \quad [3.4]$$

$$E_{el} = \sum_{i,j} \frac{q_i q_j}{e_{ij} r_{ij}} \quad [3.5]$$

$$E_{vdw} = \sum_{i,j} \epsilon_{ij} \left[\left(\frac{\sigma_{ij}}{r_{ij}} \right)^{12} - 2 \left(\frac{\sigma_{ij}}{r_{ij}} \right)^{6} \right] \quad [3.6]$$

where r_{ij} is the distance between atoms i and j; α_{ijk} the angle between atoms i,j and k; ω_{ijkl} the dihedral angle between i,j,k and l; q_i is the partial charge on atom i; ε_{ij} and σ_{ij} are Lennard-Jones parameters for van der Waals interactions; and k_{ij}^{b}, k_{ijk}^{a} and k_{ijkl}^{t} on one hand and r_{ij}^{0}, α_{ijk}^{0}, and ω_{ijkl}^{0} on the other are the force constants and equilibrium values for the bond stretch,

angle bend, and dihedral torsion deformations.

1.1.2 Periodic boundary conditions (PBCs), long range interactions

In general, the number of atoms (N) considered in an MD simulation is typically of order 10^4-10^5, though much larger systems have occasionally been studied. To minimize surface effects, and thereby simulate more closely the expected behavior of a macroscopic system, it is customary to use periodic boundary conditions. The way in which the periodic boundary conditions are applied is illustrated for the two-dimensional case in (Fig. 3.1). The system as a whole is divided into cells. Each cell is surrounded on all sides by periodic images of itself: particles that are images of each other have the same relative positions within their respective cells and the same momenta. When a particle enters or leaves a cell, the move is balanced by an image of that particle leaving or entering through the opposite edge. In the case of an ion channel in its membrane environment, what we actually simulate is in fact a multilateral stack, or a fragment of a multilayer liposome with a high density of membrane protein.

Because we simulate an infinite system, special care must be taken for the long-range interactions. The van der Waals interactions, which decay rapidly, are typically turned off beyond a certain cutoff distance (generally, 10–15 Å), which is smaller than half the box size to avoid interactions between a molecule and its own image. The electrostatic interactions, described by a coulombic function, decay much slower and truncating them beyond a few Angstroms would introduce large artifacts. In order to reduce the computational cost while keeping the error on the interaction energy as low as possible, a mathematical trick is used: Ewald summation (and its modern computational equivalent Particle Mesh Ewald - PME) consists in replacing the summation of interaction energies in real space with an equivalent summation in Fourier space. The advantage of this approach is the rapid convergence of the Fourier-space summation compared to its real-space equivalent when the real-space interactions are long-range. Because electrostatic energies consist of both short- and long-range interactions, it is maximally efficient to decompose the interaction potential into a short-range component summed in real space and a long-range component summed in Fourier space:

$$\phi(r)=\phi_{sr}(r)+\phi_{lr}(r) \quad [3.7]$$

The short-ranged part $\phi_{sr}(r)$ sums quickly in real space and the long-ranged part $\phi_{lr}(r)$ sums quickly in Fourier space. The direct summation of interaction energies between point particles is then divided into two components:

$$E_{tot}=\sum_{i,j}\phi(r_j-r_i)=E_{sr}+E_{lr} \quad [3.8]$$

a direct sum E_{sr} of the short-ranged potential in real space:

$$E_{sr}=\sum_{i,j}\phi_{sr}(r_j-r_i) \quad [3.9]$$

and a summation in Fourier space of the long-ranged part:

$$E_{lr} = \sum_{k} \tilde{\phi}_{lr} |\tilde{\rho}(k)|^2 \quad [3.10]$$

where $\tilde{\phi}_{lr}$ and $\tilde{\rho}(k)$ represent the Fourier Transform of the potential and the charge density. Since both summations converge quickly in their respective spaces, they may be truncated with little loss of accuracy and great improvement in required computational time (Toukmaji & Board 1996).

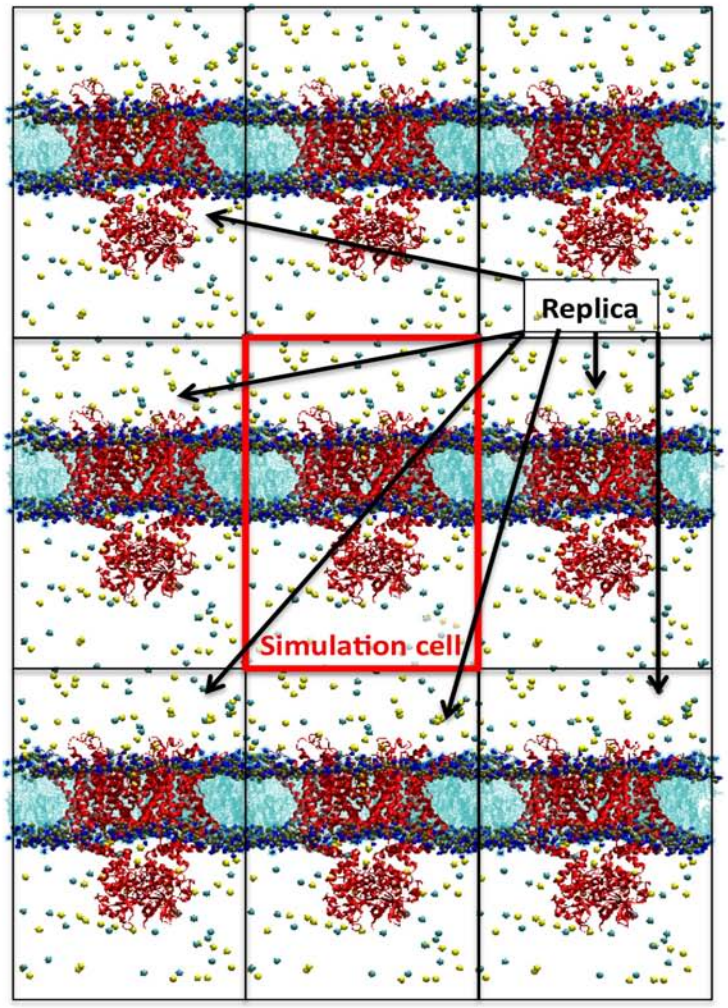

Fig. 3.1: Illustration of the use of periodic boundaries in molecular simulations. The simulation cell (in red) contains a finite number of atoms and in order to avoid size effects, it is replicated in the 3 directions of space. Here, only the first layer in 2 dimensions is shown (for clarity) as black boxes

1.1.3 Propagating the motion equations

Molecular dynamic simulations generate a set of atomic positions and velocities as a

function of time that evolve deterministically from an initial configuration according to the interaction potential *U*. MD simulations use information (positions, velocities or momenta, and forces) at a given instant in time, t, to predict the positions and momenta at a later time, $t + \delta t$, by integrating the classical equations of motion of Newton:

$$F(t) = m\,a(t) = -\nabla U(r(t)) \quad [3.11],$$

where the force *F(t),* that derives from the potential *U(r),* is equal to the product of the particle's mass *m* times its acceleration *a(t).*

To numerically integrate these equations, one of the commonly used algorithm is the Velocity Verlet algorithm, where the positions, velocities and accelerations at $t + \delta t$ are computed from their values at a time *t* (Verlet 1967) along:

$$r(t+\delta t) = r(t) + v(t)\delta t + \frac{1}{2}a(t)\delta t^2 \quad [3.12]$$

$$v(t+\frac{\delta t}{2}) = v(t) + \frac{1}{2}a(t)\delta t \quad [3.13]$$

$$a(t+\delta t) = -\frac{1}{m}\nabla V(r(t+\delta t)) \quad [3.14]$$

$$v(t+\delta t) = v(t+\frac{\delta t}{2}) + \frac{1}{2}a(t+\delta t)\delta t \quad [3.15]$$

δt is the time step, of the order of a femtosecond (10^{-15}s), and remains constant throughout the simulation. Numerical solutions of the equations of motion are thus obtained by iteration of this elementary step over the whole simulation time.

1.1.4 Constraints

Under certain circumstances, it may be desirable to freeze a subset of degrees of freedom in the course of the MD simulation through the introduction of holonomic constraints. The latter allow hard degrees of freedom that correspond to high–frequency vibrations — *i.e.* the vibration of covalent bonds involving hydrogen atoms — to be removed. By keeping through time these bond lengths at a nominal value, it is possible to increase the time step, δt, for integrating the equations of motion, without sacrificing the prerequisite of energy conservation.

Freezing certain degrees of freedom in the framework of classical MD is equivalent to solving constrained equations of motion. In the case of a fixed chemical bond length, the constraint writes:

$$\Theta_{ij}(t) = \left| r_j(t) - r_i(t)^2 \right| - d_{ij}^{\,2} \quad [3.16]$$

where d_{ij} stands for the equilibrium length of the chemical bond. It follows that, in addition to the force, F_i, due to intra– and intermolecular interactions, a constraint force, g_i, now appears in the equations of motion:

$$m_i \frac{d^2 r_i(t)}{dt^2} = F_i + g_i \quad [3.17]$$

This constraint force is defined by:

$$g_i = -\sum_j \lambda_{ij}(t) \nabla_i \Theta_{ij}(t) = -2 \sum_j \lambda_{ij}(t) r_{ij}(t) \quad [3.18]$$

where $\lambda_{ij}(t)$ is the Lagrange multiplier associated to the constraint enforced along the chemical bond connecting atoms i and j. Combined with the Verlet integrator, the equations of motion now write:

$$r_i(t+\delta t) = r_i(t) + \delta t\, v_i(t) + \frac{\delta t^2}{2m_i}[f_i(t) + g_i(t)] \quad [3.19]$$

These constrained equations of motion are solved in most cases following a Gauss–Seidel–like, iterative scheme — *i.e.* solving one by one the equations of a linear system — until each holonomic constraint is satisfied.

1.1.5 Simulation ensembles

The MD technique is a scheme for studying the natural time evolution of a classical system of N particles in a volume V. In simulations using the Newton equations of motion, the total energy E is conserved and along the trajectory, the system samples the constant NVE ensemble (also called micro-canonical ensemble). However, it is often more convenient to perform simulations in other ensembles such as the NVT (isothermal) or NPT (isothermal and isobaric) ensembles. To do so, the algorithms used have to be modified.

Constant temperature (Isothermal) MD

A number of schemes, more or less sophisticated, for carrying out isothermal MD simulations have been proposed.

Perhaps the simplest consists in rescaling periodically the velocities by a factor $\sqrt{T_0/T(t)}$, where $T(t)$ denotes the instantaneous kinetic temperature (Woodcock 1971) and T_0 the target temperature. This method however has the drawback of not letting T_0 appear explicitly in the equations that are integrated along the simulation and the fluctuations of this value can therefore not be stabilized.

Another approach, referred to as weak coupling (Berendsen et al. 1984), consists in letting

the instantaneous kinetic temperature, $T(t)$, "relax" towards the reference temperature, T_0, following:

$$\frac{dT}{dt} = \frac{(T(t) - T_0)}{\tau_t} \quad [3.20]$$

where τ_t represents precisely the relaxation time associated with the fluctuations of the temperature. The kinetic energy is modified by a quantity ΔK , defined as:

$$\Delta K = \frac{1}{2}(\lambda^2 - 1) N k_B T(t) \quad [3.21]$$

during a time–step, δt, by rescaling the velocities by a factor λ:

$$\lambda = \left[1 + \frac{\delta t}{\tau_T}\left(\frac{T_0}{T(t)} - 1\right)\right]^{1/2} \quad [3.22]$$

This aperiodic coupling to a "heat reservoir", by means of a first–order process, does not lead to oscillating responses to temperature changes. Yet, neither does it yield the correct canonical distribution.

Third, Langevin dynamics involves adding damping and random forces to simulate the influence of the external medium to the system

$$m_i a_i(t) = F_i(t) + f_i(t) - m_i \beta_i v_i(t) \quad [3.23]$$

where m_i and a_i are the mass and the acceleration of atom i. F_i is the sum of forces exerted by all other atoms on atom i, β_i is a friction term and v_i the velocity of the atom i at time t. f_i is a random force depending on the temperature and whose components follow a normal law.

$$\sqrt{\frac{2 m_i \beta_i k_B T_0}{\delta t}} \quad [3.24]$$

where T_0 is the target temperature of the system and δt the integration step.

A last approach, the most rigorous, consists in introducing in the equations of motion an additional degree of freedom, *s*. The velocity of particle *i* can, thus, be written

$$v_i = s\dot{x}_i = p_{x,i}/m_i s \quad [3.25].$$

Potential and kinetic terms are associated with the degree of freedom s, which can be envisioned as the thermostat of the system:

$$\begin{cases} V_s = \frac{1}{\beta}(f+1)\ln s \\ K_s = \frac{1}{2} Q \dot{s}^2 \end{cases} \quad [3.26]$$

where $\beta = 1/k_B T$, Q is the parameter of thermal inertia that regulates the fluctuations of temperature, and f is the number of degrees of freedom in the system — 3N-3 if the total momentum p is a constant. Such an approach is known as extended Lagrangian, owing to the fact that the latter can be expressed as

$$L_s(x; p_x) = K(p_x) + K_s(p_x) - V(x) - V_s(x) \quad [3.27]$$

The equations of motion may then be:

$$\begin{cases} \ddot{x}_i = \dfrac{f_i}{m_i s^2} - 2\dfrac{\dot{s}\dot{x}}{s} \\ Q\ddot{s} = \sum_i m_i \dot{x}_i^2 s - \dfrac{f+1}{\beta s} \end{cases} \quad [3.28]$$

This formalism, devised by Nosé (Nosé 1984), has been revisited by Hoover (Hoover 1983) (Hoover 1985), who suppressed the time–dependent parameter s. In the constrained equations of motion (31), the friction term is now given by a first–order differential equation:

$$\dot{\xi} = \frac{f}{Q} k_B (T(t) - T_0) \quad [3.29]$$

The conserved quantity, here, is the total Hamiltonian, *i.e.* that of the chemical system plus the thermostat,

$$H_s(x; p_x) = K(p_x) + K_s(p_x) + V(x) + V_s(x) \quad [3.30]$$

Constant pressure MD

Pressure control can also be achieved by an extension of the weak coupling algorithm (Berendsen et al. 1984). Just like for the constant-temperature scheme, the equations of motion are modified in response to the relaxation of the instantaneous pressure, *P(t)*, towards its reference value, P_0, according to:

$$\frac{dP(t)}{dt} = \frac{P_0 - P(t)}{\tau_P} \quad [3.31]$$

Here, τ_P is the relaxation time associated to the fluctuations of the pressure. By rescaling the atomic coordinates of the system and the size of the periodic cell by a factor κ, the total volume is modified by $\Delta V = (\kappa^3 - 1)$, leading naturally to a variation of the pressure, which can be expressed as:

$$\Delta P = \frac{\Delta V}{\beta V} \quad [3.32]$$

where β denotes the isothermal compressibility. Solving equations [3.31] and [3.32] for a

given value of κ, it follows that:

$$\kappa = \left[1 - \beta \delta t \frac{P_0 - P(t)}{\tau_P} \right]^{1/3} \quad [3.33]$$

For reasons similar to the case of constant temperature, this algorithm does not yield a well–defined thermodynamic ensemble.

Just like for keeping the temperature at a constant value, the extended Lagrangian formalism can be applied to pressure. Initially devised by Andersen (Andersen 1980) this approach implies that the system be coupled to an external variable, V, characterizing the volume of the simulation box. This coupling symbolizes the action a piston would exert on the system, to which a kinetic and a potential term is associated:

$$\begin{cases} V_v = \frac{1}{2} m_p \dot{V}^2 \\ K_V = P_0 V \end{cases} \quad [3.34]$$

where m_p can be seen as the mass of the piston, and P_0 denotes the desired pressure. Scaling of the positional variables, r, and the velocities, v, in the form $s = r / V^{1/3}$ and $\dot{s} = v / V^{1/3}$, one can rewrite the potential and kinetic energies as: $V(r) \equiv V(V^{1/3} s)$ and $K(p_x) = \frac{1}{2} m V^{2/3} \sum_i \dot{s}_i^2$. It follows that from the Lagrangian $L_v(x; p_x) = K(p_x) + K_v(p_x) - V(x) - V_v(x)$, one can establish the new equations of motion:

$$\begin{cases} \ddot{s}_i = \frac{f_i}{m_i V^{1/3}} - \frac{2}{3} \frac{\dot{s}_i \dot{V}}{V} \\ \ddot{V} = \frac{P(t) - P}{m_p} \end{cases} \quad [3.35]$$

where the force, f_i, and the instantaneous pressure, $P(t) = \frac{1}{V} (N/\beta - \frac{1}{2} \sum_i x_i . f_i)$, are evaluated from the unscaled cartesian coordinates and momenta. Here, the conserved quantity throughout the MD simulation is the Hamiltonian of the extended system, $H_v(x; p_x) = K(p_x) + K_v(p_x) + V(x) + V_v(x)$, that is its enthalpy, to which is added a kinetic contribution of $1/2\beta$ arising from the fluctuations of the volume of the simulation cell. It should be underlined that, formally, this algorithm generates an isobaric–isoenthalpic distribution, *(N, P, H)*. Its coupling to a thermostat, like the one governed by equation [3.28], yields the true isobaric–isothermal distribution. It has been observed that this scheme would lead to oscillations of P, depending upon the mass of the piston, m_P.

An alternative has been devised that suppresses this undesirable effect by damping out the

degree of freedom of the piston through a Langevin equation. Restating equation [3.31], it follows that:

$$\begin{cases} \ddot{s}_i = \dfrac{f_i}{m_i V^{1/3}} - \dfrac{2}{3}\dfrac{\dot{s}_i \dot{V}}{V} \\ \ddot{V} = \dfrac{P(t) - P}{m_p} - \gamma \dot{V} + R(t) \end{cases} \quad [3.36]$$

where γ is the collision frequency and *R(t)*, a random force taken from a Gaussian distribution of zero mean. Interestingly enough, *R(t)* satisfies the fluctuation–dissipation relationship, *i.e.*

$$\langle R(t_1) R(t_2) \rangle = \frac{2}{\beta m_P} \kappa(t_1 - t_2) \quad [3.37]$$

where $\kappa(t)$ stands for the damping factor.

In this work, we have chosen to use Langevin dynamics for both temperature and pressure control. Although it is not the most rigorous approach, it is the best that is currently implemented in NAMD.

1.2 Homology Modeling

Molecular dynamics of proteins requires a starting conformation that is close to the equilibrium structure. The best initial structure, although it also suffers from drawbacks (see Annex 1), would come from a high resolution X-ray structure. When none is available, it is possible to guess an initial conformation using homology modeling. This procedure, also termed comparative modeling or knowledge-based modeling, develops a three-dimensional model from a protein sequence (called the target) based on the structures of homologous proteins (also called the templates) (Krieger et al. 2005).

Homology modeling relies on the following assertion: for a set of proteins that are hypothesized to be homologous, their 3-D structures are conserved to a greater extent than are their sequence. It follows therefrom that even if the sequence identity between two proteins is rather low, their fold can be conserved and thus 3-D model prediction can be achieved. For this, two steps are critical: the alignment of the amino-acid sequences and the confection of a 3D atomic model.

1.2.1 Sequence alignment

The first step in homology is to generate the sequence alignment between the templates and the target. To align two sequences, two mechanisms can be used (Fig. 3.2):

Substitution involves replacing a residue in the template sequence by another one in the target.

Insertion/deletion involves either removing a residue in the target sequence or in the template sequence, resulting in the introduction of a gap in the alignment. This mechanism is useful when the sequence lengths differ in the template and the target and/or to achieve a good alignment residue-to-residue at some other neighboring point in the sequence.

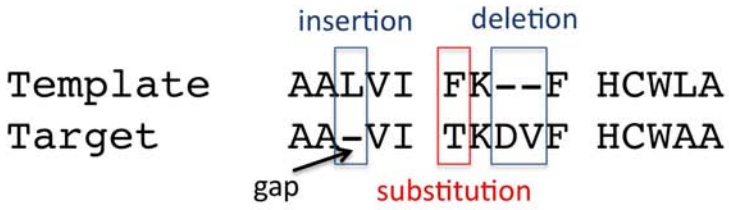

Fig. 3.2: Sample alignment of a target sequence with a template illustrating the different evolutionary mechanisms. Insertion and deletion result in a gap in the alignment while substitution exchanges a residue with another one.

In principle, it is possible, knowing the important residues or segments of the target to produce a sequence alignment with the template by hand. However, algorithms have been designed that enable to perform automatic sequence alignments. They rely on the calculation of a scoring function, that has to be maximized during the alignment procedure. This function is a combination of essentially two parameters: the cost of substituting a residue by another and the cost of inserting a gap in the sequence.

The cost of substituting a residue by another defines the probability to replace a residue in the template sequence by another in the target sequence. For each residue pair, a score is assigned. The score for identical residues are highest and exchanges between residue types with similar physicochemical properties (*i.e.* Phe → Tyr) get a better score than exchanges between residue types that widely differ in their properties (*i.e.* Phe → Lys). These values are arranged in a square matrix of 20 by 20 residues called the substitution matrix.

The cost of inserting a gap in the sequence is called the gap penalty. Biologically, it is in general easier for a protein to accept a different residue in a position, rather than having parts of the sequence chopped away or inserted. Also, a higher penalty score should be assigned for the first missing residue than for the subsequent ones. Indeed, this accounts for the fact that each genetic mutational event can insert or delete many residues at a time. These gap penalty values should result in single gaps being scarcer than substitutions.

During the alignment process, the algorithm tries to maximize the scoring function, generating the best possible compromise between the substitution of residues of different chemical natures and gap insertion. The best alignment is then the one with the largest score.

For a protein of ~200 residues, a sequence alignment with over 30% sequence identity is considered of good quality and will yield a reliable homology model. Over 60%, the model is even considered of "crystallographic" quality. Below 30%, it is very important to introduce into the alignment additional information from experiments such as conserved residues, mutations, secondary structure elements... Also, it can prove useful to resort to multiple sequence alignment. Indeed, providing sequences of intermediate identity can help bridge between two sequences of lower identity.

1.2.2 3-D model building

The information from the sequence alignment and the atomic coordinates of the template are then used to build a 3D atomic model of the target. When generating coordinates for the target structure, both the main chain atoms and side chain atoms have to be modeled.

For the structurally conserved regions, one considers that the main chain atoms of the target structure are those from the template. Side chain coordinates are also taken to be the same if the residue type in the target is identical or very similar to that in the template. If target and template residues differ, an initial guess for side chain coordinates is considered (*e.g.* taken from a side chain rotamer library). To select a correct rotamer, either manual or energy-based criteria are considered in order to take into account the interaction with the local environment.

For the variable regions, that correspond most of the time to protein loops, a variety of approaches may be applied in assigning coordinates to the target. If a loop in one of the template structures fits in the target region without making bad contacts with other atoms, it is considered a good model for the target. Otherwise, one can search fragment databases for loops in other proteins that may provide a suitable model that may then be subjected to conformational searching to identify low energy conformers. As in the case of conserved regions, coordinates for side chain atoms in these loop regions may be used if these residues are similar. In practice, side chain rotamers from libraries are required to define coordinates in these regions.

The produced model is then an initial guess that can be quite far from equilibrium. Quite often, this structure will be minimized/relaxed in vacuum or in its environment to reach the closest, stable structure.

2 Electrostatic potential (EP) calculations

The main force that drives the function of voltage gated ion channels is the presence -or not- of TM potentials, and hence of electric fields across the membrane. It is therefore very important to be able to evaluate the EP, and therefore the electric field in each point of the system. Because we use an atomistic description of the system, coordinates of each particle

are available as well as their partial charge, enabling the calculation of the EP in any given position, the so-called local EP. This section describes the methods used in this work to calculate this local electrostatic potential and to determine therefrom the TM potential, defined as the potential difference between the extracellular (top) and the intracellular (bottom) bath.

2.1 3-D EP maps

Atomistic simulations provide us with the positions of each particle at a given time. Because each particle bears a partial charge it is possible to calculate for a given system of configuration j, the electrostatic potential $\Phi_j(r, \Delta V)$ at position r can be computed by solving the Poisson's equation a 3-D grid as:

$$\nabla^2 \Phi_j(r, \Delta V) = -4\pi \sum_i \rho_i(r) \quad [3.38]$$

where the sum is running over all atoms bearing a partial charge ρ_i in the system. In practice, each partial charge is approximated by a spherical Gaussian of inverse width σ (taken to be σ = 0.25 $Å^{-1}$ here) and the equation is solved on a 1.5 x 1.5 x 1.5 $Å^3$ grid.

In order to be able to determine the EP felt on average by a particle in a given position , and therefore the local electric field acting on it (which is simply the opposite of the derivative of the EP), one has to consider the time averages of charge distributions. This may be achieved by considering EP maps that were calculated considering at least 20 to 50 frames spread over few tens of nanoseconds.

2.2 EP profiles along the membrane normal

A quantity that is particularly interesting to compare with electrophysiology experiments is the TM potential, which is defined as the voltage difference between the extracellular (top) and the intracellular (bottom) bath.

The one dimensional (1D) electrostatic potential $\phi(z)$ as a function of the position along the membrane normal *z* can be estimated using two different methods:

1 It is possible to consider averages the EP potential *x,y* slabs of thickness δ*z* of the 3D EP maps calculated as described above.

2 $\phi(z)$ can also be derived directly from the charge distribution of all atoms in the *x,y* slabs of thickness δ*z*, ρ(z). Following from the 1D Poisson equation, the EP potential can then be calculated as:

$$\phi(z) - \phi(0) = -\frac{1}{\epsilon_0} \int \int \rho(z'') dz'' dz' \quad [3.39]$$

Note that this formulation enables to distinguish the contributions of the different components of the system, such as the lipids, the protein or the water/ions.

Both means of obtaining averages of the EP along the normal to the membrane yield the same result. Figure 3.3 reports the 1D electrostatic profiles for a hydrated palmitoyl-oleoyl-phosphatidylcholine (POPC) bilayer. The charge distributions of the contributions of water and lipids long the z axis are presented separately, together with the corresponding EP profiles. The sum of the two yields the global EP potential profile: The latter is set to 0 in the solution baths and is seen to rise at the membrane water interfaces to reach a positive value at the membrane center, rationalizing the role of the membrane bilayer as a barrier for charged and polar species. Here, the membrane potential, also called "dipole potential", (the difference between the potential in the solution and the center of the bilayer) amounts to ~1.2 V. Note here that this value is highly dependent on the simulation parameters, *e.g.* the force field...

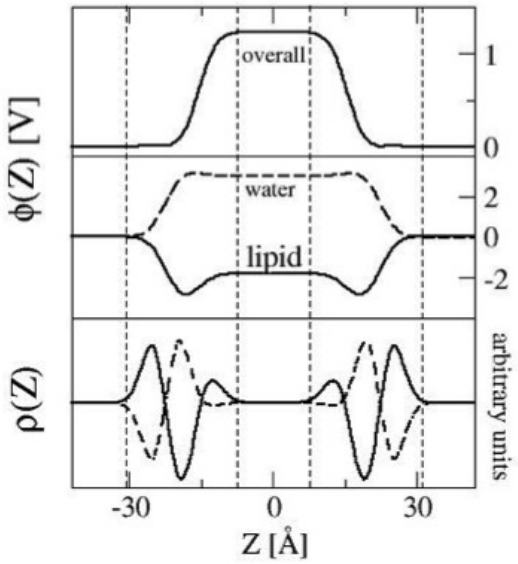

Fig. 3.3: Charge density and EP profile along the normal to the bilayer (z axis). (Top) Total electrostatic potential profile $\phi(z)$ *along the normal to the bilayer. (Middle) Contributions from the lipid (black line) and the water (dashed line) to the total EP. (Bottom) Charge density profile of the lipids and the water along the z axis. Note that the zwitterionic headgroups of the lipid give rise to a dipole at the interface (positive charges outermost and negative charges innermost) and that the water molecules orient in response to this dipole giving rise to a dipole of opposite direction. Altogether, the potential difference between the lipid center and the solution is positive and of magnitude ~1.2V.*

3 Applying a transmembrane potential

A central question to this study is the correct simulation of the applied transmembrane potential: whether when a cell membrane is naturally submitted to an electrical stress, or during a voltage clamp experiment, the TM potential always results from a local ionic charge

imbalance, *i.e.* from an excess of positive charge on one side of the membrane and an excess of negative charge on the other.

A correct simulation of such properties in simulations is challenging, mainly due to the use of PBCs and this paragraph presents the different methods that have been used to apply such a TM potential. Because of the use of PBCs in MD (Fig. 3.1), an ionic imbalance cannot be applied directly, due to the interaction of the top bath of the original system with the bottom bath of its image in the +z direction and vice versa. Two major methods have been proposed to circumvent such a technical problem and they will both be described in the following. The earliest method consists in mimicking the effect of an electric field by applying an additional force along the membrane normal on each charged particle, leading to polarization of the molecules and therefore to appearance of a TM potential. Other methods were also proposed to apply directly a charge imbalance and avoid the effect of the PBCs: 1- the double bilayer system involves separation of the internal bath from the external one by introducing two bilayers in the simulation cell and 2- the vacuum slab method, introduced by us, involves an extended system containing an vacuum slab between periodic images in the z direction to prevent the system from interacting with its images along the membrane normal.

3.1 Applying an electric field

In experiments, a charge imbalance gives rise to a TM potential -and therefore to an electric field- along the membrane normal. In MD simulations, the first strategy developed to apply a TM potential, which is also the simplest to implement technically, was then to apply a constant electric field $\vec{E}$ (Suenaga A et al. 1998) (Zhong, Moore, et al. 1998) (Tieleman et al. 2001) (Crozier et al. 2001) .

In practice, this is done by adding a force $\vec{f}_i$ to all the atoms bearing a charge q_i . Reorganization of the molecules, and most particularly of the water dipoles then induces a voltage difference $\Delta V = E \,.\, L_z$ over the whole system where L_z is the size of the simulation box along the normal to the bilayer plan (usually *z* axis). Note here that in experiments, the potential difference arising from the application of an electric field to a capacitor amounts to $E.d$ with d the thichness of the capacitor. Here, because the application of the electric field causes the reorganization of all the water molecules in the system, the dipoles add up and the application of the Poisson equation leads to a TM potential that is function of the simulation box size as opposed to the thickness of the membrane. Because of this, caution should then be exerted when comparing electric field values in simulations with values applied in experiments; the quantity that is most easy to compare is the TM potential.

This method has been successfully used so far for a wide range of studies such as membrane electroporation (Tieleman 2004) (Tarek 2005) lipid externalization (Vernier et al. 2006), voltage-gated K+ channels activation (Treptow et al. 2004) and transport properties of several ion channels (Crozier et al. 2001) (Aksimentiev & Schulten 2005) (Khalili-Araghi et al. 2006) (Sotomayor et al. 2007).

However, the electric field method introduces an artifact: in such an implementation, the particles are subject both to the force deriving from ΔV (due to the polarization of the molecules in the system) and to a constant additional force $\vec{f} \ll q_i \vec{E}$, that acts directly on charged particles. When the electric force due to ΔV is small, the additional force becomes important inducing a non-physical behavior.

3.2 Applying a charge imbalance

In patch clamp experiments, electrodes are plunged on both sides of the membrane and the TM voltage pulse is long enough to generate an ionic reorganization within the solution and subsequent charge of the membrane. To reproduce such conditions in MD simulations, other methods were introduced, that are based on an ionic charge imbalance.

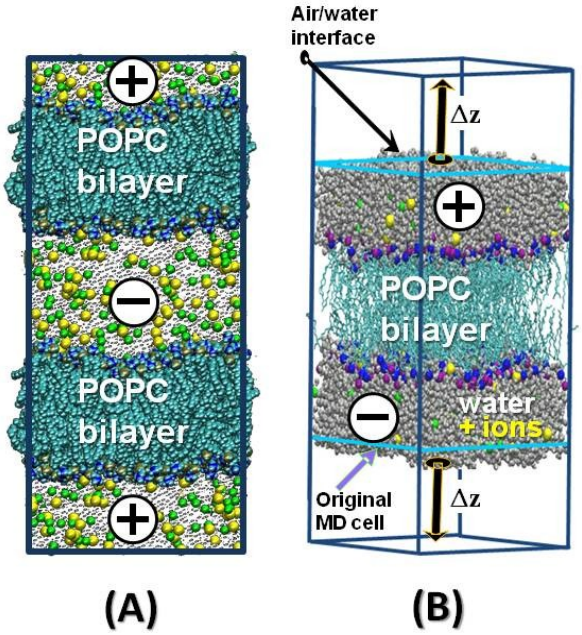

Figure 3.4: Charge imbalance setups to apply a transmembrane potential. (A) The central bath is isolated from the external media by two separate bilayers. A charge imbalance is then applied between the internal and external solutions. (B) The simulation cells, containing only one bilayer, are isolated from each other in the z direction by the presence of a vacuum slab. This vacuum slab is maintained by running the simulations at a constant volume. A charge imbalance is applied between the bottom and the top bath.

First, a method allowing simulations of realistic TM potential gradients across bilayers was proposed (Sachs et al. 2004), where TM voltages are obtained using a unit cell consisting of three salt-water baths separated by two bilayers and full 3D periodicity (Gurtovenko & Vattulainen 2005) (Kandasamy & Larson 2006), inducing therefore a TM potential generated by explicit ion dynamics (Fig. 3.4 A).

We introduced a variant of the method where consideration of the double layer is not

necessary, avoiding therefore the over-cost of a large and asymmetrical system. The method considers a unique bilayer surrounded by electrolyte baths, each terminated by an vacuum/water interface (Fig. 3.4. B).

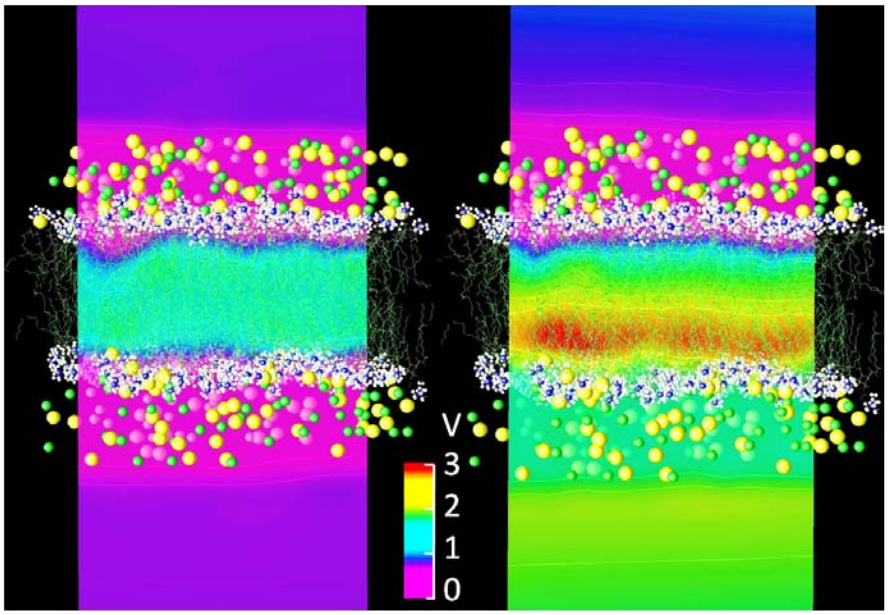

Figure 3.5: EP maps generated from the MD simulations of a POPC lipid bilayer (acyl chains: green, head groups: white) surrounded by electrolyte baths at ~ 1M NaCl. (Na^+ yellow, Cl^- green, water not shown) terminated by an air/water interface. Left: net charge imbalance Q = 0e; Right: Q = 6e.

In practice, we first consider a simple bilayer system. Constant pressure and temperature MD simulations are performed in order to equilibrate the system at a given salt concentration using 3-D PBCs. This ensures that the bilayer with its salt concentration is well equilibrated (optimum area per lipid). Then, vacuum/water interfaces are created at both sides of the system by extending the length of the original box. Simulations are then run at constant volume for further equilibration. Fig. 3.5 shows the EP (φ) maps generated from MD simulations of the bilayer in contact with water slabs each at 1M NaCl salt concentration using the Poisson equation (Eq. 3.38), considering or not a net charge imbalance Q between the electrolytes. Such a setup allows hence for a uniform voltage distribution above and below the lipid membrane. In Figure 3.6, we report the EP profiles $\varphi(z)$, generated from MD simulations of the pure bilayer in contact with salt water baths (Q varying from 0 to 8e) and calculated using Eq. 3.39. For all simulations, $\varphi(z)$ shows plateau values in the aqueous regions and an increasing potential difference between the two electrolytes: because the bilayer acts as a capacitor, the separation of the charges gives rise to a TM potential, with Q the charge imbalance per surface area and C the capacitance of the bilayer. Using this method, we can evaluate the capacitance of the bilayer for the first time using MD simulations, as the inverse of the slope of the curve of ΔV as a function of Q (Fig. 3.6 left). We find here C = 0.85 $\mu C/cm^2$, which is in good agreement with the 1 $\mu C/cm^2$ value that is traditionally assumed for

lipid bilayers.

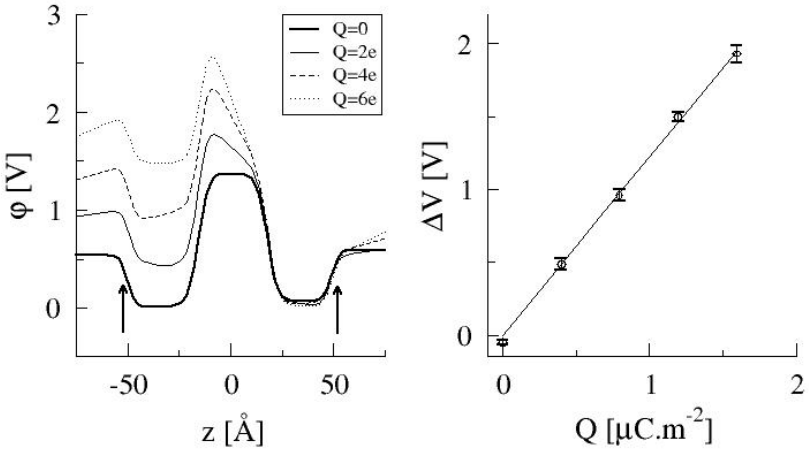

Figure 3.6: Left: Electrostatic potential φ(z) across a POPC lipid bilayer for different net charge imbalances Q between the upper and lower electrolytes. As a reference, φ was set to zero in the upper electrolyte. The arrows indicate the position of the air-water interfaces. Right: TM potential ΔV as a function of the charge imbalance Q.

4 Gating charge calculation

Gating currents are linked to the movements of charged groups (charges like ions or like charged residues, dipoles...). Within the framework of the Ramo-Shockley theorem, measured gating charges may be expressed as a function of starting and ending locations r_i of all particles bearing charges q_i and $\phi_i^{\lambda}(r_i)$, the electrostatic potentials of each configuration λ (Nonner et al. 2004). A similar formulation may be reached *via* energetic considerations .

In the particular case of voltage gated ion channels in the presence of an activating external electric force, the displacements of the charges tethered to the protein give rise to tiny transient "gating" currents (illustrated in Fig. 3.7). The time integral of the latter is called the "gating charge" (*Q*) translocated across the membrane capacitance and can be defined for a specific conformational change. This quantity, which can be measured by electrophysiology experiments (see chapter 2), can also be calculated from information extracted from molecular dynamics simulations, using the two separate methods described hereafter.

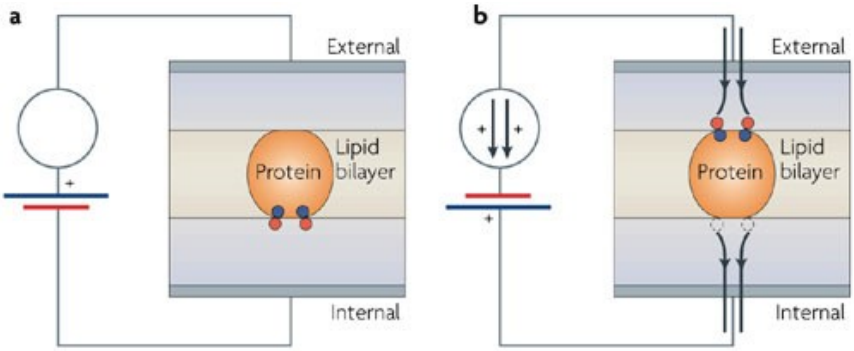

Figure 3.7: The membrane protein contains two positive charges (blue in panel a; negative countercharges are red). When the membrane voltage is reversed (panel b), these charges move from inside to outside of the membrane, crossing the entire electric field. In order to keep the membrane potential constant, the voltage-clamp circuit therefore has to remove two negative charges from inside the membrane capacitor (dotted circles) and provide two negative charges to the external side. The current recorded will therefore reflect the outwards movement of two positive charges. If the two charges of the sensor traverse only half the field, then only one external charge will be required to move. Therefore, in experimental terms, the charge transferred is the product of the magnitude of the moving charge times the fraction of the field it traverses. From (Bezanilla 2008).

4.1 Direct measurement

In general for a membrane protein system, the use of the charge imbalance method coupled to the vacuum slab enables the direct calculation of the gating charge. Indeed, the movement of charges, and most particularly of protein charges, across the membrane capacitor is reflected directly by a change in the transmembrane potential.

By considering a channel-membrane system, the time dependent voltage difference across the membrane is defined as:

$$\Delta V(t) = V_{\text{int}}(t) - V_{ext}(t) \quad [3.40]$$

V_{int} and V_{ext} are respectively the voltages of the internal and external membrane regions of the system at time *t*. Using the vacuum slab protocol, the transmembrane voltage is related to the charge imbalance between the electrolytes through:

$$\Delta V(t) = \frac{Q_0(t)}{C} \quad [3.41]$$

in which $Q_0(t)$ is the charge imbalance $q_0(t)$ per membrane area *A*, *i.e.*, $Q = q_0 / A$, and *C* is the membrane capacitance which is constant for our channel/membrane system (Stefani et al. 1994) (Treptow, Tarek, et al. 2009) in the TM voltage range we consider. $q_0(t)$ writes as:

$$q_0(t) = q_{\text{int}}(t) - q_{ext}(t) \quad [3.42]$$

q_{int} and q_{ext} being respectively the net charge within the internal and external regions

of the system. Note that $q_0(t)$ results from contributions of protein charges and of ions in solution $q_0(t)=q_0^{protein}(t)+q_0^{ion}(t)$. By combining this into eq. [3.42], we can relate $q_0^{protein}$ to $\Delta V(t)$ through:

$$q_0^{protein}(t)=-q_0^{ion}(t)+AC\,\Delta V(t) \quad [3.43]$$

that allows us to compute the gating charge associated with two conformational states of the channel λ_1 and λ_2 ,

$$Q(t)=-\frac{1}{2}\left[q_0^{protein}(\lambda_2)-q_0^{protein}(\lambda_1)\right] \quad [3.44]$$

with $q_0^{protein}(\lambda_1)$ and $q_0^{protein}(\lambda_2)$ being the charge imbalance due to protein charges in the λ_1 and λ_2 conformation, respectively.

4.2 Energetic formalism

Knowing the charge and positions of the atoms crossing the membrane, and the TM potential difference during the conformational change enables calculation of the gating charge *Q* as follows:

Q can be linked to the microscopic state of the channel through:

$$Q=\frac{\Delta G(\lambda_2,\Delta V)-\Delta G(\lambda_1,\Delta V)}{\Delta V} \quad [3.45]$$

where is the TM potential. For each channel conformation λ, $\Delta G(\lambda,\Delta V)$ is the excess free energy due to the applied voltage. It relates the conformation of the channel to δ_i^{λ} , the so-called "electrical" distance (Sigworth 1994) (Jogini & Roux 2007) (Lecar et al. 2003):

$$\Delta G(\lambda,\Delta V)=G(\lambda,\Delta V)-G(\lambda,0)=\Delta V.\sum_i q_i\delta_i^{\lambda} \quad [3.46]$$

where is the set of N atomic coordinates of the protein in a conformation λ, q_i is the i^{th}-protein charge and δ_i^{λ} is the "electrical distance" of q_i, which corresponds to the fraction of field at this charge position. The quantityis given by (Islas & Sigworth 2001) (Roux 1997):

$$\delta_i^{\lambda}=\frac{\delta}{\delta V}\phi_i^{\lambda}|_{V=0} \quad [3.47]$$

and accounts for the degree of coupling between the local-electrostatic potential and the TM potential. Note that ϕ_i^{λ} is the local-electrostatic potential (at the charge location) due to the transmembrane voltage. It must be computed without consideration of the contribution of charges belonging to the protein (Grabe et al. 2004).

In practice, four simulations have to be carried out to calculate the gating charge associated

to the conformational change λ_1 to λ_2 . Two simulation of the system in the λ_1 conformation, where the protein atoms are fixed by harmonic constraints, are carried out. One of them, carried out at constant pressure, corresponds to a resting 0 mV potential, while the other, carried out with the charge imbalance method, corresponds to a hyperpolarized potential of ~600 mV. This enables the calculation of the electrical distance δ_i^{λ} . The same is then carried out for the other conformational state λ_2 . ΔG and Q can then be derived directly therefrom.

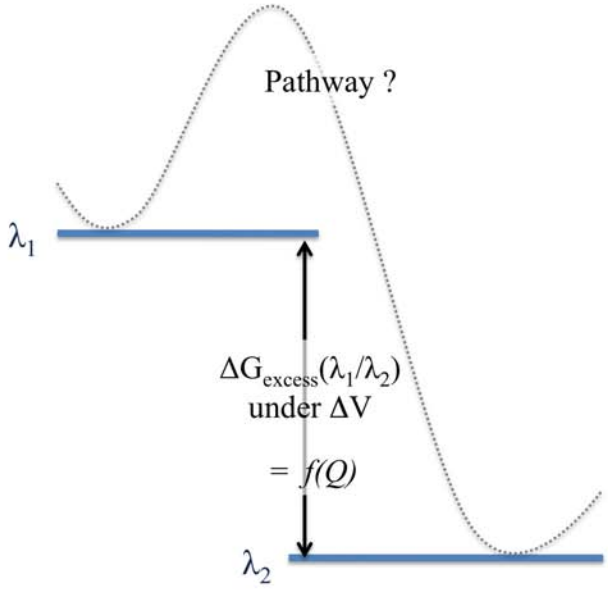

Figure 3.8: Scheme of the excess free energy surface between states $_2$ and $_2$ under given V. The free energy difference between the two states can be related directly to the gating charge whereas such a quantity does not give information about the energy pathway linking the two conformations.

The excess free energy difference due to ΔV involved in a transition from λ_1 to λ_2 can be directly related to the gating charge by Eq. 3.45. The gating charge thus gives a good estimate of the thermodynamical equilibrium under given ΔV (Fig. 3.8). Note that this free energy is related only to the transfer of protein charges across the TM electric field and does not reflect the *overall* conformational free energy associated to λ_1 / λ_2 transition. For example, rotation of a helix along the normal to the membrane does not contribute to the gating charge, as no charges are transferred across the electric field. However, its cost should be included in the overall conformational free energy.

Also, the calculation of the gating charge does not give information about the pathway associated to transition from state λ_1 to λ_2 (Fig. 3.7), meaning that it does not allow the evaluation of the free energy barriers between such states. From the gating charge calculations, no conclusions can be drawn about the kinetics of the conformational transition.

References

Aksimentiev, A. & Schulten, K., 2005. Imaging α-hemolysin with molecular dynamics: ionic conductance, osmotic permeability, and the electrostatic potential map. *Biophysical Journal*, 88, p.3745-3761.

Allen, M.P. & Tildesley, D.J., 1987. *Computer simulations of liquids*, Clarendon Press Oxford.

Andersen, H.C., 1980. Molecular dynamics simulations at constant pressure and/or temperature. *The Journal of Chemical Physics*, 72(4), p.2384.

Berendsen, H.J.C. et al., 1984. Molecular dynamics with coupling to an external bath. *The Journal of Chemical Physics*, 81(8), p.3684.

Bezanilla, F., 2008. How membrane proteins sense voltage. *Nature Reviews Molecular Cell Biology*, 9, p.323-332

Case, D.A. et al., 1999. *AMBER6*, San Francisco: University of California.

Crozier, P.S. et al., 2001. Model channel ion currents in NaCl extended simple point charge water solution with applied-field molecular dynamics. *Biophysical Journal*, p.3077-3089.

Frenkel, D. & Smit, B., 2002. *Molecular simulations - from algorithms to applications* 2e éd., Academic Press.

Grabe, M. et al., 2004. A quantitative assessment of models for voltage-dependent gating of ion channels. *Proceedings of the National Academy of Sciences*, 101(51), p.17640.

Gurtovenko, A.A. & Vattulainen, I., 2005. Pore formation coupled to ion transport through lipid membranes as induced by transmembrane ionic charge imbalance: Atomistic molecular dynamics study. *Journal of American Chemical Society*, 127, p.17570-17571.

Hoover, W.G., 1983. Nonequilibrium Molecular Dynamics. *Annual Review of Physical Chemistry*, 34(1), p.103-127.

Hoover, W.G., 1985. Canonical dynamics: Equilibrium phase-space distributions. *Physical Review A*, 31(3), p.1695.

Islas, L.D. & Sigworth, F.J., 2001. Electrostatics and the gating pore of Shaker potassium channels. *The Journal of General Physiology*, 117(1), p.69.

Jogini, V. & Roux, B., 2007. Dynamics of the Kv1. 2 voltage-gated K+ channel in a membrane environment. *Biophysical journal*, 93(9), p.3070–3082.

Kandasamy, S.K. & Larson, R.G., 2006. Cation and anion transport through hydrophilic pores in lipid bilayers. *J. Chem. Phys.*, 125, p.074901.

Khalili-Araghi, F., Tajkhorshid, E. & Schulten, K., 2006. Dynamics of K+ ion conduction through Kv1.2.

Biophys. J., 91, p.L72-L74.

Krieger, E., Nabuurs, S.B. & Vriend, G., 2005. Homology Modeling. Dans *Structural bioinformatics*. John Wiley & Sons Inc., p. 509-523.

Leach, A.R., 2001. *Molecular modeling - principles and applications* 2e éd., Pearson Education Limited.

Lecar, H., Larsson, H.P. & Grabe, M., 2003. Electrostatic model of S4 motion in voltage-gated ion channels. *Biophysical journal*, 85(5), p.2854–2864.

MacKerell Jr., A.D. et al., 1998. All-atom empirical potential for molecular modeling and dynamics studies of proteins. *The Journal of Physical Chemistry B*, 102, p.3586-3616.

Nonner, W., Peyser, A., Gillespie, D., and Eisenberg, B., 2004. Relating microscopic charge movement to macroscopic currents: The Ramo-Schockley Theorem applied to ion channels. *Biophysical Journal* 87, p.3716-3722.

Nosé, S., 1984. A molecular dynamics method for simulations in the canonical ensemble. *Molecular Physics*, 52(2), p.255-268.

Roux, B., 1997. Influence of the membrane potential on the free energy of an intrinsic protein. *Biophysical Journal*, 73, p.2980-2989.

Sachs, J.N., Crozier, P.S. & Woolf, T.B., 2004. Atomistic simulations of biologically realistic transmembrane potential gradients. *Journal of Chemical Physics*, 121, p.10847-10851.

Schuler, L.D., Daura, X. & van Gunsteren, W.F., 2001. An improved GROMOS96 force field for aliphatic hydrocarbons in the condensed phase. *Journal of Computational Chemistry*, 22(11), p.1205-1218.

Sigworth, F.J., 1994. Voltage gating of ion channels. *Quarterly Reviews in Biophysics*, 27, p.1-40.

Sotomayor, M. et al., 2007. Ion conduction through MscS as determined by electrophysiology and simulation. *Biophysical Journal*, 92, p.886-902.

Stefani, E. et al., 1994. Gating of Shaker K+ channels: I. Ionic and gating currents. *Biophysical Journal*, 66(4), p.996-1010.

Suenaga A et al., 1998. Computational observation of an ion permeation through a channel protein. *Bioscience Reports*, 18, p.39-48.

Tarek, M., 2005. Membrane electroporation: A molecular dynamics simulation. *Biophysical Journal*, 88, p.4045-4053.

Tieleman, D.P., 2004. The molecular basis of electroporation. *BMC Biochemistry*, 5, p.10.

Tieleman, D.P., Berendsen, J.H.C. & Sansom, M.S.P., 2001. Voltage-dependent insertion of alamethicin at phospholipid/water and octane water interfaces. *Biophysical Journal*, 80, p.331-346.

Toukmaji, A.Y. & Board, J.A., 1996. Ewald summation techniques in perspective: a survey. *Computer Physics Communications*, 95(2-3), p.73-92.

Treptow, W. et al., 2004. Coupled motions between pore and voltage-sensor domains: a model for Shaker B, a voltage-gated potassium channel. *Biophysical journal*, 87(4), p.2365–2379.

Treptow, W., Tarek, M. & Klein, M.L., 2009. Initial response of the potassium channel voltage sensor to a transmembrane potential. *Journal of the American Chemical Society*, 131, p.2107-2110.

Verlet, L., 1967. Computer « Experiments » on Classical Fluids. I. Thermodynamical Properties of Lennard-Jones Molecules. *Physical Review*, 159(1), p.98.

Vernier, P.T. et al., 2006. Nanopore formation and phosphatidylserine externalization in a phospholipid Bilayer at high transmembrane potential. *Journal of the American Chemical Society*, 128, p.6288-6289.

Woodcock, L.V., 1971. Isothermal molecular dynamics calculations for liquid salts. *Chemical Physics Letters*, 10(3), p.257-261.

Zhong, Q. et al., 1998. Molecular dynamics study of the LS3 voltage-gated ion channel. *FEBS Letters*, 427, p.267-270.

4- RESULTS

" People love chopping wood. In this activity, one immediately sees results."

-Albert Einstein

Afin de décrire le fonctionnement des canaux ioniques sensibles à la tension, trois modèles principaux de l'opération du domaine sensible à la tension et de l'hélice chargée positivement S4 ont été proposés. Le *modèle en vis,* décrit le mouvement de S4 lors de l'activation du canal par rapport au reste du domaine par une translation verticale de ~10 à 20 Å combiné à une rotation le long de son propre axe de 180°. Le *modèle transporteur*, quant à lui, met en jeu au contraire un mouvement de S4 d'une magnitude réduite. La charge de « gating », qui vaut 12 à 14e au total, peut être expliquée par une réorganisation conséquente du champ électrique au voisinage de S4. Il y a par ailleurs un troisième modèle, le *modèle paddle*, qui a été abandonné depuis. De nombreuses études ont été entreprises ces dernières années dans le but de réconcilier ces modèles et une vision relativement consensuelle a fini par émerger ces dernières années. Dans le modèle correspondant, S4 est translatée verticalement d'une dizaine d'angstrom et les résidus basiques de S4 forment des ponts salins avec les résidus acides de S1-S3 d'une manière séquentielle, un mécanisme qui est important pour garantir le bon fonctionnement du canal.

En 2005, pour la première fois, une structure cristallographique d'un canal voltage-dépendant a été publiée : le Kv1.2. Dans cette structure, le pore est ouvert et le domaine sensible à la tension est dans sa conformation « activée » (ouverte), *i.e.* avec S4 en position haute. Cette structure, ainsi que les études qui ont suivi, ont permis de révéler de nombreux détails du fonctionnement des canaux potassiques voltage-dépendants au niveau moléculaire. Toutefois, certaines questions fondamentales demeurent. Ainsi, le mécanisme exact de la désactivation du domaine sensible à la tension reste sujet à débat, ainsi que la structure de l'état fermé et du ou des états intermédiaires. On peut également poser la question de l'effet au niveau moléculaire de la mutation des résidus chargés de S4 qui sont impliqués dans des maladies génétiques héréditaires. Par ailleurs, le rôle des lipides qui sont proches du domaine sensible à la tension et en particulier l'effet que produit la transformation de la tête polaire de ces lipides reste à déterminer. Dans ce travail, nous nous sommes attachés à répondre à ces questions à l'aide de l'utilisation de simulations de dynamique moléculaire principalement.

La première partie de ce travail a concerné la désactivation du canal Kv1.2. Ainsi, partant de la structure cristallographique mentionnée ci-dessus, nous avons modélisé l'ensemble du canal Kv1.2, inséré dans son environnement lipidique (une bicouche lipidique de phosphatidyl-choline) et solvaté dans 150 mM de KCl. L'essentiel des résultats repose sur l'analyse d'une simulation de 2.2 μs du système soumis à un potentiel hyperpolarisé de ~ -600 mV et de simulations biaisées ultérieures conduites dans le but de générer les dernières étapes de la désactivation. Nous avons ainsi obtenu cinq conformations du domaine sensible à la tension, α, -β, γ and δ- and ε, qui correspondent aux états ouvert, intermédiaires et fermé du canal, respectivement. Lors de la désactivation, les résidus chargés de S4 se déplacent vers le bas en passant d'un résidu chargé négativement à l'autre de manière séquentielle en un mouvement vertical orienté vers le bas. Chaque transition s'accompagne du transfert de l'un résidu basique par le centre catalytique (situé à proximité du résidu conservé Phe233)

découvert récemment par le groupe de MacKinnon. Les têtes polaires des lipides jouent également un rôle essentiel dans le fonctionnement du domaine sensible à la tension puisque non seulement ceux de la couche externe entrent en interaction avec les résidus basiques du haut de S4 dans l'état activé et ceux de la couche interne avec les résidus basiques du bas de S4 dans l'état au repos mais ils jouent aussi un rôle dans la stabilisation des états intermédiaires. Au total, lors de la désactivation, S4 est translatée perpendiculairement à la membrane par 10-15 Å. Enfin, le champ électrique local est focalisé au centre du domaine sensible à la tension et n'est pas beaucoup altéré lors du changement conformationnel. L'analyse des charges de « gating » transportée par les résidus basiques de S4 révèle que l'opération du domaine sensible à la tension peut être décrite par une fonction unique qui définit le couplage électromécanique que subissent les charges du domaine sensible à la tension. Dans l'ensemble, ces résultats penchent en faveur du *modèle en vis*. Nous concluons cette première partie par une description du couplage entre l'action du VSD et la fermeture du pore à travers l'action mécanique du linker S4-S5.

Grâce à l'utilisation des configurations du Kv1.2 déterminées dans la première partie de ce travail, nous nous sommes intéressés à l'effet au niveau moléculaire de mutations de résidus chargés positivement de S4 qui sont impliquées dans des maladies génétiques. Certaines d'entre elles modifient la structure du domaine sensible à la tension car elles rompent les interactions électrostatiques dans lesquelles elles sont impliquées et donnent ainsi lieu à l'apparition d'un conduit hydrophile. Lorsqu'ils sont soumis à un potentiel transmembranaire, ces mutants donnent lieu à l'apparition de courants de fuite, appelés courant « oméga ». Ces résultats dévoilent les mécanismes moléculaire qui sont impliqués dans ces courants « oméga » détectés par électrophysiologie. Après une étude de l'effet des différentes mutations dans l'état activé et au repos du Kv1.2, nous proposons un modèle du mécanisme d'apparition des courants de fuite, indiquant quel type de résidu peut donner lieu à l'apparition de ces derniers et sous quelles conditions ces fuites peuvent être critiques et ainsi être l'origine moléculaire des maladies génétiques mentionnées ci-dessus.

Dans une troisième partie, suite à la publication récente de nouveaux résultats expérimentaux, nous nous sommes intéressés à la modulation de la fonction du Kv1.2 par la modification des têtes polaires des lipides. La simulation du Kv1.2 dans une variété des bicouches asymétriques contenant de la sphyngomyéline, du céramide-1-phosphate ou du céramide dans le couche supérieure a montré qu'en dépit du rôle essentiel des interactions entre lipides et résidus basiques de S4, la charge de « gating » n'est pas affectée par l'altération des têtes polaires des lipides. Par ailleurs, des simulations supplémentaires sous haut potentiel transmembranaire ont suggéré que les transition d'une conformation du domaine sensible à la tension à l'autre ne pouvaient être accélérées par la modification de la tête polaire des lipides, suggérant ainsi que l'altération de la tête polaire lipidique affecte surtout la cinétique ces transitions.

L'ensemble de ces trois parties participe à donner une meilleure vision du fonctionnement du canal Kv1.2 à l'échelle moléculaire et par extension des différents membres de la famille des canaux ioniques à la tension.

Since the seminal work of Hodgkin and Huxley in the 1950s that revealed that ions crossed excitable membranes using voltage-dependent ion permeation pathways through biological membranes, a lot of progress has been made in understanding the function and the modulation of voltage-gated ion channels (VGCs). As soon as the early 1970s, it was known that the molecules involved in the transport of ions across the membranes of excitable cells were membrane proteins, that could be found either in the open or in the closed state, depending on the polarization of the membrane. It was shown that when going from one VGC state to the other, conformational changes occurred within these proteins giving rise to small transient currents called gating currents. At that time, not much was known about the molecular details of VGC function. Nowadays, these channels are still the focus of intensive ongoing fundamental and applied research since they are essential to many biological functions. Furthermore, genetic modifications of these channels are known to give rise to a large number of familial genetic diseases of the heart, the neural system, etc... making it important to understand their function on a molecular level.

Electrophysiology measurements together with protein sequencing have revealed key molecular features of the function of voltage-gated potassium (Kv) channels: among the six transmembrane domains that constitute each of the four monomers, two form the pore (S5 and S6) – the region that is responsible for the transport of ions from one side of the membrane to the other. The other four (S1-S4) constitute an auxiliary domain, the voltage sensor domain (VSD) that is responsible for sensing the voltage. Among them, S4 contains a large number of positively charged residues (arginines mostly - sometimes lysines) that sense the voltage fluctuations and reorganize in response to it. VSDs are also the molecular level components responsible for the gating currents and for the gating charge, which is the integral of the latter: when the channel goes from the resting state to the activated one, 12 to 14 elementary charges are transported across the membrane electric field, most of which is comes from the contribution of these positively charged residues.

To describe the operation of the VSD, three main models have been proposed. In the first one, called the *helical screw model*, S4 moves independently from the rest of the voltage sensor domain in a screw-like motion, translating by 10-20 Å while rotating about its own axis by 180° counterclockwise when looking from the top. This model also involves characteristic features: the reorganization of salt bridges within the VSD. Indeed, to stabilize S4 in a transmembrane (TM) orientation despite its high charge, the arginines are involved in salt bridges with negatively charged residues of the other transmembrane segments (S1-S3). Based on mutagenesis studies, this model implicates that salt bridges are broken while others are formed when S4 moves with respect to the other segments of the VSD in response to the electric field. The second model involves a large reorganization of the electric field in the vicinity of S4 with only a small displacement of the positive charges of S4. This model, supported mostly by fluorescence measurements is called the *transporter model.* Finally, the *paddle model*, that has since then been abandoned, involves a large movement of the "S3-S4 paddle" from a position parallel to the membrane surface in the resting state to a vertical

position in the activated one. A lot of work was done to reconcile these various views and a rather unified model has emerged in the last years: the TM movement of S4 is of intermediate magnitude and the salt bridges within the VSD undergo important rearrangements ensuring proper function of the channel.

The event that has probably triggered the biggest advance in the comprehension of the molecular mechanism of VGCs is the resolution of the first crystal structure of a mammalian potassium channel: the Kv1.2 (Long et al. 2005). In this structure, the pore was found to be open and the VSD in an activated state, *i.e.* with S4 in an 'up' state. This structure has revealed many molecular details such as the interaction of lipid head groups with the top positive residues of S4, the salt bridge network present in the activated state of the VSD, the kink in the S6 helix important for channel gating, a possible mechanism for fast inactivation and others... However, key questions remain to be answered:

- What is the exact nature of the movement of S4 basic residues and how does the electrical driving force act upon them ?
- What do the intermediate and resting states look like ?
- What is the structural basis of coupling of the VSD activation/deactivation to the pore opening/closing ?
- How do lipids modulate the activation/deactivation of the VSD and what happens when modifying the lipids located nearby the channel?
- How can one link the genetic diseases to the mutation of selective S4 positively charged residues on a molecular level ?

To address these questions, we have used extensive molecular dynamics (MD) simulations of the Kv1.2 channel embedded in a lipid bilayer. This method, in which every atom is represented by a particle of given mass and charge, relies on the integration of the classical equations of motion, knowing all the interactions between pairs of particles in the system. When taken together with experimental results, this method enables to provide molecular-level details otherwise unreachable. Challenges however come from the need for a starting structure of biological relevance, time scales that can be reached and most importantly the importance of applying a TM potential ΔV in a way that complies with electrophysiology experiments. We have accordingly used an original method, that implies applying a charge imbalance between the top and the bottom bilayer baths and preventing the interaction between periodic images in the direction normal to the membrane by introducing an vacuum slab. Because the membrane is a capacitor, such an imbalance gives rise to a TM potential, very much as is done in patch clamp experiments.

In the following, we present the results we obtained in this work. This chapter is divided into three major sections:

In the first part, we describe the study on the deactivation of the channel. We present the

results of a large scale simulation (2.2 μs) of the activated channel submitted to ΔV = -600 mV and of subsequent steered MD simulations conducted to uncover the last steps of the deactivation. We describe here the different conformations the VSD takes during the channel deactivation and most particularly its interactions with lipids, the implication of a gating charge transfer center... We describe in details the electrical properties of the VSD among which the shape of the local electric field and the molecular components involved in the gating charge. Next, we propose a short account on the coupling of the VSD conformational change with the pore gating. We conclude this part by a discussion that places our findings within the most updated bibliographical context.

In a second part, we present the results we have obtained concerning the effect of the mutation of S4 basic residues. We start by describing the alteration of the structure following the mutation of different residues, both in the activated and in the resting states. Then we describe the appearance of leak currents (also called “omega” currents or “gating pore” currents) through the VSD when submitting the system to a TM potential. Finally, we discuss our results by proposing a mechanism explaining the appearance of state-dependent leak currents in the wide family of VGCs and their relationship to genetic diseases.

In a third part, we describe the results we obtained when altering the lipids around the channel and most particularly in the vicinity of the positive charges of S4. This study is based on experiments performed in Oocytes, that indicate that when changing the sphyngomyelin lipids of the top bilayer leaflet into negatively charged lipids (ceramides-1-phosphate) or lipids with no zwitterionic headgroup (ceramides), activation is made “easier” or “harder”, respectively. We show in particular that the gating charge does not seem to be affected by the change in top lipid headgroups, which indicate that activation kinetics is likely the most relevant quantity that is perturbed following changes in the lipid interaction with VGCS.

1 Kv1.2 deactivation

1.1 Computational details

In this study, we started with a conformation of the channel in its "activated state" based on the crystal structure of the Kv1.2. The channel was inserted at the center of a membrane patch composed by palmitoyl-oleyol-phosphatidylcholine (POPC) lipid molecules, optimizing the distance between conserved aromatic side chains (belonging to S1 through S3) and the phospholipid head groups. The complete system contains the Kv channel, 426 lipid molecules, 83,392 solvent-water molecules, 2 potassium ions located in the selectivity filter (a total of ca. 305,500 atoms, figure 4.1). To bring the ionic concentration to 150 mM and to ensure the neutrality of the system, 96 chloride ions and 138 potassium ions were distributed uniformly in the solvent. The initial dimensions of the simulation cell were 133 x 143 x 142 $Å^3$.

The system was relaxed for over 10 ns with no TM voltage applied, *i.e.* equilibrated using 3-D periodic boundary conditions at constant pressure (1 atm) and constant temperature (300 K). Vacuum/water interfaces were then created at both sides of the electrolytes by extending the length of the original box in the direction perpendicular to the membrane (z axis). Simulations were run at constant volume for further equilibration. Note that the density for bulk water is preserved through intermolecular interactions and that as long as the membrane (and protein) is far enough (~25 Å) from the air/water interface, it is not affected by the latter.

Next, we proceeded by considering a channel subjected to a hyperpolarized–TM potential ΔV using the explicit ion dynamics method (Chapter 3, paragraph 3.2). To do so a net charge imbalance q_0 between the upper and lower electrolytes was created by displacing an appropriate number of K^+ ions from the lower to the upper bath, keeping ~ constant the overall concentration of the bulk phases. Since the membrane/channel system behaves as a capacitor, the imbalance q_0 between the electrolytes creates ΔV. Here, as in electrophysiology experiments, the ionic current through the main alpha pore was inhibited throughout the MD simulations by imposing harmonic constraints on the selectivity filter backbone residues, allowing for direct measurement of voltage-sensor gating charges from ΔV (see chapter 3, paragraph 4.1).

The MD simulations were carried out using the program NAMD2. Langevin dynamics was applied to keep the temperature (300 K) fixed. The equations of motion were integrated using a multiple time-step algorithm. Short- and long-range forces were calculated every 1 and 2 time-steps respectively, with a time step of 2.0 fs. Chemical bonds between hydrogen and heavy atoms were constrained to their equilibrium value. Long-range electrostatic forces were taken into account using the particle mesh Ewald (PME) approach. The water molecules were described using the TIP3P model. The simulation used the CHARMM22-CMAP force field

with torsional cross-terms for the protein and CHARMM27 for the phospholipids (MacKerell et al., 1998). A united-atom representation was adopted for the acyl chains of the POPC lipid molecules (Hénin et al. 2008). The simulation was performed on the SGI ALTIX ICE Machine JADE at the CINES supercomputer center (Montpellier, France).

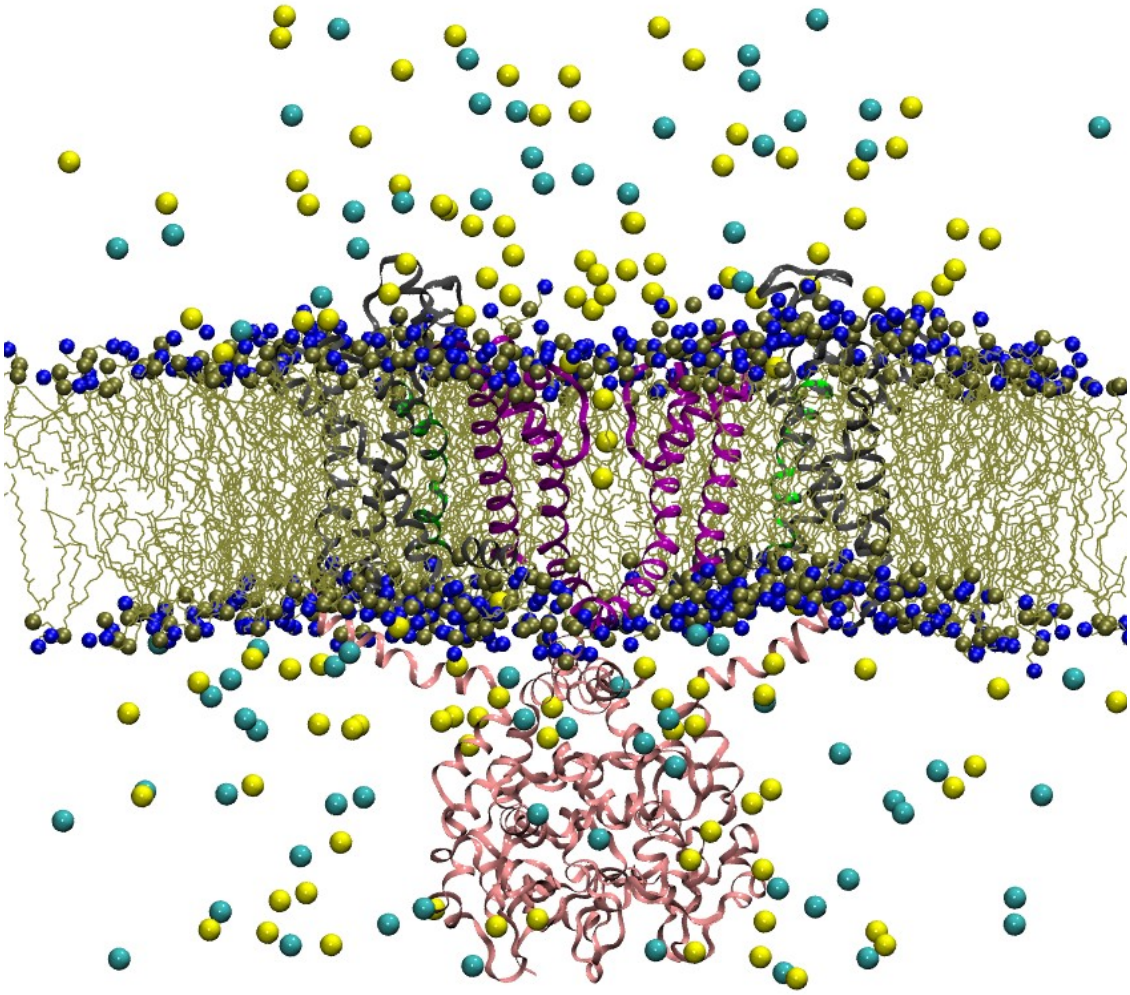

Figure 4.1: Simulation system including the channel (represented as ribbons), the lipids, represented as brown lines, with their headgroups highlighted as blue and brown spheres, the water (not represented for clarity), and the ions (represented as yellow (K^+) and cyan (Cl^-) spheres). The system is viewed from the side and only the two protein subunits in the plane of the view are represented for clarity. The channel is composed of the tetramerization (T1) domain (pink), the VSDs composed of S1-S3 (in grey) and S4 (in light green) and the pore domain (in purple). Note the presence of two K^+ ions in the selectivity filter as in normal conductance conditions.

1.2 In silico "gating charge" measurements

In electrophysiology experiments, measuring the gating charge is being done routinely to characterize the function of VGCs. In simulations, however, it is a rather new approach. Traditionally, the strategy that has been used to apply a TM potential was to apply an electric field on all charged particles (Bjelkmar et al. 2009) (Nishizawa & Nishizawa 2008) (Khalili-Araghi et al. 2010). Using this scheme, the only way to calculate the gating charge was to apply the energetic formalism (see chapter 3, paragraph 4.2) in which an estimation of the electrical distance (fraction of the transmembrane potential at a given position within the membrane) is necessary. Then, when multiplied by the partial charge of each atom, the gating charge can be deduced. This method is very useful and has been applied successfully, but as mentioned, it requires approximations, especially when accessing the electrical distance.

Interestingly enough, the use of the charge imbalance method (Delemotte et al. 2008) enables to record directly the charge that is transported across the membrane capacitor (Treptow et al. 2009). Indeed, the channel responds to the imposed TM voltage by reorganizing its charges within the electric field. Because the membrane/ion channel system is impermeable to ions (through inhibition of the current through the selectivity filter), when such reorganization occurs, the TM voltage drops and such a drop can be directly related to the amount of gating charge that is carried (see chapter 3, paragraph 4.1).

Using this method, the only quantity that has to be estimated from simulations is the TM potential. The latter is evaluated using a one dimensional profile of the electrostatic potential (EP) as a function of the position along the membrane normal *z* (see chapter 3, paragraph 2.2). In order to be able to determine the average EP in a given position, one considers the time averages of charge distributions, *i.e.* using at least 20 to 50 configurations of the system spread over few nanoseconds. Under our conditions (system size, ionic concentration, …), the TM voltage may be estimated with an error of 100 mV (17%), leading to errors on the gating charge of ~0.3e at most.

To characterize the electrical response of the system, we monitored Q(t), the total gating charge associated with the displacement of all charges in the system with respect to the membrane capacitor along the trajectory under hyperpolarization. Fig. 4.2 reports the variation of Q(t) and indicates a substantial channel electrical activity: Q(t) undergoes three major drops (I, II and III) occurring at t = ~ 0.2 μs, ~1.6 μs and ~ 2.0 μs, respectively with associated gating charges Q(t) ~ -1.4 e , -1.3 e and -1.0 e (± 0.3 e), respectively.

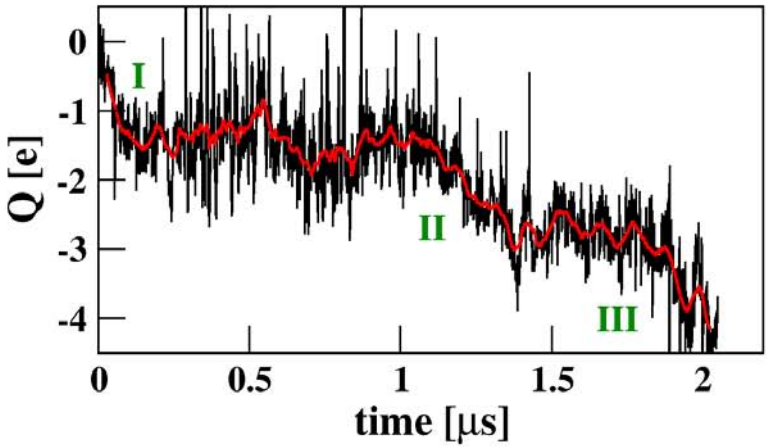

Figure 4.2: Recording of the gating charge along the 2.2 μs simulation illustrating three major gating charge drops (labelled I to III). The gating charge Q(t) was calculated via the direct method (see chapter 3, paragraph 4.1).

1.3 VSD Intermediate states along the 2.2 μs MD simulation

Further looking to analyze the response of the channel VSD to hyperpolarization, we characterized the structural changes taking place during the 2.2 μs simulation. As mentioned above, the gating charges are mainly due to the conformational rearrangements within the VSD and most particularly to the transport of charged residues across the membrane capacitor. In the following paragraphs, we will relate these rearrangements to the electrical activity of the channel and characterize which residues participate most in the gating charge.

First of all, throughout the MD simulation, we noticed that the Kv1.2 pore domain remained very stable whereas the VSD underwent substantial conformational changes involving zipper-like motion of the salt pair interactions: the changes corresponding for the largest Q(t) variations (drops I to III in Fig. 4.2) involved salt-bridge rearrangements within the VSDs with the S4 basic residues moving from external (top) to internal (bottom) binding sites along the domain. As exposed in the objects section, these binding sites are specifically the acidic amino-acids of segments S1 through S3 (E^{183}, E^{226}, D^{259} and E^{236}) and, the PO_4^- moieties of the lipid head-groups of the outer and inner bilayer leaflets (Fig. 4.5).

In order to correlate the changes in Q(t) during the MD simulation with these ion pair rearrangements, we monitored the matrix of distances between the centers of the charged moieties of the S4 basic residues and those of the acidic countercharges (Fig. 4.3). This distance matrix can be written as: $M = [r_{ij}]_{n \times m}$ where r_{ij} is the distance between the charged

moiety of a given S4 charge $j=\{R1, R2, R3, R4, K5, R6\}$ and the charge moiety of a given negatively charged group $\{PO_4^-(outer), E^{183}, E^{226}, D^{159}, E^{236}, PO_4^-(inner)\}$. In detail, r_{ij} is the distance between the geometrical centers of the i,j charged moieties, which correspond here to the side chain atoms $H_2N{=}C_\zeta(NH_2)\text{-}N_\varepsilon H\text{-}C_\delta H_2$ (Arg) and $H_3N_\zeta\text{-}C_\varepsilon H_2$ (Lys), $HOOC_\gamma\text{-}C_\beta H_2$ (Asp), $HOOC_\delta\text{-}C_\gamma H_2$ (Glu) and the lipid phosphate group PO_4^-. The rmsd profiles of the VSDs conformation were calculated according to:

$$rmsd(t)=\frac{1}{36}\sum_{i=1}^{6}\sum_{j=1}^{6}\sqrt{[r_{ij}(t)-r_{ij}(0)]^2} \quad [4.1]$$

and are reported in Fig. 4.4.

During the first Q(t) drop, the four VSDs relaxed from the initial α-state towards a metastable β-state (Fig. 4.4). During the subsequent Q(t) drop (II), further salt-bridge rearrangements occurred within a single VSD (subunit 1). This led to yet another state, called here γ, lasting for over 0.5 μs. Then, in the third Q(t) drop (III), the same VSD underwent another conformational change, leading to a state we name γ^+.

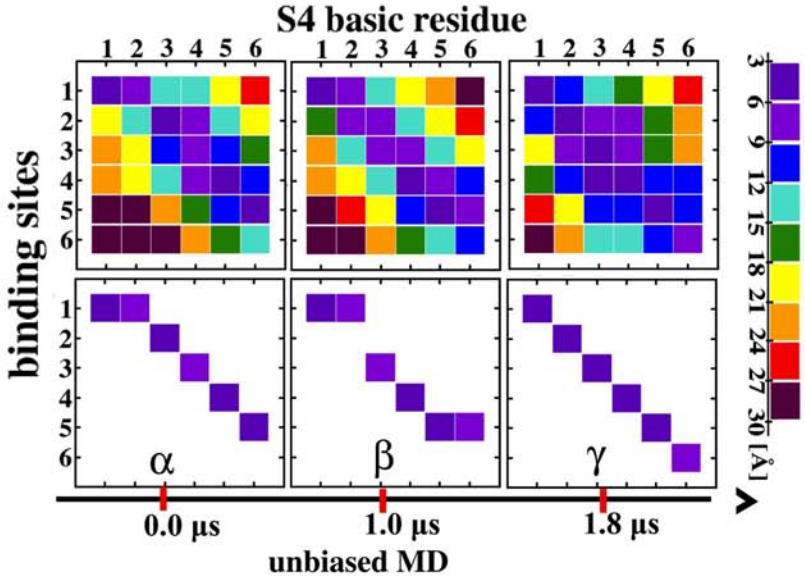

Figure 4.3:Representative conformations (α, β, γ) of the VSDs revealed during the 2.2 μs MD simulations were characterized by monitoring the distances between the S4 basic residues (numbered 1 to 6 for R1, R2, R3, R4, K5 and R6, respectively) and their binding sites (numbered 1 to 6 for top PO_4^-, E^{183}, E^{226}, D^{259}, E^{236} and bottom PO_4^-, respectively). The distances were calculated between the geometrical centers of the side chain atoms $H_2N{=}C_\zeta(NH_2)\text{-}N_\varepsilon H\text{-}C_\delta H_2$ (Arg), $H_3N_\zeta\text{-}C_\varepsilon H_2$ (Lys), $HOOC_\gamma\text{-}C_\beta H_2$ (Asp), $HOOC_\delta\text{-}C_\gamma H_2$ (Glu) and the lipid phosphate group PO_4^- from a representative conformation and averaged over all 4 subunits of the channel. The closest interacting pairs are shown in the bottom panel. Note the zipper-like motion in which, for successive transitions, the pairs involving S4 basic residues are formed with lower counter charges.

The sequential conformational changes, α → β → γ of the VSDs, and especially that of subunit 1, provide a reaction pathway for the first transition events occurring in the voltage-sensing process. Each VSD conformation α, β and γ is stabilized by a maximum number of salt bridges between the S4 basic residues and negative residues of the VSD or PO_4^- moieties of the lipids (Fig. 4.3 and 4.5). Namely, in α, R1 and R2 are in interaction with PO_4^- groups of the upper leaflet, R3 interacts with the most outer glutamic acid E^{183}, R4 with E^{226}, K5 with D^{259} and R6 with most inner glutamic acid E^{236}. However, as can be gathered from Fig. 4.3, some other interactions are also possible. For example, in α, R4 is in close proximity (3 to 6 Å between their charged moieties) to E^{183}, E^{226} and D^{259} but the closest pair (represented in the bottom panel of Fig. 4.3) is between R4 and E^{226}.

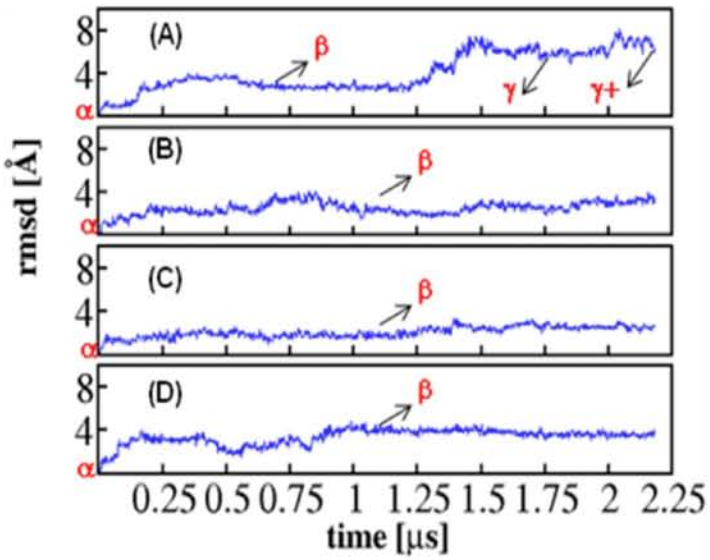

Figure 4.4: Root mean square deviation profiles for the VSD subunits 1 through 4. The profiles were calculated according to equation [4.1]. Note in (A), the VSD subunit 1 underwent significant structural transitions throughtout the MD simulation, evolving from the α state towards the γ^+ conformation. For subunits 2 (B), 3 (C) and 4 (D), the VSD relaxed towards the β conformation, remaining in this state until the end of the simulation.

In β, R1 and R2 are still in interaction with the PO_4^- groups. R3, R4 and K5 have slid down by one binding site during drop I, coming in interaction with E^{226}, D^{259} and E^{236} while R6 stayed in close proximity to E^{236}. This state, which remains stable for over 1 μs, bears strong similarity with the intermediate kinetic state previously identified in independent MD simulations by us (Treptow et al. 2009) and others. Indeed, Nishizawa et al. found that applying an electric field to an isolated VSD led to S4 displacement and salt bridge rearrangement. They identified two intermediate states, among which one of them shows a replacement of R4 by R3 to form a salt bridge with E^{226} and remains stable for several tens of nanoseconds (Nishizawa & Nishizawa 2008). Independently, the group of Lindahl led a microsecond long simulation and found salt bridge rearrangement in one of the subunits: they

followed the transition of K5 from D^{259} to E^{236} and of R2 from the lipid towards the protein (Bjelkmar et al. 2009).

In the conformation γ, while R1 is still in interaction with the top PO_4^- groups, R2 has come in interaction with E^{183}. R3, R4 and K5 remain in close proximity to E^{226}, D^{259} and E^{236}, respectively and R6 has transferred to the bottom layer PO_4^- groups. Finally, during drop III, when going to γ^+ state, the S4 basic residues have continued jumping to the next binding site along the downstream path mentioned above, without reaching a well-defined stable state. Note here that the β and γ VSD structures remain unchanged for ~μs time laps, as shown in Fig. 4.4, indicating that both conformations are stable, and can therefore be considered as representative of intermediate, metastable states of the VSD along the deactivation pathway.

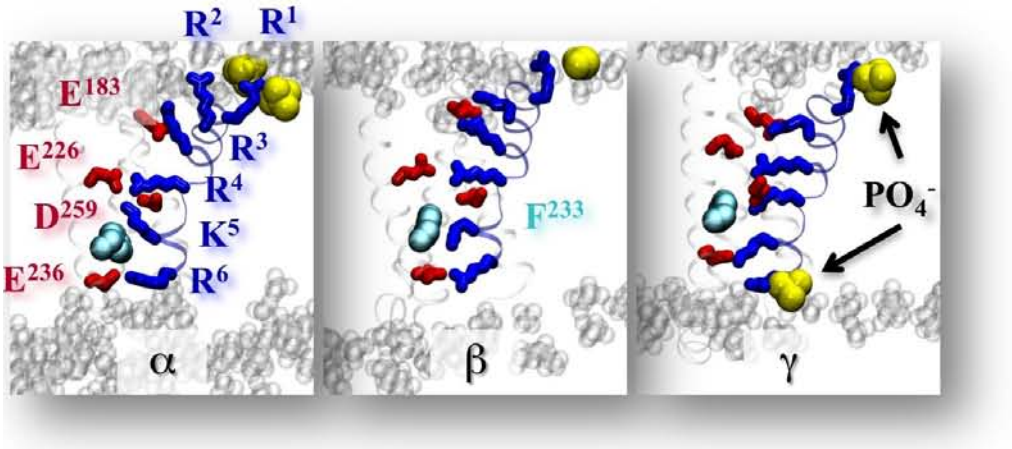

Figure 4.5: Molecular views of the VSDs in the three key conformations highlighting the position of the S4 basic residues (blue sticks) and the salt bridges they form with the acidic residues (red sticks) of the other VSD segments or with the lipid head group PO_4^- moieties (yellow). The highly conserved residue F^{233} of S2 is shown as cyan spheres.

1.4 Generation of the last two steps of the deactivation

Because of limitations in computer power, we were unable to observe the last step of the deactivation of the VSD. In order to uncover the complete VSD response from the up-state (α) to the down-state, we used biased MD to simultaneously drag all the charged moieties of the basic residues from a given binding site to the next along the downstream path revealed by the unbiased MD simulation. In practice, a further conformational change was triggered by applying "moving" harmonic constraints on the charged moieties of the S4 basic residues (corresponding here to the side chain atoms $H_2N{=}C_\zeta(NH_2)\text{-}N_\varepsilon H\text{-}C_\delta H_2$ (Arg) and $H_3N_\zeta\text{-}C_\varepsilon H_2$ (Lys)) directed towards the charged group of the next binding sites (corresponding to $HOOC_\gamma\text{-}C_\beta H_2$ (Asp), $HOOC_\delta\text{-}C_\gamma H_2$ (Glu) and the lipid phosphate group PO_4^-) with a magnitude of 1

kcal/mol/Å^2 and a velocity of 0.00003 Å/fs. More precisely, starting from the state δ, R1 and R2 are pulled towards E^{226}, R3 towards D^{259}, R4 towards E^{236} and K5 and R6 towards the bottom layer PO_4^- groups. For state ε, R1 and R2 are pulled towards D^{259}, R3 towards E^{236} and R4, K5 and R6 towards the bottom layer PO_4^- groups (Fig. 4.6). During this procedure, the C_α atom position of the protein's negative binding site were fixed by "static" harmonic constraints. Moreover, to avoid spurious effects on the channel structure, this whole procedure was performed slowly, throughout successive cycles involving short runs (~ 1 ns) with harmonic constraints turned on followed by equilibration (~ 1 ns) with harmonic constraints turned off.

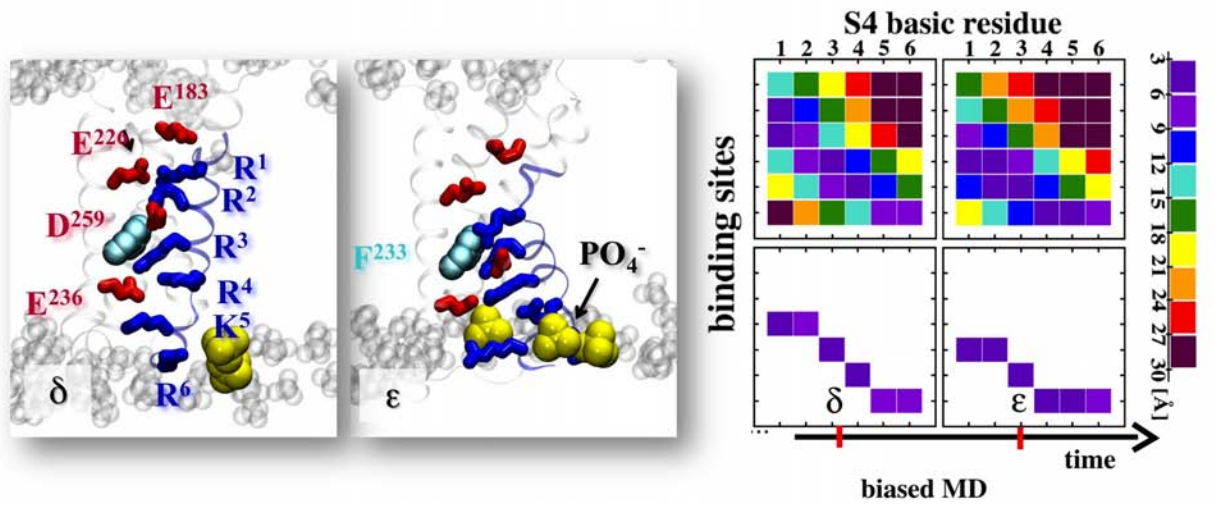

Figure 4.6: Representative conformations (δ and ε) of the VSDs revealed during the steered MD simulations. The color scheme is the same than in Fig. 4.3 and 4.5.

In order to characterize meaningful statistically averaged structural and electrical properties we have generated Kv1.2 structures in which all the VSD are in the same state. Starting from the channel conformation at *t=1.8 μs* of the *unbiased MD* simulation, in which only the VSD in the subunit 1 adopts the γ state, we have initially, dragged the VSD in the other three channel subunits into this conformation using the procedure described above, thereby generating the channel construct with the four VSDs in state γ. Proceeding further along the "reaction" pathway between α and the resting state ε, we have generated another channel construct presenting the VSDs in the state δ, which was identified here as another stable VSD conformation. Equilibration MD runs, each spanning ~15 ns, confirmed the structural stability of these additional VSD structures, for which the distance matrix rmsd profile converged to a value < 2.4 Å (Fig. 4.7). Together with β and γ, the conformation δ was therefore considered as yet another possible intermediate state of the VSD.

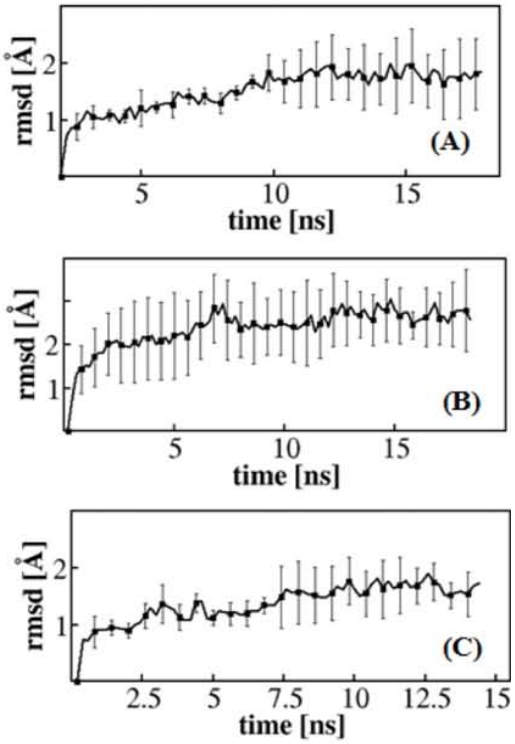

Figure 4.7: Root mean square deviation (rmsd) profile for the VSD conformations γ (A), δ (B) and ε (C) during equilibrium MD runs. The curves were computed according to equation [4.1] and presented as an average over the four subunits. Note that, the rmsd profiles converged to a value of ~ 2.0 Å, indicating the structural stability of these VSD conformations.

1.5 Validation of the resting conformational state

The molecular contacts within the VSDs in (resting) state ε agrees with a quite large number of distance probing experiments. In Table 4.1, we compare the distances measured in our equilibrated α and ε conformations to data from cysteine mutagenesis. In these experiments, the interactions are detected (by electrostatic interactions or by disulfide bridges approach) under given TM voltage conditions. If the interaction is detected under hyperpolarized voltage, it is relevant for the closed state *i.e.* when S4 is in the 'down state'. On the other hand, if the interaction is detected under depolarized voltage, it is relevant for the open state, *i.e.* when S4 is 'up'. In table 4.1, we see that most distances detected in the resting state are shorter in our ε conformation and that most distances detected in the activated state are shorter in our α conformation. This shows that our model agrees with experimental data from different sources. One should here however keep in mind that, as mentioned in Annex 1, these experimental techniques introduce point mutations that may alter slightly the structure of the channel's states as well as their function. Hence, as important it is to have a model that

agrees with most of the experimental data at hand, it is possible that some of the conclusions drawn from experiments have to be considered with caution.

We have also compared our data to other modeling studies and found that the VSD conformation in state-ε bears strong similarities with the molecular models of the VSD down state of Kv1.2 that have been proposed previously. Many of these models are based on ROSETTA membrane modeling, a method that predicts the structure of helical membrane proteins de novo by combining information from transmembrane region prediction and experimental constraints based on residue-residue interactions obtained from experiments (Yarov-Yarovoy et al. 2006) (Pathak, Yarov-Yarovoy, et al. 2007) (Catterall 2010). Other groups used restrained all-atom MD simulation of the channel embedded in it membrane environment to bias the conformation towards the hypothetical resting state: Khalili-Araghi et al. have generated a model (Khalili-Araghi et al. 2010) starting from a ROSETTA based model (Pathak, Yarov-Yarovoy, et al. 2007), in which S4 has been dragged further down to account with a total gating charge of ~12e. Along the same lines, Schow et al. have produced a down state model of KvAP VSD (Schow et al. 2010) using the biotin-avidin VSD accessibility data of Ruta et al. (Ruta et al. 2005) and information on salt bridges distances as a set of position restraints to conduct biased MD simulations.

Here, after superimposing the negatively charged residues in S1-S3 with the ones in the most recent model of Kv1.2 (Khalili-Araghi et al. 2010), we see that our present model places R1 in an even lower position (Fig. 4.8) with the S4 basic residues further down by one binding site. Indeed, whereas R1 was initially thought to be engaged in a salt bridge with E^{226} in the resting state (as mentioned in Table 4.1), a recent work of MacKinnon's group has shown that in the resting state, R1 is likely lower, close to D^{259} (Tao, Lee, et al. 2010b). We therefore propose a closed state model that agrees with this recent data.

To further validate the resting state of the VSD, we have evaluated the gating charge associated with the transition from α to ε. The latter, which was computed using the direct measurement (see chapter 3, paragraph 4.1), is most appropriate to compare with electrophysiology measurements of the gating charge. It is associated with the whole channel deactivation and for the entire system, it amounts to 12.8 ± 0.3 e (Table 4.2), is in good agreement with values obtained for *Shaker*-like channels (12 – 14 e) in the 1990s (Schoppa et al. 1992) (Seoh et al. 1996) (Aggarwal & MacKinnon 1996). If S4 had been in a higher position, the gating charge would have been smaller and we would not have been able to account for a total gating charge as large as the one measured experimentally.

Table 4.1. Comparison between experimental and computed VSD *inter residue* distances involving the S4 basic residues. The "State" column indicates in which state the residue pairs were found to interact experimentally. The values for the distances r reported in the right part of the table were computed as averages over the 4 subunits of the channel from 10 ns simulations (distances between the geometrical centers of the side chain beads) of the Kv1.2 channel. The channel states referred to are the active (open), the partially active and the resting (closed) state. Note that the disulphide-bridge approach tends to detect distances ~ 15 Å.

Experiment	State	Residue pairs	r(A)	
			Activ. (α)	Resting (ε)
Intra-subunit electrostatic interaction	Rest.	E^{226}-R1	10.7±0.3	10.5±0.7
	P.activ.	E^{226}-R3	12.0±0.3	17.9±0.5
	Activ.	E^{226}-R4	10.5±0.2	23.5±0.5
Intra-subunit disulfide bridge	Rest.	I^{177}-R1	25.9±0.4	10.4±0.6
		I^{230}-R1	22.0±0.3	10.5±0.6
Inter-subunit disulfide bridge	Rest.	S^{289}-E^{350}	19.3±0.3	13.8±0.7
		L^{293}-E^{350}	15.2±0.4	17.1±0.7
		K^{312}-F^{416}	25.9±0.4	15.0±0.6
	Activ.	A^{291}-F^{348}	15.7±0.3	13.2±0.6
		F^{348}-R1	10.1±0.3	13.7±0.7
		A^{351}-R1	12.4±0.5	19.6±0.7

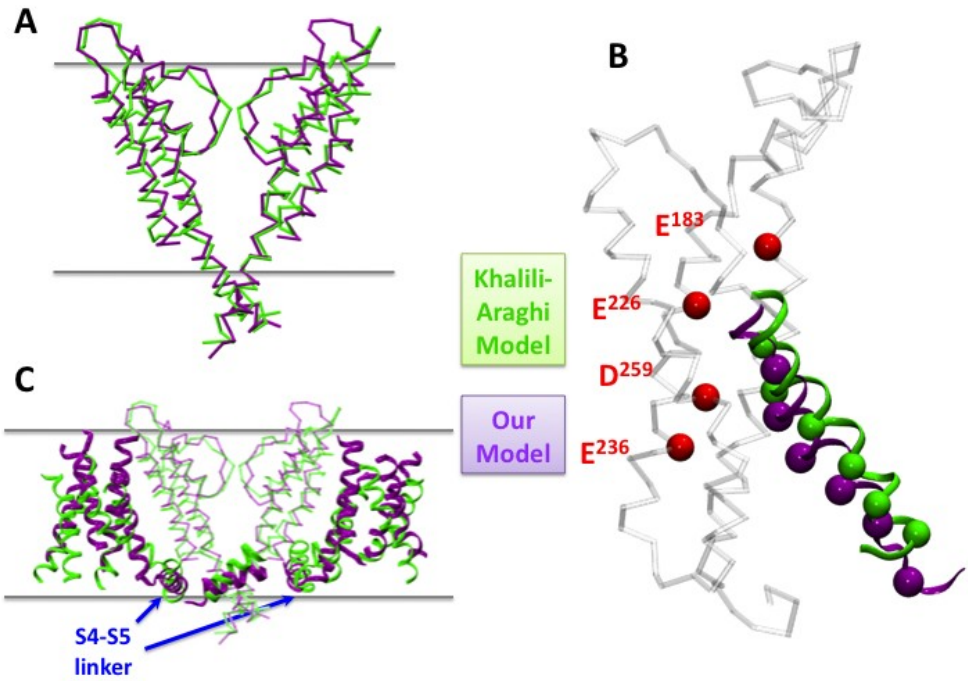

Figure 4.8: Superimposition of the pore domains of the closed state model proposed by Khalili-Araghi et al. (Khalili-Araghi et al. 2010) (green) and of our model (purple). The pore domains (S5-P-S6) were aligned. The side view in (A) indicates a good agreement between the two models. (C) The overall arrangement of the VSDs after alignment of the pore domains is similar. Discrepancies can however be observed when looking at the S4-S5 linker (more tilted in the case of the green structure) (B) Alignment of a representative VSD. Because of the high similarity of the structure of the S1-S3 packing (rmsd ~3 Å) in both structures, the positions of the negative binding sites (red spheres) are roughly superimposed and only S1-S3 of our model are represented for clarity. S4 on the other hand is higher by a few angstroms in the Khalili-Araghi model (green helix and spheres for the Cα of the basic residues) than in our model (purple helix and larger spheres for the Cα of the basic residues). Indeed, in our model, the positively charged residues of S4 are shifted down by one negative binding site (red spheres) when compared to the Khalili-Araghi model.

Finally, the position of S4 basic residues in ε were further checked by probing the effect of mutations of the arginines, R1 and R2. In agreement with electrophysiology experiments (Gamal El-Din et al. 2010), only the mutation of R1 into an uncharged homologue led to the destabilization of the VSD and to the appearance of an omega leak current through the latter under hyperpolarized voltages (see paragraph 2 of this chapter for details).

1.6 Extent of S4 displacement

To discriminate between the two models exposed in the introduction (*transporter* vs. *sliding helix* model), we analyzed the movement of S4 along the α→ε transition. Quite interestingly, the overall conformational change within the VSD involved mainly a displacement of the S4 residue with respect to the remaining other 3 helices.

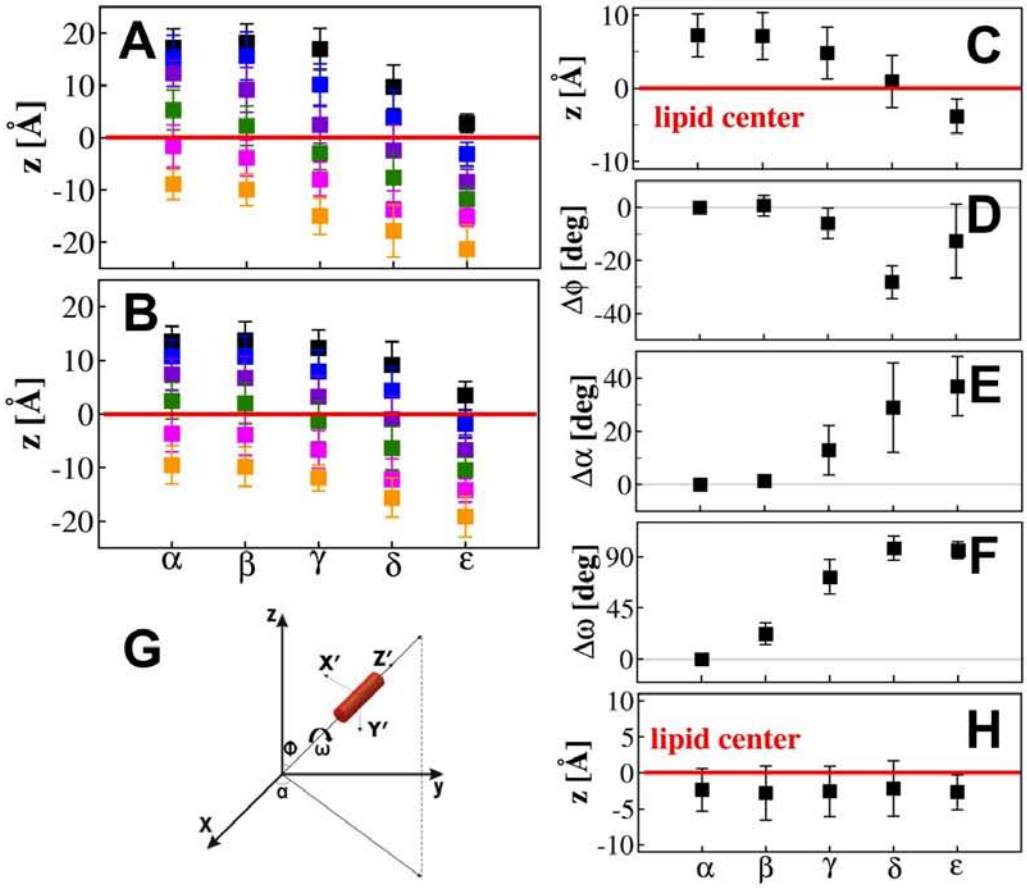

Figure 4.9: Extent of S4 motion (A and B) Positions of the S4 basic residues R1 (black) through R6 (orange) with respect to the membrane center (z=0). (A) Positions of the geometrical center of the charged moieties. (B) Positions of the main-chain C_α atoms. (C to G) Rigid-body movements of the S4 segment along the $\alpha \rightarrow \varepsilon$ transition. Only the backbone atoms of the S4 residues R1 through R4 were included in the calculation. (C) Position of the segment center of mass with respect to the membrane center (z=0). (D) Tilt Δφ with respect to z, the bilayer normal, (E) Precession Δα around z, and (F) rotation Δω about the helical main axis Z' calculated as: $\Delta\phi_i = \phi_i - \phi_\alpha$, $\Delta\alpha_i = \alpha_i - \alpha_\alpha$ *and* $\Delta\omega_i = \omega_i - \omega_\alpha$ *where* $i = \{\alpha, \beta, \gamma, \delta, \epsilon\}$ *. The S4 motions were determined after elimination of overall rotation and translation of the VSD structures, by fitting the gating charge binding sites (E^{183}, E^{226}, D^{259} and E^{236}) over the structures. (G) Coordinate systems and definition of various angles. (H) TM position (z) of the geometrical center of side chains of the charge transfer center residues (D^{259}, E^{236} and F^{233}) in each of the VSD conformational states. All the data was computed from the representative conformations considered in Fig. 4.5 and averaged over the four VSD subunits, with the error computed as the standard deviation from this average value.*

First, after superimposing the negatively charged residues in the five states, the position of the geometrical center of the charged moieties ($H_2N{=}C_\zeta(NH_2)$-$N_\varepsilon H$-$C_\delta H_2$ (Arg) and H_3N_ζ-$C_\varepsilon H_2$ (Lys)) (Fig. 4.9.A) and of their C_α backbone atoms (Fig. 4.9.B) with respect to the center of the bilayer show that during the α→ε transition, the S4 backbone atoms undergo a substantial downward translation, estimated in the range of 10 –15 Å, as the charged moieties move between 15 – 20 Å across the membrane to satisfy their electrostatic interactions with the counter charges.

We monitored additionally the rigid body motion of the backbone atoms of the segment comprising residues R1 through R4 of S4. The center of mass of this segment moves downward (~12 Å) as the VSD undergoes the 4 transitions, between the end states (Fig. 4.9.C). When viewed from the extracellular face of the membrane, this S4 motion is accompanied by a slight helical tilt (~ 15°), i.e., in state–ε, S4 becomes slightly more perpendicular to the bilayer compared to state–α, as described in early FRET and LRET experiments (Glauner et al. 1999) (Cha et al. 1999), a moderate clockwise helical precession (~ 45°) and a significant counter-clockwise helical twisting (~ 90°) (Fig. 4.9.D, E and F).

In agreement with other molecular models, significant overall translation of S4 does not occur before the rotation of the top (Pär Bjelkmar et al. 2009) (Pathak, Yarov-Yarovoy, et al. 2007) (Campos et al. 2007). Finally, in spite of significant TM displacement, the S4-side chains move relative to a rather static transfer center (see paragraph 4.1.8) during the process (Fig. 4.9.H).

1.7 Lipid participation

Recent studies have pointed to the crucial role the charges of lipid head-groups may play in modulating the gating of VGCs. The presence or absence of the phosphate groups was shown to have a dramatic influence on VGC function: the activation of K^+ VGCs may indeed be suppressed when the channels are embedded in bilayers formed by cationic lipids (Schmidt et al. 2006). Removal of the lipid head groups by enzymes also results in an immobilization of the VSD motion, thereby inhibiting VGC function (Ramu et al. 2006) (Xu et al. 2008) (Zheng et al. 2011).

Here, as inferred from electrophysiology experiments, we found that lipids, and in particular their negatively charged phosphate head group moieties, provide counter charges for the S4 basic residues, during the gating process. While earlier molecular models of the VSD (Treptow et al. 2009) (Bjelkmar et al. 2009) (Khalili-Araghi et al. 2010) have shown that lipids from the upper and lower bilayer leaflets stabilize, respectively the activated and resting states of the VSD, this study provides evidence that lipids also play this role in the intermediate states (Fig. 4.3, 4.5 and Fig. 4.10) and that in γ, both R1 and R6 interact with lipid headgroups from the upper and lower leaflet respectively at the same time.

1.8 Gating charge transfer center and conformation of S4

Mackinnon and coworkers (Tao, Lee, et al. 2010b) have recently identified an occluded site in the VSD of the K^+ VGCs formed by two negatively charged residues (D^{259}, E^{236} in *Shaker*) and the highly conserved F^{233}, which appears to "catalyse" the transfer of each of the VSD basic residues across the membrane field. As shown in Fig. 4.9.H, in each of the VSD conformations the TM position of the charge transfer center stays near the center of the bilayer. In our five conformations, however, the site is shown to be occupied by the basic residues K5, R4, R3, R2 and R1 in the VSD conformations α, β, γ, δ and ε, respectively (Fig. 4.11). Furthermore, each of the four transitions α→β, β →γ, γ→δ, δ →ε is shown to be accompanied by the translocation of a single residue (K5, R4, R3, R2, respectively) through this charge transfer region. The results from the present study confirm therefore that the VSD adopt five states along the deactivation (activation) pathway: activated, 3 intermediate and resting state that agree with the model infered by Mackinnon and co-workers based on his study.

Since the publication of the structure of the Kv1.2/2.1 paddle chimera (Long et al. 2007) and more recently of the MlotiK channel (Clayton et al. 2008), there has been a regain of interest for the problem of the secondary structure of S4 during activation. Indeed, in these two crystal structures, part of S4 is present as a 3^{10} helix. Already in the earliest models of the activation of voltage gated ion channels, the idea had been suggested that in a 3^{10} helix, the S4 basic residues located every third residue are aligned and that such a configuration would be favorable to satisfy the salt bridge interactions with the negative charges of the VSD (Kosower 1985). In their latest sliding helix model, Shafrir et al. (Shafrir et al. 2008) propose that a short stretch of S4 changes from a α-helix into a 3^{10} helix when sliding past the two negative binding sites of S2. From a computational point of view, Bjelkmar et al. found that during the initial step of the deactivation of Kv1.2, S4 underwent a 120° rotation of S4 accompanied by an extension of a 3^{10} helix stretch (Bjelkmar et al. 2009). The same authors also investigated the energetic cost of dragging S4 basic residues downwards when S4 is in a 3^{10} helical conformation when compared to a α-helical one (Schwaiger et al. 2011). For the first transition, *i.e.* when R4 passes through the gating charge transfer center, they find that the free energy is ~twice lower with the 3^{10} helix conformation and leads to less distortion of the rest of the VSD, leading them to support the hypothesis according to which S4 adopts a 3^{10} helix conformation during activation/deactivation.

We investigated the secondary structure of the S4 helix in each VSDs and in each conformation α to ε using the STRIDE program (Heinig & Frishman 2004). First of all, one should point out that in all conformations and in every subunit, the S4 helix is never a perfect α-helix (Fig. 4.12). In the α conformation, especially, even though it was equilibrated from the crystal structure, in three subunits, the bottom third of S4 is in coil structure. In the last subunit, SU1, the helix is broken at the level of R4 where two residues are coil. This suggests as expected a rather large flexibility of S4.

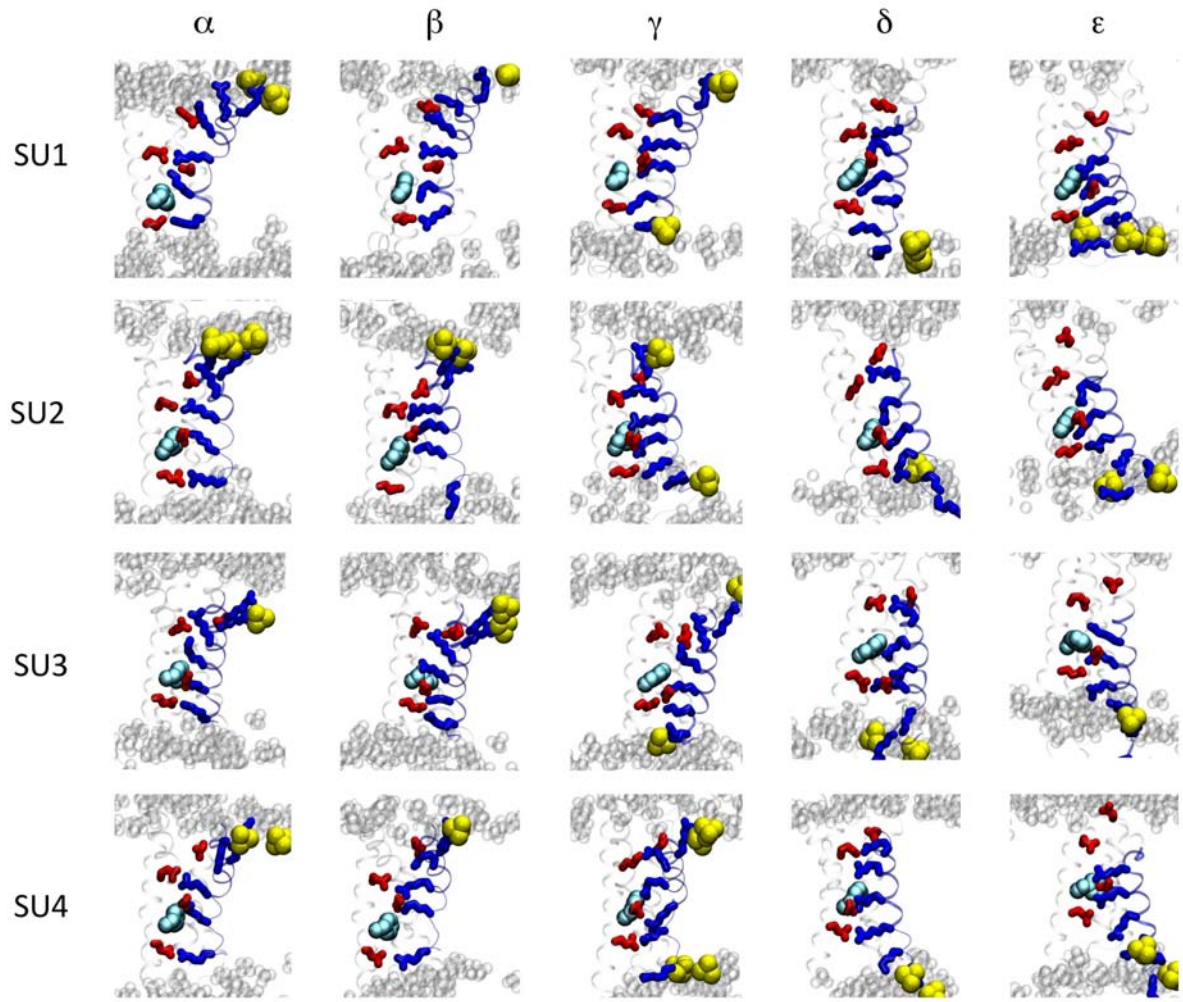

Figure 4.10: Salt bridge network in each Kv1.2 VSD subunit (coined SU1 through SU4) and in each conformation (a to e). Basic residues are in blue and acidic residues in red. F^{233} is represented as cyan spheres. Lipid PO_4^- groups within 6 Å of the basic residues are shown in yellow while the other lipid headgroups are shown as transparent spheres.

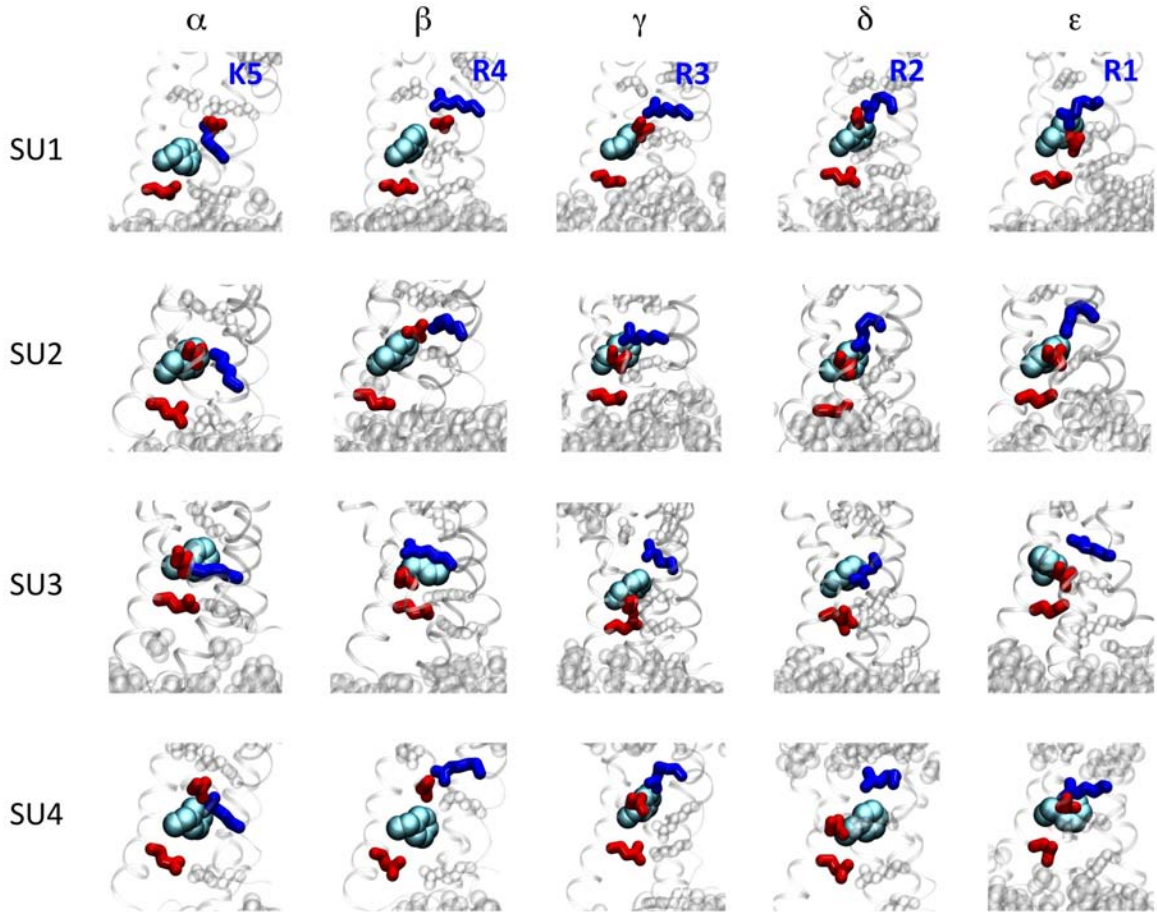

Fig 4.11: Close-up view of the gating charge transfer center in each subunit (SU1 to SU4) VSD and in each conformation (α to ε). The important residues that form the transfer center are shown: Acidic residues are represented as red sticks and the conserved phenylalanine residue F^{233} is represented as cyan spheres. In each conformation, a single basic residue is represented as blue sticks. This residue is the one that is transfers through the VSD in that particular conformation. In α, we show K5, in β, R4, in γ, R3, in δ, R2 and in ε, R1.

In three subunits, SU 1, 3 and 4, throughout the deactivation, the secondary structure of S4 does not change significantly and the secondary structure remains more or less an α helix. In subunit 2 on the other hand, the secondary structure pattern is quiet remarkable: starting from the α conformation in which the top 2/3 of S4 are in α helix and the bottom third in turn, we see that a rather large stretch in the bottom third (R4 to R6) of S4 turning into a 3_{10} helix when going to β and γ conformation. This stretch corresponds to the extent of S4 helix that is going through the gating charge transfer center. In δ, the stretch of 3_{10} helix remains roughly as long but is located in the part of S4 that is slightly higher (in the region of R2 to R4). Because S4 has slid down by ~one helix turn, this stretch is located in the gating charge transfer center. In ε, the 3_{10} helix stretch is located between R1 and R3 and corresponds once more to the section that has just transferred past the Phe^{233}. This observation is in good agreement with the model of Shafrir et al (Shafrir et al. 2008).

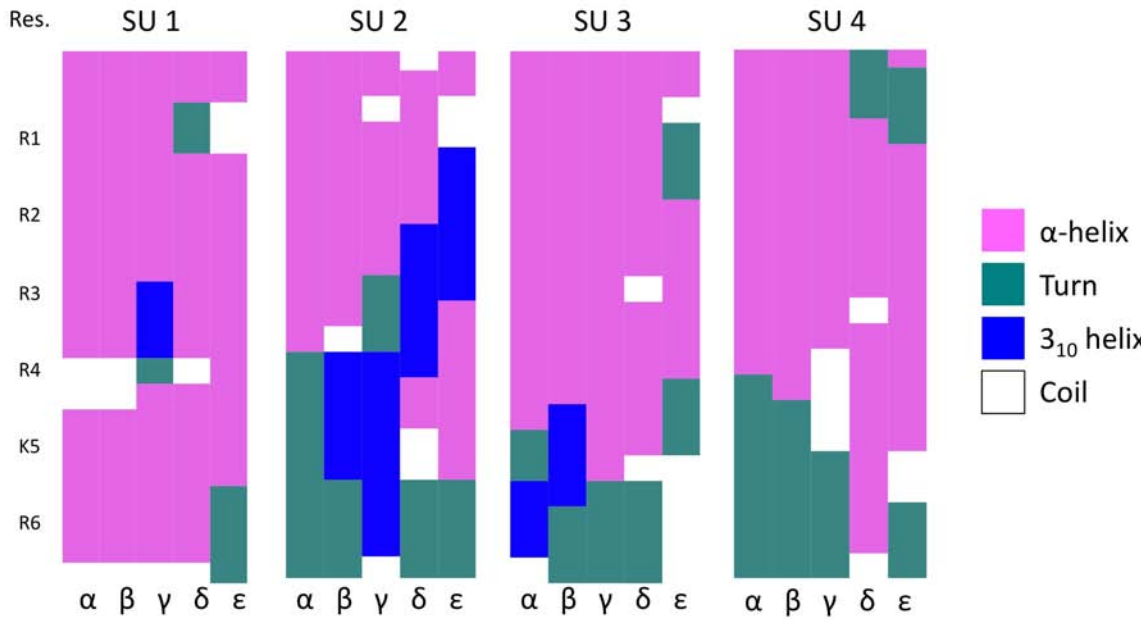

Fig 4.12: Evolution of the secondary structure of S4 in the four subunits when going from conformation α to ε as calculated with STRIDE. The position of the S4 basic residues are highlighted on the left. α-helices are figured in pink, turns in green, 3_{10} helices in blue and coil in white. Note the particularity of subunit 2 in which the stretch of 3_{10} helix evolves during the deactivation.

This disparity between the subunits indicates that the change in secondary structure is not mandatory to satisfy the electrostatic interactions described in paragraph 1.3 and 1.4 that seem to be essential for VSD function. However, due to the strong bias applied during our simulations (the -600 mV hyperpolarized potential and the subsequent steered molecular dynamics), and the disparity of S4 folds in the the four VSD it is not possible to determine clearly the most energetically favored mechanism.

1.9 Electrostatic properties

1.9.1 Transmembrane electric field

The TM-electric field is by essence the driving force for the response to membrane polarization. Here, the 2-D maps of the electric field through a VSD submitted to a 600 mV hyperpolarized potential, generated according to the procedure described in chapter 3, section 2.1, is reported for the two different states α and δ (Fig. 4.13).

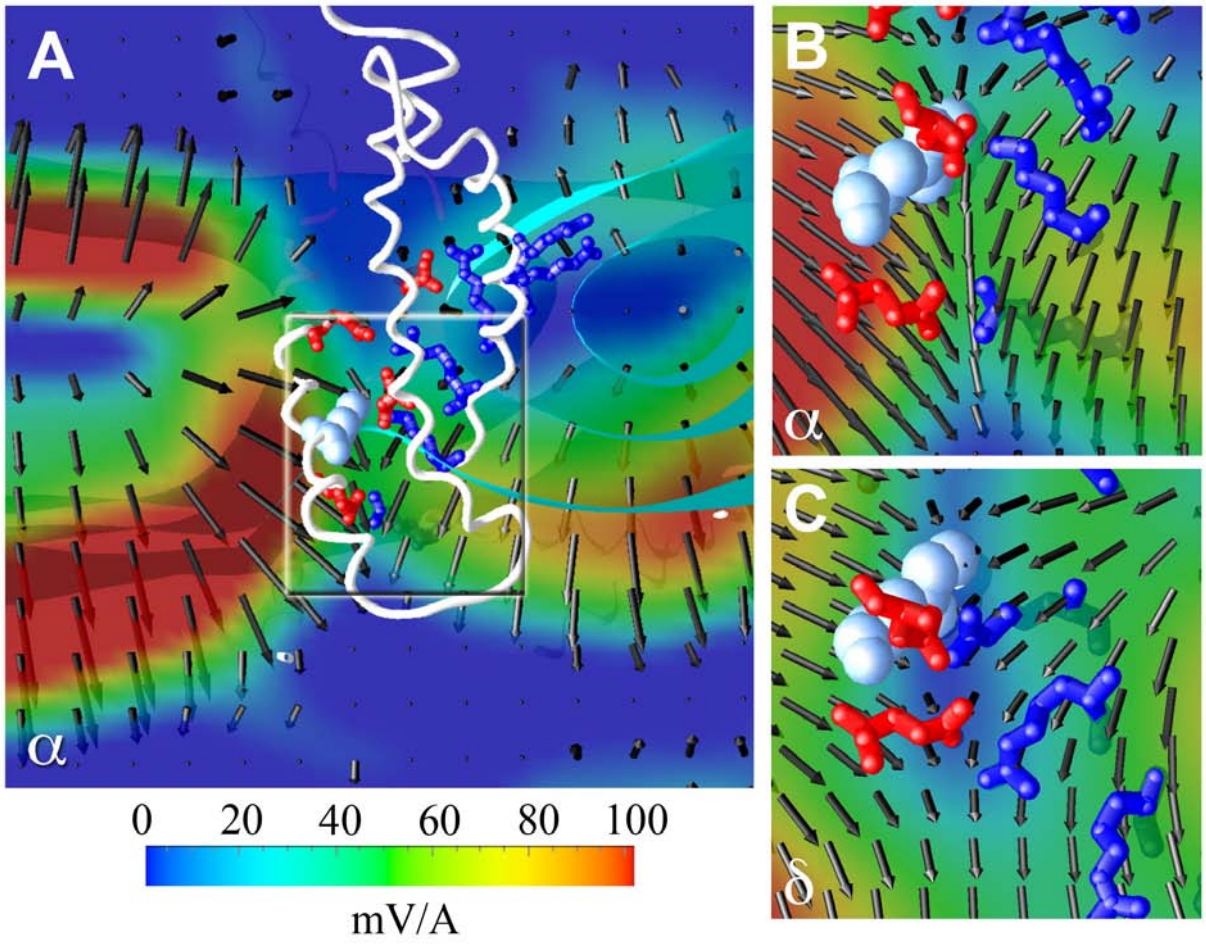

Fig 4.13: Electric field maps under a depolarized TM potential in representative VSD conformations α and δ. (A) A representative Kv1.2 (α) VSD is located in the center of the panel and for clarity, only its backbone atoms (white ribbons), the conserved F^{233} residues (cyan spheres) and the basic (blue) and acidic (red sticks) residues of its TM domain are shown. The local electric field direction is shown as black arrows. Close up view of the charge transfer center region in the α (B) and δ (C) states highlighting the electric field pointing downward and rationalizing the downwards movement of the basic residues of S4.

The maps show that the electric field is pointing down and that its magnitude is largest next to the gating charge transfer center. At this location within the VSD, the force driving the basic residues downwards is very large and interestingly, it does not seem to change drastically when going from one state to another, in contrast to what was inferred from fluorescence measurements. Indeed, one recalls that Asamoah et al. used a cysteine reactive electrochromic fluorophore to analyze the electric field in the VSD (Asamoah, Wuskell, et al. 2003) finding dynamical changes in the electric field during the gating process.

1.9.2 Gating charge calculation – Relationship to free energy

In presence of a TM potential, a number of protein tethered charges cross the resulting electric field giving rise to the experimentally measured gating charge, Q. In the following, we use the five states of the VSDs to gain further insight on the molecular/electric properties of the domain accounting for Q. We will use here the two methods described in chapter 3 (paragraph 4): the direct measurement, which provides the value of the gating charge for the entire system with little approximation and therefore little error on the gating charge value. The other method, based on a free energy description suffers from more approximation, but on the other hands enables to identify the molecular components involved in the gating charge.

The direct measurement traces back the charge imbalance and enables the direct calculation of the charge transported by the entire system between two states. As previously noted, (paragraph 1.1 of this chapter) the gating charge for the α/β transition is ~1.4e. The results for the α/γ, α/δ and α/ε transitions are reported in Table 4.2. It is interesting to note that the four transitions transport a gating charge that is not homogeneous as the gating charge in the second and third transitions transport the most gating charge: γ/δ transition has the largest gating charge with ~5.3e, followed by the β/γ transition, transporting 3.4e. The first and last transitions transport the least gating charge with 2.7e and 1.4e for the δ/ε and α/β transition, respectively.

Table 4.2 Direct measure of Q for the VSD conformations γ, δ and ε. The total Q was computed according to eq. [3.44] and considering the α state as a reference; q_0^{ion} was computed relative to the center of the bilayer; Membrane capacitance C = 0.9x10^{-22} C.V^{-1}.A^{-2}; ΔV corresponds to the voltage estimated from the average over a simulation-time window of ~ 1 ns

Conformations	ΔV [Volts]	Lipid area [Å^2]	q_0^{ion} [e]	$q_0^{protein}$ [e]	Q [e]
α	-0.81±0.05	16531.8	-36	28.5±0.5	0.0
γ	-0.98±0.05	17189.1	-48	37.3±0.5	4.8±0.3
δ	-0.95±0.05	17196.7	-58	48.8±0.5	10.1±0.3
ε	-0.57±0.05	16840.2	-60	54.6±0.5	12.8±0.3

To identify the residues that are involved in the gating charge, we have also used the free energy based calculation: we recall that for a structure undergoing a general α→β *transition* under ΔV, the gating charge Q may be linked to the variation of the free energy of the channel: $Q.\Delta V = \Delta G(\beta, \Delta V) - \Delta G(\alpha, \Delta V)$ (Treptow et al. 2009) (Grabe et al. 2004) (Jogini & Roux 2007) (Stevens 1978).

$\Delta G(\lambda, \Delta V) = G(\lambda, \Delta V) - G(\lambda, 0) = \Delta V . \sum_i q_i . \delta_i^{\lambda}$ is the excess free energy in each conformation, λ, due to the applied potential ΔV. δ_i^{λ} is the so-called "electrical distance" of the residue *i*. It accounts for the degree of coupling between the local electrostatic potential $\phi_i^{\lambda}(r_i)$ felt by q_i located at r_i and ΔV, and is expressed as $\delta_i^{\lambda} = \frac{\partial \phi_i^{\lambda}(r_i)}{\partial V}$.

This formulation allows the identification of the specific molecular components that contribute to the gating charge (Fig. 4.14.A, B and C). During the whole VSD transition from up to down states, 11.2 elementary charges were transported by the channel, of which ~10 e transported by the S4 helices. For the four consecutive transitions from α → ε, the cumulative gating charges measured for each VSD amounts to -0.52 e, -1.33 e, -2.17 e and -2.8 e, respectively (Table 4.3). As shown in Fig. 4.14.B and Fig. 4.14.C, substantial contributions arise from the S4 basic residues, which is consistent with experiments (Baker et al. 1998) (Aggarwal & R. MacKinnon 1996) (Papazian et al. 1991) and with recent MD simulations of the VSD (Pathak, Yarov-Yarovoy, et al. 2007) (Khalili-Araghi et al. 2010) (Chanda et al. 2005).

Fig. 4.14.C reports the normalized gating charges transported by the S4 basic residues during each transition. It shows that the contributions from these residues is not uniform: during deactivation, the lower S4 residues carry more charges during the early transitions, while the upper ones transport more charges during the late transitions. Evidence from the raw data suggests therefore that the electric field in which the charges physically move is not uniform across the membrane.

Table 4.3 Gating charges and cumulative free energy differences under ΔV = -100 mV per subunit computed between the α, β, γ, δ and ε states with the free energy methodology.

Transition	Direct measurement		Energetic formalism		S4 contribution	
	Q [e]	Cum. ΔG [kcal/mol]	Q [e]	Cum. ΔG [kcal/mol]	Q [e]	Cum. ΔG [kcal/mol]
α/β	-1.8	-1.74	-2.08	-2.0	-1.9	-1.83
β/γ	-3.4	-5.02	-3.24	-5.13	-2.56	-4.32
γ/δ	-4.8	-9.65	-3.36	-8.40	-3.4	-7.64
δ/ε	-2.8	-12.35	-2.52	-10.77	-2.04	-9.61

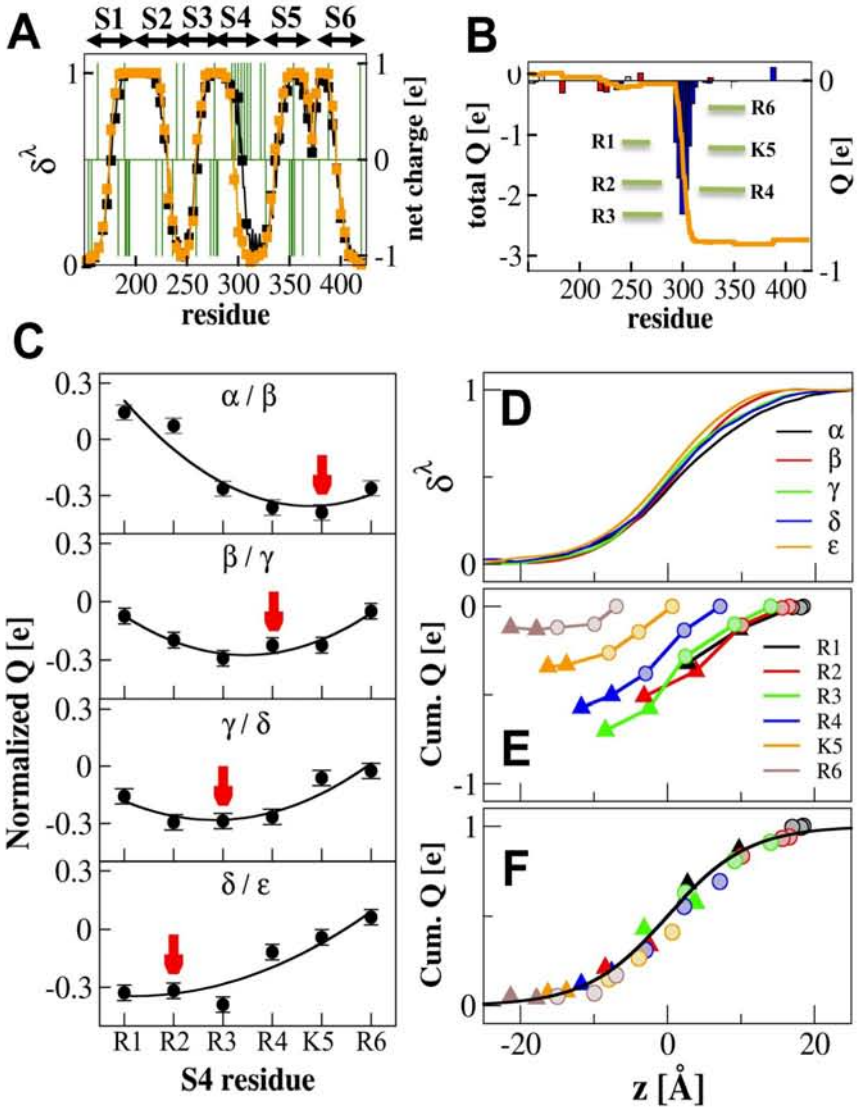

Fig 4.14: Electrical properties of the VSD (A) Top: Electrical distances, δ_i^λ for each TM residue in the α (black) and ε (orange) conformations and net charge per residue (green) along the Kv channel sequence (excluding the T1 domain). The position of the TM segments S1 to S6 is indicated by arrows. δ_i^λ was normalized assuming δ_i^λ = 1 and 0 for residues positioned, respectively above 25 Å and below -25 Å from the bilayer center. The data was averaged over the four subunits of the channel (B) Corresponding cumulative (orange line) and per-residue (bars) gating charges for the α → ε transition (basic residues in blue and acidic ones in red). (C) Contributions of each S4 basic residue to the normalized gating charge associated with each transition, enabling the identification of the residue(s) transporting most of the gating charge (red arrow). Error bars correspond to the standard deviation from the average value over the four subunits. (D) Electrical distance through the VSD in each conformation as a function of z, the normal to the bilayer. (E) Gating charge (Q) and TM position (z) for the S4 basic residues in each of the VSD states a through e. Circles represent the gating charges that were obtained with regular MD simulations while triangles stand for the configurations that were obtained with steered MD. (F) Activation master curve, describing the dependence of Q with z.

The overall conformational change from the up to down states of the VSD necessitates a large physical TM displacement of the charged moieties of R1 to R6 amounting to ~15 – 20 Å (Fig. 4.9.A). For the purpose of linking the physical displacement of these charges to the measured gating charge, it is interesting to consider $\delta_i^{\lambda}(z)$, the electrical distance of the VSD residues located at the TM position z. In each channel conformation, these values collapse onto a single sigmoidal curve that provides a good estimate of the fraction of the potential the residues are sensing across the membrane. In Fig. 4.14.D, we report this fraction of potential for the conformations α to ε of the VSD. Interestingly, $\delta_i^{\lambda}(z)$ does not seem to vary substantially from one conformation to the other. This is a clear indication that the local electric field within the VSD is not drastically reshaped during activation.

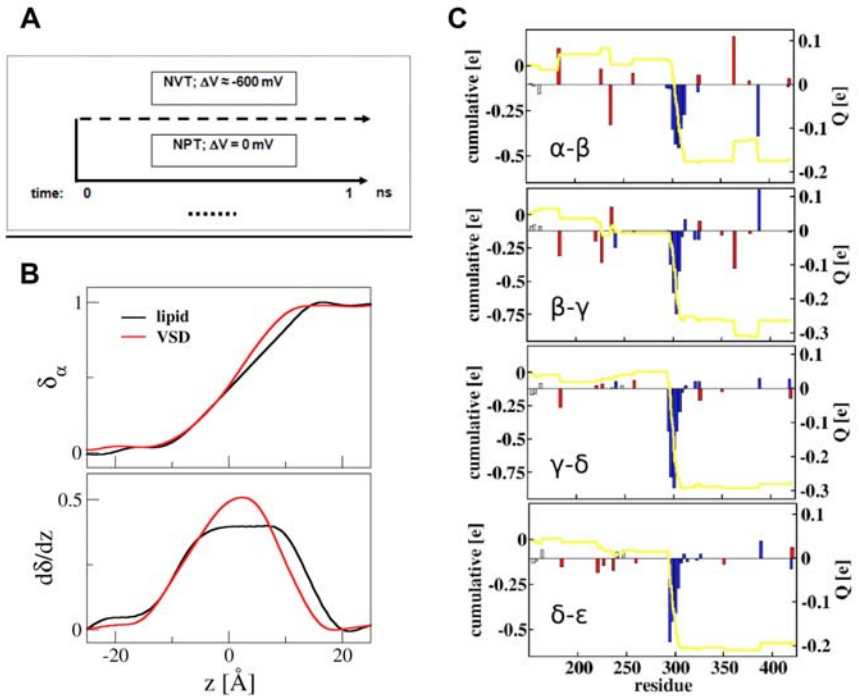

Fig 4.15: (A) Simulation protocol used for calculation of the "electrical" distance δ_i^{λ}. For both simulations, the conformational state of the channel was fixed by imposing harmonic constraints to its main-chain atoms. (B) Electrical distance profiles (top) and derivative of the latter (bottom) across the lipid zone (black line) and across the VSD (red line). Note the focalization of the electric field in the VSD when compared to the lipid. (C) Cumulative (line) and per residue (bars) gating charges calculated via the free energy formalism for the four α→β, β →γ, γ→δ, δ →ε transitions.

Fig. 4.14.E reports the cumulative gating charge evaluated for each S4 basic residue as a function of its TM position z. The data shows clearly that residues R2, R3 and R4 located in the middle of S4 carry more charges than R1, K4 and R5 during the full α to ε transition and also during the individual α/β, β/γ, γ/δ and δ/ε transitions (Fig. 4.14.C). As expected from the previous analyzes, these cumulative contributions all collapse onto a master curve, essentially

$\delta_i^{\lambda}(z)$, which itself describes the electrical activity of the VSD (Fig. 4.14.F). The gating charges for any elementary transition are directly connected to the physical displacements of the S4 basic residues across the membrane through this master curve. Comparison of the latter to the voltage fraction across a bare bilayer underlines the reshaping of the electric field within the VSD due mainly to the distribution of charges and to the presence of solvent (Fig. 4.15.B). In support of the phenomenological models developed earlier, the electric field appears to be focused in the middle of the bilayer, in the sense that identical physical displacements along z result in larger gating charges when the translocation occurs around z=0. The master curve describing the VSD electrical activity predicts that a total displacement of a given basic S4 residue of over 40 Å is necessary to carry a gating charge of 1e. However, over 70% of the latter can result from the displacement over a narrow window of 20 Å near the bilayer center.

1.10 Coupling to pore gating

Up to this point, we have focused only on the operation of the VSDs in response to a hyperpolarized voltage. The question of the coupling to the pore remains to be addressed.

Throughout the 2.2 μs unbiased simulation, as mentioned above, the original pore structure remained stable, *i.e.* the pore kept its open structure with the diameter around the gate ~8 Å. During the biased simulation, when going from γ to δ and subsequently from δ to ε, although we did not apply any force directly on the pore, it is noteworthy that the pore closed spontaneously (Fig. 4.16). The conformational change leading to pore closure occurred after reaching the δ conformation, with the pore diameter at the level of the gate dropping to ~5.5 Å and in ε to under 2 Å, thereby preventing the passage of ions through the main pore (Treptow & Tarek 2006).

The mechanism by which the coupling occurs seems to involve the S4-S5 linker in interaction with the C-terminal part of S6 (Lu et al. 2002) (Ding & Horn 2003) (Labro et al. 2008) (Nishizawa & Nishizawa 2009) In our simulations, when S4 moves downwards, the intracellular part of S4 does not translate only downwards as the energetic cost would be too high to drive the S4 hydrophobic residues into the solution. Instead, S4 bends slightly and slides along the lower leaflet lipid headgroups counterclockwise when looking from the intracellular side (Fig. 4.17).

Ferrer et al. (Ferrer et al. 2006) have shown that the linker couples the VSD movement to the activation gate. In particular, they identified a specific interaction between D^{540} and L^{666} (located, respectively, in the S4-S5 linker and in S6) in the closed state of the hERG channels. Consistently, we find that when S4 moves down, it drives the S4/S5 linker counter-clockwise and the interaction between the homologous residues in Kv1.2 (K^{312} and F^{416}) drags in turn S6 counter-clockwise and downwards, in a screw-like motion that leads to the closure of the gate.

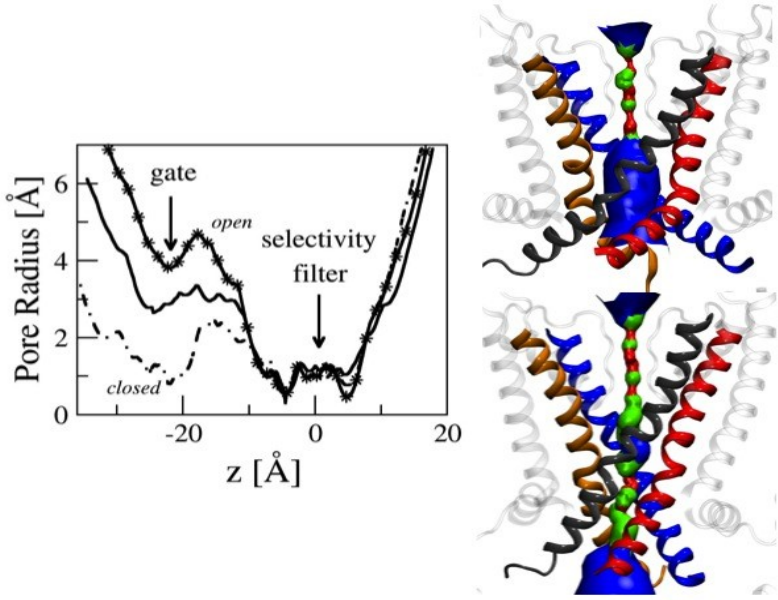

Fig 4.16: Gating of the pore region. (Left) Main pore radius along the normal to the bilayer in the open (α) state (stars), in the δ state (full line) and in the resting (ε) state (dashed line). The pore radius remains constant in the selectivity filter region while it decreases at the gate level, from ~4 Å in the open state to ~0.8 Å in the closed one. (Right) Side views of the pore in the open (top) and closed (bottom) states. S5 is represented as transparent ribbons, S6 as colored ones, the volume was calculated with the Hole program suite (Red marks places where the pore radius is below 0.6 Å, green is used where it is in the range 0.6Å to 1.15Å and blue marks places where it is above 1.15Å).

1.11 Discussion

An extensive 2.2 μs MD simulation of the membrane-bound Kv1.2 channel subject to a hyperpolarized potential, and subsequent steered MD simulations have been used to reveal the VSD response and reorganization during the channel deactivation. The conformational changes taking place within the VSD involve a zipper-like motion of the S4 basic residues in sequential ion pairing with nearby counter charges and lipid head groups from both the upper and lower membrane leaflets. This essential feature is in excellent agreement with early mutagenesis experiments (Papazian et al. 1995) (Tiwari-Woodruff, Lin, Schulteis, et al. 2000) (Zhang et al. 2005) and with the recent hypotheses from the groups of Cui and Catterall The former, probing the salt bridge interactions in the different states of Kv7.1 by charge reversal mutagenesis (Wu et al. 2010) and the latter probing these interactions in in NaChBac, a bacterial Nav channel, VSD of which is very similar to that of Kv channels, by disulfide locking (DeCaen et al. 2009) showed that, during activation, the S4 segment moves from an inward position in which R1 interacts with E2 to an outward position in which R4 interacts with E4. (cf also Catterall 2010).

In order to satisfy the charge pairing of the basic and acidic residues, some studies have suggested that the movement of S4 and particularly the passage of S4 through the catalytic

center requires the transitory switch of a stretch of S4 into a 3_{10} helix. Recent simulations have found results pointing towards this direction: Khalili-Araghi et al. found a spontaneous conversion of the 10 residue stretch of S4 located in the catalytic center into a 3_{10} helix in their Rosetta model of the resting state (Khalili-Araghi et al. 2010). The group of Lindahl (Bjelkmar et al. 2009) found an extension of 3^{10} helix stretch when submitting the open Kv1.2/2.1 paddle chimera channel to a hyperpolarized electric field. They further showed that the free energy of dragging S4 downward is ~twice lower for the 3^{10} helix conformation (Schwaiger et al. 2011).

Interestingly, in this study we have found that for one subunit, the short stretch around the residue transferring through the gating charge transfer center takes the form of a 3_{10} helix, for each of the 4 transitions. In contrast, all the other subunits underwent the 4 transitions without such secondary structure change. It is not clear therefore which mechanism would be most favorable from an energetic point of view and further investigations are needed before drawing clear conclusions. In addition, it is important to stress here that secondary structures stability and conformational changes they may undergo are highly dependent on the force field used and interpretation of any related data should be exerted with caution (Yoda et al. 2004) (Matthes & de Groot 2009).

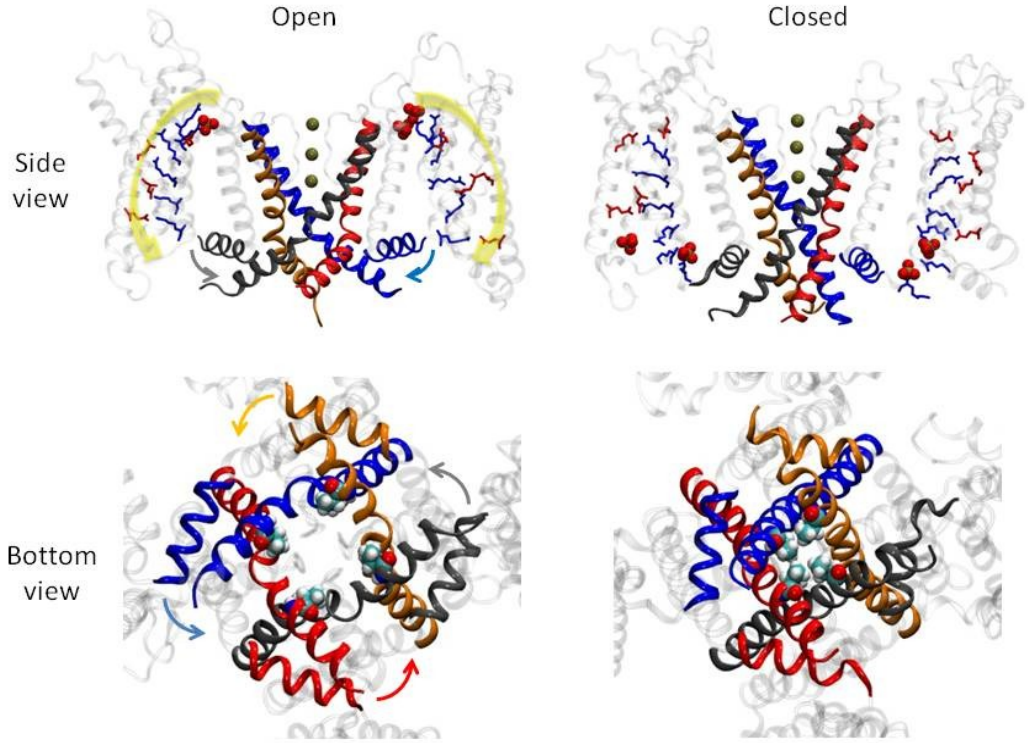

Fig 4.17: Closing mechanism of the Kv1.2. (Top) Side view of the channel illustrating the downwards motion of the S4/S5 linker coupled to the donwards motion of S4. Positive charges od the VSD are in blue, negative ones in red. The S4/S5 linker and S§ helices are represented as coloured ribbons. The PO4- groups that are closest to the gating charge are represented as red spheres. (Bottom) View from the intracellular domain illustrating the counter clockwise motion of the S4/S5 linker coupled to S6. The V^{478} residue, constituting the gate, is represented as vdw spheres.

Overall, the study has uncovered 5 states of the channel. Indeed, in addition to the α (open) state and the two intermediate states (β, γ) arising from the unbiased MD trajectory, one more (δ) was identified using biased MD simulations in which the imposed "reaction" pathway was consistent with the zipper-like motion. Importantly, the final down state (ε) arising from the biased MD could have been generated by *de novo* modeling, using the available experimental constraints from the literature, as done by others (Tombola, Pathak, et al. 2005) (Pathak, Yarov-Yarovoy, et al. 2007). It is noteworthy that while the β- and γ-states have been generated by unbiased simulation, only the δ state required assuming a pathway that follows the sequential base pairing.

This VSD activation mechanism is consistent with experiments and kinetic models devised to fit the curves of the gating current that have claimed that activation of each of the VSDs proceeded in multiple sequential steps. Interestingly, the gating charge measured here for each transition (~0.45 to 1.2e per subunit) is of the same order of magnitude than the elementary charge movements estimated from measurements of gating current fluctuations (Sigworth 1994) and as the "loose" charges, an early component of the gating current in *Shaker* channels (~1e per VSD unit) (Sigg et al. 2003), indicating that the intermediate states uncovered here are of functional significance. Naturally, early models, *e.g.* the Zagotta-Hoshi-Aldrich model (Zagotta, Hoshi & Aldrich 1994) have considered a small number of states (a minimum of 3 was required for proper fitting). Later, other groups, extending the study to a broader voltage range, have proposed the same types of models, but introducing additional states (Schoppa & Sigworth 1998) (Baker et al. 1998) (Loboda & Armstrong 2001) (Sigg et al. 2003) (Zheng & Sigworth 1998) (Kanevsky & Aldrich 1999). One of the most recent proposals suggested that the VSD can adopt five conformational states (Tao, Lee, et al. 2010b). This last investigation by Mackinnon and coworkers demonstrated indeed that the VSD transitions involve sequential passage of the S4 basic residues through a catalytic center involving the conserved F^{233} residue . Interestingly, our study captures this feature and proposes altogether five states (α and ε and three metastable β, γ and δ states) in each of which the gating charge transfer center is occupied by a different basic residue.

The unbiased simulations performed here have clearly indicated the response of the 4 VSD of the channel and particularly the intermediate transitions are not occurring in a concerted motion. This is in agreement with eletrophysiology experiments that all indicate that only the final opening transition is concerted (Zagotta, Hoshi, Dittman, et al. 1994).

The overall conformational change from the active to the resting states of the VSD results in a total gating charge in agreement with electrophysiology experiments, and necessitates a large displacement of the S4 backbone amounting to 10 – 15 Å, which is in closer agreement with estimates from avidin binding experiments (Ruta et al. 2005) than previous models (Catterall 2010). Up to 2005, two main contradictory models were competing to describe VSD activation: 1- the *helical screw model*, in which S4 moves independently from the rest of the voltage sensor domain in a screw-like motion, involving a large translation of the latter by ~ 10 to 20 Å while rotating about its own axis by 180°, advocated mostly by cysteine accessibility studies and disulfide scanning experiments and 2- the *transporter model which*

involves instead a large reorganization of the electric field in the vicinity of S4 with only a small overall displacement of S4 and that has been put forward mostly to rationalize fluorescence measurements. Since then however, several attempts had been taken at reconciling these various views (Tombola, Pathak & Isacoff 2006) (Jogini & Roux 2007) (Pathak et al. 2007). They claimed that whereas all the experiments involving mutagenesis introduce an alteration of the structure, of the function and probably of the dynamics of the channel (Durell et al. 2004), all the fluorescence studies have a tendency to underestimate measured distances (Selvin 2002). Also, avidin binding may lock the channel in extreme positions which are scarcely visited otherwise, leading altogether to overestimation of measured distances (Jiang, Ruta, et al. 2003). Taking this into account, the molecular conformations of the identified transition states in this study not only are consistent with the sliding helix model, but also comply with most experiments, providing a trustworthy picture of the complete operation of the VSD.

Perhaps the most interesting feature revealed by the present MD study is the analysis of the electrical activity of the channel and the finding that the cumulative gating charge transported by the S4 basic residues can be described by a unique function, which defines the electromechanical coupling mechanism that the VSD charges undergo. While in agreement with previous phenomenological models, this coupling results from a focused electric field within the domain, the shape and intensity of which is hardly modified during deactivation. Such a feature had already been inferred by MD studies: because water crevices protrude into the VSD from the intra- and the extra-cellular media, all the S4 basic residues lie in a solution environment, rationalizing the focused electric field necessary to transport 12-14e during activation (Treptow & Tarek 2006) (Jogini & Roux 2007) (Freites et al. 2006) (Nishizawa & Nishizawa 2008) (Krepkiy et al. 2009). However, while Jogini and Roux determined using continuum electrostatic computations that the TM potential sensed by the S4 basic residues varies mostly over the outer half of the membrane (Jogini & Roux 2007), we find that such a variation is maximal at the level of the gating charge transfer center, just under the middle of the VSD. The origin of this discrepancy is not yet understood. However, our model agrees better with the hypothesis of a catalytic transfer center at such a location (Tao et al. 2010). Finally, although the final conformations of the sensor have been generated using biased MD simulations, the ones resulting from the unbiased MD trajectory contained enough information to reconstruct the electromechanical coupling dependance, which strengthens confidence in our findings.

The molecular mechanism underlying voltage sensing has remained a matter of debate. The present computational study favors the sliding helix model and provides a molecular description of three intermediate states of the VSD. Though the present results are specific to the VSD of the Kv1.2 channel, they likely can be generalized to other VGCs. When combined with electrophysiology measurements, they will allow a better characterization of the molecular mechanisms implicated in the S4 residue mutations that underlie certain channelopathies (see paragraph 2) and in the modulation of VSD function by lipid headgroups (paragraph 3).

2 S4 basic residues mutations

As mentioned in section 2 (paragraph 3.2.3), mutations of the positively charged residues of S4 in K^+, Na^+ or Ca^{2+} VGCs have been shown to impair cellular function and have been also linked to certain inherited channelopathies, *e.g.* epilepsy, long QT syndrome, and periodic paralysis. These mutations modify several physical properties of VGCs, like sensitivity to voltage changes which in turn alters conduction through the central pore (Bao et al. 1999) (Jurkat-Rott et al. 2000) (Soldovieri et al. 2007).

In the case of K^+-VGCs, specific mutations of S4 positively charged residues to uncharged or smaller amino-acids lead to the appearance of another current component aside from the alpha conduction (Tombola, Pathak, et al. 2005). This so-called "omega" or gating-pore current was attributed to leakage of cations through a conduction pathway within the VSD. In Nav channels (Sokolov et al. 2005), measurements correlated such currents with mutations that cause *normo*- and *hypo*-kalemic periodic paralysis (Sokolov et al. 2007) (Struyk & Cannon 2007) (Sokolov et al. 2008).

In this section, we investigate the molecular mechanisms involved in these currents. To do so, we have used molecular dynamics simulations of the Kv1.2 channel embedded in its lipid environment, in its open and closed state, after mutating different sets of residues.

2.1 Computational details

Here, we considered the Kv1.2 channel both in the open/activated state (corresponding to the starting structure of paragraph 1, which is also the α state) and the channel in its closed/resting state (corresponding to the ε state). We have used the same protocols and methods as in the previous study. Especially, the channel was always considered to be embedded in a model membrane and solvated in a 150 mM KCl solution.

To apply TM voltage to the systems, as in paragraph , we used the charge imbalance combined with the vacuum water interface scheme (chapter 3, paragraph 3.2).

We considered mutants of the channel that contain a single (or a double) mutation of a positively charged residue of S4 into an uncharged residue (Table 4.4). Whereas in experiments mutants have to be engineered by mutagenesis, in simulations, it is very easy to replace an amino acid by another one. Here, we engineered artificial mutants in which the arginine (or lysine) is replaced by its uncharged homolog. This simply implies to set the partial charges of the atoms that constitute the charged moiety of the residue to zero. We thereby mimic the mutation to glutamine. To ensure neutrality of the system, either negative ions are added to the system or a negative residue of the protein that is not in the VSD region (typically far away in the T1 domain) is also mutated to an uncharged homologue.

2.2 Effect of S4 basic residue mutation on the structure

We first investigated the effect of selected mutations of the S4 basic residues on the stability and conduction properties of the Kv1.2. Two key conformations of the channel have been considered: the first corresponds to the X-ray crystal structure of the open channel, the above-mentioned α state (Long, Campbell, et al. 2005a), while the other corresponds to the closed state, in which the VSD has the resting conformation (conformation ε). MD simulations (#0, 11, see table 4.4) of these both conformations correspond to the equilibration runs stated in the previous paragraph and extended over 50 ns. They enabled to show that the structures of the VSDs remain stable.

We recall here the networks of salt bridges between the positively charged residues of S4 and negatively charged residues of the other segments of the VSD in both conformations:

- In the open (α) conformation (Fig. 4.18.A), the top residues R1 and R2 are located at the membrane-water interface and interact with lipid -PO_4^- groups of the top leaflet of the membrane and R3 is close to E^{183} (S1). Deeper within the VSD, R4, K5 and R6 are respectively involved in salt bridges with E^{226} (S2), D^{259} (S3) and E^{236} (S2).
- In the closed (ε) conformation (Fig. 4.18.D), the network of electrostatic interactions is different. Here, R1 interacts with both E^{226} and D^{259}; R2 and R3 are involved respectively in salt bridges with D^{259} and E^{236}; and R4, K5 and R6, which are located near the inner membrane-water interface interact with the lipid-PO_4^- groups as highlighted in other proposed models of the closed state.

In both conformations, the VSD topology delimits an hourglass-like structure in which water penetrates from the extra and the intracellular sides. In agreement with previous investigations (Sokolov et al. 2005) (Krepkiy et al. 2009) (Bezanilla 2005), salt bridges involving bottom residues in the open conformation and top ones in the closed conformation, are found to participate in the constrictions, which prevent communication between the lower and the upper water crevices (Fig. 4.18.B, E).

Next, several MD simulations of the open channel conformation were performed, in which selected S4 positively charged residues were substituted by uncharged counterparts, thereby mimicking their mutations to glutamine (see Table 4.4). Mutation of the residues not involved in the water constriction does not change the overall topology of the VSD: In R1/R2 and R3/R4 double mutants, the constriction prevents communication between the intra and extra cellular baths. Mutating K5 and R6, on the other hand, opens up a hydrophilic path (omega pore), drastically changing the topology of the VSD. During the MD simulation of the latter by contrast (Sim #3), the K5-D^{259} and R6-E^{236} electrostatic interactions were severely reduced as the average distance between their moieties increased from ~3 Å to ~8 Å within 1 ns. As a result, the VSD adopted a swollen-stable structure in which a connected hydrated pathway (so called omega pore) opened up between the intra- and extracellular media.

Simulation #4 indicated that the single mutation of K5 is enough to destabilize the VSD in a similar manner (Fig. 4.18.C).

For the closed state conformation on the other hand, the constriction in the VSD involves R1 and R2. Accordingly, we studied only the R1/R2 double and the R1 and R2 single mutants (Sim. #12, #14, #13). Only the breaking of the salt bridges involving R1 led to the appearance of an omega pore (Fig. 4.18.F).

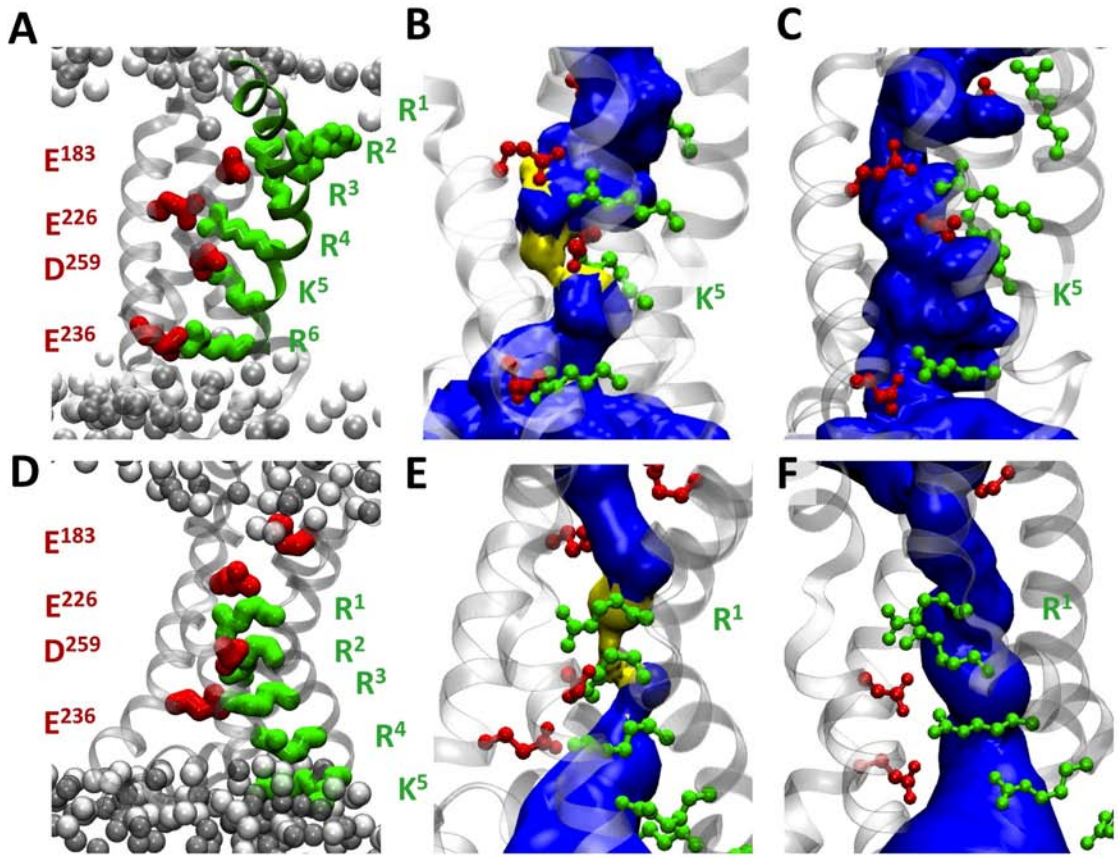

Figure 4.18: (A) VSD topologies for the open (S4 'up'; top panels) and closed (S4 'down'; lower panels) Kv1.2 channel conformations. (A) and (D) highlight the location of the S4 basic residues (green) and the salt bridges they form with basic charges (red) of the VSD, (B) and (E) the solvent accessible volume (blue) (as determined with the HOLE program) within the VSD of the WT channels. The most constricted region (pore radius < 1.15 Å) is depicted in yellow. (C) and (F) the accessible volume respectively for the K4 and R1 mutants.

Table 4.4: Summary of all MD simulations of the VSD mutants. *Applied voltage is 0.6 V for the open state and -0.6 V for the closed one. [1] Under 0 mV [2] Under TM voltage conditions

#	State	Channel	Voltage*	Time (ns)	Omega pore [1]	Leak[2]
0/5	Open (α)	WT	No/Yes	50/60	-	-
1/6		R1/R2	No/Yes	20/60	-	-
2/7		R3/R4	No/Yes	40/40	-	-
3/8		K5/R6	No/Yes	40/150	YES	YES
4/10		K5	No/Yes	60/100	YES	partial
11/15	Closed (ε)	WT	No/Yes	100/40	-	-
12/16		R1/R2	No/Yes	12/40	YES	YES
13/17		R2	No/Yes	12/40	-	-
14/18		R1	No/Yes	12/40	YES	YES

2.3 Leaks through the VSD

The conduction properties of the omega pores have been investigated by submitting the systems to TM potentials. Explicit ion dynamics has been employed (see chapter 3, paragraph 3.2) (Delemotte et al. 2008) (Treptow et al. 2009), with applied voltages six times larger than under physiological conditions (+/- 600 mV), to thereby enhance the ionic conduction. The prevention of the main pore conduction was achieved by restraining the motion of the selectivity filter residues. As expected, both the WT channels and mutants in which the VSD constriction was preserved (Sims. #5, 6, 7, 15, 17) displayed no conduction over the time scales explored. Even under such high TM voltages, in each of the simulations carried out, the VSDs remained very stable, maintaining the specific constriction.

In contrast, mutants where omega pores formed under equilibrium conditions were partly (for the open K5 single mutant) or totally permeable to K^+ ions (for the open K5/R6 mutant and for the closed R1/R2 and R1 mutant) (Sims. #8, 10, 16 and 18).

2.3.1 Conduction through the activated K5/R6 double mutant

The MD simulation (Sim. #8) of the K5/R6 double mutant subject to a depolarized TM potential shows that the hydrophilic pathway within the VSD enables cation conduction from the intra to the extracellular media. Indeed, within the simulation run (150 ns), a total of 9 K^+ ions translocated through the mutated VSDs. The channel subunits 1, 2 and 4 carried respectively six, two and one K^+ ions. No crossing event occurred through subunit 3, due its partial obstruction by a lipid tail during the simulation. In general, one expects that the

specific nature of the amino-acids lining up a hydrophilic pathway controls the molecular diffusion of ions within the gating pore. In the present case, due to the neutralization of the basic residues K5 and R6, the resulting omega pore contains an excess of negative charges (Glutamates). Accordingly, in agreement with experiments, the omega pores formed following the S4 basic residues mutations are likely to be selective to cations.

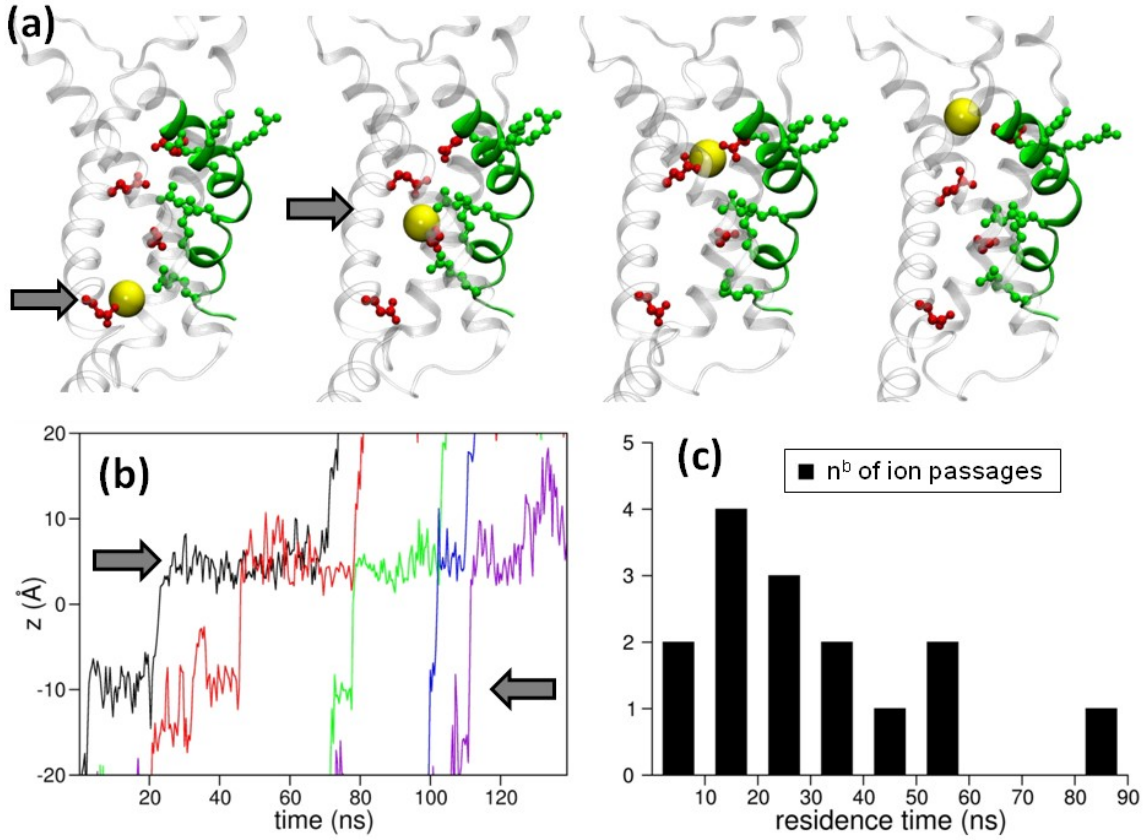

Figure. 4.19: (a) Snapshots from a single translocation event of a K+ ion (yellow) trough a Kv1.2 VSD captured in the MD simulation (Sim. #8) of the K5/R6 double mutant. (b) Trajectories of selected K+ translocations through a single VSD under depolarized potentials indicate the presence of long lived binding sites along the pathway. These sites, indicated by arrows, correspond to the location of the acidic residues E^{236}, D^{259}, and E^{226} as shown in (a). (c) Distribution of the residence times of K^+ ions inside the VS pores, during the translocation events estimated from the MD simulations. The intrinsic conductance of a mutated channel subject to a TM potential ΔV, giving a rough estimate of the leak current may be computed as $G_i = I_i / \Delta V$ *where* I_i *is the intrinsic gating pore current. The latter is a function of <dz/dt>, the average residence time of a translocating cation in the VSD, and of Lz, the length of the hydrophilic pore (~40 Å):* $I_i = \frac{q}{L_z}\frac{dz}{dt}$.

In the present study, despite the presence of chloride ions in the electrolyte baths, none translocated through the VSD during the simulation under TM potential, which suggests that the omega pores formed following the S4 basic residuesmutations are indeed selective to cations. This is in agreement with experiments (Gamal El-Din et al. 2010).

Furthermore, the negatively charged residues E^{183}, D^{259}, E^{226} and E^{236} lining the hydrophilic VS pore provide stable binding sites for diffusing K^+ ions (Fig. 4.19.a,b). Hence, translocation of cations within the mutated VSD is not a simple free diffusion in a hydrophilic pore but is rather stochastic, *i.e.* follows a jump diffusion model in which E^{236}, located at the inner entrance of the domain (z ~ -10 Å) constitutes the first binding site, and D^{259} (z ~ 7 Å) the second.

An additional simulation was performed at a hyperpolarized potential and showed that the mutated VSD can transport K^+ ions also at negative TM potentials (within a time scale too short to permit conformational rearrangements towards the β-state). Under these conditions, K^+ ions translocate from the extra to the intra-cellular media. No significant differences were noticed neither in the average number of ions transported per unit time nor in their residence time inside the VSD. The molecular pathway for K^+ ions translocation through the VSD was mainly reversed, *i.e.* the translocating ion first reached D^{259} before jumping to E^{236}. The intrinsic gating pore current estimated (cf. Fig. 4.20) from the cationic translocation events through the VSD of the double mutant (Fig. 4.20.c) is ~ 5.3 pA. The corresponding intrinsic conductance measured hence under the TM potential conditions considered here, *e.g.*, $U = \pm$ 600 mV, amounts to ~8.3 pS (~ $3\ 10^7$ ions/s).

The global conduction per gating pore of the mutated channel may only be estimated here from the total number of crossing events over the overall length of the simulation. The data at hand (15 crossing ions for the whole channel over ~310 ns) lead to an average conduction of ~$1.25\ 10^7$ ions/s per VSD at the electrolyte KCl salt concentration of 150 mM considered here. Extrapolating these "measured" omega currents to physiological TM potentials (~ 100 mV), and to low salt concentrations lead to leaks through the VSDs of the order of ~ 10^6 ions/s, over one order of magnitude below the alpha currents (~ 10^7 ions/s).

2.3.2 Conduction through the K5 open mutant and R1 closed mutant

When considering the K5 single mutant under depolarized potentials (Sim. #9), the hydrophilic pathway of one VSD allowed for translocation of a cation from the intracellular medium up to the residue D^{259} to which it remained bound for over 60 ns. The sampled trajectory shows that the pathway is not as highly permeable to cations as in the case of the K5/R6 mutant. This is in good agreement with Gamal El-Din et al. who find that in the activated state of Shaker channels, mutation of two residues is necessary to give rise to omega currents (Gamal El-Din et al. 2010).

For the closed channel, and during simulations lasting ~40 ns, two K^+ passages were witnessed through the VSD of subunit 1 in the R1 single mutant and no translocation occurred in the WT or in the R2 mutant.

2.4 Discussion – Relationship to diseases

Using the configurations of Kv1.2 determined in the first part of this work, we have studied the molecular level effect of selected mutations of S4 positively charged residues involved in genetic diseases. Specific mutations (that of R1 in the closed state and that of K5 in the open one) disrupt the VSD structure, open a hydrophilic pathway and when submitted to TM potential, lead to the appearance of leak "omega" currents. "Omega" currents have been recorded by electrophysiology measurements and were shown to be state dependent. We have here unveiled the the atomic level perturbation that occurs after the mutation of specific basic residues of S4. For the first time, we were able to show the leak at a molecular level. We propose here a cartoon model that summarizes our observations in the case of the Kv1.2 and extends them to other members of the large VGC family.

The results obtained may be summarized as follows (Fig. 4.20):

- At rest, VGCs are in a closed non-conducting conformation and S4 is in the so-called 'down' state. Within the VSD, the salt bridges that maintain the constriction between the intra- and extra-cellular water crevices involve the top S4 residues and only their mutation leads to omega currents (Fig. 4.20.a).
- Upon activation, *i.e.*, under depolarized TM potentials, S4 positive residues are dragged upwards (S4 moves to the 'up' state) and the VGCs adopt the open conformation. Within the VSD, bottom S4 basic residues become critical in maintaining the constriction (Tombola, Pathak, et al. 2005) (Nishizawa & Nishizawa 2008). Accordingly, mutations of the latter destabilize the VSDs and lead to omega currents (Fig. 4.20.b).
- Hence, mutations of the S4 basic residues give rise to state dependant omega currents. These results are consistent with experiments showing that (*i*) mutations (synthetic or genetic) of the S4 top basic residues of the Na^+ VGCs Nav1.2a (Sokolov et al. 2005) and Nav1.4 (Sokolov et al. 2007) and of *Shaker* channels (Tombola, Pathak, et al. 2005) lead to inward omega currents under hyperpolarized potentials and (*ii*) mutations of the S4 bottom basic residues of Nav1.2a (Sokolov et al. 2005) and Nav1.4 (Sokolov et al. 2008) lead to outward omega currents under depolarized potentials.

It is noteworthy that we have chosen to study the specific case of mutation of S4 basic residue. However, as can be gathered from the OMIM database, a large number of channelopathies result from a variety of other mutations. Almost all of these diseases (as varied as paramyotonia congenita, hyperkalemic periodic paralysis, erythromelalgia,

erythema, short and long QT syndromes to cite only a few...) have dominant inheritance and are caused by gain of-function mutations that result mostly in enhanced activation or impaired inactivation (both fast and slow) of VGCs. Such mutations can be found all along the VGC sequence, in both VSD and pore domain and in the inactivation gate. Therefore, it is not possible to propose a single molecular mechanism to explain the defect in ion channel function in all of these diseases.

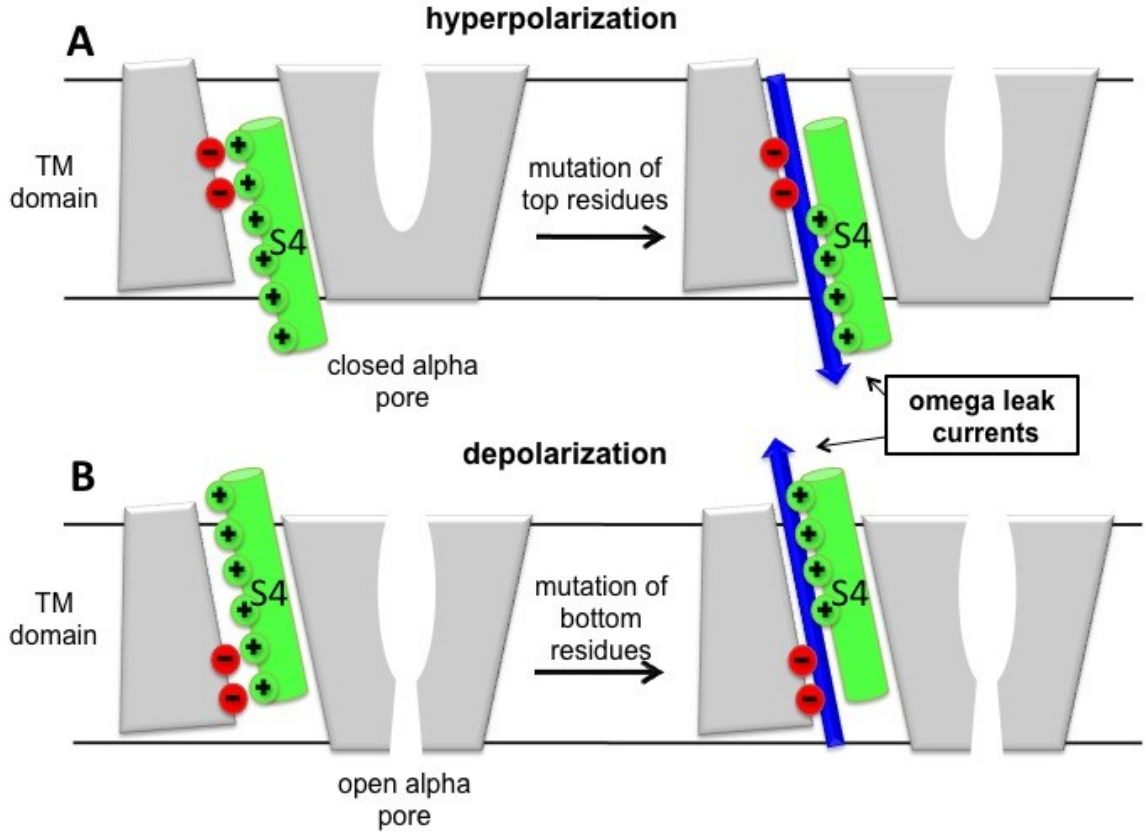

Figure. 4.20: (A) Under hyperpolarized potentials, the VGC is closed. Omega currents represent an inward cation leak (blue arrow). (B) Under depolarized potentials, the channel is open. Omega outward currents are a modulation of the alpha (central pore) current.

However, for the specific case of S4 basic residues mutations, a pattern emerges. Indeed, in VGCs, the positive residues of S4 are the main sensors of the TM voltage and are directly implicated in the conformational changes of the VSD, which control switching (gating) of the channels from open to closed conformations (Schoppa et al. 1992) (Seoh et al. 1996). Mutation of any S4 basic residue alters the sensitivity of the channels and modifies their gating kinetics as shown for several VGCs. The present work has: (*i*) identified the mutations that are critical for the stability of α and ε VSD conformation, and (*ii*) determined in which conformational state these mutations give rise to omega currents. Note that the mutations considered here involved neutralization of the S4 basic residues. The qualitative results summarized in Fig. 4.20 remain however relevant as experiments indicate that mutation of the S4 basic residues to any neutral residue has similar consequences on the VGC.

Under hyperpolarized TM potentials, omega currents affect directly the channel's function since they constitute a leak through a closed channel supposedly impermeable to ions. Quite interestingly, most mutations associated with genetic diseases *e.g.*, epilepsy, hypo- or hyper-kalemic periodic paralysis, or long QT syndrome fall in this category. Under depolarized TM potentials, VGCs are open and omega currents are a mere modulation of the main alpha current (the omega pore conductance is ~2 orders of magnitude lower than the alpha pore conductance (Sokolov et al. 2005) (Sokolov et al. 2007) (Sokolov et al. 2008). Such small conductance must however have a more dramatic consequence on VGCs that undergo N-type inactivation – *i.e.*, become non-conductive under extended depolarized potentials – as shown for Nav1.4, for which omega leak currents were implicated in NormoPP symptoms (Sokolov et al. 2008).

Owing to the structural similarity between the members of the large family of VGCs (Nav, Cav and Kv), mutations of key residues within their VSD are expected to result in similar effects to those characterized here for Kv1.2. However, precise knowledge of (*i*) the salt bridges network, and (*ii*) the specific S4 basic residue involved in the VSD constriction, (and hence an accurate model of the 3d structure) would be necessary to determine which specific mutation detected in a given channelopathy gives rise to omega currents.

Finally, although it is the easier to characterize using MD simulations, one should also note that the appearance of omega currents is most likely not the only effect of such S4 basic residues mutations. Indeed, mutating such charges probably results in alteration of the response of the VSD to TM voltage change, as manifested by shifts in G/V and Q/V curves and modified kinetics of ON and OFF currents (Miceli et al. 2008). To understand the molecular origin of such experimental observations, due to the long timescale over which such response occurs (see paragraph 1 of this chapter), classical MD simulations are not well adapted. It would therefore be of most interesting to characterize the free energy surface of activation/deactivation in the WT and mutant channels using special MD schemes such as metadynamics (Laio & Gervasio 2008) or adaptative biaising force (ABF) (Hénin & Chipot 2004), which would further enable to account for the electrophysiology results mentioned above.

3 Modulation by lipids

It has been shown recently that VGCs are unable to function in the absence of negatively charged particles in the headgroup of the lipids (Schmidt et al. 2006) (Zheng et al. 2011). The results presented in paragraph 1 of this chapter clearly show that the lipid phosphate PO_4^- groups are important for the function of the VSD since they provide counter-charges for the binding of S4 positively charged residues and thereby stabilize not only the activated and resting state of the VSD but also the intermediate kinetic states.

In most cells, VGCs are embedded in complex membranes made of a variety of lipids rather than in pure POPC bilayers, as we have used for our model membranes in parts 1 and 2 of this chapter. Particularly, these membranes are often asymmetrical: for example, sphingomyelin (SPGM) is found mainly in the outer leaflet of plasma cell membranes (Koval & Pagano 1991). It can represent as much as 50% of the lipids in certain tissues, though it is usually lower in concentration than phosphatidylcholine. In brain cell membranes, for instance, it makes up about 10% of the lipids. The brown spider *Loxosceles reclusa* takes advantage of this asymmetry as its venom contains an enzyme, sphingomyelinase D (SMase D), that catalyses a reaction in which the positively charged choline group of zwitterionic sphingomyelin is removed, yielding the negatively charged lipid ceramide-1-phosphate (POCP) (Fig. 4.21). This has the effect of favoring the activated conformation of the channels at TM potentials for which the Kv1.2 channels are usually in their resting state (Fig. 4.22) (Ramu et al. 2006). Another enzyme, sphyngomyelinase C (SMase C), cuts sphyngomyelin at the level of the bond between the phosphate group and the hydrophobic tails of the lipids, yielding a polar molecule, ceramide (POCR), that has no zwitterionic headgroup (Fig. 4.21). This has the opposite effect of stabilizing the resting state of the channel (Fig. 4.22) (Xu et al. 2008).

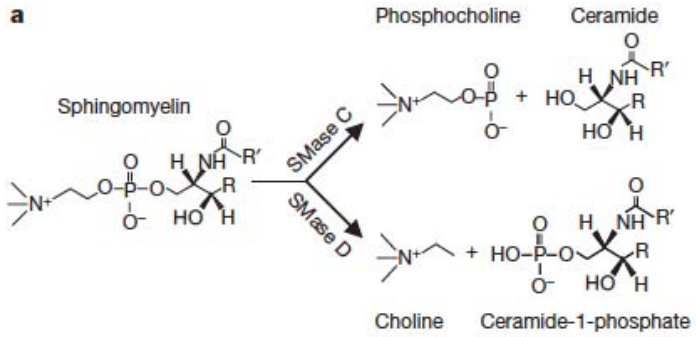

Figure 4.21: Action mechanism of sphyngomyelinase C and D on a sphygomyelin molecule. From (Xu et al. 2008).

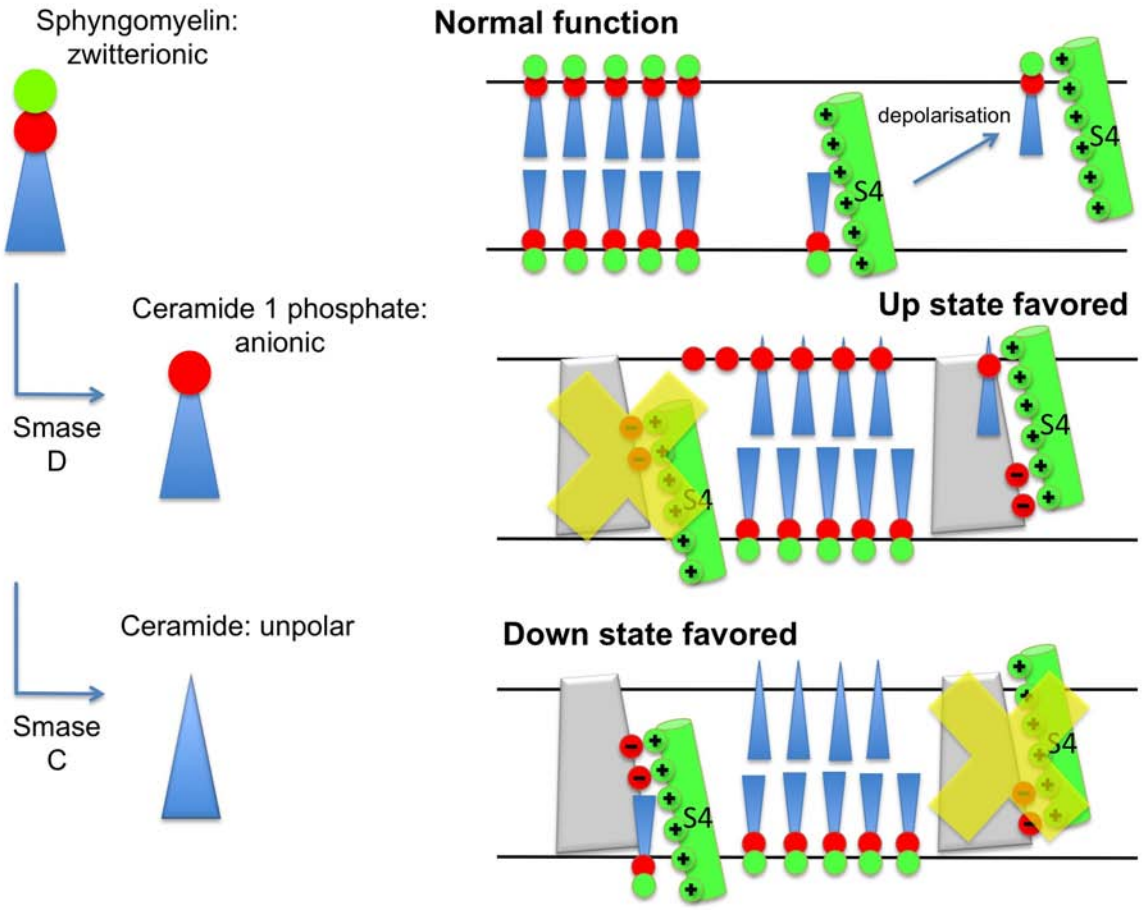

Figure 4.22: Scheme of the function of Smase C and D enzymes indicating the effect on channel conformational stability.

To explain the molecular level effect of such enzymatic reactions, two main hypotheses may be put forward: the TM potential changes when the lipid headgroup is altered, leading the channel to respond differently (manifested by a shift in the Q/V curves) and/or the local interactions between lipid headgroups of the products and S4 basic residues differ when changing the lipid headgroup.

To investigate this, we have studied the properties of the open (α), intermediate (γ) and closed (ε) conformations of the channels in asymmetric bilayer made of POPC in the inner leaflet and either SPGM, POCP or POCR in the outer (top) leaflet. To enhance the effect due to lipid headgroup removal, we have chosen asymmetrical bilayers with 100% SPGM, POCP or POCR in the top layer. This also ensures that these specific lipid headgroups will interact directly with the top S4 gating charges, in agreement with experimental hypotheses. Indeed, in real cells such as Xenopus oocytes, SPGM is thought to interact preferably with the Kv channel VSDs over other lipids such as POPC (Xu et al. 2008). Whereas the change in TM voltage is easy to monitor by evaluating the TM potential in the different asymmetric systems, the local interactions are more difficult to probe. To contribute to the evaluation of such properties, we have evaluated the gating charge associated to activation of the Kv1.2 in the different systems. This should give us access to the excess free energy associated to such conformational change in the varied environments. The present section summarizes our initial results. We first report our findings on the electrical properties of the bare solvated bilayers (without the channel embedded in them) and in a second part, of the different channel conformations in the lipids.

3.1 Computational details

We started by building three model asymmetrical bilayers: in each of them, the bottom layer is composed of POPC lipids whereas the top layer is made of sphyngomyelin, ceramide-1-phosphate or ceramide, all lipids having for simplicity palmitoyl-oleoyl lipid chains. We then equilibrated these lipid bilayers in a 150 mM NaCl solution. Next, we considered the Kv1.2 in the three conformations that represent the activated/open state (α state from section 1), the intermediate state (γ state) and the resting/closed state (ε state). We inserted each of these configurations in each of the three pre-equilibrated asymmetrical bilayers. To avoid close contact, we deleted all the lipid and water molecules that had at least one atom less than 2 Å away from the protein. We then solvated and ionized the entire system to a concentration of ~150 mM. The details of the different systems are reported in table 4.5.

The force field parameters we used are the same as above for the protein, water and ions (CHARMM27 with CMAP correction, TIP3P water). For POPC, we considered all atom lipids from the CHARMM32 force field. For the sphygomyelin, ceramide-1-phosphate and ceramide lipids, we have considered the force field proposed by Hyvonen et al. (Hyvönen & Kovanen 2003) to model the headgroups while keeping the tail parameters as those of POPC. Note that Hyvonen et al. are derived from CHARMM parameters. For ceramide-1-phosphate, we have cut the sphyngomyelin lipid after the phosphate group and taken the CHARMM

parameters of the phosphate to ensure proper charge of -1. For ceramide, we proceeded in the same way by removing the phosphate group and replacing it by a primary alcohol group from the classical CHARMM force field. Details for all these parameters can be found in the annex.

For the MD simulations, we used the same protocols as in the two previous studies. To equilibrate the systems, we proceeded in the following way: in the simple bilayer systems, we simply equilibrated the systems for ~10 ns, in the NPT ensemble at 300K and 1 atm, until reaching a stable lateral density. In the channel systems, we started by equilibrating the water and lipids by constraining the position of all the atoms of the channel (4 ns), we then let the side chains of the channel to relax (10 ns) before finally letting the complete system to relax (at least 20 ns). The rmsd from the initial structure of the channel calculated for the backbone atoms reached equilibrium values after ~25 ns.

To apply TM voltage to the systems, as in the previous paragraphs, we used the charge imbalance combined with the vacuum water interface scheme (see chapter 3, paragraph 3.2).

Table 4.5: Summary table of the asymmetrical bilayer systems

	Channel state	Lipid composition	Water molecules	Ions	Total atom Nb	Size (Å^3)
0.1	No	SPGM (49) POPC (49)	5 168	56 NaCl	28 895	53x56x94
0.2	No	POCP (49) POPC (49)	5 026	72 Na/23 Cl	27 570	57x48x96
0.3	No	POCR (49) POPC (49)	5 182	49 NaCl	27 845	55x52x96
1	Open	SPGM (319) POPC (331)	84 909	141 K/97 Cl	368 254	153x159x146
2	Open	POCP (297) POPC (318)	78 345	392 K/51 Cl	338 665	165x141x142
3	Open	POCR (320) POPC (330)	86 143	143 K/99 Cl	364 923	157x148x153
4	Interm.	SPGM (315) POPC (323)	85 106	142 K/98 Cl	367 227	150x152x156
5	Interm.	POCP (313) POPC (320)	75 374	534 K/177 Cl	332 192	157x142x155
6	Interm.	POCR (320) POPC (326)	84 482	141 K/97 Cl	359 400	152x146x158
7	Closed	SPGM (323) POPC (333)	97 757	159 K/115 Cl	407 650	153x151x171
8	Closed	POCP (306) POPC (316)	88 136	424 K/74 Cl	368 896	162x132x167
9	Closed	POCR (326) POPC (323)	84 506	141 K/97 Cl	359 760	155x143x158

3.2 Bare asymmetrical bilayers

We expect the electrical properties in asymmetrical systems to be particular: the difference in the lipid headgroup between the two leaflets of the bilayer should give rise to a global dipole and therefore to a TM potential at rest. Indeed, previous simulations of POPC/POPE (phosphatidyl-ethanolamine, a zwitterionic lipid) or POPC/POPS (phosphatidyl serine, a negatively charged lipid) asymmetric bilayers have shown that a non-zero TM potential exists, of same polarity for the two systems, and the magnitude of which was found to be of the order of ~200 mV (Gurtovenko & Vattulainen 2008).

To investigate the TM potential in the asymmetric systems described above, we have evaluated from the charge distributions the total electrostatic potential profiles along the normal to the bilayer (see chapter 3, paragraph 2.2), as well as the contributions from the different constituents of the system: lipids, water and ions (Fig. 4.23).

The electrostatic potential (EP) profile of the contributions of water, ions and lipids along the z axis are presented separately, together with the corresponding total EP profiles. In each system, in the lower leaflet (POPC), the EP is the same as in symmetric, pure POPC bilayers : the dipole due to the lipid headgroup is partly canceled out by the reorientation of water dipole and ion reorganization at the membrane/solution interface. The EP profile shows a presence of a dipole potential (potential difference between the center of the membrane and the middle of the bottom bath) amounting to ~1.0V.

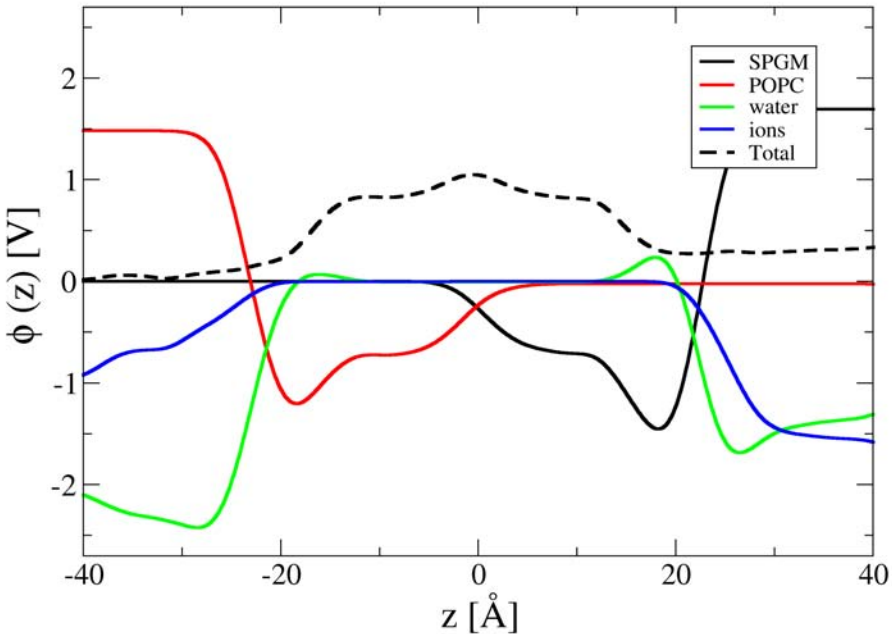

Figure 4.23: EP profiles along the normal to the bilayer in the sphyngomyelin asymmetrical systems. On the z axis, 0 is located at the center of the bilayer. In the top layer, SPGM is figured as a black line In the bottom layer, POPC is represented as red lines. The contribution from water is in green and that from ions in blue. The sum of all contributions is figured as thick dashed lines.

In the upper leaf on the other hand, the lipids give rise to very different profiles: SPGM, which is a zwitterionic lipid, has the same behavior as POPC. Starting from 0 at the center of the membrane, the contribution of the lipid to $\varphi(z)$ goes down to negative values at the lipid/water interface (~20-25Å) before rising back up to positive values. As in the case of POPC, the ions reorganize to counteract the zwitterionic dipole of the headgroups, along with water dipoles. When comparing to the bottom leaflet of POPC, a positive contribution of the water arises around 20Å, indicating that water at the interface is more organized, *i.e.* the dipoles are more polarized than in POPC (Fig. 4.23). The sum of these contributions leads to a dipole potential of ~0.8V, and an overall TM potential of ~0.2V, therefore with a possible implication for VGC function.

In POCP, because the lipid head group is negatively charged, the contribution of the ceramide-1-phosphate only gives rise to a huge positive potential. However, the excess of positive ions counterbalances this contribution and quite amazingly, when taken together with the contribution from water, the membrane potential for the upper leaflet amounts also to 0.8V, leading to a similar TM potential of ~0.2V (Fig. 4.24).

Finally, in POCR, the entire zwitterionic headgroup has been chopped off. Because of the lack of lipid dipoles at the interface, the contribution of the lipid only gives rise to a -2V potential, with a opposite polarity to the one in SPGM. Ion reorganization also tends to reduce this potential, *i.e.* displaying a positive contribution (Fig. 4.25). Against our expectations, however, when summing these contributions with the one from water, the TM potential amounts here also to ~0.2V.

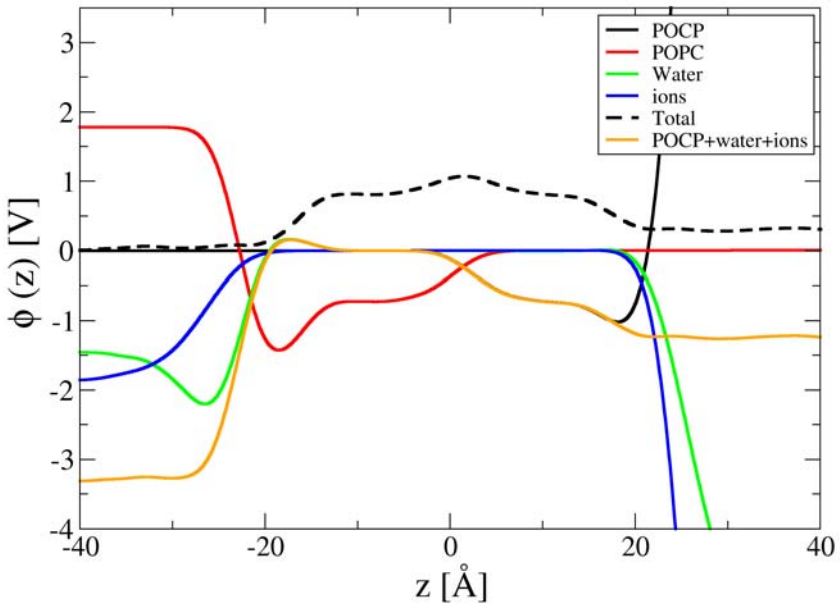

Figure 4.24: EP profiles along the normal to the bilayer in the ceramide-1-phosphate asymmetrical system. The color code is the same than above. Because the lipid is negatively charged, the potential profile of POCP reaches very high values. Similarly, the contribution due to ions accumulating at the interface reach very low ones. For clarity, we have therefore represented in orange the sum of these two contributions together with water, which converges to a finite value.

Changes in lipid headgroups modify the individual contributions of the lipid components to the total EP. However, contrary to what is expected, when considering sum of the individual contributions from lipid, water and ions, the global TM potential amounts to ~200 mV for all 3 systems.

No major difference in the electrostatic properties (*e.g.* in the TM potential) can be seen between the three asymmetric systems in which 100% of the lipids of the top leaflet are sphyngomyelin or one of its derivatives. We may therefore conclude from this that, most likely, the experimental modulation of Kv channel function (witnessed by a shift in G/V and Q/V curves) cannot be explained by change in TM potential after action of sphyngomyelinase.

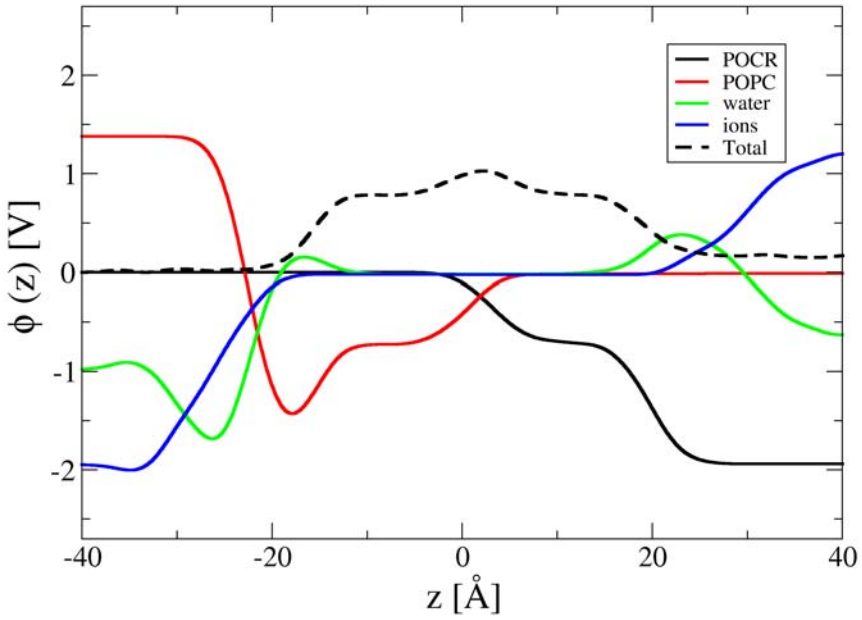

Figure 4.25: EP profiles along the normal to the bilayer in the ceramide asymmetrical system.The color scheme is the same than in Fig. 4.23.

3.3 Kv1.2 in asymmectrical bilayers

In order to investigate if the modulation of Kv function as probed experimentally can be linked to a change in specific channel/lipid interactions, we have considered systems in which Kv1.2 is embedded in the same bilayers.

3.3.1 Interaction of the basic S4 residues with the lipid headgroups

We considered the Kv1.2 channel in the three asymmetrical bilayers, SPGM/POPC,

POCP/POPC and POCR/POPC (Fig. 4.26). To look at specific interactions, we have chosen 3 conformations that represent the kinetically relevant states of the channel: activated/open state (α), one intermediate state (γ) and resting/closed state (ε). All these conformations come from the study presented in paragraph 1. We recall that the three conformations are stable on the tens of nanosecond time scale enabling the characterization of the salt bridge network within the VSD that packs the VSD structure together.

Following long simulations of the three systems (Table 4.5), in shyngomyelin, as expected from the zwitterionic nature of the lipid, the salt bridges network remains the same as in POPC.

- In α, R1 and R2 are found to be close to the lipid headgroups of the sphyngolmyelin, while the three others are engaged in salt bridges with the negatively charged residues of S1-S3 (Fig. 4.27.A).
- In γ, R2 has transferred to the first negatively charged residue while R1 remains in contact with the negative group of sphyngomyelin. R6, on the other hand has come in interaction with the PO_4^- groups of the POPC of the bottom layer (Fig. 4.27.B).
- In ε, R1 is in turn in transmembrane position, in interaction with the top negatively charged residues. R4, K5 and R6 are all in interaction with the POPC headgroups of the bottom layer (Fig. 4.27.C).

In the POCP/POPC system, *i.e.* after removing the choline groups from the top leaflet, the VSD is close to negatively charged headgroups of the top layer. As expected from the strongest interactions between R1/R2 and the negative headgroups of POCP, in α and γ, the salt bridge network does not reorganize. These conformations are most likely stabilized by such. In ε also, contrary to what was expected, the salt bridge network does not rearrange during the 30 ns simulations. Even if this conformation is probably less stable than in the SPGM configuration because of the excess of negative charges at the top membrane/solution interface, the energy barriers arising from the local electrostatic interactions seem to be to high to be overcome on this time scale.

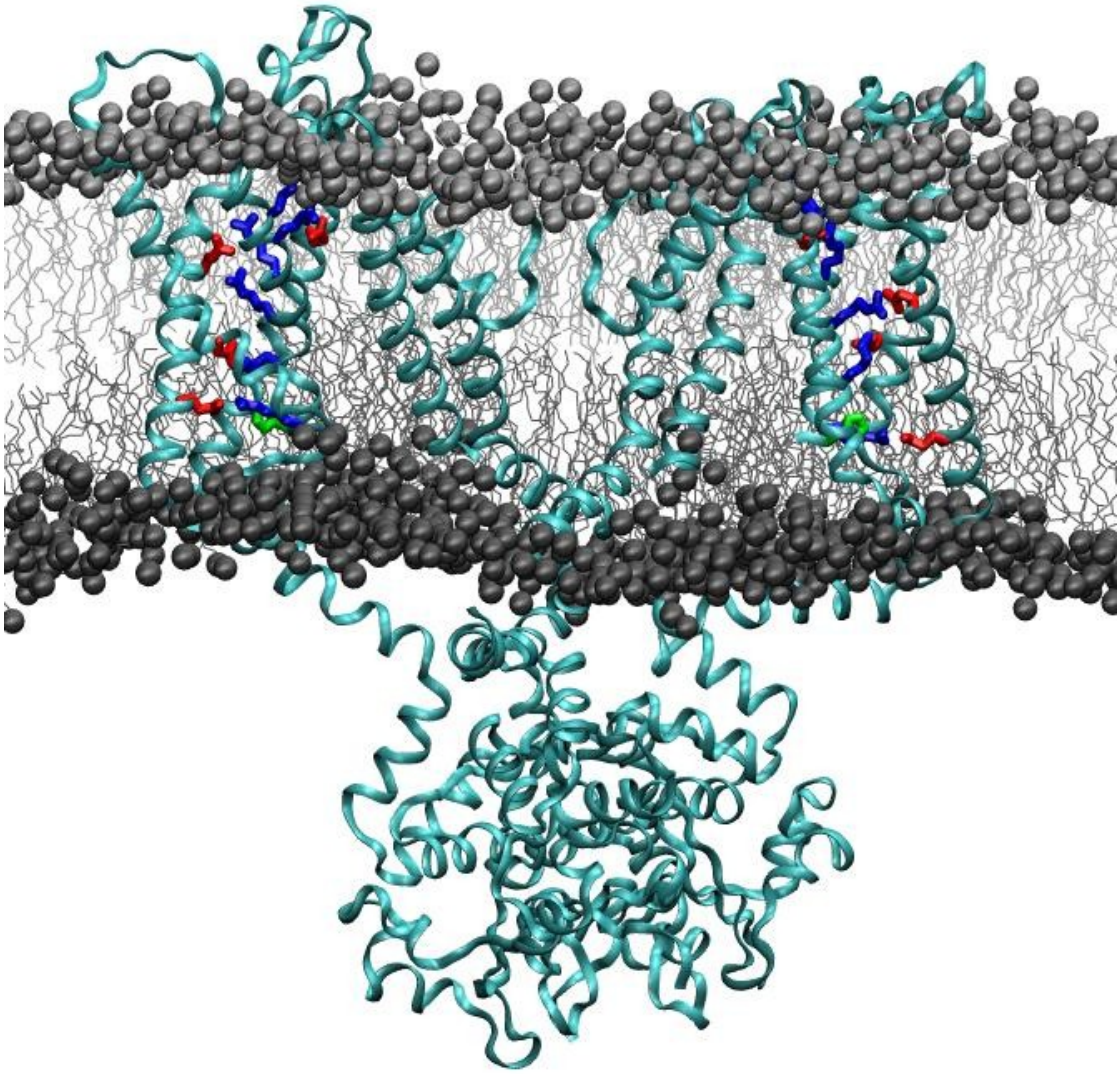

Figure 4.26: Simulation system containing the channel (cyan ribbons), inserted in a bilayer. The lipid head-groups are represented as van der waals spheres (light grey fro SPGM, and dark grey for POPC) whereas their tails are represented as lines. The charged residues within the VSD are represented as sticks (blue for positive charges, red for negative ones). The ionic solution is not represented for clarity.

Finally, POCR is neutral and does not bear any zwitterionic headgroup, and therefore does not have the negative group that is essential for VSD function. Interestingly, starting from the same configurations as in the other lipids, the salt bridge network remains stable in all three states within the ~60 ns run. In the open α state, especially, we expected the salt bridges to reorganize to let the top basic residues R1 and R2 come in contact with the first binding site within the VSD. However, no transfer of R1 and R2 occurs over.

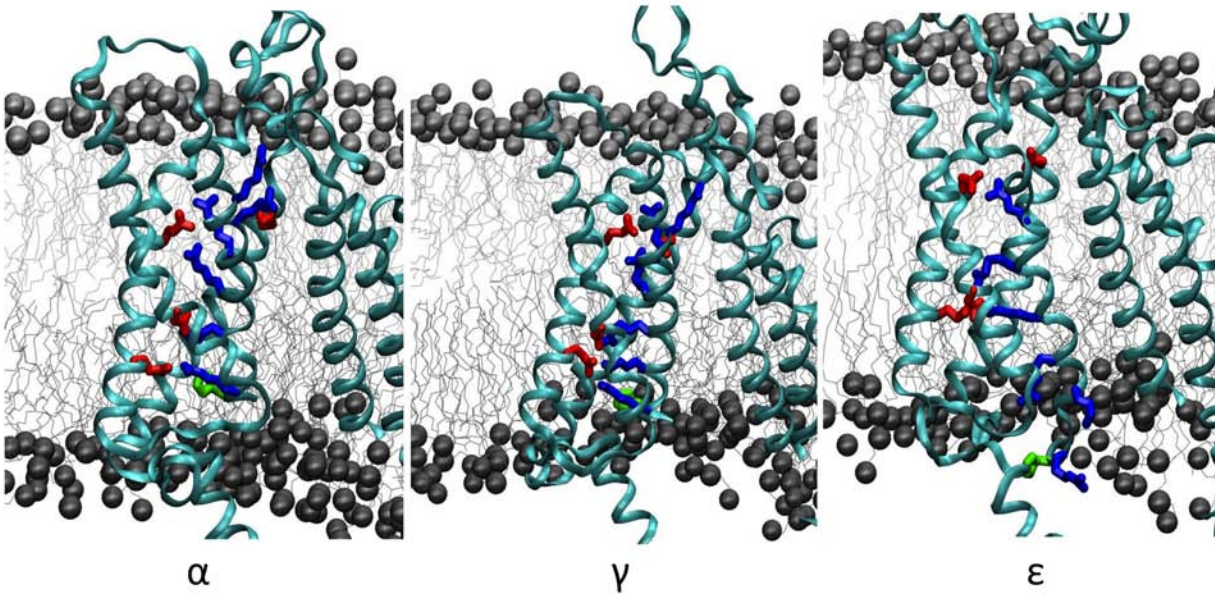

Figure 4.27: Representation of one of the four VSDs embedded in their membrane environment in the asymmetrical SPGM/POPC system. Three configurations are represented: α (A), γ (B) and ε (C). (A) S4 is in its 'up' position, with R1 and R2 in interaction with the top headgroups. (B) S4 is in its 'intermediate' position, with R1 in interaction with the top headgroups and R6 with the bottom ones. (C) S4 is in its 'down' position, with R4, K5 and R6 in interaction with the bottom headgroups of POPC. Colors and representations are the same than in Fig. 4.26.

Taken together, our calculations show that on the tens of nanosecond timescale, no dramatic reorganization of the salt bridge network within the VSD occurs when altering the lipid headgroups of the top leaflet. It seems that, even if the VSD is not in its most stable conformation, the electrostatic interactions within the salt bridge network in the VSD define free energy barriers that are too high to enable substantial reorganization on the tens of ns time scale.

3.3.2 Deactivation of the VSD in POCR

To study in more details the hypothesis of high energy barriers between different metastable VSD conformations, we have submitted the channel in the γ state in the POCR

asymmetrical system to a hyperpolarized potential of ~600 mV. In this system, because of the missing negatively charged groups in the top layer, the states in which there is a maximum of S4 basic residues in interaction with the bottom layer headgroups (*i.e.* resting state) are expected to be lower in energy. In principle, such conditions should favor the transitions to state ε.

In a POPC bilayer, as mentioned in part 1 of this chapter, the response of the channel to a 600 mV hyperpolarized potential takes place on the microsecond time scale, making it difficult to generate the entire deactivation. In POCR/POPC system, we expected this reorganization to happen on a shorter time scale.

We performed a simulation of the γ state in the POCR/POPC asymmetrical system (simulation #6) under these conditions for several tens of nanoseconds. Starting from state γ, the salt bridge network seemed very stable and no significant reorganization of the electrostatic interactions took place within the VSD. Even in the presence of a 600 mV TM voltage, the intermediate to closed transition was not favored after 120 ns, endorsing further the hypothesis of high energy barriers between VSD metastable conformations.

3.3.3 Gating charge calculations in the different lipids

The electrostatic environment (*i.e.* the membrane dipole potential) around the VSDs is similar in the three different bilayers, indicating that the driving force for VSD activation/deactivation is comparable in all three environments.

To confirm that this will not yield major changes in the gating charge values, we thus calculated the latter associated to the VSD deactivation during the α/γ transition, the γ/ε and finally the entire α/ε transition in the three different environments. For this purpose, we used the two different methods at hand: the direct measurement and the energetic formalism as presented in chapter 3, paragraph 4. The results are presented for a single VSD in table 4.5.

Table 4.5: Gating charges associated to the conformational changes in the three asymmetric bilayers. The first value is the one calculated by the direct measurement (chapter 3, paragraph 4.1), while the second one was calculated by the energetic formalism (chapter 3, paragraph 4.2). Values are estimated at ± 0.3e, mainly due to the 0.2 V error when estimating the TM volatge.

	***Q*(α/γ) [e]**	***Q*(γ/ε) [e]**	***Q*(α/ε) [e]**
SPGM	-1.0/-0.9	-2.5/-1.6	-3.5/-2.5
POCP	-0.9/-0.7	-2.2/-1.7	-3.1/-2.4
POCR	-1.0/-1.0	-2.4/-1.3	-3.4/-2.3

First, we note that the values seem quite different according to the method used to evaluate the gating charge, especially for the γ/ε transition. Since this difference does not seem to come from the contribution of the protein, we are still in the process of looking to identify its origin.

However, the results from either of the methods indicate that the gating charge values are similar for all transitions when changing the lipidic environment. Focusing most particularly on the values estimated by the direct measure (a method that introduces less approximation), we can see that during the α/γ transition, the per subunit gating charge amounts to ~1.0 e in the three lipids. During the γ/ε, Q amounts to 2.2 to 2.5e. Since the error was estimated to 0.3e, the difference between the different systems is not significant. In conclusion, not too surprisingly, following from the fact that the electrostatic environment is not drastically altered, the gating charge is the same in the three systems.

However, one should note here that we deliberately inserted the Kv1.2 channel in the three defined configurations in the various lipids and calculated the gating charge therefrom. If the free energy barriers between states are very different in the different lipids, one or more of these states may then never be reached. The resulting gating charge would then be completely different.

3.3.4 Discussion and model

We have studied the effect of altering the lipid headgroups on the activation/deactivation of the Kv1.2. Experimentally, activation is favored in the presence of POCP (negative headgroups in the outer layer) while deactivation is favored in the presence of POCR (no zwitterionic headgroup in the outer layer. Although one can expect effects on a molecular level, such as 1- in POCP, an electric field is expected to arise that would guide the S4 basic residues toward the active state and 2- in POCR, the lack of stabilizing interactions through the PO_4^- groups should stabilize the resting state of the VSD, it remained unclear from an energetic point of view if it is rather the thermodynamics (relative stability of states) or the kinetics (free energy barriers between states) of activation/deactivation that are modified when changing the lipid headgroup environment.

We have considered three asymmetrical bilayer environments: the lower leaflet is always constituted of POPC whereas the upper one is made of sphyngomylein or one of its derivatives (ceramide-1-phosphate, which has the choline group chopped off and is therefore negatively charged and ceramide, which is lacking the entire zwitterionic headgroup). Although experimentally, sphingomyelin and its derivatives form 10 to 50% of the lipid volumes, we have chosen to model 100% SPGM (or POCP, POCR) in the top bilayer to increase the effect associated to change in lipid headgroups.

The study of bare asymmetrical bilayers has shown that in each of these systems, the TM potential of amounts to ~200 mV, *i.e.* chopping off part or totality of the headgroup does not give rise to a change in the TM potential.

The study of Kv1.2 embedded in the bilayer has shown that changing the lipidic environment of the channel does not trigger a spontaneous reorganization of the salt bridge network within the VSD, even under a 600 mV hyperpolarized potnetial. Most importantly, the gating charge calculations give a direct estimate of the excess free energy due to applied

TM voltage (see chapter 3, paragraph 4.2). Here, the gating charge estimate is similar in the three asymmetric bilayers, indicating that the difference in the excess free energy due to the TM voltage (gating-charge related) during activation is equivalent in the different lipidic environments.

Altogether, these observations show that the experimental results can be explained most likely by kinetic considerations, *i.e.* by change in the height of the energy barriers between metastable states. However, to confirm this, it is necessary to conduct an altogether different study using free energy methods. This should enable to characterize the entire free energy surface associated to the deactivation of the Kv1.2 channel in the different asymmetric lipids.

References

Aggarwal, S.K. & MacKinnon, R., 1996. Contribution of the S4 segment to gating charge in the Shaker K+ channel. *Neuron*, 16(6), p.1169–1177.

Asamoah, O.K. et al., 2003. A fluorometric approach to local electric field measurements in a voltage-gated ion channel. *Neuron*, 37(1), p.85–98.

Baker, O. et al., 1998. Three transmembrane conformations and sequence-dependent displacement of the S4 domain in Shaker K channel gating. *Neuron*, 20(6), p.1283-1294.

Bao, H. et al., 1999. Voltage-insensitive gating after charge-neutralizing mutations in the S4 segment of Shaker channels. *The Journal of General Physiology*, 113(1), p.139 -151.

Bezanilla, F., 2005. The voltage-sensor structure in a voltage-gated channel. *Trends in biochemical sciences*, 30(4), p.166–168.

Bjelkmar, P. et al., 2009. Conformational changes and slow dynamics through microsecond polarized atomistic molecular simulation of an integral Kv1.2 ion channel *PLoS Computational Biology*, 5(2), p.e1000289.

Campos, F.V. et al., 2007. Two atomic constraints unambiguously position the S4 segment relative to S1 and S2 segments in the closed state of Shaker K channel. *Proceedings of the National Academy of Sciences*, 104(19), p.7904 -7909.

Catterall, W.A., 2010. Ion channel voltage sensors: structure, function, and pathophysiology. *Neuron*, 67(6), p.915-928.

Cha, A. et al., 1999. Atomic scale movement of the voltage-sensing region in a potassium channel measured via spectroscopy. *Nature*, 402(6763), p.809-813.

Chanda, B. et al., 2005. Gating charge displacement in voltage-gated ion channels involves limited transmembrane movement. *Nature*, 436(7052), p.852-856.

Clayton, G.M. et al., 2008. Structure of the transmembrane regions of a bacterial cyclic nucleotide-regulated channel. *Proceedings of the National Academy of Sciences*, 105(5), p.1511 -1515.

DeCaen, P.G. et al., 2009. Sequential formation of ion pairs during activation of a sodium channel voltage sensor. *Proceedings of the National Academy of Sciences*, 106(52), p.22498.

Delemotte, L. et al., 2008. Modeling membranes under a transmembrane potential. *The Journal of Physical Chemistry B*, 112(18), p.5547-5550.

Ding, S. & Horn, R., 2003. Effect of S6 tail mutations on charge movement in Shaker potassium channels. *Biophysical Journal*, 84(1), p.295-305.

Durell, S. R, Shrivastava, I.H. & Guy, H. R, 2004. Models of the structure and voltage-gating mechanism of the

Shaker K+ channel. *Biophysical journal*, 87(4), p.2116–2130.

Ferrer, T. et al., 2006. The S4-S5 linker directly couples voltage sensor movement to the activation gate in the Human Ether-a'-go-go-related gene (hERG) K+ channel. *The Journal of Biological Chemistry*, 281, p.12858-12864.

Freites, J. A, Tobias, D. J & White, S. H, 2006. A voltage-sensor water pore. *Biophysical journal*, 91(11), p.L90–L92.

Gamal El-Din, T.M. et al., 2010. Double gaps along Shaker S4 demonstrate omega currents at three different closed states. *Channels*, 4(2), p.93-100.

Glauner, K.S. et al., 1999. Spectroscopic mapping of voltage sensor movement in the Shaker potassium channel. *Nature*, 402(6763), p.813-817.

Grabe, M. et al., 2004. A quantitative assessment of models for voltage-dependent gating of ion channels. *Proceedings of the National Academy of Sciences of the United States of America*, 101(51), p.17640.

Gurtovenko, A.A. & Vattulainen, I., 2008. Membrane potential and electrostatics of phospholipid bilayers with asymmetric transmembrane distribution of anionic lipids. *The Journal of Physical Chemistry B*, 112(15), p.4629-4634.

Heinig, M. & Frishman, D., 2004. STRIDE: a web server for secondary structure assignment from known atomic coordinates of proteins. *Nucleic Acids Research*, 32(Web Server issue), p.W500-W502.

Hénin, J., Shinoda, W. & Klein, M.L., 2008. United-atom acyl chains for CHARMM phospholipids. *Journal of Physical Chemistry B,* 122, p.7008-7015

Hénin, J. & Chipot, C., 2004. Overcoming free energy barriers using unconstrained molecular dynamics simulations. *Journal of Physical Chemistry*, 121, p.2904-2914.

Hyvönen, M.T. & Kovanen, P.T., 2003. Molecular dynamics simulation of sphingomyelin bilayer. *Journal of Physical Chemistry B*, 107(34), p.9102-9108.

Jiang, Y. et al., 2003. The principle of gating charge movement in a voltage-dependent K+ channel. *Nature*, 423(6935), p.42–48.

Jogini, V. & Roux, B., 2007. Dynamics of the Kv1. 2 voltage-gated K+ channel in a membrane environment. *Biophysical journal*, 93(9), p.3070–3082.

Jurkat-Rott, K. et al., 2000. Voltage-sensor sodium channel mutations cause hypokalemic periodic paralysis type 2 by enhanced inactivation and reduced current. *Proceedings of the National Academy of Sciences*, 97(17), p.9549.

Kanevsky, M. & Aldrich, Richard W., 1999. Determinants of voltage-dependent gating and open-state stability in the S5 segment of Shaker potassium channels. *Journal of General Physiology*, 114(2), p.215 -242.

Khalili-Araghi, F. et al., 2010. Calculation of the gating charge for the Kv1.2 voltage-activated potassium channel. *Biophysical Journal*, 98(10), p.2189-2198.

Kosower, E.M., 1985. A structural and dynamic molecular model for the sodium channel of Electrophoruselectricus. *FEBS Letters*, 182(2), p.234-242.

Koval, M. & Pagano, R.E., 1991. Intracellular transport and metabolism of sphingomyelin. *Biochimica Et Biophysica Acta*, 1082(2), p.113-125.

Krepkiy, D. et al., 2009. Structure and hydration of membranes embedded with voltage-sensing domains. *Nature*, 462(7272), p.473-479.

Labro, A.J. et al., 2008. Kv channel gating requires a compatible S4-S5 linker and bottom part of S6, constrained by non-interacting residues. *The Journal of General Physiology*, 132(6), p.667 -680.

Laio, A. & Gervasio, F.L., 2008. Metadynamics: a method to simulate rare events and reconstruct the free energy in biophysics, chemistry and material science. *Reports on Progress in Physics*, 71, p.126601.

Loboda, A. & Armstrong, C.M., 2001. Resolving the gating charge movement associated with late transitions in K channel activation. *Biophysical Journal*, 81(2), p.905–916.

Long, S.B., Campbell, E.B. & MacKinnon, R., 2005. Crystal structure of a mammalian voltage-dependent Shaker family K+ channel. *Science*, 309(5736), p.897 -903.

Long, S.B. et al., 2007. Atomic structure of a voltage-dependent K+ channel in a lipid membrane-like environment. *Nature*, 450(7168), p.376-382.

Lu, Z., Klem, A.M. & Ramu, Y., 2002. Coupling between voltage sensors and activation gate in voltage-gated K+ channels. *The Journal of General Physiology*, 120(5), p.663 -676.

Matthes, D. & de Groot, B.L., 2009. Secondary structure propensities in peptide folding simulations: a systematic comparison of molecular mechanics interaction schemes. *Biophysical Journal*, 97(2), p.599-608.

Miceli, F. et al., 2008. Gating consequences of charge neutralization of arginine residues in the S4 segment of Kv7.2, an epilepsy-linked K+ channel subunit. *Biophysical Journal*, 95(5), p.2254-2264.

Nishizawa, M. & Nishizawa, K., 2009. Coupling of S4 helix translocation and S6 gating analyzed by molecular-dynamics simulations of mutated Kv channels. *Biophysical journal*, 97(1), p.90–100.

Nishizawa, M. & Nishizawa, K., 2008. Molecular dynamics simulation of Kv channel voltage sensor helix in a lipid membrane with applied electric field. *Biophysical journal*, 95(4), p.1729–1744.

Papazian, D.M. et al., 1995. Electrostatic interactions of S4 voltage sensor in shaker K+ channel. *Neuron*, 14(6), p.1293-1301.

Papazian, D.M. et al., 1991. Alteration of voltage-dependence of Shaker potassium channel by mutations in the S4 sequence. *Nature*, 349(6307), p.305-310.

Pathak, M.M. et al., 2007. Closing in on the resting state of the Shaker K+ channel. *Neuron*, 56(1), p.124-140.

Ramu, Y., Xu, Y. & Lu, Z., 2006. Enzymatic activation of voltage-gated potassium channels. *Nature*, 442(7103), p.696-699.

Ruta, V., Chen, J. & MacKinnon, R., 2005. Calibrated measurement of gating-charge arginine displacement in the kvap voltage-dependent K+ channel. *Cell*, 123(3), p.463-475.

Schmidt, D., Jiang, Q.-X. & MacKinnon, R., 2006. Phospholipids and the origin of cationic gating charges in voltage sensors. *Nature*, 444(7120), p.775-779.

Schoppa, N.E. & Sigworth, F. J., 1998. Activation of Shaker potassium channels: II. Kinetics of the V2 mutant channel. *The Journal of general physiology*, 111(2), p.295.

Schoppa, N. et al., 1992. The size of gating charge in wild-type and mutant Shaker potassium channels. *Science*, 255(5052), p.1712 -1715.

Schow, E.V. et al., 2010. Down-state model of the voltage-sensing domain of a potassium channel. *Biophysical Journal*, 98(12), p.2857-2866.

Schwaiger, C.S. et al., 2011. 310-helix conformation facilitates the transition of a voltage sensor S4 segment toward the down state. *Biophys J.*, 100(6), p.1446-1454.

Selvin, P.R., 2002. Principles and biophysical applications of lanthanide-based probes. *Annual Review of Biophysics and Biomolecular Structure*, 31, p. 275-301.

Seoh, S.A. et al., 1996. Voltage-sensing residues in the S2 and S4 segments of the Shaker K+ channel. *Neuron*, 16(6), p.1159–1167.

Shafrir, Y., Durell, Stewart R. & Guy, H. Robert, 2008. Models of voltage-dependent conformational changes in nachbac channels. *Biophysical Journal*, 95(8), p.3663-3676.

Sigg, D., Bezanilla, F. & Stefani, E., 2003. Fast gating in the Shaker K+ channel and the energy landscape of activation. *Proceedings of the National Academy of Sciences*, 100(13), p.7611.

Sigworth, F.J., 1994. Voltage gating of ion channels. *Quaterly Reviews in Biophysics.*, 27, p.1-40.

Sokolov, S., Scheuer, T. & Catterall, W.A., 2008. Depolarization-activated gating pore current conducted by mutant sodium channels in potassium-sensitive normokalemic periodic paralysis. *Proceedings of the National Academy of Sciences*, 105(50), p.19980 -19985.

Sokolov, S., Scheuer, T. & Catterall, W.A., 2007. Gating pore current in an inherited ion channelopathy. *Nature*, 446(7131), p.76-78.

Sokolov, S., Scheuer, T. & Catterall, W.A., 2005. Ion permeation through a voltage-sensitive gating pore in brain sodium channels having voltage sensor mutations. *Neuron*, 47(2), p.183-189.

Soldovieri, M. V. et al., 2007. Correlating the clinical and genetic features of benign familial neonatal seizures (BFNS) with the functional consequences of underlying mutations. *Channels*, 1, p.228-233.

Stevens, C.F., 1978. Interactions between intrinsic membrane protein and electric field. An approach to studying nerve excitability. *Biophysical Journal*, 22(2), p.295-306.

Struyk, A.F. & Cannon, S.C., 2007. A Na+ channel mutation linked to hypokalemic periodic paralysis exposes a proton-selective gating pore. *The Journal of General Physiology*, 130(1), p.11.

Tao, X. et al., 2010. A gating charge transfer center in voltage sensors. *Science*, 328(5974), p.67-73.

Tiwari-Woodruff, S.K., Lin, M.A., Schulteis, C.T., et al., 2000. Voltage-dependent structural interactions in the Shaker K+ channel. *The Journal of General Physiology*, 115(2), p.123.

Tombola, F., Pathak, M.M. & Isacoff, E.Y., 2006. How does voltage open an ion channel? *Annual Review of Cell and Developmental Biology*, 22(1), p.23-52.

Tombola, F., Pathak, M.M. & Isacoff, E.Y., 2005. Voltage-sensing arginines in a potassium channel permeate and occlude cation-selective pores. *Neuron*, 45(3), p.379-388.

Treptow, W. & Tarek, M., 2006. Environment of the gating charges in the Kv1. 2 Shaker potassium channel. *Biophysical journal*, 90(9), p.L64–L66.

Treptow, W. & Tarek, M., 2006. Molecular restraints in the permeation pathway of ion channels. *Biophysical Journal*, 91(3), p.L26-L28.

Treptow, W., Tarek, M. & Klein, M.L., 2009. Initial response of the potassium channel voltage sensor to a transmembrane potential. *Journal of the American Chemical Society*, 131(6), p.2107-2109.

Wu, D. et al., 2010. State-dependent electrostatic interactions of S4 arginines with E1 in S2 during Kv7.1 activation. *The Journal of General Physiology*, 135(6), p.595 -606.

Xu, Y., Ramu, Y. & Lu, Z., 2008. Removal of phospho-head groups of membrane lipids immobilizes voltage sensors of K+ channels. *Nature*, 451(7180), p.826-829.

Yarov-Yarovoy, V. Baker, D. & Catterall, W.A., 2006. Voltage sensor conformations in the open and closed states in rosetta structural models of K+ channels. *Proceedings of the National Academy of Sciences*, 103(19), p.7292 -7297.

Yoda, T., Sugita, Y. & Okamoto, Y., 2004. Secondary-structure preferences of force fields for proteins evaluated by generalized-ensemble simulations. *Chemical Physics*, 307(2-3), p.269-283.

Zagotta, W.N., Hoshi, T., Dittman, J., et al., 1994. Shaker potassium channel gating. II: Transitions in the activation pathway. *The Journal of General Physiology*, 103(2), p.279 -319.

Zagotta, W.N., Hoshi, T. & Aldrich, R.W., 1994. Shaker potassium channel gating. III: Evaluation of kinetic models for activation. *The Journal of general physiology*, 103(2), p.321.

Zhang, M. et al., 2005. Interactions between charged residues in the transmembrane segments of the voltage-sensing domain in the herg channel. *Journal of Membrane Biology*, 207(3), p.169-181.

Zheng, H. et al., 2011. Lipid-dependent gating of a voltage-gated potassium channel. *Nature Communications*, 2, p.250.

Zheng, J. & Sigworth, F.J., 1998. Intermediate conductances during deactivation of heteromultimeric Shaker potassium channels. *The Journal of General Physiology*, 112(4), p.457 -474.

Appendix 2

Table A.1 : Topology of the sphyngomyelin, ceramide-1-phosphate and ceramide headgroup in the CHARMM format

```
RESI SPGM           0.00
GROUP                 !            H15B
ATOM N NTL -0.60      !             |
ATOM C13 CTL5 -0.35   !       H15A-C15-H15C
ATOM H13A HL 0.25     !             |
ATOM H13B HL 0.25     !      H13B   |    H14A
ATOM H13C HL 0.25     !       |     |     |
ATOM C14 CTL5 -0.35   ! H13A-C13----N----C14-H14B (+)
ATOM H14A HL 0.25     !       |     |     |
ATOM H14B HL 0.25     !      H13C   |    H14C
ATOM H14C HL 0.25     !             |
ATOM C15 CTL5 -0.35   !             |
ATOM H15A HL 0.25     !             |
ATOM H15B HL 0.25     !             |
ATOM H15C HL 0.25     !             |
ATOM C12 CTL2 -0.10   !      H12A--C12---H12B
ATOM H12A HL 0.25     !             |
ATOM H12B HL 0.25     !             |
GROUP                 !
ATOM C11 CTL2 -0.08   !             |
ATOM H11A HAL2 0.09   !      H11A--C11---H11B
ATOM H11B HAL2 0.09   !             |
ATOM P PL 1.50        !        O13 O12
ATOM O13 O2L -0.80    !         \\ /
ATOM O14 O2L -0.80    !       (-) P
ATOM O11 OSL -0.55    !         // \
ATOM O12 OSL -0.55    !        O14 O11
ATOM C1 CTL2 -0.08    !             |
ATOM HA HAL2 0.09     !        HA---C1---HB
ATOM HB HAL2 0.09     !             |
GROUP                 !             |
ATOM C2 CTL1 0.02     !        HS---C2- - - - - - -
ATOM HS HAL1 0.09     !             |         |
ATOM N21 NH1 -0.50    !            N21-HN
ATOM HN HL 0.28       !        O22 |
ATOM C21 CL 0.55      !         \\ /          |
ATOM O22 OBL -0.54    !          C21
ATOM C22 CTL2 -0.08   !           |           |
ATOM H2R HAL2 0.09    !    H2R---C22---H2S
ATOM H2S HAL2 0.09    !           |           |
GROUP                 !
ATOM C3 CTL1 -0.04    !           |           |
ATOM HX HAL1 0.09     !                  HX---C3---O3--HO
ATOM O3 OHL -0.60     !           |           |
ATOM HO HOL 0.43      !                       |
ATOM C34 CEL1 -0.14   !                     C34---H4X
ATOM H4X HEL1 0.15    !           |          //
ATOM C35 CEL1 -0.14   !                    C35---H5X
ATOM H5X HEL1 0.15    !

...

!BONDING FROM PC
```

```
BOND N     C13       N     C14      N     C15     N     C12
BOND C13   H13A      C13   H13B     C13   H13C
BOND C14   H14A      C14   H14B     C14   H14C
BOND C15   H15A      C15   H15B     C15   H15C
BOND C12   H12A      C12   H12B     C12   C11
BOND C11   H11A      C11   H11B
BOND P     O12       P     O11      P     O14     P     O13
BOND O12   C11
BOND O11   C1

BOND C1    HA        C1    HB       C1    C2      C2    HS
BOND C2    N21
BOND N21   HN        N21   C21
DOUBLE O22 C21
BOND C21   C22       C22   H2R      C22   H2S


BOND C2    C3        C3    HX       C3    O3       O3    HO
BOND C3    C34       C34   H4X
DOUBLE C34   C35
BOND C35   H5X       C35   C36      C36   H6X      C36   H6Y

IMPR O22 N21 C22 C21
IMPR N21 C2  C21 HN
PATCHING FIRS NONE LAST NONE

RESI POCP         -1.00
GROUP                                  H1
ATOM P1   PL      1.50 !               |
ATOM O13  O2L    -0.82 !     (-) O3   O1
ATOM O14  O2L    -0.82 !           \ /
ATOM O11  OHL    -0.68 !           P1 (+)
ATOM O12  OSL    -0.62 !           / \
ATOM H1   HOL     0.34 !    (-) O4   O2
ATOM C1   CTL2   -0.08 !               |     alpha1
ATOM HA   HAL2    0.09 !        HA---C1---HB
ATOM HB   HAL2    0.09 !               |     theta1
GROUP                  !               |
ATOM C2 CTL1 0.02      !         HS---C2- - - - - - -
ATOM HS HAL1 0.09      !               |         |
ATOM N21 NH1 -0.50     !             N21-HN
ATOM HN HL 0.28        !         O22 |
ATOM C21 CL 0.55       !          \\ /          |
ATOM O22 OBL -0.54     !           C21
ATOM C22 CTL2 -0.08    !            |           |
ATOM H2R HAL2 0.09     !     H2R---C22---H2S
ATOM H2S HAL2 0.09     !            |           |
GROUP                  !
ATOM C3 CTL1 -0.04     !            |           |
ATOM HX HAL1 0.09      !                   HX---C3---O3--HO
ATOM O3 OHL -0.60      !            |           |
ATOM HO HOL 0.43       !                        |
ATOM C34 CEL1 -0.14    !                      C34---H4X
ATOM H4X HEL1 0.15     !            |          //
ATOM C35 CEL1 -0.14    !                     C35---H5X
ATOM H5X HEL1 0.15     !

...
```

```
!BONDING FROM PA
BOND P1    O11       P1    O12      P1    O13     P1    O14
BOND O11   H1        O12   C1

BOND C1    HA        C1    HB       C1    C2      C2    HS

BOND C2    N21
BOND N21   HN        N21   C21
DOUBLE O22 C21
BOND C21   C22       C22   H2R      C22   H2S


BOND C2    C3        C3    HX       C3    O3       O3    HO
BOND C3    C34       C34   H4X
DOUBLE C34   C35
BOND C35   H5X

...

IMPR O22 N21 C22 C21
IMPR N21 C2  C21 HN
PATCHING FIRS NONE LAST NONE



RESI POCR           0.00
GROUP                 !
ATOM HO1 H 0.43       !        HO1
ATOM O1 OH1 -0.66     !        |
ATOM C1 CT2 0.05      !        O1
ATOM H1R HA 0.09      !        |
ATOM H1S HA 0.09      ! H1R ---C1---H1S
GROUP                 !             |
ATOM C2 CTL1 0.02     !        HS---C2- - - - - - -
ATOM HS HAL1 0.09     !             |         |
ATOM N21 NH1 -0.50    !            N21-HN
ATOM HN HL 0.28       !        O22 |
ATOM C21 CL 0.55      !         \\ /          |
ATOM O22 OBL -0.54    !          C21
ATOM C22 CTL2 -0.08   !           |           |
ATOM H2R HAL2 0.09    !    H2R---C22---H2S
ATOM H2S HAL2 0.09    !           |           |
GROUP                 !
ATOM C3 CTL1 -0.04    !           |           |
ATOM HX HAL1 0.09     !                 HX---C3---O3--HO
ATOM O3 OHL -0.60     !           |           |
ATOM HO HOL 0.43      !                       |
ATOM C34 CEL1 -0.14   !                    C34---H4X
ATOM H4X HEL1 0.15    !           |        //
ATOM C35 CEL1 -0.14   !                   C35---H5X
ATOM H5X HEL1 0.15    !

...

!BONDING FROM PA

BOND HO1 O1 O1 C1
BOND H1R C1 H1S C1 C1 C2
BOND HS  C2 C2 N21 N21 HN
```

```
BOND N21 C21

DOUBLE O22 C21
BOND C21 C22
BOND H2R C22 H2S C22

BOND C2    C3        C3    HX       C3    O3       O3    HO
BOND C3    C34       C34   H4X
DOUBLE C34   C35
BOND C35   H5X

...

IMPR O22 N21 C22 C21
IMPR N21 C2  C21 HN
PATCHING FIRS NONE LAST NONE
```

Table A.2 Bonded and Lennard-Jones parameters of sphyngomyelin, ceramide-1-phosphate and ceramide in the CHARMM format.

```
BONDS
!
!V(bond) = Kb(b - b0)**2
!
!Kb: kcal/mole/A**2
!b0: A
!
!atom type Kb          b0
!
NH1   CL    370.000     1.3450  ! from protein NH1 C
NH1   CTL1  320.000     1.4300  ! from protein NH1 CT1
NH1   HL    440.000     0.9970  ! from protein NH1 H
CTL1  CEL1  365.000     1.502

ANGLES
!
!V(angle) = Ktheta(Theta - Theta0)**2
!
!V(Urey-Bradley) = Kub(S - S0)**2
!
!Ktheta: kcal/mole/rad**2
!Theta0: degrees
!Kub: kcal/mole/A**2 (Urey-Bradley)
!S0: A
!
!atom types     Ktheta    Theta0   Kub     S0
CTL1 NH1  CL     50.0      120.00 ! from protein CT1 NH1 C
HL   NH1  CL     34.0      123.00 ! from protein H NH1 C
HL   NH1  CTL1   35.0      117.00 ! from protein H NH1 CT1
NH1  CL   CTL2   80.000    116.5000 ! from protein NH1 C CT2
OBL  CL   NH1    80.0      122.5 ! from protein O C NH1
CTL2 CTL1 NH1    70.0      113.5 ! from protein NH1 CT1 CT2
HAL1 CTL1 NH1    48.0      108.0 ! from protein NH1 CT1 HB
NH1  CTL1 CTL1   70.0      113.5 ! from protein NH1 CT1 CT1
CTL1 CTL1 OHL    75.700    110.10
CTL1 CTL1 CEL1   32.00     112.20
HAL1 CTL1 CEL1   45.00     111.50
```

```
OHL  CTL1 CEL1   75.700    110.10
CTL1 CEL1 HEL1   40.00     116.00
CTL1 CEL1 CEL1   48.00     123.50

DIHEDRALS
!
!V(dihedral) = Kchi(1 + cos(n(chi) - delta))
!
!Kchi: kcal/mole
!n: multiplicity
!delta: degrees
!
!atom types             Kchi    n   delta
!
X    CTL2 CEL1 X           1.2     3   180.0
CTL2 CEL1 CEL1 CTL2        0.36    1     0.0
CTL2 CEL1 CEL1 CTL2        3.55    2   180.0
HEL1 CEL1 CEL1 CTL2        3.45    2   180.0
X    CEL1 CEL1 X           3.55    2   180.0
CTL2 X    X    CEL1       70.0     0     0.0
CEL1 X    X    CEL1      150.0     0     0.0
HEL1 X    X    CEL1       75.0     0     0.0
HAL2 X    X    CEL1       75.0     0     0.0
CL   CTL1 NH1  CL          0.2     1   180.0
CL   CTL2 NH1  CL          0.2     1   180.0
CTL1 CL   NH1  CTL1        1.6     1     0.0
CTL1 CL   NH1  CTL1        2.5     2   180.0
CTL1 CTL1 NH1  CTL1        1.8     1     0.0
CTL2 CL   NH1  CTL1        1.6     1     0.0
CTL2 CL   NH1  CTL1        2.5     2   180.0
CTL2 CL   NH1  CTL2        1.6     1     0.0
CTL2 CL   NH1  CTL2        2.5     2   180.0
CTL2 CTL1 NH1  CL          1.8     1     0.0
CTL2 NH1  CL   CTL1        1.6     1     0.0
CTL2 NH1  CL   CTL1        2.5     2   180.0
HL   NH1  CL   CTL1        2.5     2   180.0
HL   NH1  CL   CTL2        2.5     2   180.0
HL   NH1  CTL1 CTL1        0.0     1     0.0
HAL1 CTL2 NH1  CL          0.0     3     0.0
HAL1 CTL2 NH1  HL          0.0     3     0.0
HAL2 CTL2 NH1  CL          0.0     3     0.0
HAL2 CTL2 NH1  HL          0.0     3     0.0
NH1  CL   CTL2 CTL2        0.0     1     0.0
OBL  CL   NH1  CTL1        2.5     2   180.0
OBL  CL   NH1  HL          2.5     2   180.0
CTL2 CTL1 NH1  HL          0.0     1     0.0
CTL1 NH1  CL   OBL         2.5     2   180.0
CTL1 CTL1 CEL1 HEL1        0.12    3     0.00
CTL1 CTL1 CEL1 CEL1        0.4     3     0.00
HAL1 CTL1 NH1  HL          0.0     3     0.00
HAL1 CTL1 NH1  CL          0.0     3     0.00
CL   NH1  CTL1 CTL1        1.8     1     0.0
HAL1 CTL1 CEL1 HEL1        0.87    3    0.00
HAL1 CTL1 CEL1 CEL1        0.12    3    0.00
OHL  CTL1 CEL1 HEL1        0.87    3    0.00

IMPROPER
!
!V(improper) = Kpsi(psi - psi0)**2
```

```
!
!Kpsi: kcal/mole/rad**2
!psi0: degrees
!note that the second column of numbers (0) is ignored
!
!atom types           Kpsi                   psi0
!
!lipid section
OBL  X    X    CL         100.00    0     0.00 ! acetic acid
HEL2 HEL2 CEL2 CEL2         3.00    0     0.00 ! ethene, yin,adm jr., 12/95
OCL  X    X    CL          96.00    0     0.00 ! acetate
OCL  X    X    CCL         96.00    0     0.00 ! for POPS


NONBONDED nbxmod  5 atom cdiel shift vatom vdistance vswitch -
cutnb 14.0 ctofnb 12.0 ctonnb 10.0 eps 1.0 e14fac 1.0 wmin 1.5
               !adm jr., 5/08/91, suggested cutoff scheme
!
!V(Lennard-Jones) = Eps,i,j[(Rmin,i,j/ri,j)**12 - 2(Rmin,i,j/ri,j)**6]
!
!epsilon: kcal/mole, Eps,i,j = sqrt(eps,i * eps,j)
!Rmin/2: A, Rmin,i,j = Rmin/2,i + Rmin/2,j
!
!atom  ignored    epsilon      Rmin/2   ignored   eps,1-4       Rmin/2,1-4
!
HOL      0.0       -0.046     0.2245
OBL      0.0       -0.12      1.70 0.0 -0.12 1.4
OCL      0.0       -0.12      1.70
OHL      0.0       -0.1521    1.77
OSL      0.0       -0.1521    1.77
NTL      0.0       -0.20      1.85 ! as all other nitrogens
NH1      0.0       -0.20      1.85 0.0 -0.20 1.55
```

5- ONGOING WORK

"Enjoyment is not a goal, it is a
feeling that accompanies
important ongoing activity"
-Paul Goodman

Enfin, souhaitant étendre les résultats du chapitre précédent à d'autres membres de la famille des canaux ioniques qui ont une fonction biologique importante nous avons entrepris une étude de plusieurs membres de la famille de Kv7. Ceux-ci jouent un rôle physiologique important puisque ces cinq membres, les Kv7.1, Kv7.2, Kv7.3, Kv7.4 and Kv7.5 se retrouvent dans le cœur, le cerveau, les muscles, l'estomac, l'oreille interne... Ils sont donc très étudiés comme cibles potentielles pour traiter des maladies qui proviennent de l'altération de l'excitabilité de la membrane.

De la même manière que les autres canaux Kv, ces canaux Kv7 sont des tétramères de six hélices transmembranaires. S5-S6 forment le pore tandis que S1-S4 froment le domaine sensible à la tension. Par rapport au Kv1.2, S4 contient un nombre réduit de résidus chargés positivement. Dans Kv7.2 et Kv7.4, R3 est remplacée par une glutamine, neutre et S4 porte donc 5 arginines en tout. Dans Kv7.5, en plus de cette mutation, la lysine en position 5 est remplacée par une histidine, portant le nombre total de charges de S4 à 4. Les autres résidus chargés du domaine sensible à la tension sont conservés, ainsi que la phenylalanine de S2 qui est impliquée dans le centre catalytique. Dû à ce nombre réduit de charges positives, les courants de « gating » sont plus petits dans les Kv7 et la charge de « gating » n'a pas pu être mesurée à ce jour.

La mutation de résidus chargés de S4 donne lieu a des maladies génétiques dans deux membres de la famille des Kv7. Ainsi, la mutation de R2 dans Kv7.1 donne lieu a l'apparition du syndrome du QT long du cœur tandis que la mutation de R4 dans Kv7.2 fait apparaître différentes maladies neurologiques telles que des attaques bénignes familiales néonatales ou encore une forme de surdité progressive. Nos collaborateur italiens (groupe du Pr. Taglialatela) ont pu enregistrer des courants de fuite « oméga » dans les mutants R4 du Kv7.4, qui sont très proches en séquence et en structure du Kv7.2. Il semble donc plausible que les maladie génétiques du Kv7.2 proviennent de ces courants de fuite.

Ainsi, nous avons construit des modèles moléculaires du domaine sensible à la tension des Kv7.1, Kv7.2 et Kv7.4 dans leurs conformations ouverte et fermée qui sont en accord avec ceux du Kv1.2. Après équilibration, le réseau de ponts salins dans les domaines sensibles à la tension a subi un réarrangement consécutif à la modification de la séquence de S4. Nous avons ensuite débuté l'étude de leurs propriétés électrique : leur charge de « gating » mesurée in silico est de magnitude réduite par rapport au Kv1.2 (~9e pour le Kv7.4 et ~6e pour le Kv7.1) en accord avec le nombre réduit de résidus basiques sur S4. Nous avons également entamé l'étude de l'effet de mutations de résidus basiques de S4 qui pourraient donner lieu à l'apparition de courant « oméga » dans le domaine sensible à la tension. Alors que nous n'avons à ce jour pas pu encore observer ce type de phénomène, la comparaison de nos résultats avec les données expérimentales est aujourd'hui en cours.

The voltage-gated potassium channel Kv7 family, which is encoded by the KCNQ genes, has an important physiological role, as its five members Kv7.1, Kv7.2, Kv7.3, Kv7.4 and Kv7.5 can be found in the heart, brain, muscles, stomach, inner ear and others… As such, they have been more and more studied as potential targets to treat diseases resulting in the alteration of membrane excitability (Miceli, Soldovieri, Martire, et al. 2008). Furthermore, four out of the the five members of this family have so far been found to be implicated in channelopathies, leading to long QT syndrome, neonatal epilepsy, neuromyotonia… (Maljevic et al. 2010).

As all other Kv channels, the channels pertaining to this family are tetramers of 6 TM segments in which S1-S4 constitute the VSD and S5-S6 making up the pore domain. In Kv7.1, the S4 segments contain each 4 basic residues (Fig. 5.1) which is the lowest number found in the Kv family. Sequence alignment of this channel with the Kv1.2, shows that R3 is replaced by a glutamine and K5 by a histidine, leaving only four arginines, R1, R2, R4 and R6. In Kv7.2 and Kv7.4 on the other hand five basic residues are present: R1, R2, R4, R5 and R6. Compared to the Kv1.2 sequence, only the third residue is replaced by a glutamine. One should also note the presence of an acidic residue (aspartic acid, named hereafter D^{S4}) at the bottom of S4, just before R6, that is characteristic to the Kv7 family.

Concerning the other TM segments of the VSD, the four negatively charged residues of S1, S2 and S3 are conserved within the Kv7s. As in Kv1.2, S1 contains an glutamic acid, S2 two glutamic acids and S3 and aspartic acid. The Phenylalanine residue in S2 that is thought to be implicated in the gating charge transfer (Tao et al. 2010) is also present as in all other members of the Kv family.

Kv1.2	287-AMSL	AILRVIRLVRVFRIFKLSRH	SKGLQ
Kv7.1	221-VFAT	SALRGIRFLQILRMLHVDRQ	GGTWR
Kv7.2	191-VFAT	SALRSLRFLQILRMIRMDRR	GGTWK
Kv7.4	197-IFAT	SALRSMRFLQILRMVRMDRR	GGTWK

Figure 5.1: Sequence of the S4 helix in the Kv7.1, Kv7.2 and Kv7.4 channel. Kv7.1 contains four basic residues, R1 (R228), R2 (R230), R4 (R236) and R6 (R242). Kv7.2 and Kv7.4 are more similar in sequence: they contain five basic residues R1, R2, R4, R5 and R6 (R198, R201, R207, R210 and R213 in the Kv7.2 numbering scheme and R204, R207, R213, R216 and R219 in the Kv7.4 numbering scheme). Note the presence of a glutamic acid residue (D^{S4}) at the bottom of S4 that is characteristic of the Kv7 family.

Due to the low number of basic residues on S4, gating currents are smaller than in the Kv1 family and the VSD movement are particularly slow (Wu, Delaloye, et al. 2010), leading to technical difficulties when conducting electrophysiology experiments. None the less, these gating currents were successfully measured in two members of the family: Kv7.4 and Kv7.5 (Miceli et al. 2009). The single channel gating charge, on the other hand, was never measured due to difficulties to count precisely Kv7 channels in the plasma membrane.

From a medical point of view, two members of the family, the Kv7.1 and the Kv7.2 were

found to be affected by mutations in the S4 region, and most particularly at the level of the basic residues. In Kv7.1, which is a channel that is found mainly in the heart, Lupoglazoff et al reported that the mutation of R2 (R^{231}) into cysteine led to Long QT syndrome of type 1 and to Fetal brachycardia (Lupoglazoff et al. 2003). The mutation of the top negative residue of S2, $E^{160}K$ (E2K), was also shown to lead to long QT syndrome (Splawski et al. 2000). In Kv7.2, a brain channel, mutation of R2 or R4 (R^{207} and R^{214}), leads to Benign Neonatal Familial Seizures (BNFS), myokymia and Peripheral Nerve Hyperexcitability (PNH) (Dedek et al. 2001) (Castaldo et al. 2002) (Wuttke et al. 2007).

Electrophysiology measurements of S4 mutants of the Kv7.2 channel were recently reported (Miceli, Soldovieri, Hernandez, et al. 2008). All the mutations of basic residues modify the G/V relationship, indicating that each of the S4 basic residue is important for the voltage-dependent gating. Mutation of R2 (R^{201}), especially, yields channels that "behave as K^+-selective leak channels that are largely open at all test potentials". Also, mutation of R4 (R^{207}) to tryptophane induces a larger change in the G/V curve than mutation to glutamine, probably because of its necessary translocation through the gating charge transfer center during activation. In Kv7.4, recent experiments have shown that the mutation of R4 into glutamine or tryptophane causes a G/V right-shift associated to slower activation/deactivation current kinetics. Interestingly, upon pore current blockade, in these mutants causing PNH, a persistent "omega" current was recorded in the active state of the VSD. The authors hypothesize that the mutations of R4 cause a persistent leak current responsible for the PNH condition (Miceli et al. 2011).

Homology models of the Kv7.1 channel have already been proposed mostly by Sanders and co-workers (Smith et al. 2007). The open state model was built on the basis of the open Kv1.2 X-ray structure whereas the closed state model is based on the closed state of the same Kv1.2 model proposed by Yarov-Yarovoy et al (Yarov-Yarovoy et al. 2006). They further proposed models of the interaction between Kv7.1 and KCNE1 (Kang et al. 2008) (Van Horn et al. 2011).

In this chapter, we present the preliminary results of a study of the molecular level properties of members of the Kv7 family. For this purpose, we have built a homology model of the Kv7.1, Kv7.2 and Kv7.4 using activated and resting Kv1.2 conformations as templates. After relaxing the channels in their membrane environment using molecular dynamics simulations, we focused on the the structure of the VSDs. Most particularly, we compared them with Kv1.2 VSDs and examined the rearrangement of the salt bridge networks within these VSDs that lack some of S4 basic residues with respect to the Kv1.2. We then proceeded to estimate the gating charge and found that these are are much smaller than for the Kv1.2 channel. Using the free energy formalism described earlier, we identified the molecular components that contribute the most to the gating charge and analyzed the effect of the lack of some of the S4 basic residues on this quantity. These results will be described in details below. In the final section of this chapter, we will present the preliminary results concerning the molecular level effect of the mutation of the Kv7.1 and Kv7.4 S4 basic residues incriminated in genetic diseases.

1 Model of the Kv7 channels in the activated and resting states

As a starting point for the molecular dynamics study, we have built homology models of chosen Kv7 family members using the activated (α) state and resting (ε) state of Kv1.2 models previously determined as templates. We first present the multiple sequence alignment of Kv7.1, Kv7.2 and Kv7.4 with Kv1.2. We then describe the 3D atomistic models of the channels produced by comparative modeling and subsequent equilibration in their lipidic environment using MD simulations.

1.1 Sequence alignment

We performed a multiple sequence alignment of the Kv7 family members of interest with all the identified homologs in the sequence database (FASTA search) using clustalW (Larkin et al. 2007). We chose the Gonnet substitution matrix, a gap penalty of 10 for the first residue in a gap and a 0.2 gap penalty for each additional gap residue. Trying other exchange matrices (Blosum, PAM) and varying the gaps penalty values did not alter substantially the alignments in the conserved TM segments and pore regions. After this automatic multiple alignment procedure, we extracted the alignment of Kv1.2 with Kv7.1, Kv7.2 and Kv7.4.

The pore domain is correctly aligned, probably due to the high sequence similarity (~38%). We checked especially that the selectivity filter, *i.e.* the signature sequence TXGYG (X being a hydrophobic residue), and the proline residue responsible for the kink in the S6 helix were well aligned (Fig. 5.2).

The alignment of the VSD domains, on the other hand, was not as successful. In the S1-S4 region, the sequence similarity falls down to ~17%, which is within the bulk of bad quality alignments. However, we know that stability and function of the VSD is governed by the electrostatic interactions and that the charged residues (positive on S4 and negative on the other segments) are conserved in all Kv channels. In S2 (E2 and E3), S3 (D4) and S4 (R1, R2, R4, (R5) and R6), the charged residues were well aligned in all four sequences. In S1, on the other hand, the glutamic acid at the top (E1) was not aligned. We therefore manually edited the alignment to make this residue match in the four sequences. This meant sliding the Kv7 sequence by 2 (for Kv7.2 and Kv7.4) or 3 residues (for Kv7.1). It is rather interesting to note that in regions other than S1, our alignment of Kv7.1 with Kv1.2 is close to the one proposed elsewhere (Smith et al. 2007). In S1, on the other hand, Smith et al. chose the “automatic” alignment, that yields a higher score by aligning the hydrophobic residues. This discrepancy is discussed in paragraph 5. The final alignment is reported in figure 5.2.

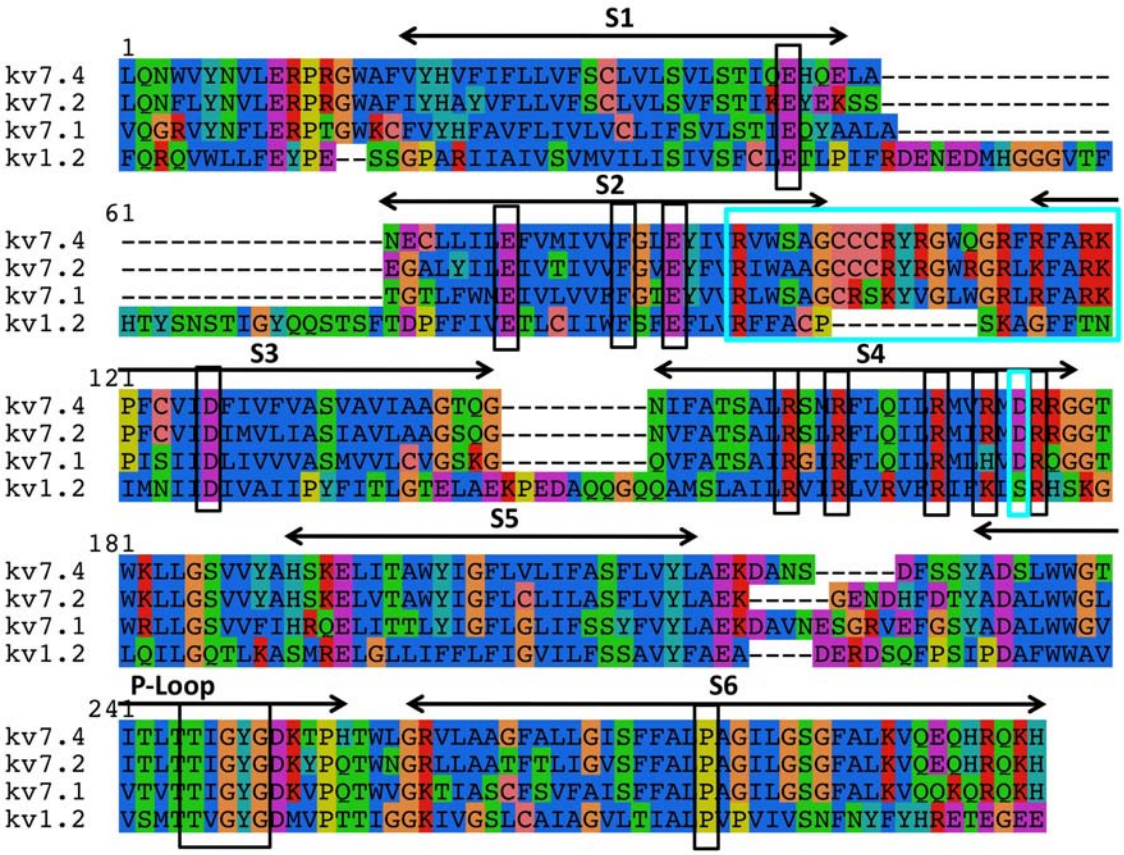

Figure 5.2: Sequence alignment of the Kv7.1, Kv7.2 and Kv7.4 with the Kv1.2 highlighting the importance of S4 basic residues and of the acidic countercharges of S1-S3. Other residues such as the conserved phenylalanine residue in S2, the TXGYG selectivity filter, the proline in S6 are highlighted. Two regions of special interest are highlighted in cyan: the S2/S3 linker in the Kv7 channels is much longer and contains a lot of positively charged residues, and in the D^{S4} residue at the bottom of S4.

In contrary to the TM segments, which are well conserved, the connecting loops are very different in the Kv7 family when compared to the Kv1.2. Indeed, in Kv1.2, the S1-S2 and the S3-S4 extracellular loops are quite long and the S2-S3 loop is short. In the Kv7 family, it is the opposite: the extracellular loops are particularly short (as illustrated by the wide gaps in the alignment) while the S2-S3 linker is much longer. It is noteworthy that this particular loop contains a large number of basic residues (Fig. 5.2) and is a region that concentrates a large number of mutations involved in Kv7.1 channelopathies (Pan et al. 2009), stressing the possible importance of a correct 3-D model of these S2-S3 linkers.

1.2 3-D model in the closed and open state

Based on this alignment, we built a model of each Kv7 channel in the open and in the closed state by comparative modeling, using the spatial restraints method with the modeller

program (Eswar et al. 2006). This method consists in generating many restraints on the structure of the target, using its sequence alignment with the template as a guide. These homology-derived restraints are generally obtained by assuming that distances between aligned residues and dihedrals in the template and the target structures are similar. Stereochemical restraints on bond lengths, bond angles, dihedral angles..., obtained from the CHARMM22 force field (MacKerell Jr. et al. 1998), are also added. The model is then iteratively obtained by minimizing the violations of all the restraints. Here, the tetrameric assembly of Kv1.2 in its α and ε conformations were taken as templates, introducing thereby a diversity among the subunits that is also naturally present.

For the loops, extra care was taken. Indeed, as previously stated, whereas the S1-S2 and the S3-S4 loops are very short and yield a straightforward model, the S2-S3 loop on the other hand is much longer, making it possible to generate many different conformations. To build a correct starting model of this loop, we used the conformational search method also implemented in modeller (Eswar et al. 2006). This method is based on optimization-based approach and relies on conjugate gradients and molecular dynamics with simulated annealing. The pseudo energy function is a sum of many terms, including some terms from the CHARMM22 force field and spatial restraints based on distributions of distances and dihedral angles in known protein structures (Fiser et al. 2000). For each of the six tetramers, we built up to five different S2-S3 loop conformations. For each channels, we chose a configuration in which all the four S2-S3 loops are extending towards the solution and away from the VSD intracellular entrance. Altogether, we have 24 different loops (6 models with four loops each) before beginning the equilibration, possibly reflecting a natural diversity.

Table 5.1: Summary table of the Kv7 channel/bilayer systems

#	System	Channel state	Voltage	Duration [ns]
1	Kv7.1	Activated	No/Yes	60/25
2	Kv7.1	Resting	No/Yes	25/25
3	Kv7.2	Activated	No	25
4	Kv7.2	Resting	No	25
5	Kv7.4	Activated	No/Yes	40/10
6	Kv7.4	Resting	No/Yes	40/50
7	Kv7.1 R2 mutant	Resting	No/Yes	10/60
8	Kv7.4 R4 mutant	Activated	No/Yes	20/20

We then inserted the channels in a fully hydrated POPC bilayer, and equilibrated the six systems under normal NPT conditions (298 K, 1 atm) in a 150 mM KCl solution (Table 5.1). Fig. 5.3 presents the Kv7.4 open channel system (corresponding to Sim. #6). Following a

similar strategy as in the case of the Kv1.2, we started by constraining the positions of all the atoms of the channels during 1 ns to let the solution and lipids reorganize around the protein. Then, we constrained the backbone atoms during 8 ns, letting the side chains free to rearrange in response to the environment. Finally, we constrained only the backbone of the selectivity filter, letting the entire channel relax and equilibrate. The rmsd profiles for the backbone of the transmembrane segments of the open and closed Kv7.4 channels (Sim. #5 and #6) indicate that the channel structure is stabilized after ~36 ns (Fig. 5.4). In the other systems, the profiles look alike (data not shown).

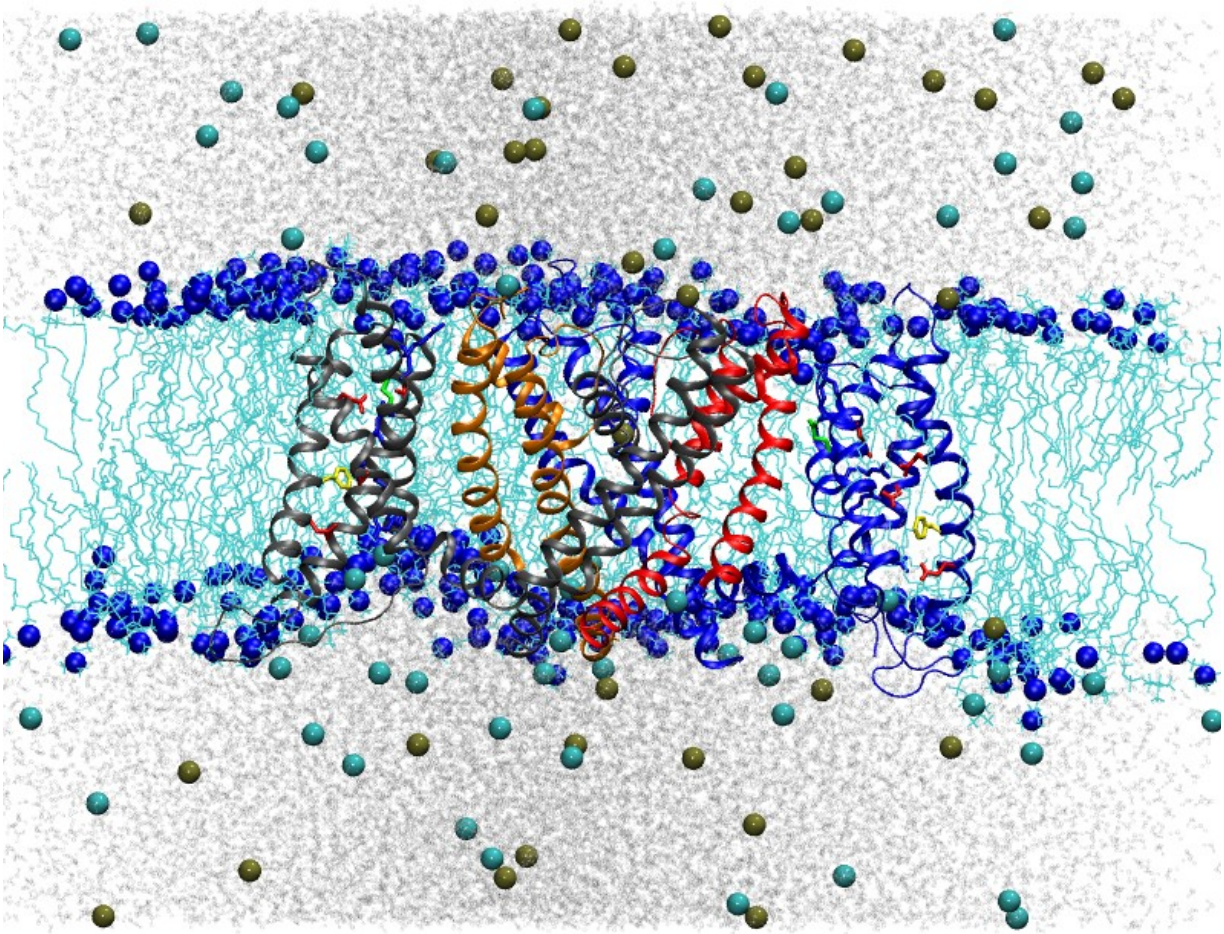

Figure 5.3: Side view of the open Kv7.4 inserted in a POPC lipid bilayer. The different subunits are represented by ribbons of different colors (blue, red, grey and orange). The conserved residues within the VSDs of two subunits are figured as sticks (blue for basic residues, red for acidic ones, green for the glutamine and yellow for the phenylalanine).The lipid headgroups are represented as blue spheres and the lipidic part as cyan lines. The water is transparent and the ions as cyan and green spheres.

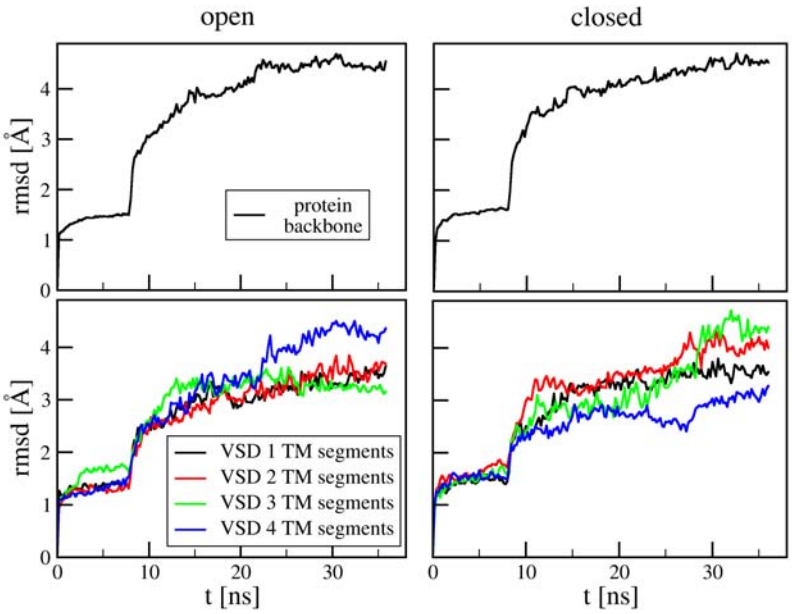

Figure 5.4: Rmsd profiles of the open (left) and closed (right) conformations of the Kv7.4. We present the rmsd profile for the ensemble of the protein heavy atoms after superimposing the position of the pore domain in all the frames of the simulation (top) and the rmsd profiles for the individual VSD transmembrane segments heavy atoms after fitting the individual VSDs in all the frames (bottom). In all graphs, note the jump in the rmsd values around 8 ns when the constraints on the backbone atoms were released and the convergence of the rmsd after few tens of nanoseconds indicating a stabilization of the structures.

2 Salt bridge network rearrangement

In Kv1.2, we recall that S4 contains six basic residues that interact with four negative residues within the VSD and with the top lipid phosphate groups in the activated state and with the bottom ones in the resting state. In Kv7.4 (and Kv7.2), S4 has lost one positive residue: the arginine in position 3 is changed into a glutamine. In Kv7.1, there are two substitutions: the third and fifth basic residues are exchanged for a glutamine and a histidine residue, respectively. Note that in our model, the histidine was considered in its uncharged state, despite the fact that its protonation state could be altered by the environment.

From the change in S4 sequence when compared to Kv1.2, we expect salt bridge rearrangements to take place during the multi-nanosecond equilibration. We describe hereafter the organization of the salt bridges network found for the 3 Kv7 studied channels.

Before equilibration, as in the open state of the Kv1.2, in the activated Kv7 models, R1 and R2 were in interaction with the lipid headgroups of the top bilayer, Q3 was pointing towards the first binding site D1, R4 towards D2, H5 (or R5) towards D3 and R6 towards E4. In the

resting state, R1 was engaged in a salt bridge with D3, R2 with E4 and Q3, R4, H5 (or R5) and R6 were pointing towards the lipid headgroups of the bottom layer of the membrane. Due to the lack of electrostatic interactions for Q3 and H5, the particular salt bridges involving these residues were disrupted during equilibration and such electrostatic interactions replaced by others:

In Kv7.4 and Kv7.2, which are the channels with the least difference with respect to Kv1.2, in the open state, R1 and R2 interact with the phosphate groups of the lipids of the top layer, R4 is in interaction with two negative charges, E1 and E2, replacing thereby R3. K5 and R6 interact with D3 and E4, respectively (Fig. 5.5.C). In the resting state, R3 was in interaction with the lipid headgroups of the bottom bilayer and its mutation to glutamine has not led to a very specific reorganization of the salt bridges: (Fig. 5.5.D).

In Kv7.1, due to the loss of one more positively charged residue in S4, the rearrangement was more drastic. In the open state, R1 remains in interaction with lipid headgroups while R2 has taken the position of R3 and is in interaction with both E1 and E2. R4 has transferred from the top of the VSD to the bottom and interacts mostly with D3 and R6 with E4 (Fig. 5.5.A). In the resting state, similarly to what is found in the case of the Kv7.4, no major reorganization can be seen (Fig. 5.5.B). It is interesting to note here that the "activated state" of the VSD looks very much like the β state of the Kv1.2, indicating that the total S4 translocation during Kv7.1 deactivation is probably reduced when compared to the one for Kv1.2. Accordingly, the gating charge is probably also drastically reduced both due to the loss of charge and to the reduced transfer distance.

Similarly to Kv1.2, in all Kv7 channels, the topology of the water accessible volume is similar to the one found in the Kv1.2 (chapter 4, paragraph 2.2). Indeed, it defines a hourglass like structure in which water can access the top half of the VSD from the extracellular medium and the bottom half of the VSD from the intracellular one. In both the open and the closed state, the center of the hourglass is located around the salt bridge involving the D3 binding site. In this region, water and other solutes (*i.e.* ions) are prevented from circulating.

3 Kv7 gating charges

Using the configurations presented above, we calculated the gating charge for the Kv7.1 and Kv7.4 channels using the direct measurement and the free energy formalism described in the methods section (paragraph 3.2). These results are compared to the values obtained for the Kv1.2 channel in table 5.2.

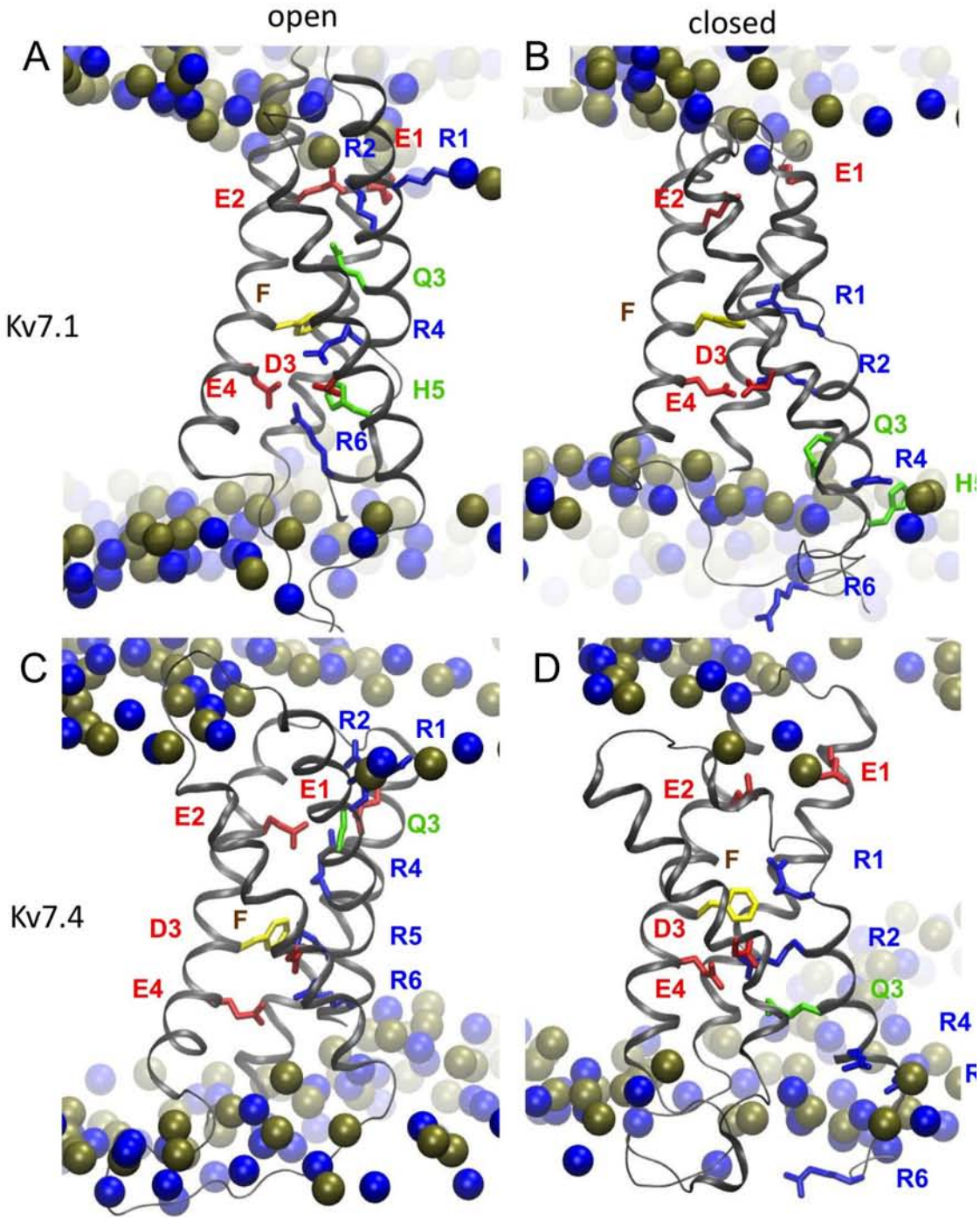

Figure 5.5: Side view of the Kv7.1 (top) and Kv7.4 (bottom) VSD in the open (left) and resting (right) equilibrated conformation. The VSD backbone is represented as grey ribbons and the lipid phosphate and choline groups as green and blue spheres, respectively. The conserved residues within the VSD are figured as sticks (blue for basic residues, red for acidic ones, green for the glutamine and yellow for the phenylalanine).

In Kv7.4, the total gating charge amounts to ~ 9e, compared to ~13e in Kv1.2. As expected from the basic residue sequence, the gating charge is drastically reduced. Indeed, it seems that mutation of R3 (Kv1.2) in Q3 (Kv7.4) leads to a drop in the gating charge of ~4e. In Kv1.2, each R3 charge translocates through almost the entire electric field and accounts for ~ 4 x 0.75 = 3e when going from α to ε states (Fig. 4.11). If the mutation R3Q would lead to no reorganization within the VSD, i.e. the extent of S4 movement would not be altered, we would expect the loss in gating charge to be ~3e. Because the salt bridges have also been shown to reorganize, it is not too surprising that the drop in gating charge is even larger.

In Kv7.1, the direct measurement gives a value of ~6 e for the gating charge, that is a reduction by almost 7e when compared to Kv1.2. Following the same reasoning, because K5 transports ~0.4e per subunit, the net loss consecutive to mutation of R3 and K5 into uncharged residues should be ~4.6e. Due to the large salt bridge rearrangement in the open state, it is altogether not too surprising to have a 7e drop for the entire channel.

Table 5.2: Gating charge computed between the open-activated and the resting-closed state in the Kv7.1, Kv7.2 and Kv7.4

Channel	Direct Measurement Q[e]	Energetic Formalism Q[e]	S4 contribution
Kv7.1	-5.85		
Kv7.4	-8.9	-8.0	-7.5
Kv1.2	-12.8	-11.2	-9.9

We completed the study for Kv7.4, by applying the energetic formalism to identify the residues that contribute the most to the ~8.9e gating charge. Here, as seen in the case of Kv1.2, the total gating charge calculated with the energetic formalism amounts to ~8.0e, which is slightly lower than with the direct measurement.

Also as in the case of Kv1.2, the biggest contribution to the gating charge comes from S4 and its contribution amounts to ~7.5e (Table 5.2 and Fig 5.6). In Fig 5.6.C, we distinguish between the contributions of the different residues of S4 to the gating charge. R2 is the charge that conducts the most, with ~-0.6e per subunit, in agreement with its large displacement within the VSD, along the normal to the membrane plane (Fig.5.5). Residues R1 and R4 contribute by ~ -0.45e per subunit each, whereas the contributions of R5 and R6 are smaller.

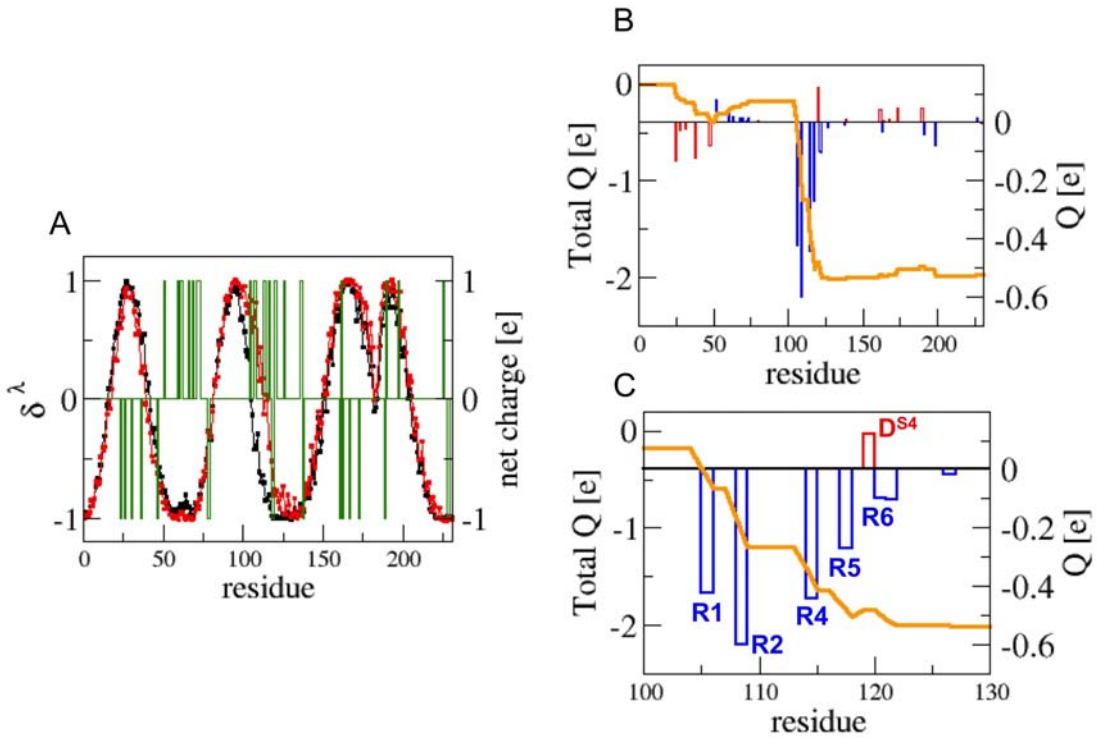

Figure 5.6: Electrical properties of the Kv7.4 VSD (A) Top: Electrical distances, δ_i^λ for each TM residue in the α (black) and ε (orange) conformations and net charge per residue (green) along the Kv channel sequence (excluding the T1 domain). The position of the TM segments S1 to S6 is indicated by arrows. δ_i^λ was normalized assuming δ_i^λ = 1 and 0 for residues positioned, respectively above 25 Å and below -25 Å from the bilayer center. The data was averaged over the four subunits of the channel (B and C) Corresponding cumulative (orange line) and per-residue (bars) gating charges for the α → ε transition (basic residues in blue and acidic ones in red) for the entire sequence (B) and zooming on the S4 segment (C).

4 Preliminary results on the effect of S4 basic residue mutations in Kv7.1 and Kv7.4

As previously noted, in the Kv7 family, a large number of S4 basic residues mutations lead to inherited channelopathies. In Kv7.1, mutation of R2 into an uncharged residue leads to a familial form of Long QT1 syndrome and Fetal brachycardia (Lupoglazoff et al. 2003). In Kv7.2, mutation of R2 or R4 leads a few different brain nervous system diseases like BNFS, myokymia and PNH (Dedek et al. 2001) (Castaldo et al. 2002). The molecular mechanism implicated in these diseases have not yet been identified, mostly because of the difficulty to express these channels in large enough quantities.

In Kv7.4, on the other hand, there are no known S4 mutations implicated in diseases.

However, this channel is easier to express. Because of the high sequence homology with Kv7.2, this channel was hence used to study the effect of mutating R4 (R213 in Kv7.4). The group of Taglialatela found not only that R4Q or R4W mutants alter the gating properties (G/V right shift, slower kinetics of activation and deactivation...) (Miceli et al. 2011) but also that when blocking the ionic current through the central pore, the R4Q mutant gives rise to outwards leak "omega" currents through the activated VSD. This observation is in quite good agreement with our model of the state dependent currents. Indeed, we have shown in Kv1.2, that mutation of *top residues* would lead to outward leak "omega" currents in the activated state of the channel whereas mutation of *bottom residues* would lead to inward "omega" currents in its resting state (chapter 4, paragraph 2.5). Accordingly, although no experiments exist on the Kv7.1 corresponding to the R2 mutant, we thought it would be a good candidate to test for inwards omega currents in the resting state.

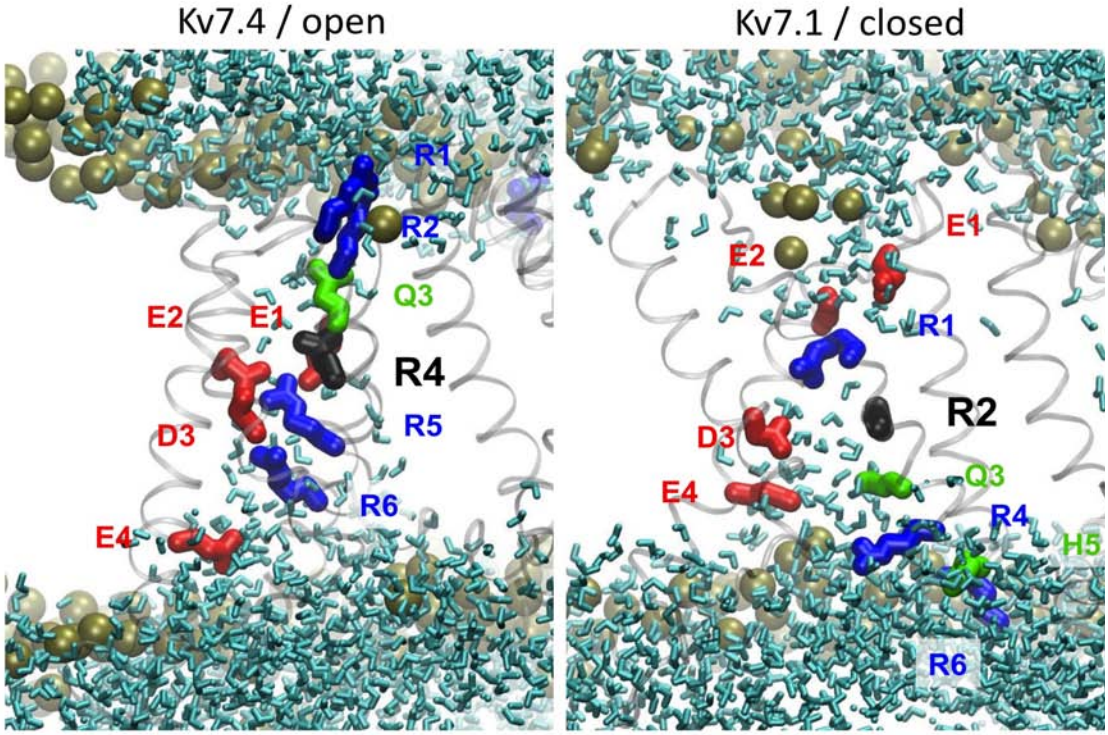

Figure 5.7: Side view of the open Kv7.4 R4 mutant (left) and closed Kv7.1 R2 mutant (right) VSD. The VSD backbone is represented as grey ribbons and the lipid phosphate and choline groups as green spheres, respectively. The conserved residues within the VSD are figured as sticks (blue for basic residues, red for acidic ones, green for the glutamine and histidine). The mutated residue is especially highlighted as thick black sticks. The water molecules are figured in cyan.

We have prepared systems of the Kv7.4 R4 mutant in the open state and of the Kv7.1 R2 mutant in the closed state by mutating either R4 or R2 to glutamine. The work is still on its way but preliminary MD simulations (Table 5.1) in NPT conditions seem to indicate that the disruption of the VSD structure in Kv7.1 and Kv7.4 is not as important as in the Kv1.2 VSD.

Indeed, one can see that the water constriction around the D3 salt bridge has not been disrupted (Fig. 5.7). However, after 10 to 20 ns, it is difficult to draw conclusions.

We submitted the mutants to +/- 600 mV after restraining the positions of the selectivity filter atoms to prevent ionic conduction through the main pore. The simulations are also still to short to draw any irrevocable conclusions but the preliminary results show no transport of ions through the VSD after few tens of nanoseconds, in contrast to what was expected.

5 Discussion

Within the scope of characterizing the function and modulation of Kv7 channels, we have built homology models of three members of this family (Kv7.1, Kv7.2 and Kv7.4) based on the Kv1.2 structure.

Let us first discuss some particularities arising from the choices we made. Whereas most of the alignment in the transmembrane regions is unambiguous, in the S1 region, uncertainties remain. Indeed, on can choose to align the hydrophobic residues, in which case the negative residues (E1) present at the top of S1 are not aligned in the four sequences. They will therefore not be able to serve as a binding site for S4 basic residues in the 3D structure. Such an alignment has been considered by another group for Kv7.1 (Smith et al. 2007). We, on the other hand, considered a different alignment in which we aligned E1 in the top of S4. In our opinion, the salt bridge network governs proper function of the VSD and the number of salt bridges should be maximal within the VSD. However, because of the lower number of basic residues in the S4 sequence in Kv7 channels, it is conceivable that a negative binding site in S1 is missing. This would then reduce the number of binding sites to match the number of S4 basic residue. This question is still open and it would be interesting to test by mutagenesis if E1 is a binding site for positive charges of S4 in the Kv7 family. This would enable to determine with certainty which of the two alignments is correct.

Next, after MD equilibration of the channels in their membrane environment, we studied the salt bridge network in the two conformations of the three channels. We were able to see that the replacement of R3 by a glutamine in all the Kv7 channels and of K5 by a histidine in Kv7.1 only leads to a state-dependent reorganization of the electrostatic interactions within the VSD. A recent charge reversal mutagenesis study revealed that in Kv7.1, the top negatively charged residues of S2, E2, interacts with various S4 gating charges (R1 to R4) in a state-dependent manner (Wu, Delaloye, et al. 2010). The authors interpret their electrophysiology measurements by positing that R4 is close to E2 in the open state whereas R1 is the residue close to E2 in the resting state . It is rather interesting to note that our model is quite different. Indeed, we find R2 close to E2 in the activated state (R4 has transferred to D3) and no basic residue in the vicinity of E2 in the resting state. Whereas these experimental results should be considered, it is rather important to note that charge reversal mutagenesis probably induces a rather large perturbation of the VSD function. Indeed, the same experiments indicate that

single mutation of E2 into lysine modifies drastically the electrostatic environment in the top half of the VSD even making the channels non functional (Wu, Delaloye, et al. 2010). Moreover, the mutation of a S4 basic residue into a negative charge probably alters the structure even more, possibly pairing this residue to the only positive binding site (E2 mutated to lysine) in the VSD. In our model, the salt bridge network was built on the basis of the one of Kv1.2. There is also no experimental evidence showing that this is an accurate way to proceed. From this, it is rather difficult to conclude as to which of the VSD model is the most trustworthy, and additional experiments are needed to validate one with respect to the other.

Thanks to the use of the charge imbalance/air slab method to apply a TM voltage, we have also measured the gating charge in two of these channels. We find that a loss of one basic residue leads to a drop of ~ 4e in the single channel gating charge (Q ~ 9e in Kv7.4) when compared to the Kv1.2, probably due both to the missing positive charge, and to the salt bridge rearrangement. Also, the loss of two basic residues leads to a gating charge reduction of almost 7e, with a resulting gating charge of ~6e for the Kv7.1. Both Aggarwal et al. and Seoh et al. found in 1996 that mutating any of the first 4 positively charged residues of S4 gave rise to a drop of at least 4e for the whole channel (Aggarwal & MacKinnon 1996) (Seoh et al. 1996). It is interesting to note that the single mutation of R3 to glutamine in Kv7.4 leads to a similar drop. Because each R3 residue transports ~0.75e, a drop of ~3 e would have been expected if the electrostatic network was strictly conserved from Kv1.2 to Kv7.4. The larger drop of 4e, in agreement with the experiments in Shaker, indicates that the electrostatic network reorganization we observe is very plausible.

Finally, we tackled the question of the effect of S4 basic residues mutation on a molecular level. We conducted MD simulations of the Kv7.4 R4Q mutant in the open state and of the Kv7.1 R2Q mutant in the closed state. Kv7.4 R4Q, in particular, was experimentally shown, to give rise to outwards leak “omega” currents through the activated VSD. Contrary to this, our simulations do not show any sign of VSD conduction. We identified several explanations for this discrepancy. The most obvious is that the simulations are too short to enable complete reorganization of the VSD after mutation and subsequent ionic transport. This will be addressed by extending the simulations. Next, it is possible that our model of the VSD, built on the basis of the Kv1.2 is too far from the actual VSD structure. Along the same line, an error in the S1 alignment could have led to a poor model that doesn't allow the conduction of ions in the mutant. This is however unlikely because E1 is quite far from the water constriction that is critical for the appearance of omega currents. Also, the highly positively charged S2-S3 loop could define an electrostatic barrier, preventing ionic conduction. This is especially true in the depolarized state where K^+ ions reach the VSD from the intracellular side. It is then possible that our model of this loop should be reworked. Finally, the electrophysiology experiments that were conducted in Kv7.4 are recent and could also be a source of error, by the authors' own admission (private communication).

A few questions still remain. First, in the near future, we wish to investigate the gating charge of Kv7.2. Indeed, as the S4 sequence is very similar to Kv7.4, one expects the results for both channels to be similar. However, a change in structure may arise from the subtle

discrepancies in sequence and this channel is the most relevant to study the effect of genetic mutations since it is effectively implicated in diseases. Finally, because of the existence of a histidine in position of K5, is is possible to expect a proton transport through the VSD in the activated state, similarly to what is seen in Shaker (Starace & Bezanilla 2004). This would change the channel operation quite drastically. Although such an investigation is not possible using classical MD simulations, it would be interesting to investigate such a possibility by both experimental or theoretical means.

References

Aggarwal, S.K. & MacKinnon, R., 1996. Contribution of the S4 segment to gating charge in the Shaker K+ channel. *Neuron*, 16(6), p.1169–1177.

Castaldo, P. et al., 2002. Benign familial neonatal convulsions caused by altered gating of KCNQ2/KCNQ3 potassium channels. *Journal of Neuroscience*, p.199.

Dedek, K. et al., 2001. Myokymia and neonatal epilepsy caused by a mutation in the voltage sensor of the KCNQ2 K+ channel. *Proceedings of the National Academy of Sciences*, 98(21), p.12272 -12277.

Eswar, N. et al., 2006. Comparative protein structure modeling using modeller. Dans A. D. Baxevanis et al., éd. *Current Protocols in Bioinformatics*. Hoboken, NJ, USA: John Wiley & Sons, Inc.

Fiser, A., Do, R.K. & Sali, A., 2000. Modeling of loops in protein structures. *Protein Science: A Publication of the Protein Society*, 9(9), p.1753-1773.

Van Horn, W.D., Vanoye, C.G. & Sanders, C.R., 2011. Working model for the structural basis for KCNE1 modulation of the KCNQ1 potassium channel. *Current Opinion in Structural Biology*, In Press.

Kang, C. et al., 2008. Structure of kcne1 and implications for how it modulates the KCNQ1 potassium channel. *Biochemistry*, 47(31), p.7999-8006.

Larkin, M.A. et al., 2007. Clustal W and Clustal X version 2.0. *Bioinformatics*, 23, p.2947-2948.

Lupoglazoff, J.-M. et al., 2003. Long QT syndrom in neonates: Conduction disorders associated with HERG, mutations and sinus bradycardia with KCNQ1 mutations. *Journal of the American College of Cardiology*, 43, p.826-830.

MacKerell Jr., A.D. et al., 1998. All-atom empirical potential for molecular modeling and dynamics studies of proteins. *Journal of Physical Chemistry B*, 102, p.3586-3616.

Maljevic, S. et al., 2010. Kv7 channelopathies. *Pflügers Archiv - European Journal of Physiology*, 460(2), p.277-288.

Miceli, F., Soldovieri, M.V., Hernandez, C.C., et al., 2008. Gating consequences of charge neutralization of arginine residues in the S4 segment of Kv7.2, an epilepsy-linked K+ channel subunit. *Biophysical Journal*, 95(5), p.2254-2264.

Miceli, F. et al., 2009. Neutralization of a unique, negatively-charged residue in the voltage sensor of KV7.2 subunits in a sporadic case of benign familial neonatal seizures. *Neurobiology of Disease*, 34(3), p.501-510.

Miceli, F., Soldovieri, M.V., Martire, M., et al., 2008. Molecular pharmacology and therapeutic potential of neuronal Kv7-modulating drugs. *Current Opinion in Pharmacology*, 8(1), p.65-74.

Miceli, F. et al., 2011. Gating currents from neuronal Kv7 channels carrying BFNS-causing mutations in the S4 segment of the voltage sensing domain. *Biophysical Journal*, 100(3, Supplement 1), p.426a.

Pan, N. et al., 2009. A hydrophobicity-dependent motif responsible for surface expression of cardiac potassium channel. *Cellular Signalling*, 21(2), p.349-355.

Seoh, S.A. et al., 1996. Voltage-sensing residues in the S2 and S4 segments of the Shaker K+ channel. *Neuron*, 16(6), p.1159–1167.

Smith, J.A. et al., 2007. Structural models for the KCNQ1 voltage-gated potassium channel. *Biochemistry*, 46(49), p.14141-14152.

Splawski, I. et al., 2000. Spectrum of mutations in long-QT syndrome genes : KVLQT1, HERG, SCN5A, KCNE1, and KCNE2. *Circulation*, 102(10), p.1178-1185.

Starace, D.M. & Bezanilla, F., 2004. A proton pore in a potassium channel voltage sensor reveals a focused electric field. *Nature*, 427(6974), p.548-553.

Tao, X. et al., 2010. A gating charge transfer center in voltage sensors. *Science*, 328(5974), p.67-73.

Wu, D., Delaloye, K., et al., 2010. State-dependent electrostatic interactions of S4 arginines with E1 in S2 during Kv7.1 activation. *The Journal of General Physiology*, 135(6), p.595-606.

Wuttke, T. V. et al., 2007. Peripheral nerve hyperexcitability due to dominant-negative KCNQ2 mutations. *Neurology*, 69(22), p.2045 -2053.

Yarov-Yarovoy, V., Baker, D. & Catterall, W.A., 2006. Voltage sensor conformations in the open and closed states in rosetta structural models of K+ channels. *Proceedings of the National Academy of Sciences*, 103(19), p.7292 -7297.

6- SUMMARY & CONCLUSION

"To succeed, jump as quickly at opportunities as you do at conclusions."

-Benjamin Franklin

Les canaux ioniques sensibles au voltage sont des protéines membranaires ubiquitaires qui sont responsables du transport de l'influx nerveux dans toutes les cellules excitables, *e.g.* celles du coeur, du système nerveux, des muscles squelettiques, des organes sensoriels tels que l'oreille interne, l'oeil et de nombreux autres. Ainsi, ces protéines sont sensibles à un grand nombre de *facteurs de modulation*, *e.g*. l'action de peptides d'inactivation, drogues ou anesthésiants, l'altération des lipides qui les entourent... D'une manière similaire, la mutation génétique de ces canaux peut avoir un effet dramatique et donner lieu à un grand nombre de maladies familiales (appelées canalopathies) comme le syndrome du QT long du coeur, une variété de maladies neurologiques comprenant l'épilepsie, les attaques ou les paralysies périodiques de différents types, la surdité progressive...

Une caractéristique particulière des canaux ioniques sensibles au voltage est qu'ils produisent des courants électriques transitoires et de très petite magnitude (200 fois plus petits que les courant ioniques au travers de la membrane) lorsqu'ils passent de l'état fermé à ouvert. L'intégrale de ces courants dits de « gating » est appelée la charge de « gating » et est une propriété fondamentale de ces canaux. Lorsque les premiers canaux ioniques sensibles au voltage ont été séquencés, on a découvert qu'ils ont une structure tétramérique commune, chaque monomère contenant six hélices transmembranaires. Les deux dernières s'assemblent pour former le pore, la région qui est responsable pour le transport des ions d'un côté de la membrane à l'autre. Les quatre autres (S1-S4) constituent un domaine auxiliaire qui est responsable de la sensibilité au voltage: le domaine sensible à la tension (DST). Parmi elles, la quatrième hélice (S4) compte un nombre important de résidus chargés positivement (4 à 7, la plupart étant des arginines) qui sentent et répondent aux variations du potentiel transmembranaire (*i.e.* du champ électrique local). Ces résidus sont les composants responsables des courants de « gating » au niveau moléculaire: en effet, après activation, soit quand le canal ionique va de l'état fermé (au repos) à l'état ouvert (activé), la charge de gating totale (~ 12 à 14 charges élémentaires par canal) est transportée au travers de la membrane essentiellement par les résidus basiques de S4.

Malgré le grand intérêt de la communauté scientifique pour ces protéines chargées de transporter les ions au travers de la membrane des cellules excitables d'une manière dépendante du voltage et en dépit des découvertes capitales des dernières années (parmi lesquelles la résolution de la structure cristallographique de l'état activé du canal Kv1.2, un canal voltage-dépendant mammalien), des nombreux mystères demeurent quant à leur fonctionnement au niveau moléculaire et plus particulièrement quant au mécanisme de leur désactivation.

Dans ce travail, nous avons abordé nombreuses de ces questions en utilisant des simulations de dynamique moléculaire état de l'art et une procédure spéciale qui permet d'appliquer un potentiel transmembranaire d'une manière cohérente avec les expériences de

« patch clamp ».

Les résultats principaux peuvent être résumés comme suivent :

- A partir d'une simulation de 2.2 μs du canal Kv1.2 (inséré dans un analogue de son environnement lipidique (une bicouche de phosphatidylcholine) et solvaté dans une solution ionique de KCl, puis soumis à un potentiel désactivant de ~ -600 mV) et de simulations biaisées ultérieures, nous avons découvert cinq états du DST, les conformations desquels α, -β, γ et δ- et ε correspondent respectivement aux états ouvert, intermédiaires et fermé du canal. Les changements conformationnels intervenant dans le DST mettent en jeu un mouvement de fermeture éclair des résidus chargés de S4 en interaction consécutivement avec les résidus chargés négativement du DST. Le transfert d'un état à l'autre est accompagné par la transition de l'un des résidus basiques par le centre « catalytique » de transfert, en accord avec l'hypothèse de MacKinnon. Nous démontrons également que les lipides participent non seulement à la stabilisation des états ouvert et fermé par leur interaction avec des résidus basiques du haut et du bas de S4 respectivement, mais aussi dans la stabilisation des états intermédiaires. Dans l'état γ, notamment, le premier résidu positif de S4 interagit avec des groupements phosphate de la couche supérieure de la membrane tandis que le dernier interagit avec des groupements phosphate de la couche inférieure. Le changement conformationnel global de l'état activé à « au repos » du DST donne lieu à une charge de « gating » totale en accord avec les données expérimentales (12.8e) et nécessite un déplacement vertical de S4 de 10 à 15 Å. La caractéristique la plus frappante révélée ici provient sans doute de l'analyse de l'activité électrique du canal et du fait que la charge de « gating » transportée par les résidus basiques de S4 peut être décrite pas une fonction unique, qui définit le couplage électromécanique que les charges du DST subissent. Pris dans leur ensemble, ces résultats favorisent le modèle conceptuel *en vis* plutôt que le modèle *transporteur*.

- Grâce aux configurations du Kv1.2 déterminées dans la première partie de ce travail, nous avons étudié l'effet au niveau moléculaire de la mutation des résidus basiques de S4 qui sont impliquées dans des maladies génétiques et qui donnent lieu à l'apparition de courants de fuite (courant « oméga ») au travers d'un passage non identifié. On montre que certaines de ces mutations cassent les ponts salins qui maintiennent l'intégralité du DST et ouvrent un passage hydrophile au travers de celui-ci. Lorsqu'on les soumet à un potentiel transmembranaire d'une magnitude de quelques centaines de millivolts, ceci donne lieu à la conduction d'ions K^+ le long de ce chemin. Ces résultats révèlent donc les processus élémentaires impliqués dans ces courants « oméga ». A partir d'une étude extensive des mutations de la plupart de ces résidus dans les états ouvert et fermé, nous proposons un modèle du mécanisme, dans lequel la mutation des résidus du haut de S4 donne lieu à l'apparition de courants « oméga » vers l'intérieur dans l'état au repos tandis que la mutation des résidus du bas de S4 donne lieu à l'apparition de courants « oméga » vers l'extérieur dans l'état activé. Ce modèle indique également dans quelles conditions ces courants peuvent être critiques.

- Nous concentrant ensuite sur la modulation de la fonction des DST par les lipides, nous avons étudié l'impact de la modification de la nature des têtes polaires des lipides sur l'activation des DST. Nous avons ainsi utilisé des simulations du Kv1.2 dans différentes bicouches asymétriques contenant de la sphyngomyéline, du céramide-1-phosphate ou du céramide dans la couche supérieure de la membrane, montrant qu'en dépit de leur rôle clé dans la stabilisation des résidus basiques de S4, la charge de « gating » est peu affectée par la modification des caractéristiques des têtes polaires des lipides. Ces résultats indiquent que le changement des têtes polaires des lipides affecte en majorité la cinétique de transition d'une conformation du DST à l'autre. Pour confirmer ceci, une étude extensive de la surface d'énergie libre de l'activation (désactivation) du Kv1.2 serait nécessaire.

- Finalement, en souhaitant étendre les résultats précédents à d'autres membres des la famille des canaux ioniques voltage-dépendants qui sont intéressants d'un point de vue pharmacologique, nous avons entrepris l'étude de quelques membres de la sous-famille des Kv7. De tels canaux ont un nombre réduit de résidus basiques sur S4 par rapport au Kv1.2, et donc une charge de « gating » plus petite. Nous avons donc construit des modèles moléculaires du domaine transmembranaire des Kv7.1, Kv7.2 et Kv7.4 dans leurs états fermés et ouverts, en cohérence avec ceux du Kv1.2. Les résultats préliminaires indiquent que le réseau de ponts salins dans le DST est réorganisé par rapport au Kv1.2 suite à la perte de charges sur S4. Leur charge de « gating » vaut ~9e pour le Kv7.4 et ~6e pour le Kv7.1 (à comparer avec les ~13e du Kv1.2). Nous avons également débuté l'étude des l'effet des mutations génétiques des résidus basiques du DST qui sont impliquées dans le syndrome du QT long, dans les attaques bénignes familiales néonatales, ou dans une forme de surdité progressive. Bien que nous n'ayons pas pu à ce jour enregistrer de courants « oméga » dans de tels mutants, ainsi que l'expérience l'indique, la comparaison de résultats de simulations plus longues avec les données expérimentales est en cours.

Ainsi, tout au long de ce travail débuté en 2008, le contexte bibliographique a continué d'évoluer et l'apparition de nouveaux résultats expérimentaux nous a mené vers de nouvelles directions parfois imprévues. Ainsi, la résolution du mécanisme de désactivation a été cruciale pour commencer de nouvelles études sur la modulation du Kv1.2. Elle nous a également servi de base pour débuter l'étude d'autres membres de la famille élargie des Kv. Enfin, il faut aussi noter que cette étude n'aurait pas pu être réalisée sans moyens de calcul conséquents et c'est grâce à la quantité d'heures généreuse pourvue par GENCI et le CINES que nous avons pu toujours essayer de rester à la pointe des questions scientifiques concernant les canaux ioniques voltage-dépendants.

Aujourd'hui, à la lumière de nos résultats, il semble difficile, afin de s'intéresser aux différents aspects de la modulation des canaux Kv, d'éviter la question de l'énergie libre de l'activation. Bien que ce soit une question capitale, elle est également compliquée à attaquer car elle implique de choisir une coordonnée de réaction loin d'être évidente et parce qu'elle nécessite d’échantillonner cette dernière sur des échelles de temps très longues. Nous somme

en train de considérer la question.

La modulation des canaux voltage-dépendants par des molécules médicamenteuses joue un rôle central en pharmacologie en agissant essentiellement via deux mécanismes : l'activation et le blocage. Ainsi, les molécules activantes des Kv peuvent permettre d'hyperpolariser la membrane fournissant ainsi une approche thérapeutique pour traiter l'hyperexcitabilité neuronale, impliquée dans l'épilepsie, les migraines... Les molécules bloquantes d'autre part sont utilisées comme analgésiques, anti-douleurs ou encore comme anesthésiants.

Tandis que dans cette étude, nous avons abordé la modulation des canaux Kv par leur mutation génétique ou encore par la modification des lipides qui les entourent, les résultats que nous avons obtenus quant au fonctionnement des domaines sensibles à la tension de ces canaux permettront de comprendre mieux les mécanismes impliqués dans leur modulation par ces molécules provenant de l'extérieur (petites molécules médicaments, anesthésiants, peptides, toxines).

Comme nous avons entrepris de le montrer avec l'exemple des Kv7, il est possible de s'intéresser à différents membres de la famille des canaux ioniques voltage-dépendants, notamment au fur et à mesure de la publication de structure cristallographiques de différents membres. Ainsi, nous pouvons envisager d'étudier immédiatement l'interaction de certaines molécules médicaments avec les différents états des canaux choisi (activé, intermédiaires, au repos) et également imaginer participer à la conception ou l'amélioration de molécules qui permettraient de contraindre ce canal dans l'un ou l'autre de ces états.

Voltage gated ion channel are crucial, ubiquitous membrane proteins that are responsible for the transport of the nervous influx in all excitable cells, *e.g.* the ones of the heart, of the nervous system, of skeletal muscles, of sensory organs like the inner ear, the eyes and many others. As such, these proteins are sensitive to a large number of *modulating factors*, *e.g.* the action of inactivation peptides, drugs or anesthetics, the alteration of the lipids embedding them... Similarly, *genetic mutations* of these channels can have dramatic effects and give rise to a large number of familial genetic diseases (so-called *channelopathies*) like long QT heart syndromes, several neurological diseases including epilepsy, seizures or periodic paralyzes of different kinds, deafness...

One particular feature of VGCs is that they produce tiny, transient currents that were named *gating currents* when going from closed to open state. The integral of these currents is called the *gating charge* and is a fundamental property of the channels. When the first VGCs were sequenced, it was found that they have a common structure with 4 units each containing six transmembrane helices. The fold and assembly of the two helices at the N-terminus of each unit (S5 and S6) form the pore, the region that is responsible for the transport of ions from one side of the membrane to the other.

The other four (S1-S4) constitute an auxiliary domain that is responsible for sensing the TM voltage change: the *voltage sensor domain (VSD)*. Among them, the fourth transmembrane segment (*S4*) contain a large number *positively charged residues* (4 to 7, mostly arginines) that sense and respond to the TM voltage changes (*i.e.* the local electric field). These residues are the molecular level components responsible for the gating currents: indeed, following activation, *i.e.* when VGCs go from the resting (closed) state to the activated (open) one, the total gating charge (~12 to 14 elementary charges) is transported across the membrane mostly by the S4 basic residues.

Despite the great interest for these proteins that are known to transport ions across the excitable membranes in a voltage dependent manner and the breakthrough discoveries of the last decades (among which the resolution of a crystal structure of the activated state of the Kv1.2, a mammalian potassium VGC), many mysteries remain about their function on a molecular level, and most particularly what is the mechanism of their deactivation.

In this work, we have addressed several of these questions using state of the art molecular dynamics simulations together with a special scheme we devised that allows to apply a TM potential in a way that complies with patch clamp experiments.

The main results of this work can be summarized as follow:

- Based on a 2.2 μs simulation of the entire Kv1.2 channel (embedded in a mimic of

lipid environment (a phosphatidyl-choline lipid bilayer), solvated in KCl salt solution and submitted to a deactivating TM potential of ~ -600 mV) and of subsequent biased (steered) MD simulations, we uncovered 5 states of the channels VSDs along the deactivation, conformation of which α, -β, γ and δ- and ε correspond respectively to the open, intermediates and closed states of the channel. The conformational changes taking place within the VSD involve a zipper-like motion of the S4 basic residues in sequential ion pairing with nearby counter charges from the VSD. The transfer from one state to another is accompanied by the transition of one of the basic residues through the newly discovered gating charge transfer center, in agreement with the hypothesis of MacKinnon et al. We also show that the lipids not only participate in the stabilization of the activated and resting state through interactions with top and bottom of S4 basic residues respectively but also in the intermediate states. In γ, for instance, the first residue of S4 interacts with the phosphate groups of the top bilayer while the last residue of S4 interacts with the bottom residues of S4. The overall conformational change from the active to the resting states of the VSD results in a total gating charge in agreement with electrophysiology experiments (12.8e), and necessitates a large displacement of the S4 backbone amounting to 10 – 15 Å. Perhaps the most interesting feature revealed by the present MD study lies in the analysis of the electrical activity of the channel and the finding that the cumulative gating charge transported by the S4 basic residues can be described by a unique function, which defines the electromechanical coupling mechanism that the VSD charges undergo. Taken together, these findings favor the sliding helix model over the transporter one.

- Using the configurations of Kv1.2 determined in the first part of this work, we then studied the molecular level effect of selected mutations of S4 positively charged residues involved in genetic diseases and that were shown by electrophysiology to give rise to leak currents (called “omega currents”) through an unidentified pathway. Some well-defined mutations are shown to disrupt the salt bridges that maintain the integrity of the voltage-sensor domain and to open a hydrophilic pathway through the VSD. When submitted to a transmembrane potential of a few hundreds of millivolts, this lead to the conduction of K+ ions along this pathway. These results hence reveal the key elementary molecular processes involved in these “omega” currents. Based on an extensive study of most mutations performed both for the open and closed conformations of the Kv1.2, we propose a model of the mechanism involved, indicating that top S4 residues may lead to the appearance of inward omega currents in the resting states while bottom S4 residues may lead to the appearance of outward omega currents in the activated state and describing under which condition these leaks may be critical.

- Focusing on the modulation of VSD function by lipids, we studied the impact associated to modification of the nature of polar head groups on the VSD activation. We have used simulations of the Kv1.2 channel in a variety of asymmetric lipid bilayer containing sphygomyelin, ceramide-1-phosphate or ceramide in the upper leaflet to show that despite their key role in the stabilization of S4 basic residues, the gating

charge is not drastically affected by the change in the lipid headgroups characteristics. These results indicate that the change in the lipid head groups affects mostly the kinetics of transition from one VSD conformation to the other. In order to confirm this hypothesis, an extensive study of the free energy surface of Kv1.2 activation/deactivation would be necessary.

- Finally, wishing to extend the previous findings to other members of the VGC family which are implicated in genetic diseases and that are interesting from a pharmaceutical point of view, we have undertaken the study of several members of the Kv7 subfamily. Such channels have less S4 basic residues than the Kv1.2, leading to a reduces gating charge. In this scope, we have built molecular models of the transmembrane domain of Kv7.1, Kv7.2 and Kv7.4 channels in their open and closed conformation that are consistent with those of the Kv1.2. The preliminary results indicate that the salt bridge network within the VSD is reorganized due to the change in S4 sequence. Their gating charge amounts to ~9 e for Kv7.4 and ~6 e for Kv7.1 (compared to 12-13e in Kv1.2). We have also initiated a study of the effect of VSD basic residue mutations that are implicated in long QT syndrome, in benign familial neonatal seizures or in slowly progressive deafness. Although we have no yet been able to record any “omega” current in such mutants, as expected from electrophysiology measurements, comparison of our findings with experimental data based on longer simulations are still in progress.

Along this work that started in 2008, the bibliographical context has kept evolving and the appearance of new experimental work has led us into new, unexpected, directions. As such, the resolution of the deactivation mechanism has been crucial to start the other parts of the study on the modulation of the Kv1.2. It has also served as a basis for the initiation of the study of other members of the wide Kv family. Finally, we should stress that none of this would have been possible without the computer power and it is thanks to the generous amount of time provided by GENCI and by the CINES computer center that we have always been able to try to keep ahead of the scientific questions.

Today, in the light of our results, it seems difficult, in order to understand many phenomena along the modulation of VGKCs, to escape the question of the free energy landscape of activation. Although this is an important issue, it is also a complicated one to tackle because it involves choosing a reaction coordinate that is not straightforward and because it requires sampling on very long time scales. We are now considering the question.

The modulations of VGKCs by drugs plays a central role in pharmacology by acting essentially via two mechanisms: activation and blockade. Indeed, activators enable hyperpolarization of the membrane, thereby providing a therapeutical approach to treat neuronal hyperexcitability that is involved in epilepsy, migraines... Blockers on the other hand are used as analgesics, pain-killers or else anesthetics.

In this work, we have started the study of the modulation of Kv channels by their genetic mutation or by the alteration of the lipids embedding them. The results we have obtained on

the function of their VSDs will help understand better the mechanisms involved in their modulation by external molecules (small drugs, anesthetics, peptides, toxins).

As we have started demonstrating with the example of the Kv7 family, it is possible to study different members of the voltage gated ion channel family, especially as crystal structures are published in the future. Indeed, we can imagine to study immediately the interaction of a specific drug with the different states of a given channel (activated, intermediate, resting) and also to participate in the design of molecules that would stabilize the channel in a given desired state.